THE STUDY OF MIXED-PHASE ELECTRODES IN SOLID STATE CELLS

A Thesis

presented for the degree of

Doctor of Philosophy

in the Faculty of Science of the

University of St.Andrews

TO MY PARENTS

DECLARATION

I declare that this thesis is my own composition, that the work of which it is a record has been carried out by me, and that it has not been submitted in any previous application for a Higher Degree.

This thesis describes results of research carried out in the Department of Chemistry, United College of St.Salvator and St.Leonard, University of St.Andrews under the supervision of Dr. C.A. Vincent since 1st. of October 1981.

August 1984 Ian A. Nairn

CERTIFICATE

I hereby certify that Ian Alexander Nairn, B.Sc., has spent twelve terms of research work under my supervision, has fulfilled the conditions of the Resolution of the University Court, 1967 No. 1, and is qualified to submit the accompanying thesis in application for the Degree of Doctor of Philosophy.

August 1984

C.A. Vincent

Director of Research

ACKNOWLEDGEMENTS

I would like to thank Dr. C.A. Vincent for his help and encouragement throughout this work, and the Science and Engineering Research Council for a Research Scholarship award and travel grants.

Thanks are also due to Professor Lord Tedder and Professor Wyatt for providing research facilities.

I gratefully acknowledge the help provided by Mr. C.D. Sinclair as well as to other members of staff within the Chemistry Department for the help provided during the course of this research.

SUMMARY

The aim of the work presented in this thesis has been to develop an electrochemical measurement technique with which to study a mixed phase or composite electrode, with a view to optimising it for maximum power.

The technique selected is based on the analysis of the voltage transient recorded during the application of a galvanostatic pulse to a solid state, three-electrode cell. The working electrode consists of a mixed phase or composite region in which the electronic and ionic conductors are mixed as powders and then subjected to pressure treatment in order to form the electrode. The solid state electrode material used in this study was NbS_2 and the solid electrolyte was an iodotungstate glass.

The measurement technique has been optimised, so far as the analysis of the voltage transient and application of the galvanostatic pulse are concerned, and the effect of particle size distribution and other parameters in the mixed phase region has been studied.

A computational model has been developed to study the effect of composition and particle size disparity on the mixed phase region.

CONTENTS

1 Introduction.

1.1 Electrochemical Cells and Energy Storage.

An electrochemical power source is a device in which the energy of a chemical reaction is directly converted into electrical energy.[1] Other devices exist for the indirect conversion of chemical energy into electrical energy, for example thermal power plant and diesel engine/generator sets. In these converters the energy of fuel combustion is transformed, first into thermal energy (in furnaces or combustion chambers), then into mechanical energy (in turbines or cylinders of internal combustion engines), and finally into electrical energy (in electrical generators). In contrast to these multiple-step processes, electrochemical cells operate on a one-step basis, avoiding intermediate transformations into other types of energy and the energy losses associated with them.

Electrochemical power sources vary in size, structural features and the nature of the chemical reactions involved. They may be classified under the following headings,

(a) Primary Cells.

These are single-discharge cells, containing finite quantities of reactants; once these have been consumed on completion of discharge the primary cell cannot be used again.

(b) Secondary Cells.

These are multiple-cycle cells also known as accumulators or rechargeable cells. On completion of cell discharge, a secondary cell can be recharged by forcing the electric current through the cell in the reverse direction. This results in regeneration of the initial reactants from the reaction products. Thus during charge electric energy supplied by an external power source is 'accumulated' in the secondary cell in the form of chemical energy. On discharge this energy is released. Most storage cells allow a large number of such charge/discharge cycles.

(c) Fuel Cells.

Reactants may be fed into a fuel cell while the reaction products are continuously removed. Hence, fuel cells can discharge on a continuous basis.

In order to characterise (and hence compare) the practical performance of a given cell a number of terms have been introduced, based upon available capacity, available energy and the power that can be delivered.(2)

The theoretical capacity (Q_T) of a cell (or half-cell) is defined as

$$Q_T = xnF$$

where x is the theoretical number of moles of reaction associated with the complete discharge of the cell. The practical capacity (Q_P) or actual number of coulombs (or ampere hours, Ah) delivered is lower than Q_T if utilisation of electroactive material is not 100%. This may be due to some chemical side-reaction occurring in the cell which consumes some of the reactants. The rated capacity is the practical capacity of a cell which has been discharged under prescribed conditions until the cell voltage has fallen to a pre-determined level.

The coulombic efficiency of a cell is defined as Q_P/Q_T and the specific capacity (theoretical or practical) is defined as the capacity divided by the mass of the cell (or half-cell) and is usually given in units of Ah kg^{-1}. Sometimes a volume-based specific capacity is preferred (e.g. Ah dm^{-3}).

The theoretical available energy (En_T) for one mole of reaction (not for complete discharge) is given by,

$$En_T = nFE_{cell}$$

where E_{cell} is the E.M.F. of the cell. The actual amount of energy delivered for one mole of reaction, or practical available energy (En_P) is,

$$En_P = \int_0^{nF} E_{cell} dq = \int_0^t E_{cell} i \, dt$$

and is dependant on the manner in which the cell is discharged since the cell voltage (E_{cell}) deviates progressively from its (maximum) thermodynamic value as the rate of discharge increases. Hence the energetic efficiency (En_P/En_T) is a variable quantity, which must be associated with closely defined conditions if it is to be meaningful.

The theoretical and practical energies can also be expressed in terms of the complete discharge of a cell,

$$En_T = xnFE_{cell}$$

$$En_P = \int_0^{xnF} E_{cell} dq$$

where x is again the number of moles of reaction associated with the complete discharge.

The energy density (or specific energy) is defined as the (theoretical or practical) energy divided by the mass of the cell (units usually $Ah\ kg^{-1}$). As with the specific capacity it is sometimes more useful to consider a volume-based energy density (units $Wh\ dm^{-3}$).

The power rating of a battery specifies whether or not it is capable of sustaining a large current drain without undue polarisation. As more and more current is drawn from a cell, the power initially rises until it reaches a maximum (the maximum power point, P_{max}) and then drops as the cell voltage falls away due to polarisation effects (figure 1).

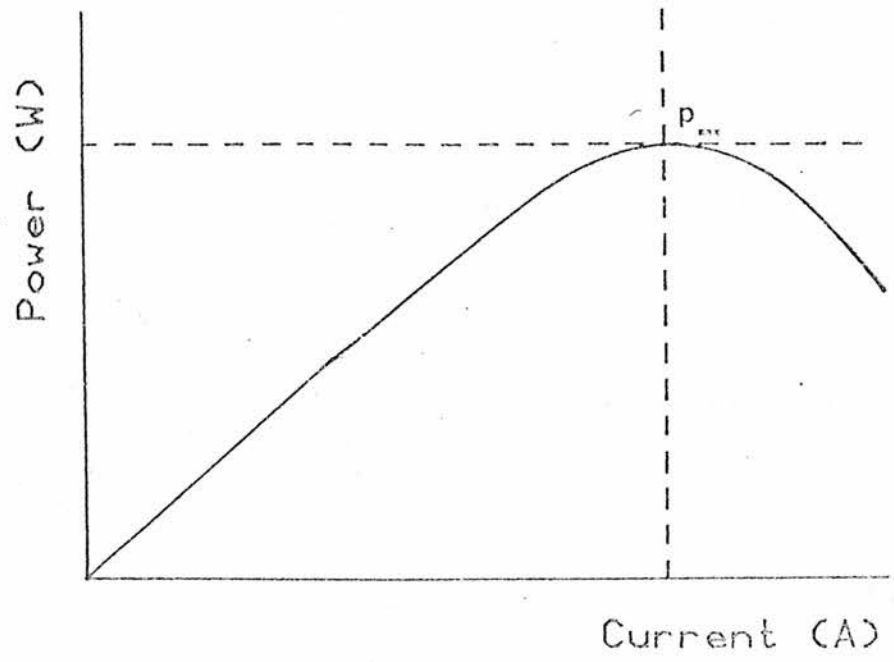

Figure 1: The power of a typical electrochemical cell as a function of discharge current.

For secondary cells then the ability of the cell to accept charge or be (re-)charged is measured in terms of the capacity and energy efficiencies of the charge/discharge cycle. The capacity or ampere-hour efficiency of a cell cycled under stated conditions of rate and depth is defined as,

$$\frac{\int_0^t i_{dis}\, dt}{\int_0^t i_{ch}\, dt}$$

where i_{dis} and i_{ch} refer to the currents flowing during discharge and charge respectively. The overall cycling energy efficiency is given by,

$$\frac{\int_0^t E_{dis} i_{dis} \, dt}{\int_0^t E_{ch} i_{ch} \, dt}$$

where E_{dis} and E_{ch} are the cell voltages during discharge and charge respectively. The ability of a cell to accept charge is dependant on the way in which the charging operation is carried out and so the above efficiency ratings are not absolute quantities. In practice, cycle efficiencies are quoted in terms of particular charge-rates for charge and discharge to fixed depth.

1.2 Current flow in an Electrochemical Cell.

For any cell that is undergoing charge or discharge, there are three general divisions that can be made to describe transmission of charge within the cell. These are

(a) electron flow in the electronic conductors. (e.g. electrode materials, terminal connectors, load resistor, etc.)

(b) ion flow in the electrolyte (this may be an aqueous solution, solid electrolyte, molten salt, etc.) and

(c) charge transfer reactions at the electrode/electrolyte interface.

The rates at which each of these processes occurs determine the total current that the cell can deliver and if any one of the rate processes is unable to maintain as high a rate as the others then it becomes the current limiting process.

When any electrochemical cell is delivering a particular current then the voltage that is observed for the cell is lower than its equilibrium value. When the cell is being charged then the observed voltage is higher. This difference in values is called the polarisation voltage or overpotential and has two main causes,

(I) 'Ohmic' or 'iR' drop in the bulk of the electrolyte phases, separators and sometimes in the electrode phases and connectors, and

(II) 'Electrode losses' which include the 'activation overvoltage', connected with the charge transfer step and/or 'nucleation' or 'crystallisation' processes at each electrode/electrolyte interface, and the 'concentration overvoltage' related to the depletion or accumulation of electroactive species near the electrode surfaces.

The iR potential drop is due to the internal resistance of the bulk phases within the cell and if the current distribution (within the cell) is uniform then the total iR drop for the cell can be found by summing the individual resistances for each phase.

It is found in practice however that the current distribution is rarely uniform and depends upon many factors, such as the cell geometry and electrode surface characteristics. In certain situations however, difficulty is encountered when trying to distinguish ohmic and electrode polarisation, for example in situations where porous electrodes are involved, or where electrode and electrolyte phases are finely mixed, (as in some solid state cells), or where the electroactive material is also responsible for carrying all the current in the electrolyte phase.

In porous electrodes the electrolyte conductivity and ohmic loss is determined by the number of pores, their size, shape and tortuosity. A conductivity attenuation factor can be derived (for various pore geometries) which relates the conductivity the electrolyte has in a free mobile solution, to the conductivity it would have when it is immobilised within a pore. de Levie[3] has derived relationships not only for the electrolyte conductances but also for the effect of porous electrodes and surface roughness on the other rate determining processes within the cell (e.g. charge transfer and mass transport reactions).

In order to minimise the polarisation losses due to iR drop, considerable attention must be paid to a number of factors when designing a battery. These include maximisation of the ionic conductance in the electrolyte phases, reducing the resistivities of the electrode materials and supplying adequate current collectors, balancing the advantages (from the point of view of electrode polarisation) of high interfacial areas against the drawbacks of high resistance paths in the bulk phases, and optimising cell geometry to minimise the effective distance between electrodes which maintaining a uniform current distribution.

Polarisation losses due to electrode processes can involve many different phenomena,[4] but in general the overvoltage can be divided into two general processes involving respectively, charge transfer reactions and mass transport of the electroactive species. Under certain circumstances one of the contributing factors become dominant, in which case it is possible to say that the electrode process is, for instance, 'mass transport' or 'charge transport' limited.

When the electrode process is charge transfer controlled (i.e. the current is determined by the rate of electron or ion transport at the electrode/electrolyte interface) then the rate of the process is determined directly by the potential difference across the double layer, and hence by the potential of the electrode. 'Charge transfer' is considered here to include the whole process of chemical bond formation and scission, solvation changes, etc. which must accompany the successful transfer of an electron or ion across an

electrode/electrolyte interface.

In addition to the basic interfacial charge transfer reaction, many processes involve a further step in the vicinity of the phase boundary. For example a 'crystallisation' overvoltage can be distinguished which is caused by a hindrance in the inclusion or release of 'ad-atoms', into or from, respectively, the ordered lattice of the solid metal electrode. Another example is a 'reaction' overvoltage which is due to some slow chemical reaction, whose rate is independent of the electrode potential.

The total current density for a cell which is charge transfer limited can be related to the overpotential by the Butler-Volmer equation,

$$i = i_0[\ \exp(-c_t F\,\eta/RT) \ - \ \exp(\{1-c_t\}F\,\eta/RT)\ ]$$

where i_0 is the exchange current (i.e. the cathodic {or anodic} current that exists when the cell is at equilibrium), c_t is the transfer coefficient or symmetry factor and is generally close to 0.5, F is Faraday's constant (96490 C equiv^{-1}), R is the gas constant (8.314 J K^{-1}mol^{-1}), T the temperature and η the overvoltage of the cell.

When the electrode process is mass transport controlled the current is restricted by the availability of the electroactive species at the electrode surfaces. Mass transport of the electroactive species may involve either diffusion in a concentration gradient or

migration in an electric field. In addition convection effects are important in cells with liquid phases.

If a high concentration of ions is present in the electrolyte which are not involved in the electrode process, (i.e. supporting or indifferent electrolyte) then the transport by electromigration is small. But if the electroactive species are responsible for carrying all the current in the electrolyte phase then it is not possible to distinguish mass transport polarisation and ohmic potential drop.

If mass transport is due to pure diffusion (i.e. diffusion of species in a concentration gradient only) then the concentration of the electroactive species can be found for simple systems by solving Fick's equations with appropriate boundary equations.

Most of the work done in this thesis is concerned with cells which are limited by this type of transport control. Solutions of Fick's equations for various boundary conditions can be found in appendix I.

1.3 Solid State Cells.

Most of the problems associated with conventional batteries, either primary or secondary, can be traced to the use of a liquid electrolyte, whether it be an aqueous, non-aqueous or molten salt system.[5] The ideal electrolyte would be both chemically and

physically invariant, i.e. its composition and structure should remain unchanged during the life of the battery. It should at the same time provide a path for ionic transport and a barrier to electronic transport. The electrolyte should also poses a high decomposition potential, thus permitting the use of couples with a high E.M.F. and consequently high energy density.

Many of the above attributes are met by the use of all solid state cells, which utilise solid electrolytes and therefore eliminate problems associated with spillage, leakage, or the emission of dangerous fluids or vapours. Such cells generally have very long shelf lives and the possibility of operation over a wide temperature range.

A 'solid electrolyte' is a phase which has an electrical conductance wholly due to ionic motion within the solid lattice and an example of these can be seen in the commercially available small low power primary batteries for use in pacemakers, watches and various electronic devices operating at or near room temperature. Some of these battery systems, for the very low current (microamperes) applications, involve lithium iodide as a Li^+ ion conducting solid electrolyte.[6] For these systems, the use of a thin layer of electrolyte is necessary to reduce the resistance to an acceptable level since LiI is a poor Li^+ ion conductor. But other solid electrolytes exist which have higher ionic conductances for other electroactive species and do not require to be used in thin layers (e.g. $Ag_6I_4WO_4$, $RbAg_4I_5$, sodium beta alumina, etc.).

In order to attain high energy densities cells must contain reactants of low equivalent weight and high free energy of reaction. In other words reactions between the more electropositive metals, (e.g. lithium and sodium), and highly oxidising elements or compounds, (e.g. sulphur, oxides, and sulphides).

Reactions between alkali metals (lithium in particular) and various compounds, such as the copper halides, have been extensively studied for battery applications. They are not, however, readily reversed at ambient temperatures. During reaction the crystalline host lattice is totally destroyed which necessitates the difficult task of rebuilding it during recharge.[7] Other problems encountered in cycling such cells is the formation of metal dendrites which can cause short circuit, and preferential deposition/depletion of electroactive species at the electrode/electrolyte interface which result in morphological changes at the interface leading to loss of contact between the conducting phases and/or distortion of the electrode. Thus an ideal reversible electrode is a compound that not only has a high free energy of reaction with alkali metals but one which also retains its crystalline structure during reaction. One such class of compounds are the solid solution electrode (SSE) materials.

1.4 Solid Solution Electrodes (SSE).

The concept of SSE materials was introduced by Steele[8] and Armand,[9] who discussed the requirements for a mixed conducting, non-stoichiometric electrode, A_xMX_y, which could incorporate the electroactive species A.

First the free energy of the reaction, $xA + MX_y \rightarrow A_xMX_y$ should be high in order to obtain high energy densities for the cell. The electrode material (MX_y) should show a high mobility of both ionic species, A, and electrons, in order to maintain high current densities and so that electronically conducting diluents should not be required. The host should have a substantial capacity for the guest species and the free energy of formation of the A_xMX_y compound should be fairly constant over the range of composition. The structural change associated with the incorporation of the electroactive species, A, into the host should be minimal. Finally the SSE material should be capable of forming stable interfaces with the electrolyte used, and transfer across the electrode/electrolyte interface should be rapid.

If these criteria are fulfilled by two different electrode materials for the same guest species, and a suitable electrolyte is available then a cell such as that shown in figure 2(a) may be visualised. This is the so-called "rocking chair" cell, in which two SSE materials are used with the active species (A), transferred between them in charge/discharge cycles.

FIGURE 2 (a)

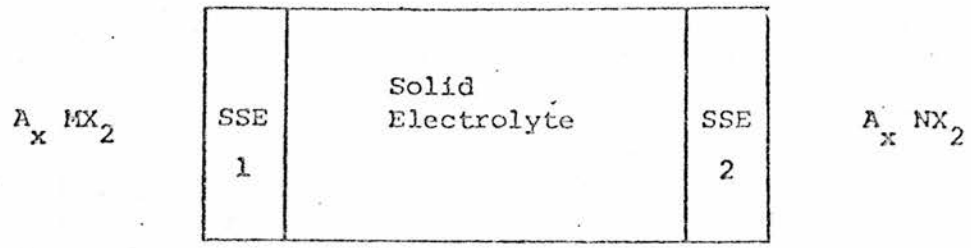

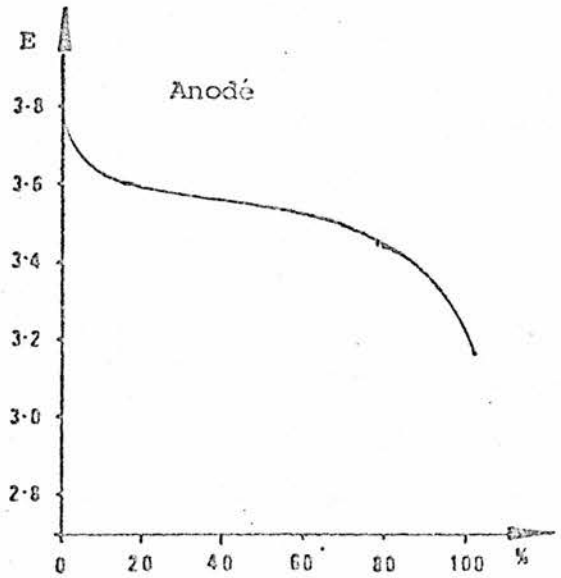

FIGURE 2 (b): Potential Versus Percentage Anode Capacity A_xMX_2

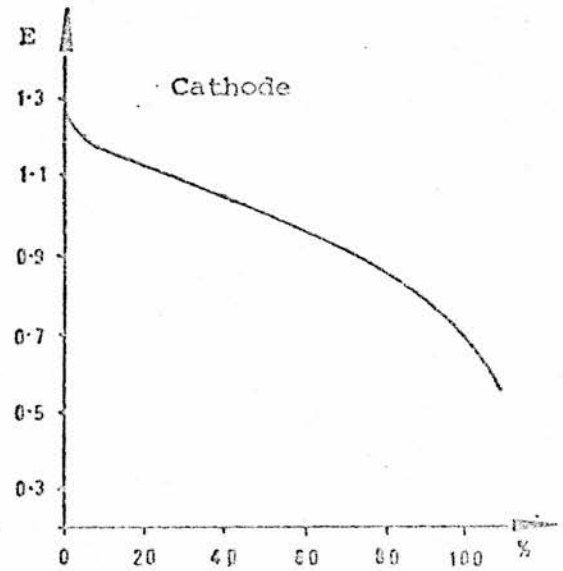

FIGURE 2 (c): Potential Versus Percentage Cathode Capacity A_xNX_2

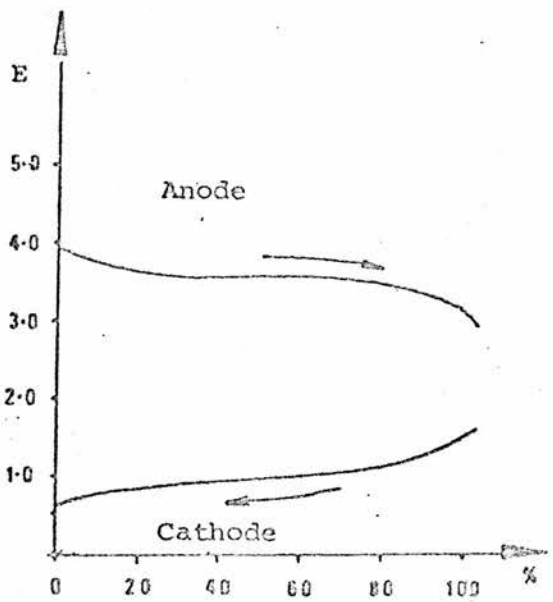

FIGURE 2(d): Individual Electrode Potentials During Cell Operation

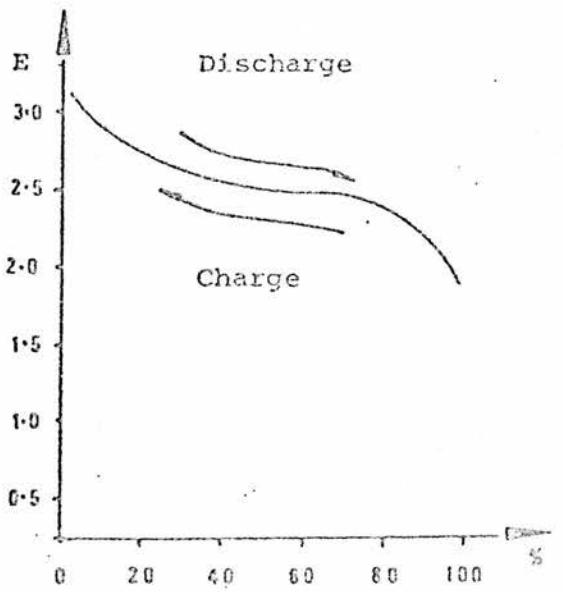

FIGURE 2(e): Overall Cell Potential.

Individual potential versus composition profiles for the two electrodes, {figures 2(b) and 2(c)}, potential versus composition of anode and cathode combined, {figure 2(d)}, and the cell potential versus composition, {figure 2(e)}, for a hypothetical ideal cell are included to illustrate the operation of this type of cell. A number of cyclable cells using this design have been discussed.[10,11]

A large number of compounds which satisfy some, if not all, of the attributes of a good SSE material have been reported. Of these the most promising candidates have either "layer" or "open-channel framework" type lattices into which intercalation of alkali metals can occur.

Strictly defined, intercalation involves the insertion of an atomic or molecular species into a host lattice. Like the insertion of days into the calendar, (e.g. February 29), the process is ideally reversible. The most familiar intercalation reactions are those involving graphite as the host material, as discussed by Kagan.[12] However, the free energy of reaction between graphite and the alkali metals is both small and discontinuous with composition,[13] so that graphite itself is of limited interest as a cathode. Because graphite is amphoteric, it has a low free energy of reaction with both electron donors and acceptors. Thus in principle, it could serve as a "container" for other electroactive elements, such as bromine. An electrochemical cell could then be devised that would use graphite compounds as both electrodes, (i.e. a "rocking chair" cell), e.g.

(anode) C_8K/Electrolyte/C_8Br (cathode).

The voltage of this cell would be within 0.5 V of that of a pure K/Br_2 cell, (i.e. 3.99 V). It has also been proposed that metal oxide intercalates, such as CrO_3 with graphite,[9] would make high energy cathodes. These cells have been tested both with lithium and sodium anodes and are partially reversible, but it is questionable whether such materials are true intercalates or merely physical mixtures of graphite and chromium oxides.[14]

Other layered intercalation compounds include the dichalcogenides of the early transition metals, which were originally studied because of their superconductivity,[15] and also because they fill the requirements of a high energy density cathode.[16] These compounds are described (synthesis and structure) in more detail in the next section.

FeOCl,[17] another layered compound with the attraction of low cost, exhibits no change in the lattice parameters as lithium is inserted. The host structure is capable of reversibly incorporating 0.5 moles of lithium per mole of FeOCl.

Initial results reported for the $NiPS_3$ layered host structure, suggesting that a maximum capacity of up to 3 lithium atoms per mole of host material, (1000 Wh kg^{-1}), were very encouraging. However, subsequent research indicates that only 1.5 lithium atoms per mole are reversibly incorporated. A range of these compounds, (formula MPX_3, where M = transition metal and X = S, Se) have been investigated by

Rouxel.[18] The results indicate that certain members of this series could perform satisfactorily over a limited range of guest concentrations.

The possibility of using $Li_xM_yV_{1-y}S_2$ electrode materials (where M = Cr, Fe) has been investigated by Murphy et al[10] in liquid electrolyte systems. This type of compound may be considered to be based on the Li_xVS_2 system. The results indicate that the substitution of some of the vanadium metal atoms in this host structure by chromium results in an extension of the maximum lithium capacity to 0.6 moles per mole of host. Replacement of vanadium by iron results in an extension of the lithium capacity to 0.8. In both these systems the potential versus composition profiles for a lithium reference electrode were considerably improved relative to Li_xVS_2.

Many transition metal oxides have been reported to have three-dimensional framework structures with tunnels formed from suitable geometrical arrangements of static ions, where the tunnels serve as sites for inserted alkali metal ions. These materials show a range of behaviour in most of the aspects of importance as SSE's, (i.e. electronic conductivity, potential composition profiles, charge/discharge behaviour, and rate of diffusion of guest species within the host lattice). For example the tungsten and vanadium bronzes[19] are perhaps the best known materials with linear tunnel structures, however the diffusion coefficients of alkali metal ions in these hosts are too small to be of practical importance in secondary batteries.[20,21] V_6O_{13},[22] on the other hand has a similar structure, but a higher diffusion coefficient and this material is

currently being developed for vehicle propulsion in cells using polymer electrolytes and lithium anodes.[23]

Up to now many of the SSE materials that have been described have been using lithium as the electroactive species since this metal, being the most electronegative and one of the lightest elements, gives very high energy densities. However, lithium has a low melting point, is highly corrosive and presents difficulties in material selection and cell design. Also, lithium dissolves appreciably in the chloride salts typically used in high temperature cells, causing self-discharge due to the corresponding increased electronic conduction in the molten salt electrolyte. These problems may be reduced or avoided by the use of certain solid lithium alloys as anode materials. Huggins and co-workers[24] have studied the diffusion coefficient for lithium in the LiAl system over a wide temperature and composition range and Garrean et al[25] have studied the various processes which limit the performance of the system as an anode.

1.5 Transition Metal Dichalcogenides.

The layered compounds of the transition metal dichalcogenides, shown schematically in figure 3, adopt one of the two types of 6:3 coordination. As shown in figures 4(a) and 4(b), the metal ion situated between two sheets of chalcogen atoms may be in either a trigonal prismatic or octahedral site, depending on the relative position of the chalcogen sheets. The host structure is made up of

ordered stacks of Ch-T-Ch layers. As there are very many permutations of relative layer positions within the stacks of several layers, and compounds exist with mixed coordination, (trigonal prismatic and octahedral in different layers), it follows that the structures of this class of compounds are numerous and complicated.

In reference to different structures of one compound, free use is frequently made of the terms polymorph and polytype. As defined by Verma and Krishno,[26] polymorphism is the ability of some compounds to exist in more than one structural form. Polytypism is defined as a special kind of one dimensional polymorphism shown by only a few groups of compounds, one of which is the layered TCh_2 compounds.

Various systems of nomenclature and representation have been developed to uniquely describe complicated layer structures. The 'ABC' notation is the simplest and describes the relative positions of atoms within a TCh_2 layer. The three sites in the plane of a hexagonally close packed sheet of atoms are designated A, B or C, (figure 5), to indicate the anion, a, b or c, lower case letters, indicates the transition metal position, and [a], [b], and [c], the intercalated guest species.

H																	He
Li	Be											B	C	N	O	F	Ne
Na	Mg											Al	Si	P	S	Cl	Ar
K	Ca	Sc	Ti	V	Cr	Mn	Fe	Co	Ni	Cu	Zn	Ga	Ge	As	Se	Br	Kr
Rb	Sr	Y	Zr	Nb	Mo	Tc	Ru	Rh	Pd	Ag	Cd	In	Sn	Sb	Te	I	Xe
Cs	Ba	La	Hf	Ta	W	Re	Os	Ir	Pt	Au	Hg	Tl	Pb	Bi	Po	At	Rn
Fr	Ra	Ac															

Trigonal Prismatic

Octahedral

FIGURE 3 Periodic Table showing the Transition metals that form layered chalcogenides with octahedral or trigonal prismatic coordination.

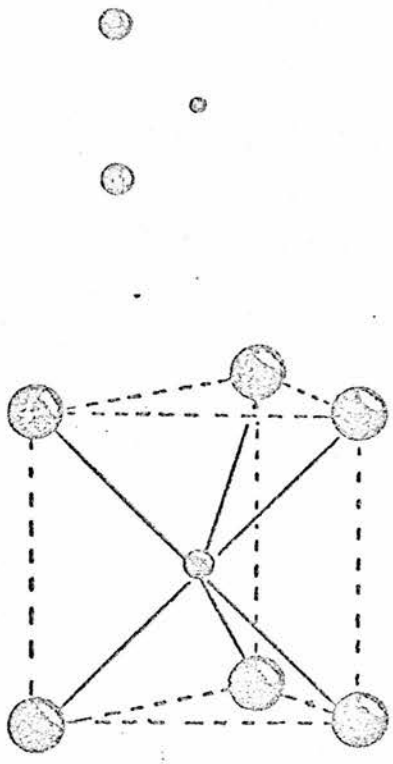

FIGURE 4(a): Trigonal Prismatic Stacking Order

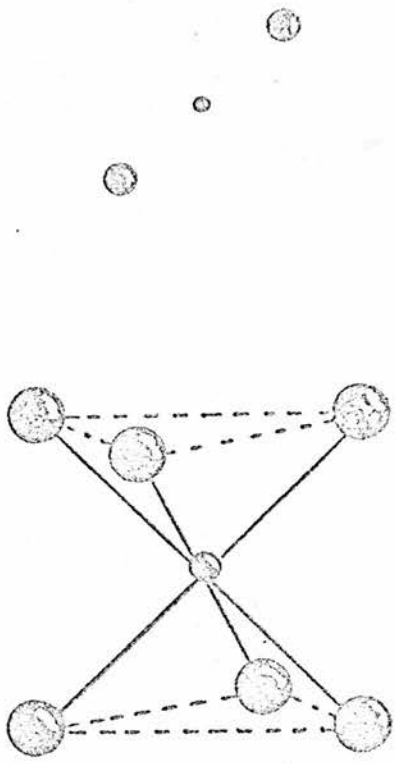

FIGURE 4(b): Octahedral Stacking Order

Where a description of the layer disposition is required, this may be achieved by indicating the number of layer units in the c-direction of the lattice repeat unit, 1, 2, 3, etc., and the symmetry of the chalcogenide atoms round the transition metal atom by T (trigonal), H (hexagonal) or R (rhombohedral). If there is more than one polytype of a given compound they may be distinguished by subscription or a lower case letter, this letter indicating the order of discovery.

Three dimensional representation of the compounds is usually very difficult. It is more common to find $(11\bar{2}0)$ sections.

These three methods of description are probably more readily understood with reference to examples, and figure 6 has included a selection of representations for some TCh_2 compounds.

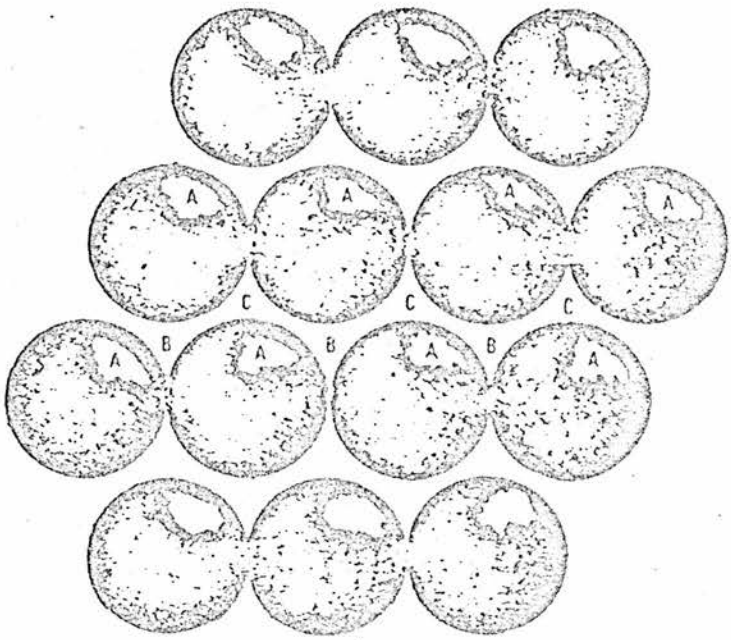

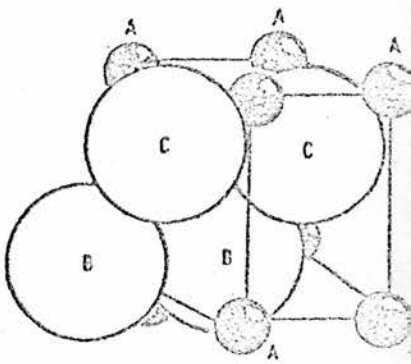

FIGURE 5 A B C notation, 001 section through lattice showing atomic positions and three-dimensional representation

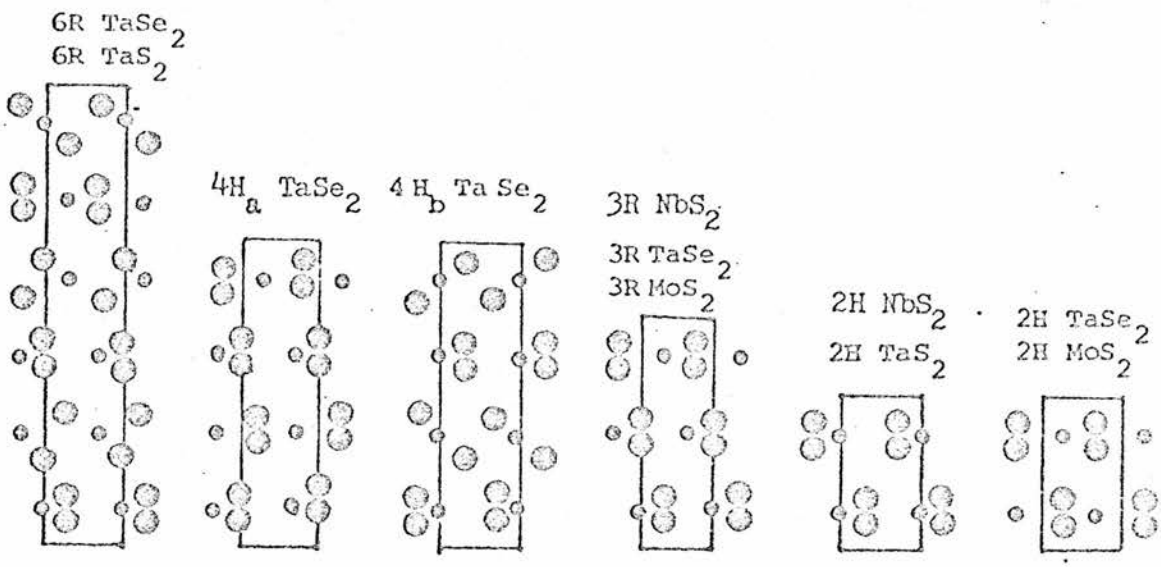

FIGURE 6 Sections through (1120) plane of polymorphic or polytypic phases, illustrating nomenclacture schemes.

1.5.1 Synthesis of TCh_2 Compounds.

TCh_2 compounds may be synthesised in simple crystal and polycrystalline form by a variety of methods.[27] Various chemical transport techniques[28] have been used in the production of large single crystals used in x-ray analysis investigations of structure. Preparations involving reduction of metal oxides with CS_2 or reaction of metal chlorides with H_2S at elevated temperatures have also been successful for certain compounds. Probably the simplest and most commonly used method for the production of polycrystalline samples is that of direct combination of the elements in sealed quartz ampoules, at elevated temperatures, i.e. as described in Chapter 2. Different polytypes of a given TCh_2 compound may be synthesised depending on oven temperatures, reaction duration and annealing or quenching procedures.

An important aspect of the structure, as far as applications as electrode materials are concerned, is the stoichiometry of the resultant compound. Compounds of the type $T_{1+x}Ch_2$ may be found under certain conditions, with quite different electrochemical properties. This feature of the compound structure is therefore very important and will be discussed further in the next section.

1.5.2 Structure of the Intercalates, A_xTCh_2

Layered TCh_2 compounds of transition metal elements form compounds arising from intercalation of molecules or ions into the host structure in such a manner as to permit return to the initial compound through appropriate physical or chemical treatment. A large number of elements in the periodic table react directly or indirectly with these structures to form well-defined compounds. In addition to the many inorganic compounds reported, there are a variety of organic intercalation products, where the organic molecule is considered to bond weakly with the TCh_2 layers. Molecules of the Lewis base type, amides, N-heterocycles, S, P and N oxides, have been reported as forming stable compounds.[29]

The structural consequences, on the host, of the intercalation reaction are either, a) a lateral movement of layers to form a different polytype, or b) vertical dilation of the van der Waals gap to accommodate the guest species. These modifications are shown schematically in figure 7. Figure 8 shows the geometries of the two types of site available to the guest species, (a) trigonal prismatic, or (b) octahedral/tetrahedral.

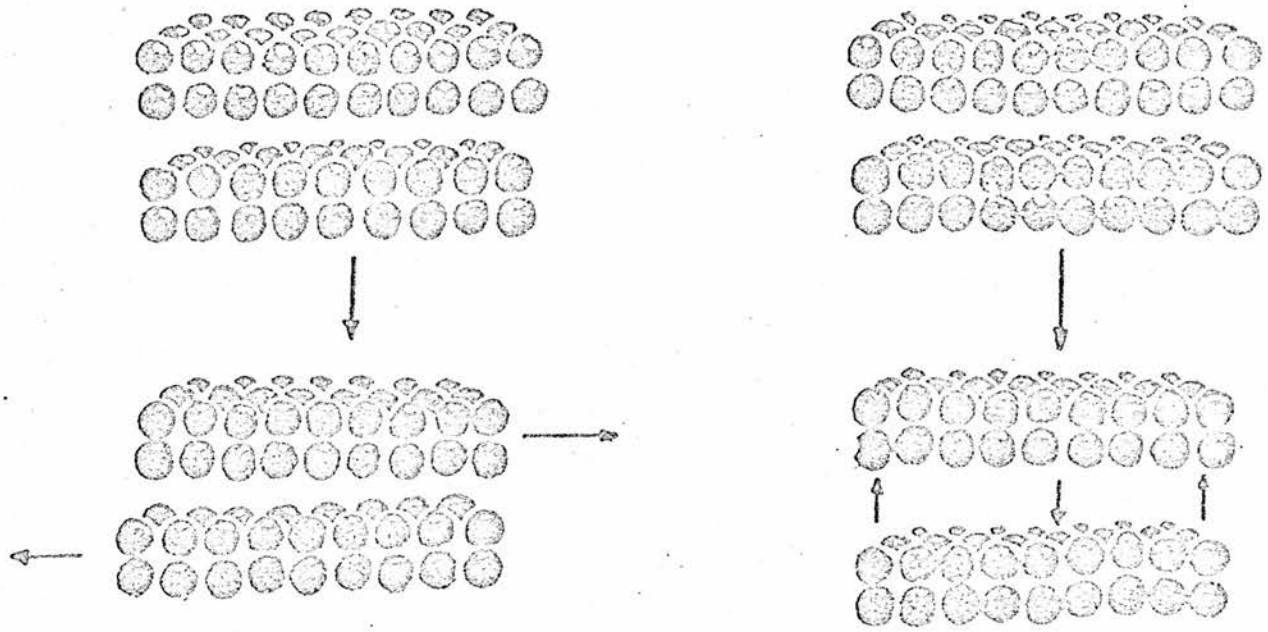

FIGURE 7 On intercalation of guest species, (a) lateral shift of host layers, (b) c - lattice parameter dilation of host

In some cases intercalation compounds have been reported as forming stage type phases.[30] These staged phases have been found in many layered phases, notably graphite compounds.[31] In these structures, not all the van der Waals gaps are occupied, figure 9.

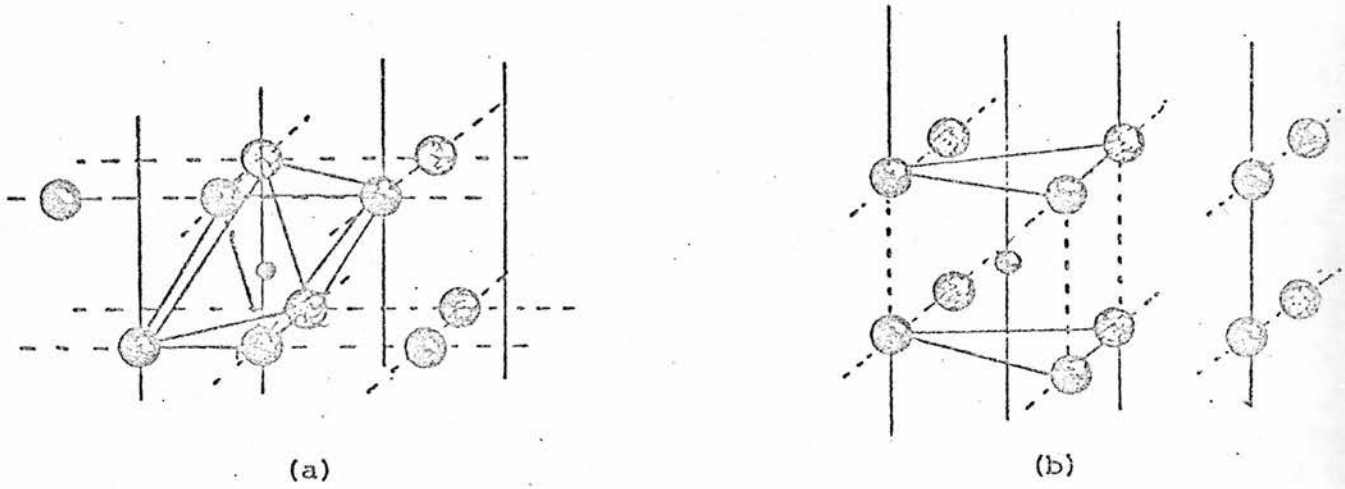

FIGURE 8 (a) Octahedral and (b) Trigonal Prismatic sites in $A_x TCh_2$ complexes

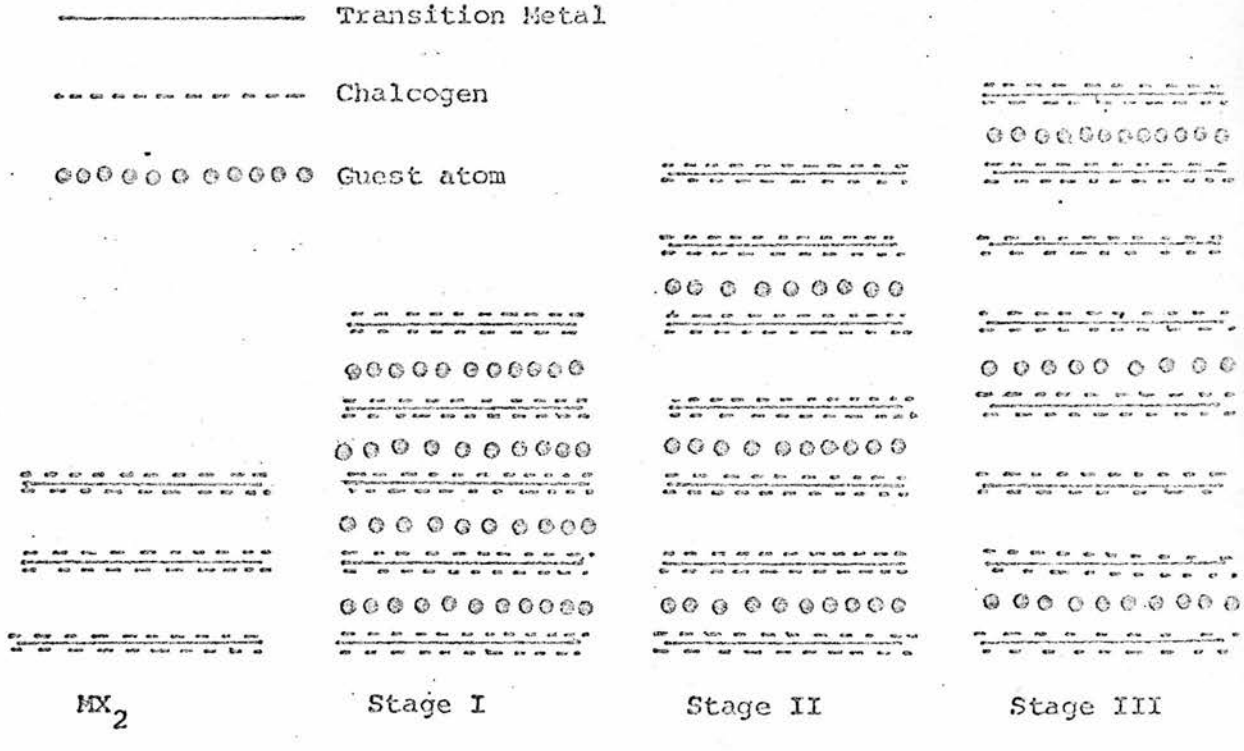

FIGURE 9 Schematic representation of first, second and third stage complexes

Metal rich phases of TCh_2 compounds may also form intercalation compounds. The rate of guest intercalation into the host has been reported as less rapid than with a near stoichiometric host. The excess metal is resident in the van der Waals gap and a correlation between metal rich non-stoichiometry and an inhibition of c-axis dilation on intercalation has been found.[9] An explanation has been proposed in terms of a 'structure pinning' effect due to excess metal bonding with adjacent sulphur layers. This has a derogatory influence on the rate of diffusion of the guest species in the lattice and also on the electrode material capacity.

1.5.3 Synthesis of the Intercalated Compounds.

The intercalated compounds can be produced in a number of ways, they may be prepared by direct reaction of the elements at high temperatures, or by reaction of the host material with solutions of the guest species; e.g. alkali metals in ammonia or butyllithium in hexane etc. But the easiest and most versatile method available is one involving electrolysis of the materials.

This method has been used to prepare several intercalated layer compounds in both single crystal and polycrystalline samples from solid, and liquid, electrolyte cells. The TCh_2 sample is made the cathode in a cell with an electrolyte to transport the guest ion and

an anode either of the metal guest or a suitable source of the metal. This method has the advantage of producing phases of precisely known stoichiometry of the guest species. The reaction rate is controlled by the current and the state of the reaction is related to the cell potential.

1.6 Mixed Phase Electrodes.

In all-solid-state cells the power that may be obtained from a particular chemical system is dependent, as described earlier, not only on the conductance of the solid electrolyte and the charge-transfer or the diffusion-limited impedance of the electrode reactions, but also on the magnitude of the operative contact area between the electronic and ionic conducting phases. In order to optimise this interfacial area and hence reduce its impedance, it has been practice to mix the electronic and ionic conducting phases and subject them to heat or pressure treatment in order to form the electrode.[32] This type of electrode is called a mixed phase or composite electrode and so far very little discussion of the effects and advantages of this region are to be found in the literature.[33]

The structure of a composite electrode is sketched in figure 10. It is essential that the SSE material and the electrolyte form two interwoven contiguous networks with maximum contact area and that the number of voids or isolated particles is at a minimum. The realization of such a structure is difficult; it can however, be

facilitated using a 'soft' electrolyte, (e.g. $Ag_6I_4WO_4$ glass), or a small amount of polymeric electrolyte to improve the contact between the electrolyte and electrode particles. The properties associated with this region will be affected by such variables as its depth, the component ratio, their relative conductance's, the particle size, the proportion of voids, etc.

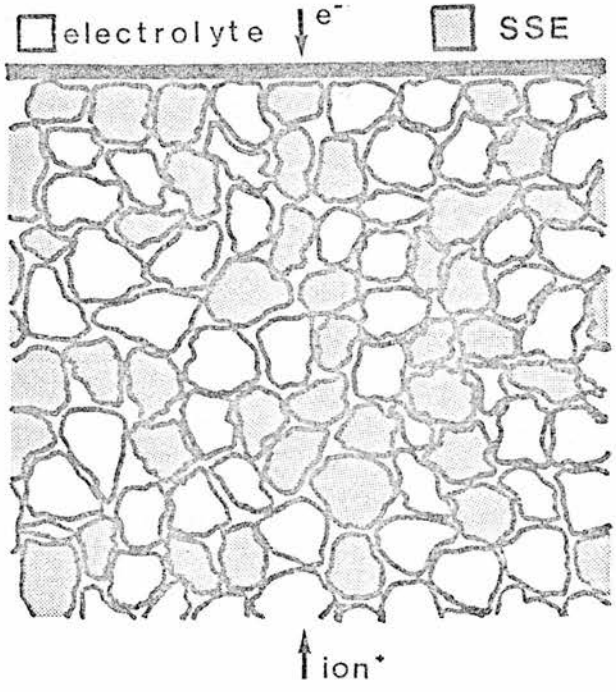

Figure 10: Composite Electrode.

In this thesis we first discuss a simple computer model which enables predictions to be made on the effect of varying some of the above parameters which define such a composite. We then discuss the analysis of the chronopotentiometric response of a mixed phase region under the influence of a short galvanostatic pulse as a means of characterising and comparing the merits of a particular configuration

or method of electrode formation. Finally we apply the above analysis to two various configurations where the component ratio has been altered and the mixed phase region has been tempered for a short time.

References.

[1] Bagotzky, V.S., Skundin, A.M., 'Chemical Power Sources', 1980, Academic Press, London.

[2] Vincent, C.A., 'Modern Batteries', 1984, Arnold Publ. Ltd., London.

[3] De Levie, R, "Electrochemical Response of porous and rough electrodes.", in 'Advances in Electrochemical and electrochemical Engineering.', Eds. Delahay, Tobias, Vol. 6, 1967, Wiley, New York, p. 329

[4] Vetter, K.J., 'Electrochemical Kinetics, theoretical and experimental aspects.', 1967, Academic Press, New York/London.

[5] Bockis, J.O'M., Conway, B.E., Yeager, E., White, R.E., "Comprehensive Treatise of Electrochemistry, Electrochemical Energy Conversion and Storage.", Vol. 3, Plenum Press, New York/London

[6] Schneider, A.A., Greatbatch, W., Mead, R., "Performance characteristics of a long life pacemaker cell", in 'Power Sources 5, Proc. of the 9' Int. Symp. in 1974', Ed. D.H. Collins, 1975, Academic Press, London, p. 651

[7] Whittingham, M.S., "The role of ternary phases in cathode reactions.", J. Electrochem. Soc., Vol. 123, No. 3, 1976, p. 315

[8] Steele, B.C.H., "Chemical Diffusion", in 'Fast Ion Transport in Solids', Ed. W. Van Gool, 1973, North Holland Press, Amsterdam, p. 103.

[9] Armand, M.B., "New electrode materials", in 'Fast Ion Transport in Solids', Ed. W. Van Gool, 1973, North Holland Press, Amsterdam, p. 665.

[10] Murphy, D.W., Carides, J.N., DiSalvo, F.J., Cros, C, Waszczak, J.V., "Cathodes for nonaqueous lithium batteries based on vanadium(IV) sulphide", Mat. Res. Bul., Vol. 12, No. 8, 1977, p. 825.

[11] Lazzari, M., Scrosati, B., "A cyclable lithium organic electrolyte cell based on two intercalation electrodes", J. Electrochem. Soc., Vol. 126, 1980, p. 773.

[12] Kagan, H.B., "Graphite insertion compounds as reagents in organic chemistry", Chemtech., Vol. 6, No. 8, 1976, p. 510.

[13] Aronson, S., Salzano, F.J., Bellafiore, D., "Thermodynamic properties of the potassium-graphite lamellar compounds from solid-state EMF measurements", J. Chem. Phys., Vol. 49, No. 1, 1968, p. 434.

[14] Ebert, L.B., Huggins, R.A., Brauman, J.I., "Nature of the chromium trioxide intercalation in graphite", Carbon, Vol. 12, No. 2, 1974, p. 199.

[15] Gamble, F.R., Osiecki, J.H., Cais, M., Pisharody, R., DiSalvo, F.J., Geballe, T.H., "Intercalation complexes of Lewis bases and layered sulphides. Large class of new superconductors", Science, Vol. 174, 1971, p. 493.

[16] Whittingham, M.S., "Electrical energy storage and intercalation chemistry", Science, Vol. 192, 1976, p. 1126.

[17] Coic, L., Palvadean, P., Portier, J., Rouxel, J., "The lithium and molecular intercalates of FeOCl.", Mat. Res. Bul., Vol. 13, 1978, p. 221.

[18] Brec, R., Rouxel, J., "Lithium intercalation in layered transition chalcogenophosphates.", in 'Proc Meet. Prospects battery app., subsequent R & D requirements', EUR 6350, 1979, p. 237.

[19] Dickes, P.G., Wiseman, P.J., "Oxide bronzes and related phases", in 'MTP Internat. Rev. of Science, Inorganic Chemistry, Series Two', Ed. L.E.J. Roberts, Vol. 10, 1975, Univ. Park Press, London, Butterworth, Baltimore, p. 211.

[20] Steele, B.C.H., "Measurement of chemical diffusion coefficients in nonstoichiometric oxides using solid state electrochemical techniques", in 'Mass Transport Phenomena in Ceramics', Eds. Cooper & Heuer, Vol. 9, 1975, London, Plenum Press, p. 269.

[21] Steele, B.C.H., "Electrical conductivity in ionic solids", in 'MTP Internat. Rev. of Science, Inorganic Chem., Series One', Ed. L.E.J. Roberts, Vol. 10, 1972, Universal Park Press, London, Butterworths, Baltimore, p. 117.

[22] Murphy, D.W., Christian, P.A., DiSalvo, F.J., Carides, J.N., "Vanadium oxide cathode materials for secondary lithium cells", J. Electrochem. Soc., Vol. 126, 1979, p. 497.

[23] Dell, Jenson, Tofield, "Materials Research for Advanced Batteries.", EUR 7595 EN, Vol. 1&2, 1980.

[24] Wen, C.J., Boukamp, B.A., Huggins, R.A., "Thermodynamic and Mass Transport properties of 'LiAl'.", J. Electrochem. Soc., Vol. 126, No. 12, 1979, p. 2258.

[25] Garreau, M., Thevenin, J., Fekir, M., "The processes responsible for the degradation of the aluminium-lithium electrode used as anode materials in lithium aprotic electrolyte batteries", J. of Power Sources, Vol. 9, 1983, p. 235.

[26] Verma, A.R., Krishna, P., "Polymorphism and Polytypism in Crystals.", 1966, John Wiley & Sons. Inc., New York/London.

[27] Leith, R.M.A., 'Preparation and Crystal Growth of Materials with layered structures', 1977, Reidel Publ. Co., Dordrecht, Holland, Boston-USA.

[28] Balchin, A.A., 'Crystallography and Crystal Chemistry of Materials with Layered Structures', Ed. F. Levy, 1976, Reidel Publ. Co., Dordrecht, Holland, Boston-USA.

[29] Whittingham, M.S., "Chemistry of intercalation compounds: Metal guests in chalcogenide hosts", Prog. Solid State Chem., Vol. 12, 1978, p. 41.

[30] Rouxel, J., "Alkali metal intercalation compounds of transition metal chalcogenides: TX_2, TX_3, TX_4 chalcogenides.", Phys. Chem. Mat. layered struct., Vol. 6, 1979, p. 201.

[31] Whittingham, M.S., Gamble, F.R., "The lithium intercalates of the transition metal dichalcogenides", Mat. Res. Bull., Vol. 10, 1975, p. 363.

[32] Oxley, J.E., Owens, B.B., "Solid State Batteries", in 'Power Sources 3, Proc. of the 7' Int. Symp. at Brighton in 1970', Ed. D.H. Collins, 1971, Oriel Press, Newcastle, p. 537.

[33] Atlung, S., Zachau-Christiansen, B., West, K., Jacobsen, T., "The composite insertion electrode. Theoretical Part. Equilibrium in the insertion compound and linear potential dependence", to be published in J. Electrochem Soc.

2 Experimental Details

2.1 Silver Iodide (γ AgI)

Silver iodide was prepared by dropwise addition of approximately 0.5 molar potassium iodide to a slight excess of silver nitrate, of the same concentration, under conditions of minimum light and slight acidity. Stirring was maintained throughout the addition. The product, a bright yellow, fine precipitate, was recovered by filtration and washed thoroughly with distilled water and AnalaR acetone. The solid obtained was dried and stored in darkness over phosphorous pentoxide desiccant.

2.2 Silver Tungstate (Ag_2WO_4)

Silver tungstate was prepared by precipitation from approximately 0.5 molar solutions of sodium tungstate and silver nitrate under conditions of minimum light. During the dropwise addition of the silver nitrate solution to the sodium tungstate, the solution temperature was maintained at approximately 80^{o}C and the pH retained between 9 and 10 by the occasional dropwise addition of dilute sodium hydroxide.[1] The white product obtained was filtered, washed with distilled water and AnalaR acetone, then dried and stored, in

darkness, over phosphorous pentoxide desiccant.

2.3 Iodotungstate Glass Electrolyte ($Ag_6I_4WO_4$)

The iodotungstate glass[2] was prepared by melting a finely ground mixture of silver iodide and silver tungstate, in a 4:1 molar ratio, in a pyrex melting tube with a narrow bore side arm. The melt was quenched by decanting the liquid through the side arm, in fine droplets, into a dewar of liquid nitrogen. The electrolyte was finely ground in an agate mortar and pestle and stored, in the dark, over phosphorous pentoxide desiccant.

2.4 Determination of the Iodotungstate Electrolyte conductivity.

The conductivity of the electrolyte was assessed by preparing a cell with two non-blocking electrodes comprising of a 2:1 mixture (by weight) of electrolyte and silver powder, finely ground in an agate mortar and pestle. Approximately 0.2g of this mixture was pressed at 0.5 tonne pressure in a 13mm Specac die. A layer of approximately 0.3g pure electrolyte was pressed over the electrode layer at 1 tonne. Finally, a further 0.2g of the electrode mixture was pressed onto the cell at 3 tonnes pressure to complete the cell.

The area of the electrodes was assumed to be the geometric area and the length of the cell, for purpose of calculating the cell constant, was obtained by sectioning the cell and using a travelling microscope to determine the electrolyte layer depth after the conductivity measurements had been carried out.

Figure 1 shows the detail of the cell-holder and pyrex envelope design used to measure the two-electrode cell conductivity. The envelope was located in a horizontal tube furnace with an electronic temperature control unit and was flushed with nitrogen prior to heating, a slow flow of gas being maintained during the experiments. Screened electrical connections were made with the external circuit through BNC connectors sealed into the 7mm cones on the envelope-head with "Araldite" epoxy resin.

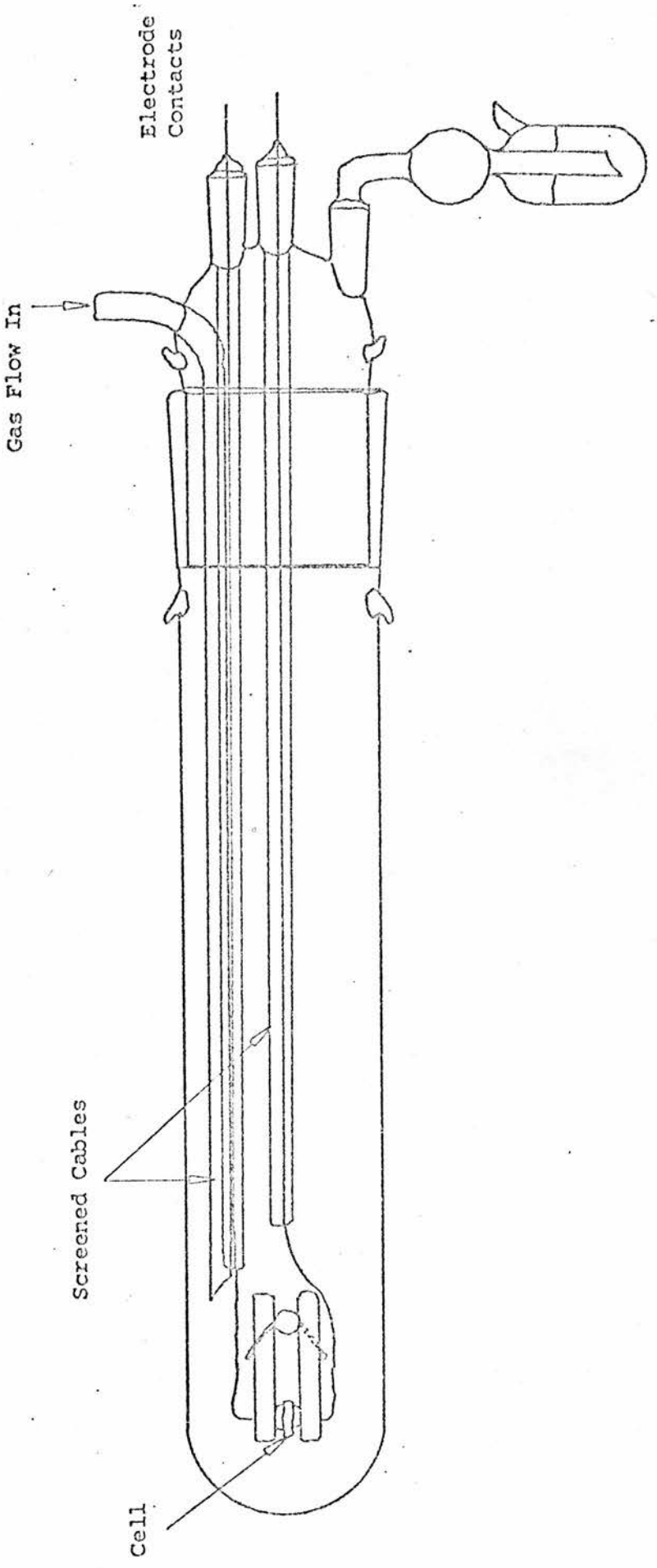

Figure 1: Detail of Cell Holder used for AC conductivity measurements.

One of the most powerful techniques available for the investigation of electrolytes is a.c. frequency response analysis. Typical applications are in the determination of total electrolyte resistance, (due to a combination of grain boundary and bulk resistances), double layer capacitance and geometrical capacitance. Data obtained by the application of a range of a.c. frequencies to a cell and recording the change in the resistance and capacitance of the equivalent circuit of the cell with frequency may be treated in a variety of ways to highlight the parameters of interest. While it is possible to use different plots and formalisms to evaluate the components of intergranular and bulk impedances, in the present case the technique has been used at its simplest level, as a means of determining the total resistance of a cell at specific temperatures. It is generally true that a frequency independent region in the log conductivity versus log frequency spectra corresponds to the d.c. conductivity of a cell with non-blocking electrodes and this value of conductivity obtained from the plateau is the value quoted for the electrolyte at a given temperature.

Using this technique it was found that the ionic conductivity of the iodotungstate electrolyte was typically 0.04 S cm^{-1} at room temperature and 0.09 S cm^{-1} at 50^{o}C, the temperature at which all the measurements on the three-electrode cells were carried out at. The transport number for the silver ion was unity.[3]

2.5 Niobium Disulphide

Various polymorphs of niobium disulphide were prepared by reaction of elemental niobium and sulphur in the appropriate molar ratios (eg. 1g Nb to 0.6903g S) in evacuated quartz ampoules. The free volume in the ampoule was kept to a minimum so as to ensure that the gaseous sulphur would react with the niobium metal quickly and not build up to such an extent that the ampoule might explode. Suitable precautions must be taken in this area and slow heating rates (approx. 50^{o}C per hour) are advisable to ensure adequate reaction of sulphur.

The exact phase found during reaction is dependant upon the maximum reaction temperature and the cooling process. In all cases the final sample is a mixture of phases, with the hexagonal and rhombohedral forms being the most predominant at reaction temperatures around 900^{o}C.

The phase best suited for an electrochemical cell was found to be the hexagonal form[4] since this gave an overpotential of approximately 0.4 V with respect to a silver reference electrode, whereas the rhombohedral form gave only 0.25 V. Thus it was desirable to prepare samples of NbS_2 which most closely resembled the pure hexagonal form.

Analysis of the predominant phase was undertaken by X-ray powder diffraction on a Philips PW1384 using CuK_α radiation and in order to simplify interpretation of the resultant spectra use was made of a program called POWD on the Aberdeen IBM mainframe computer which can predict the X-ray powder diffraction pattern for a sample, given the unit cell coordinates and dimensions, its space group and the atomic scattering factors for the atoms present.

Figures 2 and 3 are the X-ray powder patterns which would be expected for the pure hexagonal and rhombohedral phases as predicted by POWD given the relevant data. Figure 4 is the sum of figures 2 and 3.

The data that POWD requires for the hexagonal form of NbS_2 is that the space group is $P6_3/mmc$ (no. 194),[5] its unit cell dimensions[6] are, a = 3.31 Å, b = a, c = 11.89 Å and the cell coordinates are, for Nb (0, 0, $\pm$0.25) and for S ($\pm$0.333, $\pm$0.667, $\pm$0.125) and ($\pm$0.333, $\pm$0.667, $\pm$0.375). For the rhombohedral form, the space group is R3m (no. 160),[5] its unit cell dimensions[6] are, a = 3.33 Å, b = a, c = 17.92 Å and the cell coordinates are, for Nb (0, 0, 0); (0.333, 0.667, 0.667); (0.667, 0.333, 0.333) and for S (0, 0, 0.246); (0.333, 0.667, 0.913); (0.667, 0.333, 0.580) and (0, 0, 0.420); (0.333, 0.667, 0.867); (0.667, 0.333, 0.753). The atomic scattering factors[7] for the atoms are given in table 1, the wavelength of the x-ray beam was 1.54056 Å.

	Scattering Factors			Scattering Factors	
Sin(θ/λ)	Nb	S	Sin(θ/λ)	Nb	S
0.00	41.000	16.000	0.50	21.336	7.017
0.05	39.970	15.484	0.60	19.156	6.254
0.10	37.606	14.177	0.70	17.268	5.505
0.15	34.916	12.583	0.80	15.533	4.790
0.20	32.305	11.109	0.90	13.915	4.138
0.25	29.881	9.927	1.00	12.427	3.570
0.30	27.692	9.039	1.10	11.098	3.092
0.35	25.760	8.376	1.20	9.945	2.699
0.40	24.077	7.856	1.30	8.972	2.384

Table 1

As can be seen from figure 4 many of the lines overlap, but there are several lines which are unique to each of the forms and these occur mainly between 30° and 60°. The lines at 32°, 34.7°, 38.7°, 43.8° and 56.4° being characteristic of the hexagonal form and the lines at 32.6°, 37.1°, 40.2°, 47.6° and 51.8° the rhombohedral form. Thus by studying the intensities of these characteristic angles for each sample it may be decided qualitatively which phase is predominant. Unfortunately a quantitative analysis cannot be carried out using the relative intensities because there are a great many uncontrollable factors which influence these intensities, such as the morphology (more or less lamellar) and size of the crystals and the preparation and exposure of the sample (flat or cylindrical sample holder) to the X-ray beam. But despite this a semi-quantitative analysis is still possible.

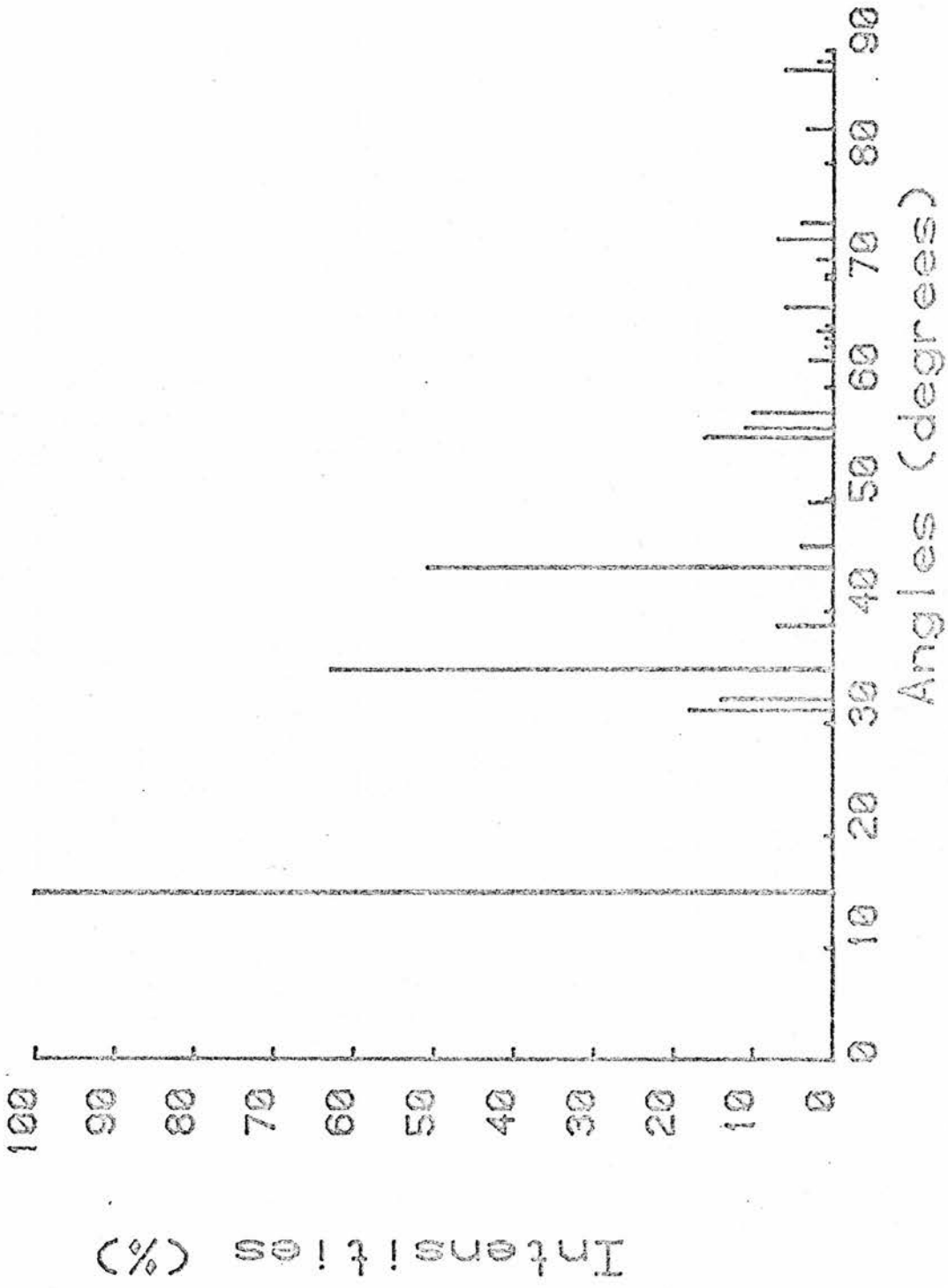

Figure 2: Hexagonal NbS_2

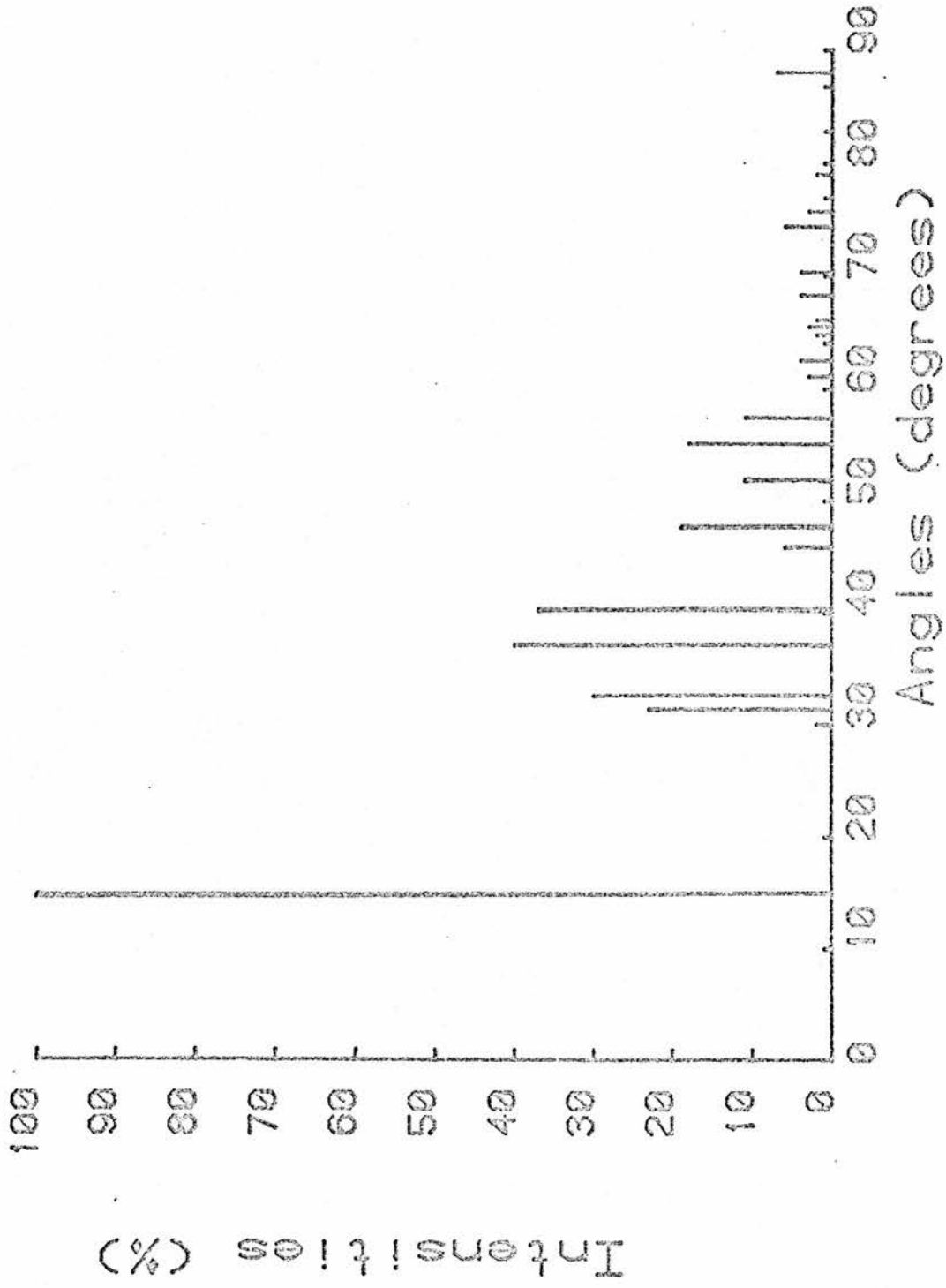

Figure 3: Rhombohedral NbS_2

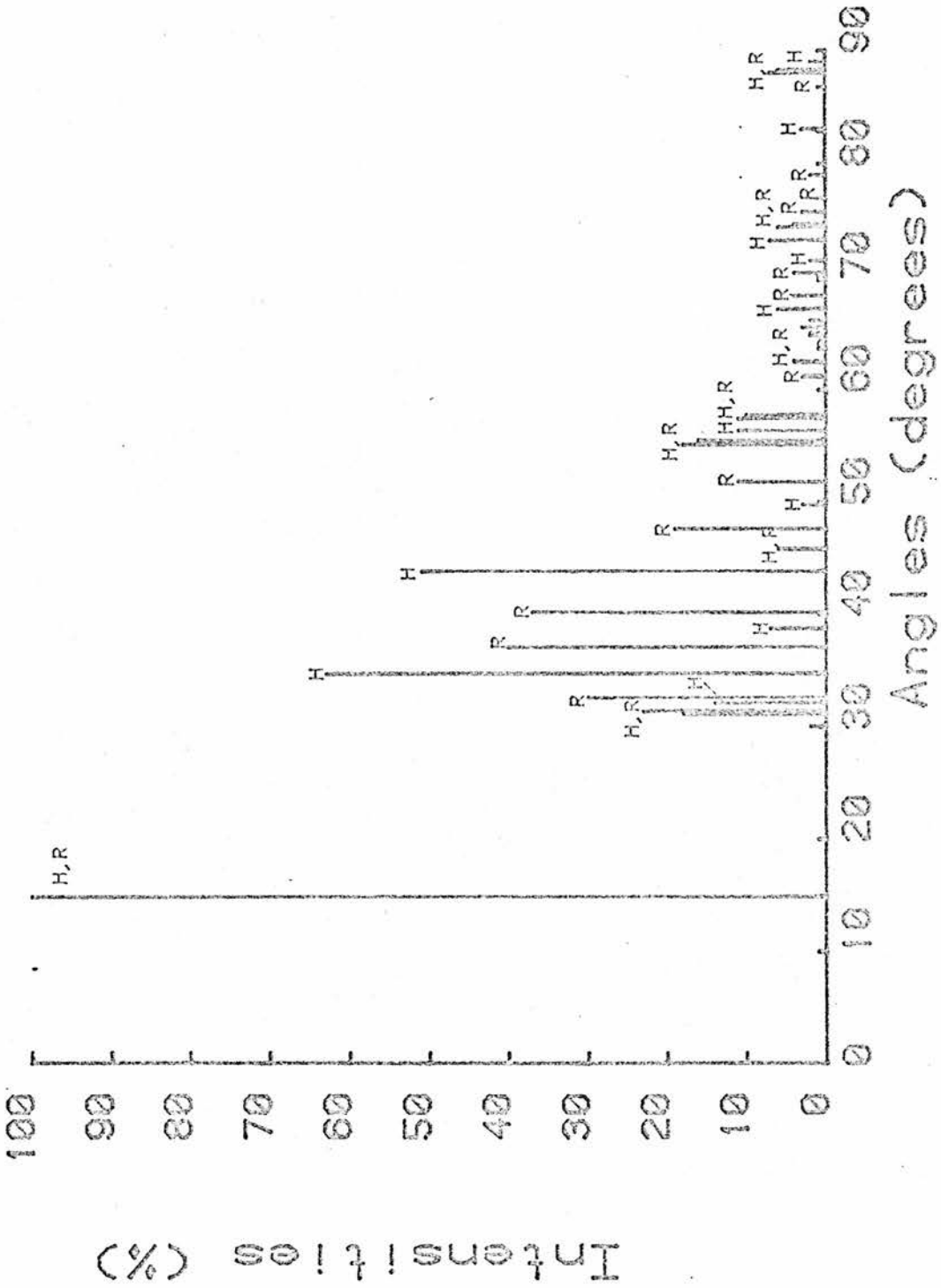

Figure 4: Hexagonal AND Rhombohedral NbS_2

Kadijk and Jellinek[6,8] have prepared various phases of niobium disulphide at different temperatures and they describe the best temperature for preparing the hexagonal form to be above 850°C. As a consequence all but one of the samples prepared and analysed had a maximum reaction temperature of 1000°C, the only other difference between the samples being the method of cooling employed.

In each of figure 5 to 8 the sample was heated to 1000°C for ten days before being cooled. In figure 5 the sample was cooled in air, in 6 quenched in ice-water, in 7 the method used for sample 6 was repeated on the same sample (i.e. the sample was heated to 1000°C and quenched in ice-water twice) and in figure 8 the sample was quenched in liquid nitrogen. In all these cases the apparent crystallinity of the samples was found to be approximately the same.

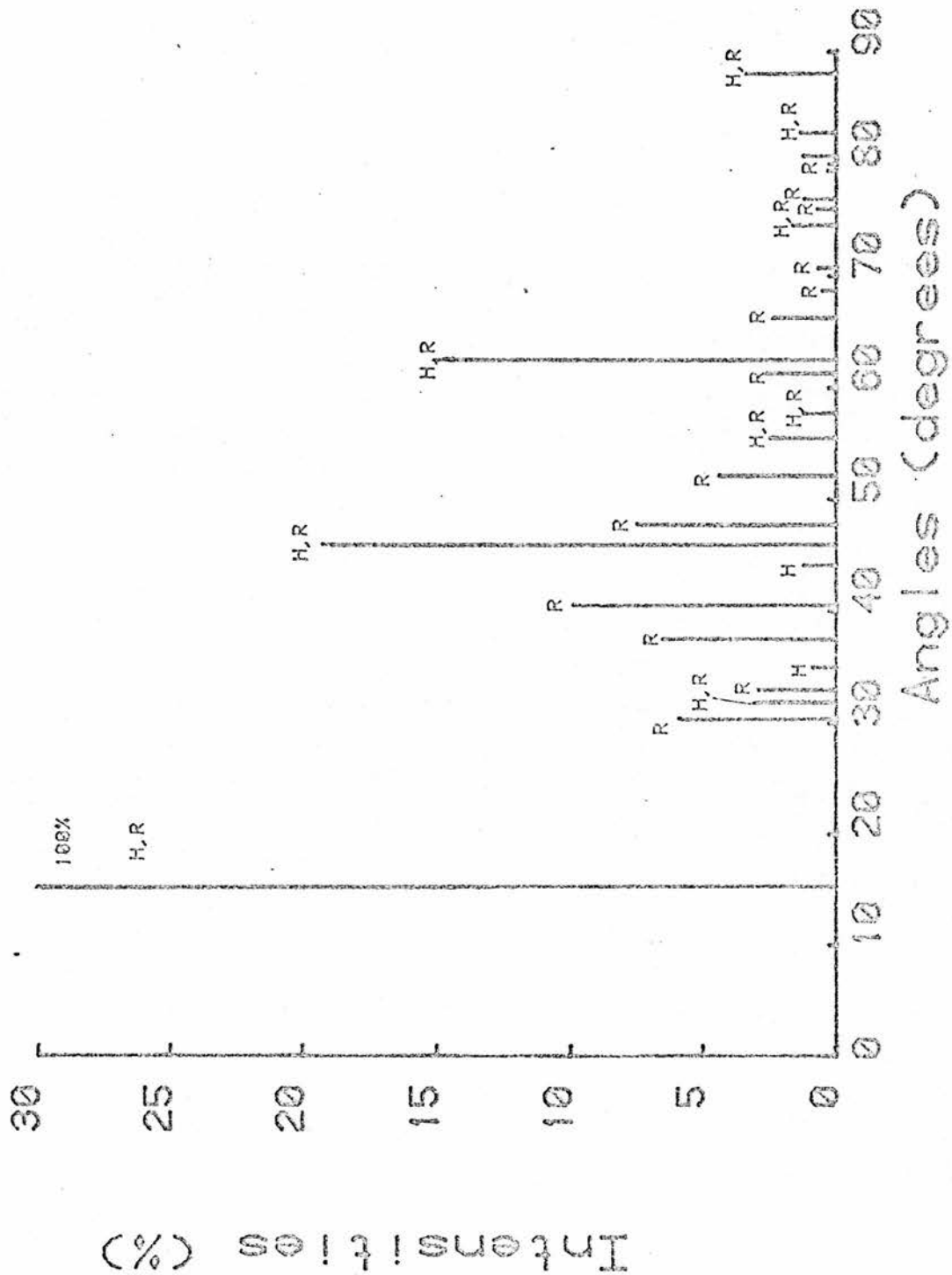

Figure 5: 1000°C, cooled in air

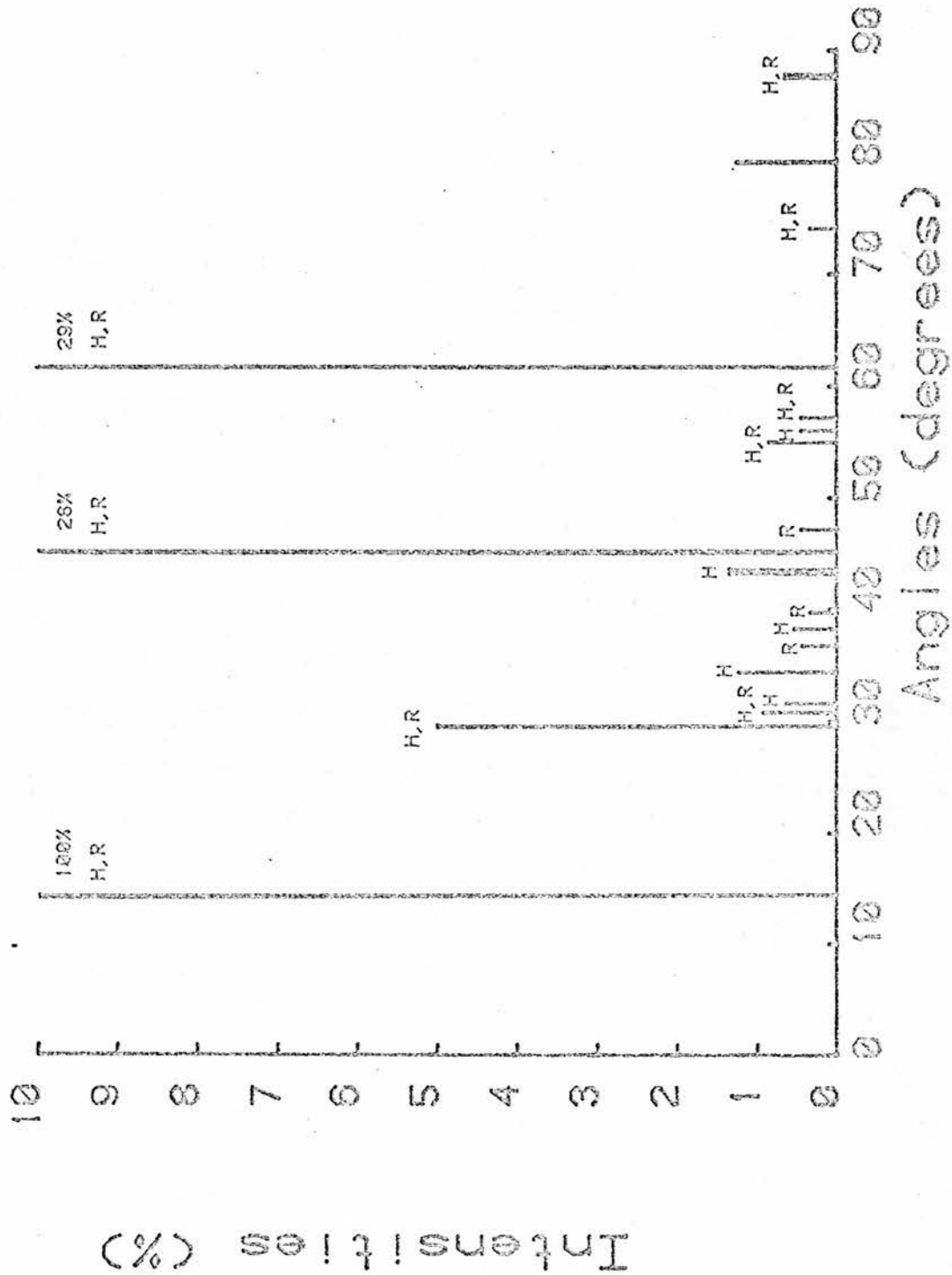

Figure 6: 1000°C, quenched in ice-water

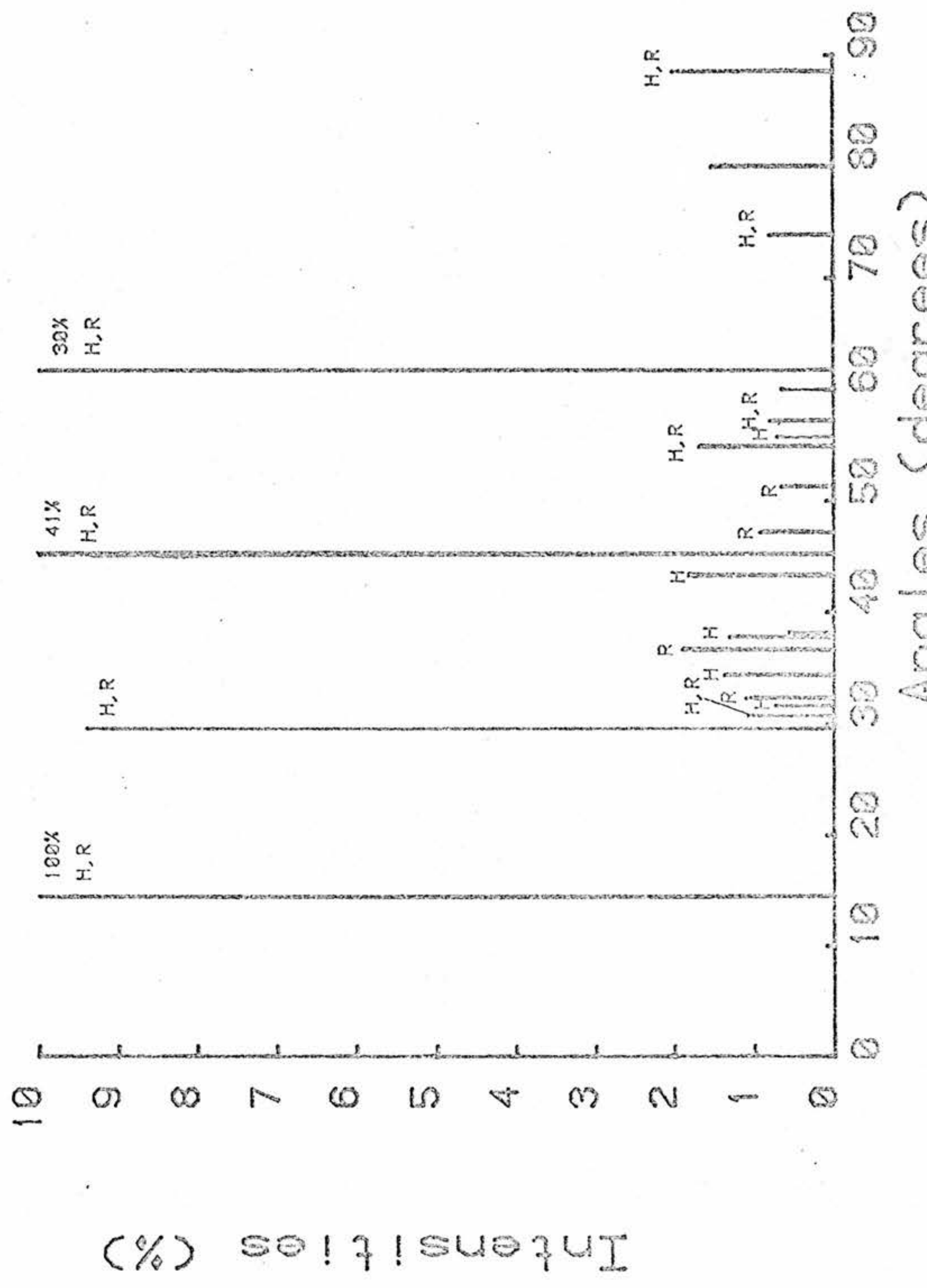

Figure 7: 1000°C, quenched in ice-water (repeated)

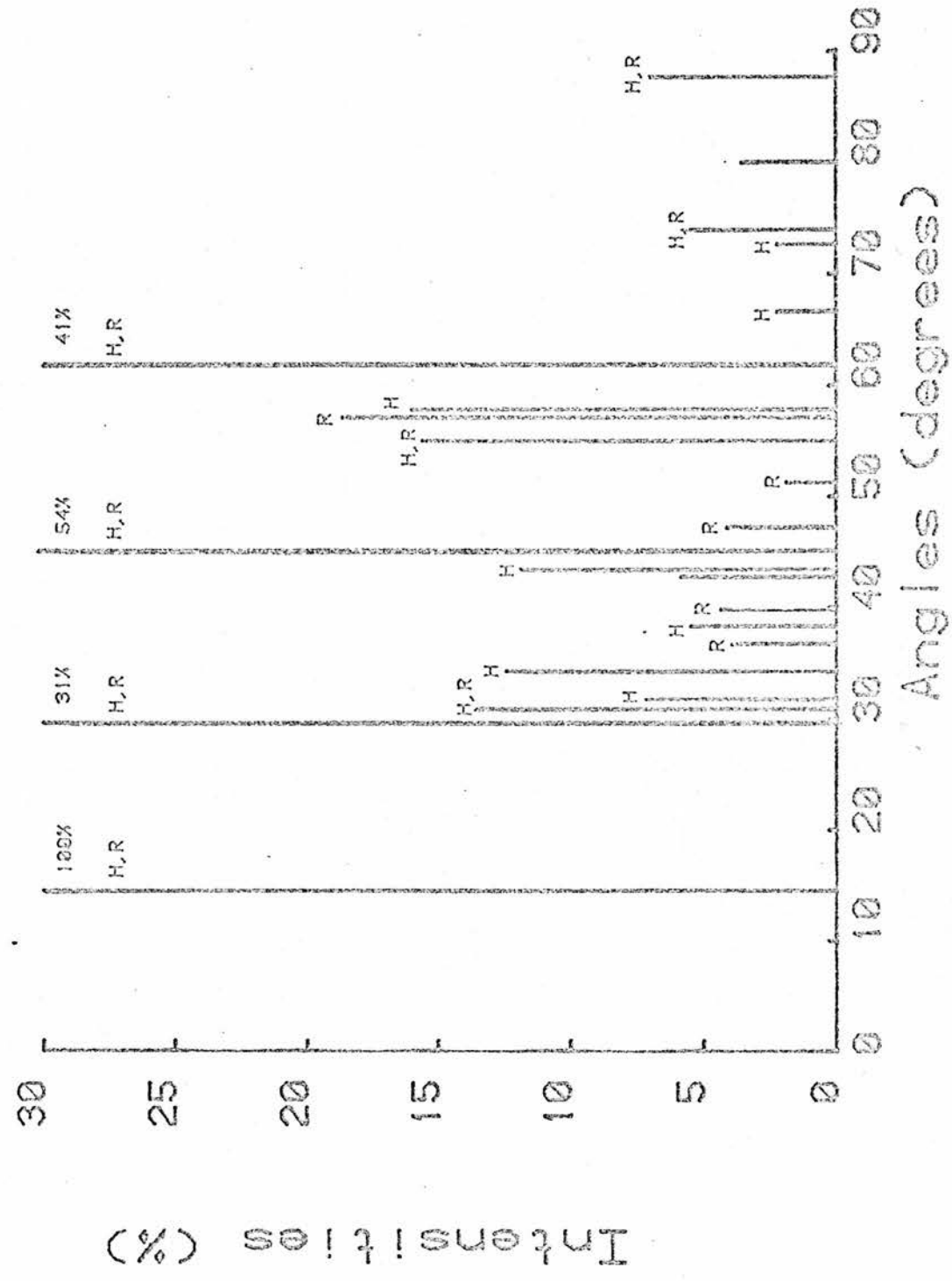

Figure 8: 1000°C, quenched in $N_2(l)$

As can be seen from the figures there is always a mixture of the two phases, but the more rapid the cooling then the more predominant the hexagonal phase becomes. In the case where the treatment was repeated (i.e. fig. 7) then there is less of the hexagonal phase present than in the case of a single heating/cooling cycle. Thus the best method to produce a sample of hexagonal niobium disulphide is to heat the elements at 1000°C for ten days then rapidly quench. (eg. in liquid nitrogen)

The sample produced by this method (i.e. shown in fig. 8) is the sample of niobium disulphide which has been used throughout this work in all the three-electrode cells constructed.

The molar volume for (hexagonal) NbS_2 is 33.97 cm^3 per mole.[9]

A sample of predominantly rhombohedral phase was also prepared by heating the elements at 750°C for ten days and then allowing the sample to cool slowly in air, the X-ray powder diffraction pattern for this sample is shown in figure 9 and is characteristic of the rhombohedral phase.

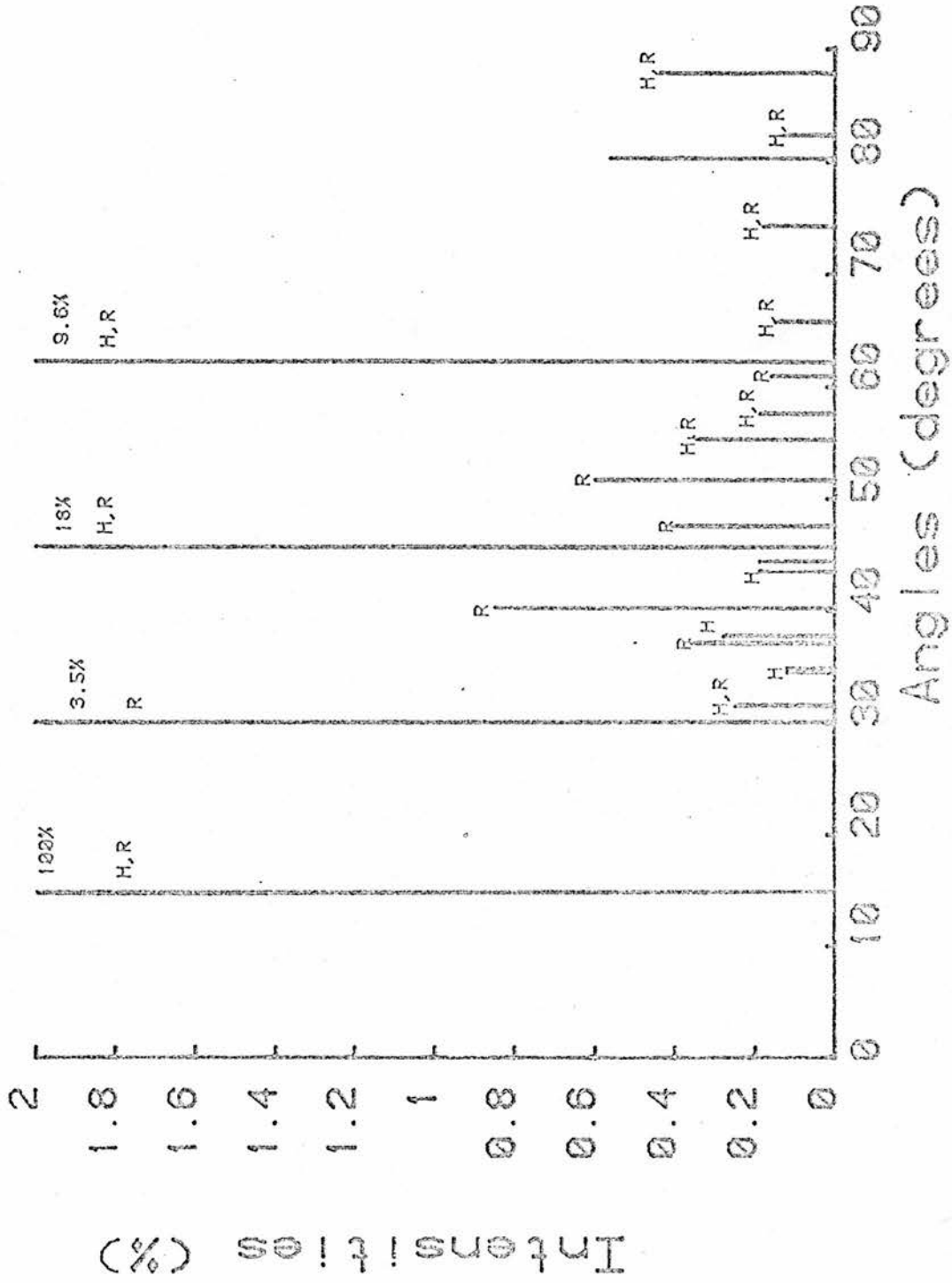

Figure 9: 750°C, cooled in air

2.6 Three-Electrode Cell Construction

The configuration of the three electrode cell is shown in figure 10. Figure 11 give step by step details of the pressing procedure, with dimensional details of the dies included in figure 12.

Slight modifications to quantities used, or pressures with which segments are applied, may be necessary for different electrode materials or electrolytes. The technique described in detail below was found suitable for the transition metal dichalcogenide electrode material (NbS_2) and silver iodotungstate electrolyte ($Ag_6I_4WO_4$) used here.

A finely ground mixture of approximately 0.12g of electrolyte and 0.07g powdered silver metal, (particle size < 100 micrometers) was pressed at 0.5 tonne pressure to form the outer reference ring of the cell. [fig. 11 a)] The internal former was pressed clear of the cell using one of the alternative base plates as shown in figure 11 b).

The die arrangement shown in figure 11 c) was then used to press approximately 0.15g of pure electrolyte at 1 tonne, to form the electrolyte separating ring. The internal former was then pressed clear of the electrolyte ring using the die arrangement of figure 11 d)

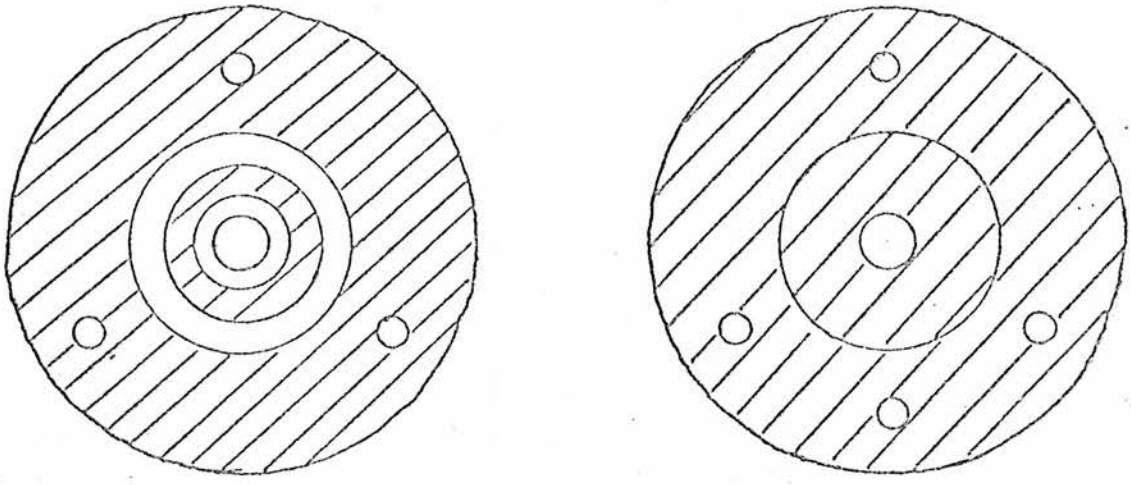

Figure 10 (a) Detail of Cell-Holder

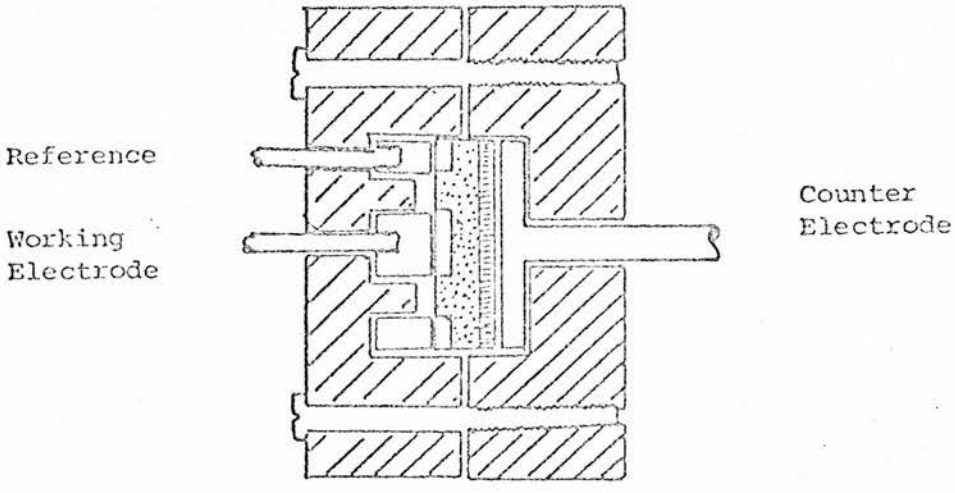

Figure 10 (b) Detail of 3 Electrode Cell. (1) Working Electrode Mixture, (2) Reference Ring, (3) Electrolyte Ring, (4) Counter Electrode

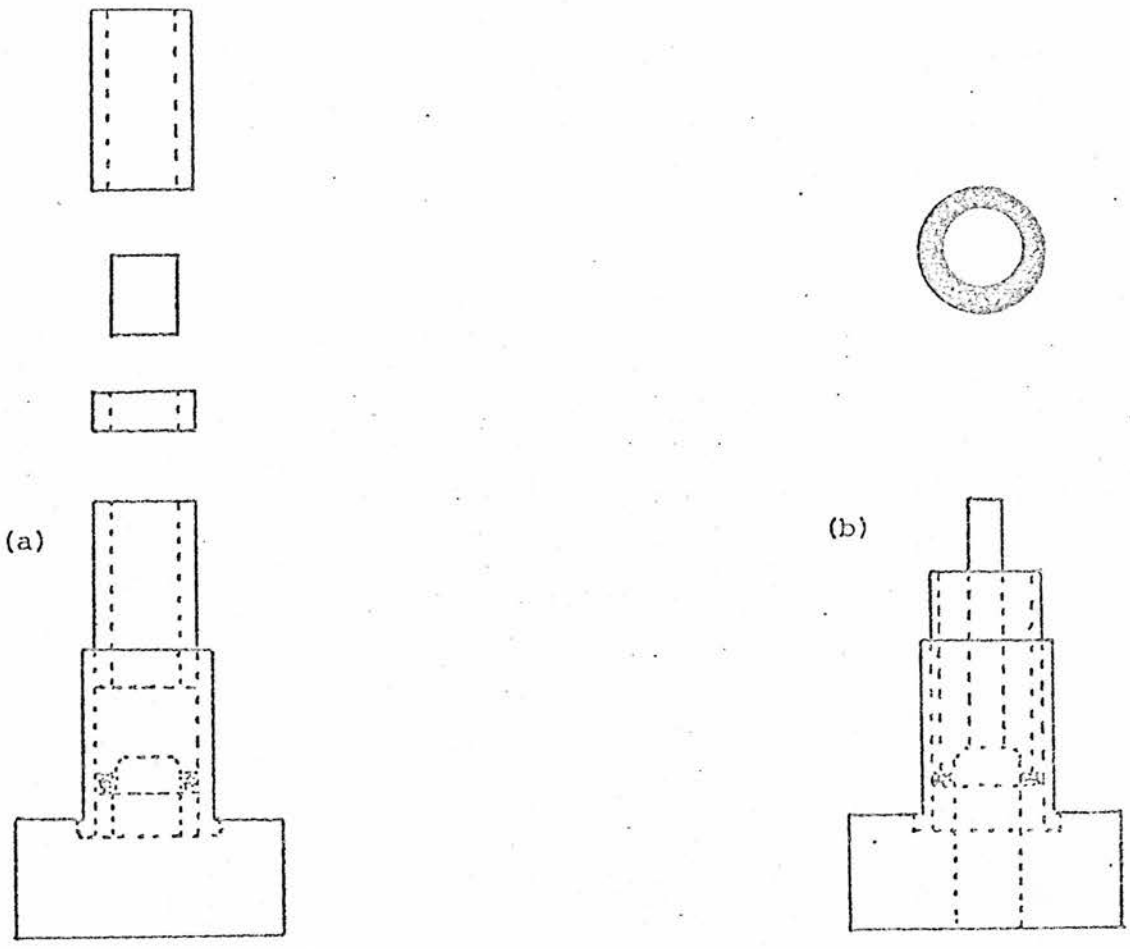

Figure 11 Detail of Cell Pressing Procedure

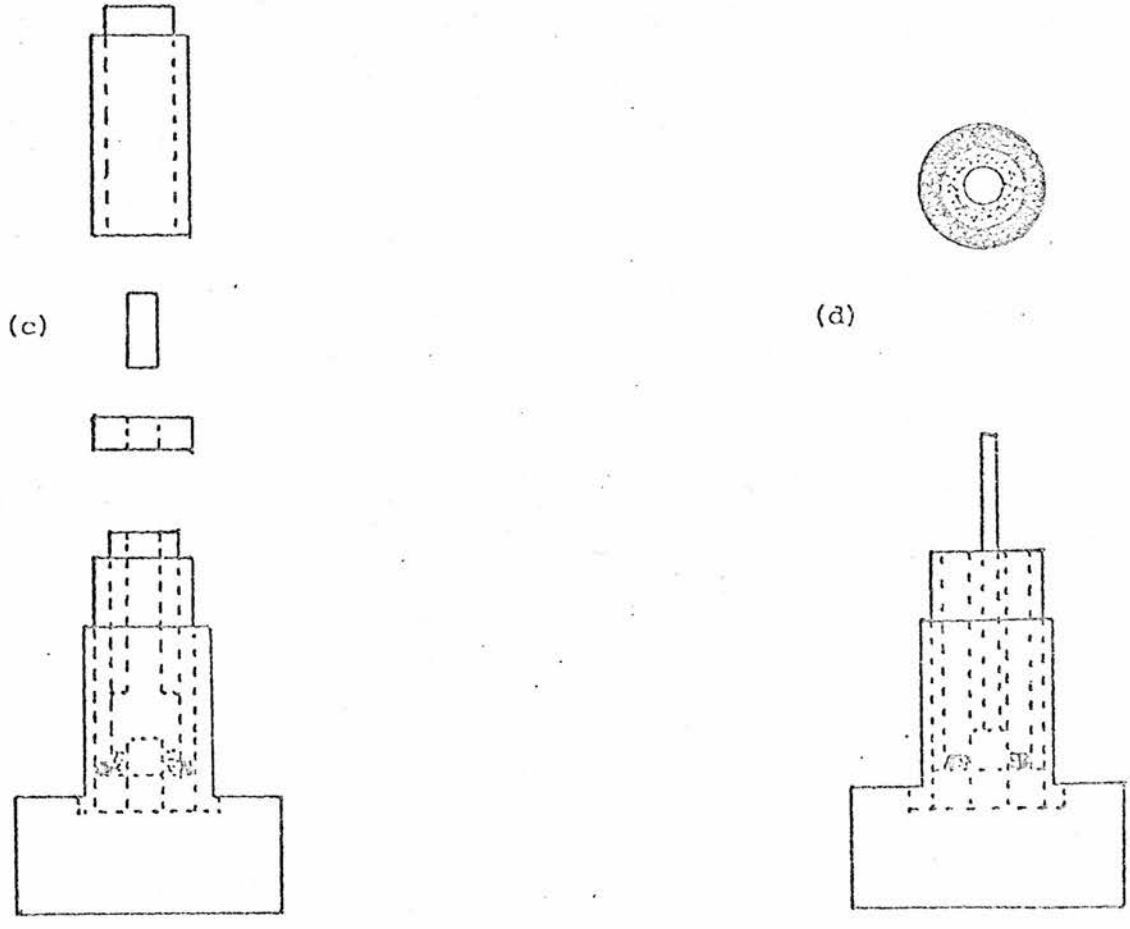

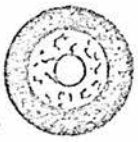

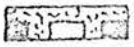

(e)

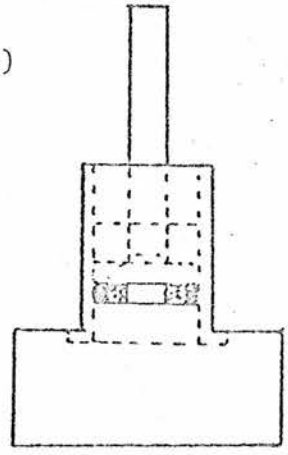

(f)

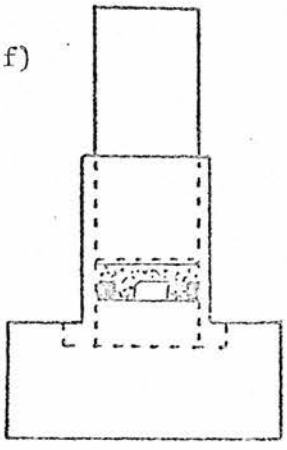

Figure 11 Detail of Cell Pressing Procedure

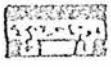

(g)

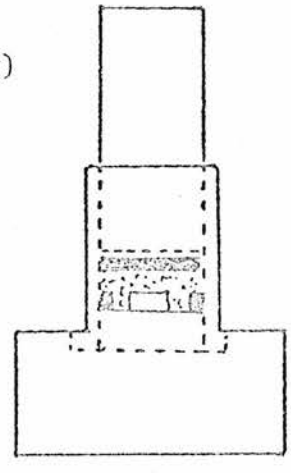

(h)

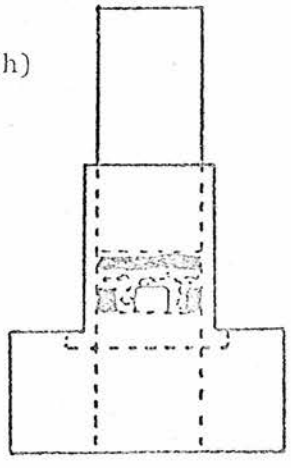

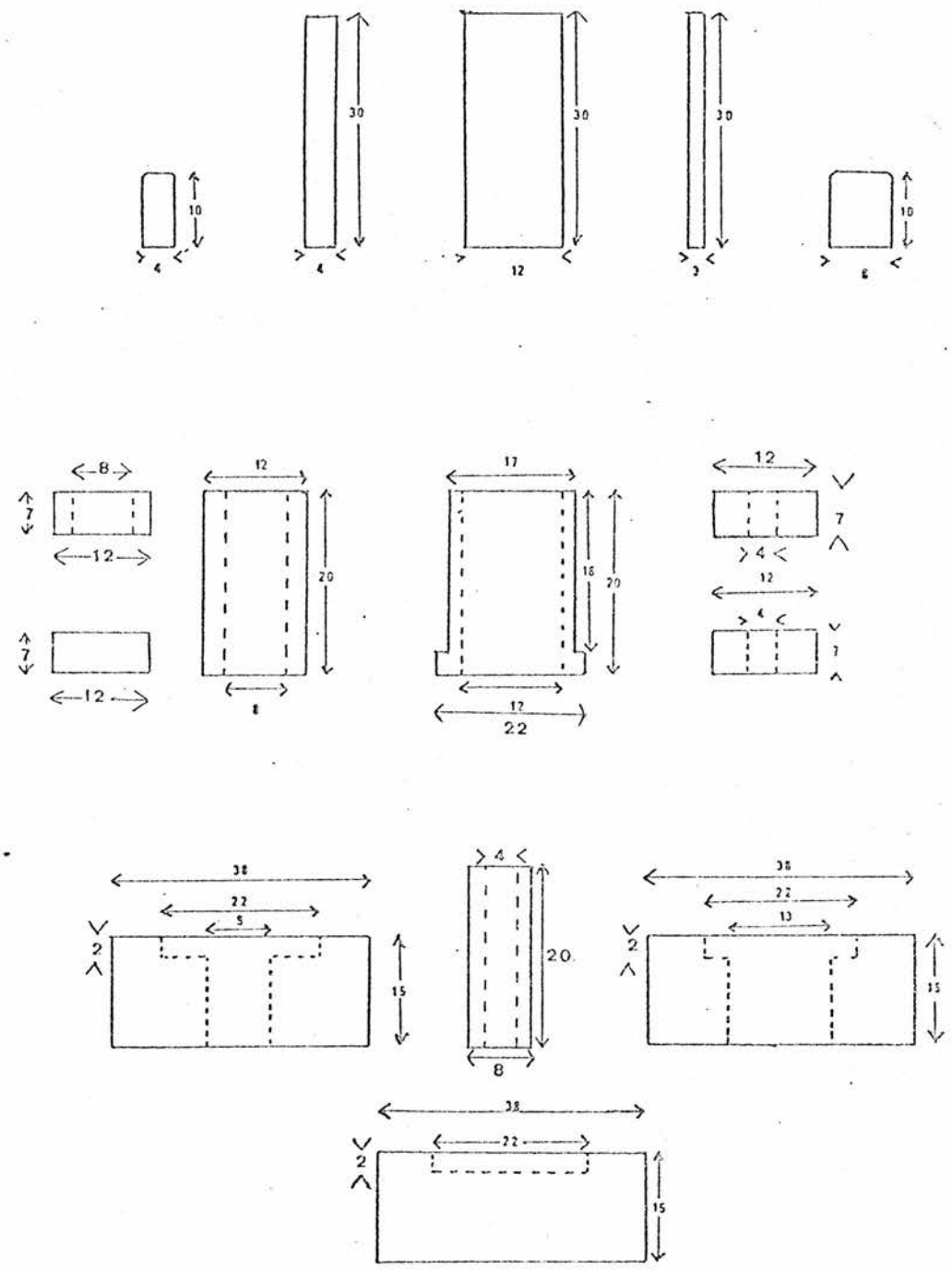

Figure 12 Detail of die dimensions (mm)

The working electrode, approximately 0.02g of an electrolyte/solid state electrode (SSE) material ground mixture, (eg. a 2:1 ratio by weight), was then pressed into the pill, as shown in figure 11 e), at finger pressure. The plunger guide, inserted in the die, was made of teflon to prevent short circuit of the cell, between working and reference electrodes during this process. Figure 11 e) does not show the presence of a teflon insulating disc, cut from thin teflon sheet, located between the cell and the lower anvil, used to prevent short circuiting of the cell at this and later stages of cell fabrication.

Figure 11 f) shows the arrangement of die pieces used to press about 0.3g of electrolyte, at 2 tonne pressure, onto the reference and working electrode section. Figure 11 g) shows the final arrangement used to apply the counter electrode, 0.3g of a silver/electrolyte mixture of the same composition as used for the reference electrode, at about 3 tonne pressure.

The completed cell was then removed from the die as shown in figure 11 h) and stored in a sample bottle, in darkness, over phosphorous pentoxide desiccant until immediately prior to installation in the cell-holder.

2.7 Three Electrode Cell Holder and Pyrex Cell Envelope.

The cell was mounted in a teflon cell holder, using gold electrode contacts, detail of which is shown in figure 10. The contacts to the external circuit were made through the pyrex tube-head by means of tungsten rods sealed into the 7mm cones. The detail of the cell holder pyrex envelope is shown in figure 13. This arrangement allowed the experimental environment of the cell to be carefully controlled. A continuous flow of dry, thermostated nitrogen was supplied to the cell envelope.

Thermostating of the cell envelope was achieved with the use of a Townson-Mercer oil bath and the inert gas flow to the cell was thermostated prior to entry by passage through a molecular sieve drier and thermostated coils submerged in the bath liquid. All the experiments on the three electrode cells were carried out at 50^{o}C.

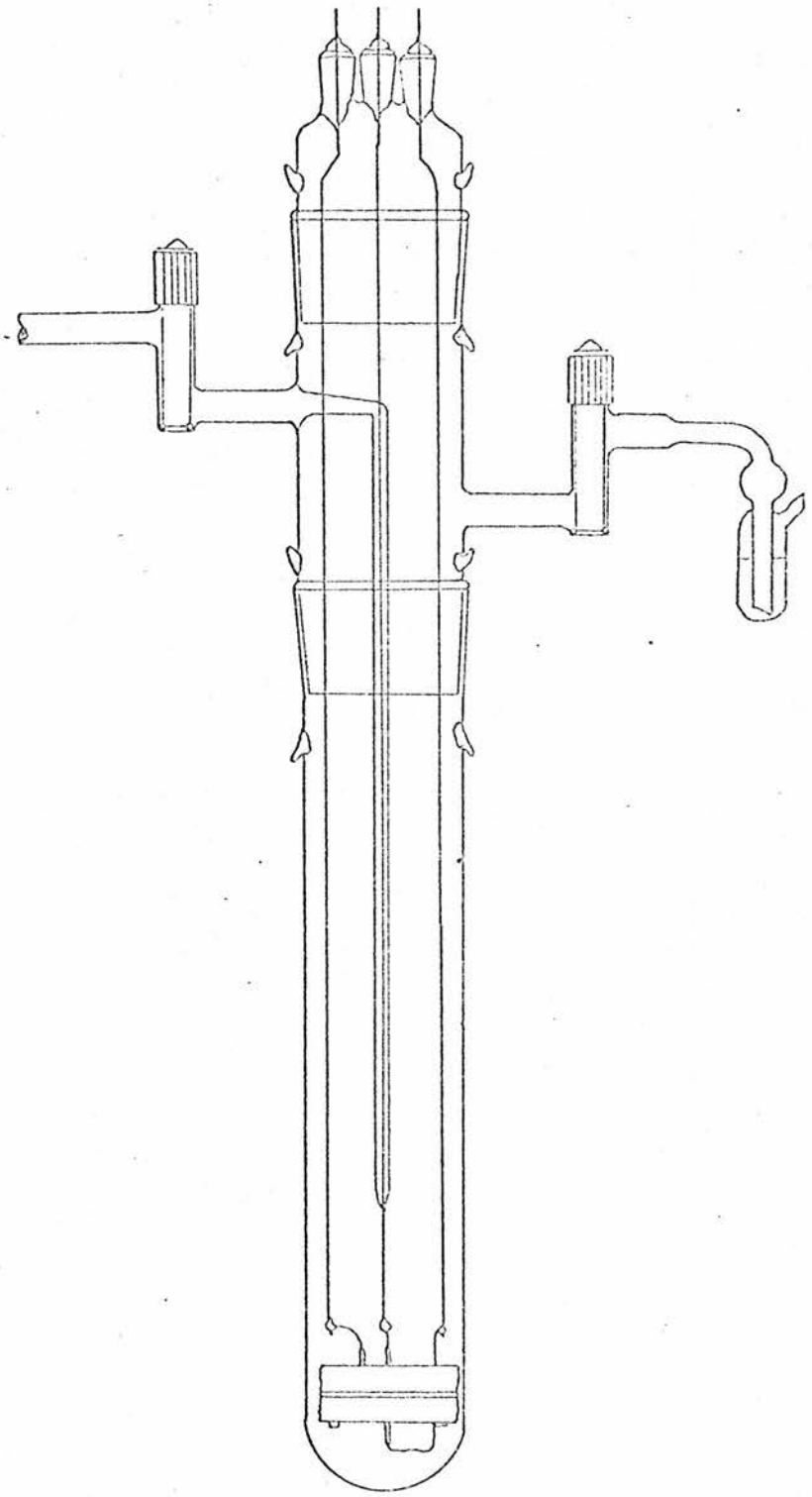

Figure 13 Cell Envelope.

2.8 Temperature Measurement.

All the cell holders used were designed to accommodate a copper/constantan thermocouple, close to the cell location, for temperature measurement. The temperature reading device was either a Comark Type 1625 electronic thermometer, with an internal standard, or a Solartron 7065 microprocessor voltmeter, with an ice-triple point cell as external standard.

In both cases the readings given by these devices were checked with the use of standard mercury thermometers and found to agree within $0.2^{o}C$ over the temperature range of interest.

2.9 Open Circuit Potential Measurement.

The three electrode cells described in section 6 were used to obtain a coulometric titration curve for cells containing (hexagonal) NbS_2 as the working electrode. (A ratio of 2:1, by weight, of electrolyte to SSE material was used in these cells) The cell holder and envelope described in section 7 were used to hold the cell. The temperature of the latter was kept constant at $50^{o}C$.

The cells were first completely deintercalated potentiostatically and allowed to equilibrate before the coulometric titration was begun. At the beginning of the titration only a very small amount of charge was passed, since at very low intercalation levels the relative change in potential can be great. But as the intercalation level increased larger amounts of charge were passed. Typical currents used were in the milliamp range and after each intercalation the potential was monitored until it was stable to within 1mV for over 24 hours, before the titration was continued.

2.10 Standardisation of Intercalation Level.

All the three electrode cells used in this work were initially intercalated to a fixed level, namely $Ag_{0.05}NbS_2$, after construction.

This was done by holding the cell at a constant voltage just above its normal open cicuit value (0.42 V) until the current that passed was negligible. The cell was then allowed to completely equilibrated (i.e. the potential was constant to within 1mV for over 24 hours) before being intercalated galvanostaticaly to the required level (using currents of 5 mA or less). All the cells treated in this way had potentials that were within 2% of each other after they had been allowed to equilibrate.

2.11 Voltage Transient Recording

2.11.1 Instrumentation

A block diagram of the experimental set up used to obtain a voltage transient is shown in figure 14.

a) Digital Voltage Recorder.

Two types of recording device were used, depending upon the pulse length of the experiment.

I Stardel Datarecorder.

This digital signal analyser (produced in St.Andrews) was used for pulse lengths of less than 100 s and provided a means by which the voltage response of the three electrode cell to a galvanostatic pulse could be recorded with respect to time. After each pulse was applied, the data obtained was transferred to a Tektronix 4052 microcomputer via the RS-232 serial port of the device, where it was averaged with previously recorded pulses.

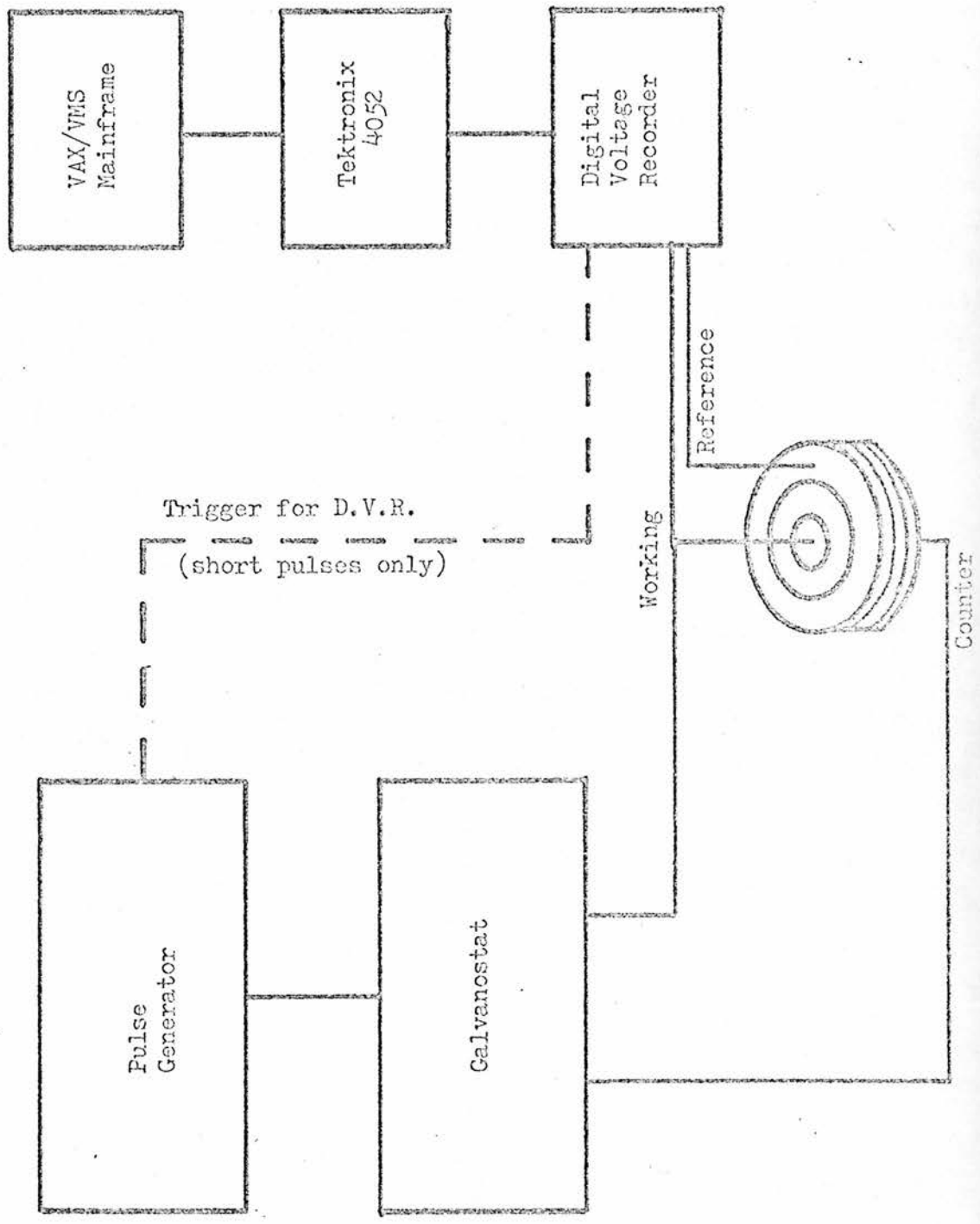

Figure 14

Block circuit diagram of apparatus used in voltage transient recording.

Periodically a calibration graph for the analogue-digital convertor of the datarecorder was obtained by applying a range of voltages to the datarecorder over the appropriate voltage scale and this graph was used to obtain absolute values of potential for each transient.

II Solartron 7065 Microprocessor Voltmeter.

For pulse lengths greater than 100 s a Solartron 7065 DVM was used to record the transient. The Solartron was programed to output a potential reading every second and this reading was transferred to a Tektronix 4052 via the IEEE-488 parallel port of the unit where it was stored on magnetic tape. The timing was carried out by the internal digital clock of the DVM and was accurate to within 2.5 ms.

b) Tektronix 4052 Microcomputer.

For the case of the data obtained from the datarecorder, this was first averaged with similar transients previously recorded and then stored on magnetic tape. A plot of the transient could be obtained on the screen of the Tektronix at any time and this was examined until a sufficiently low signal to noise ratio was obtained for the transient. A example of this type of signal averaging technique is shown in figure 15. In the case of the data received from the Solartron DVM signal averaging was not required and the data were stored directly on magnetic tape.

Once a suitable transient had been obtained, it was transferred to the VAX/VMS mainframe computer (via the RS-232 serial port) for storage and further processing by the programs described in the appendixes.

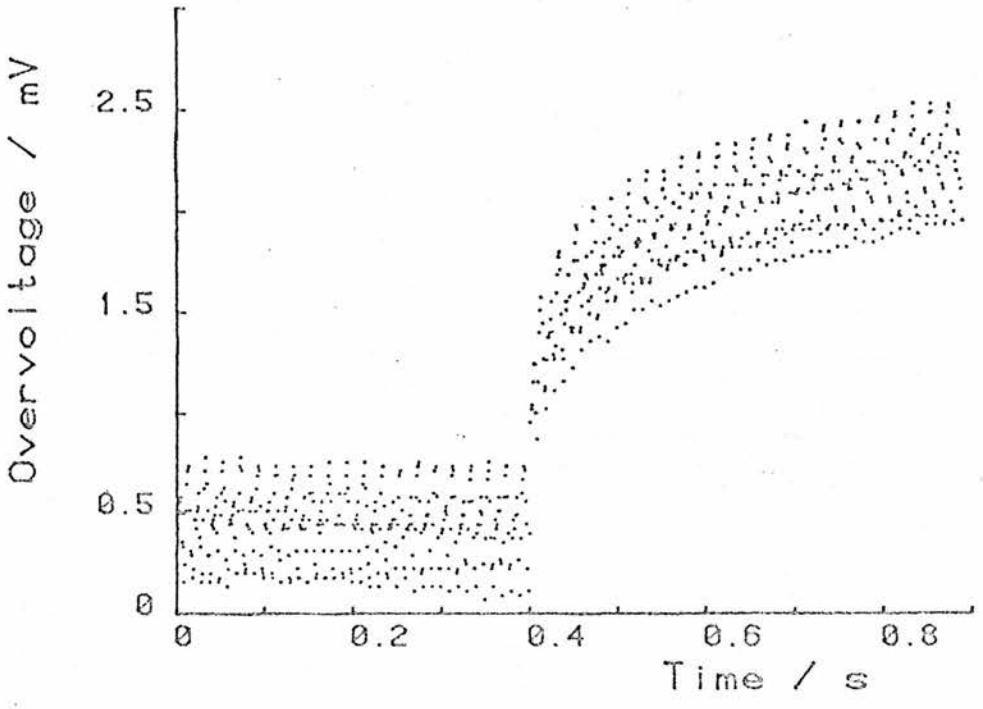

Figure 15 (a)
Example Transient, 1 run.

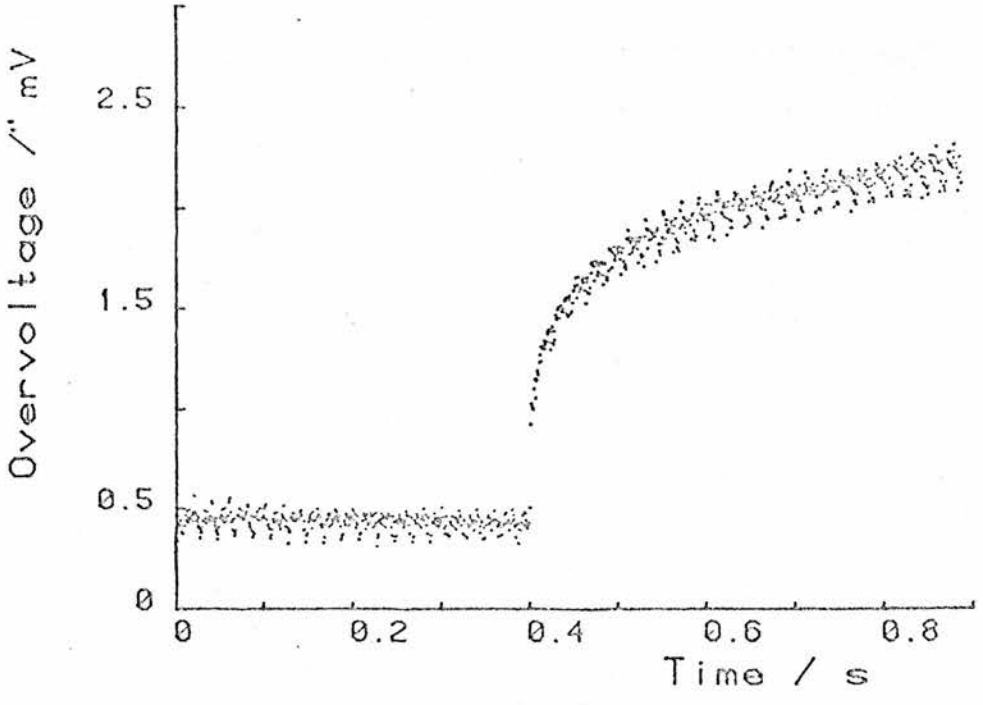

Figure 15 (b)
Example Transient, several runs.

C) Pulse Generator.

Here again two types of generating device were used depending upon the pulse length applied to the cell.

I Potentiostat.

For pulse lengths greater than 1 sec then a simple potentiostat was used which had an On/Off switch and a voltage output which could be set to any value in the range 0 to 2 volts. Timing for these lengths of pulse was done using the internal digital clock of the Solartron 7065 DVM and was accurate to within 2.5 ms.

II Short Pulse length Generating Unit.

For pulse lengths less than 1 sec then a pulse generator which could produce accurately timed short pulses was used. A block diagram of the pulse generator components is shown in figure 16.

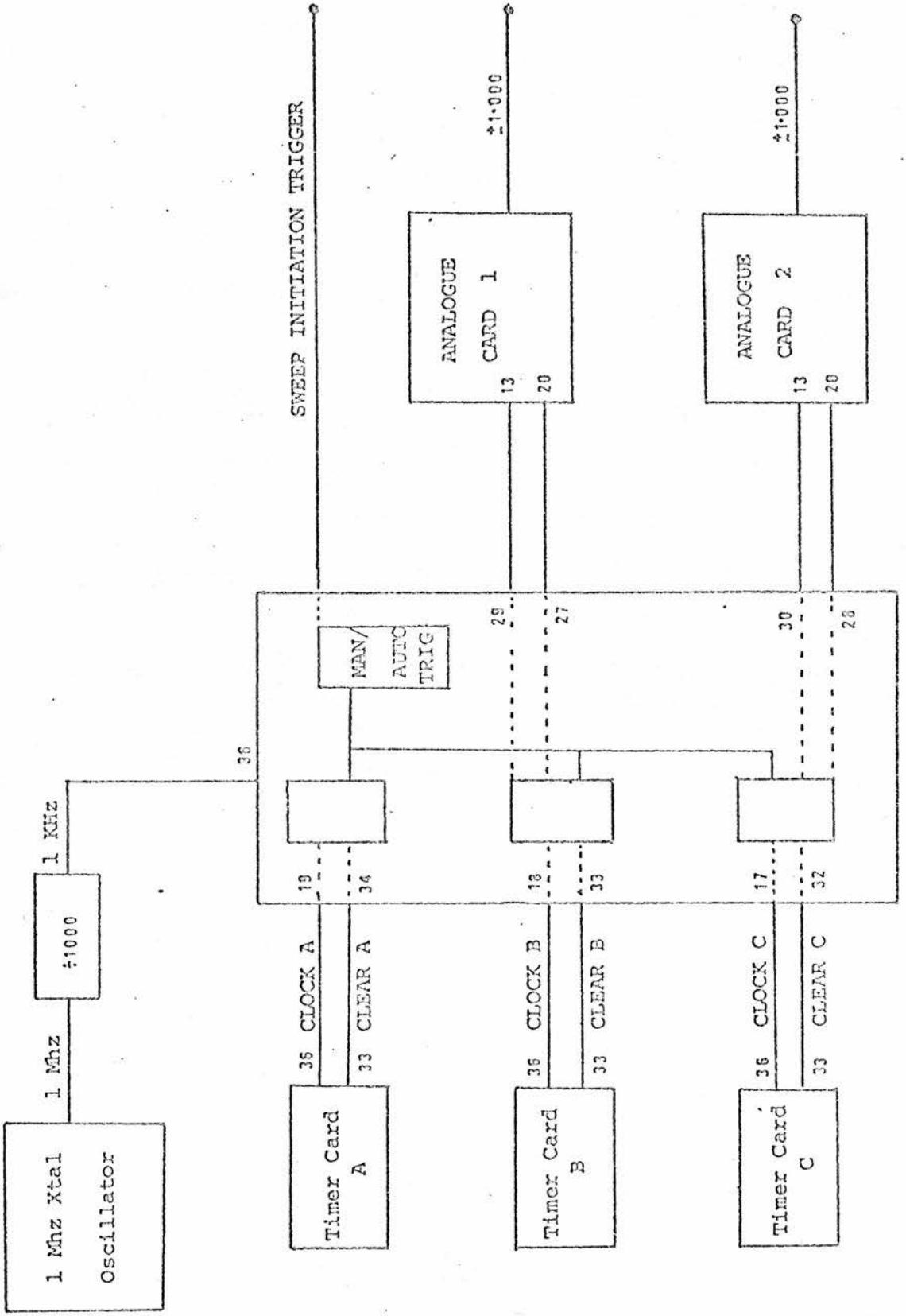

Figure 16: Block circuit component diagram of short pulse generator.

The unit uses an internal time reference signal to synchronise three timer cards, accurate to within 1 ms. Card A provides a variable time delay between the initiation signal and the beginning of the first pulse. The initiation may be either manual or automatic. Timer card B controls the length of the pulse delivered to the analogue card 1. Timer card C determines the length of the pulse delivered by analogue card 2. Analogue cards 1 and 2 allow the signal generated to be set between $\pm$ 1.000 V.

The output signal from the pulse generator analogue units can thus be varied in both duration and height and, by using a combination of the two analogue cards, a pulse of the type shown in figure 17 may be produced.

(a) Pulse from trigger output of pulse generator to external trigger input of D.S.A. starts recording sweep at zero time.

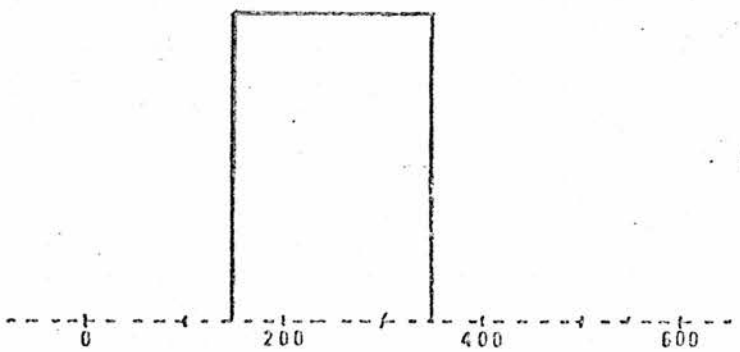

(b) Analogue unit 1 delivers pulse to galvanostat auxilliary input after delay

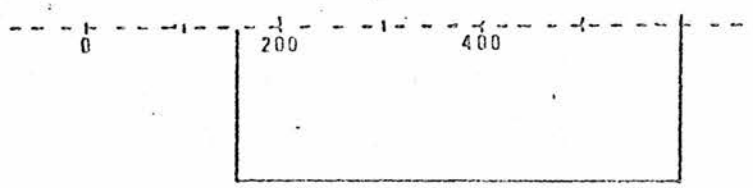

(c) Counterpulse delivered to galvanostat by analogue unit 2

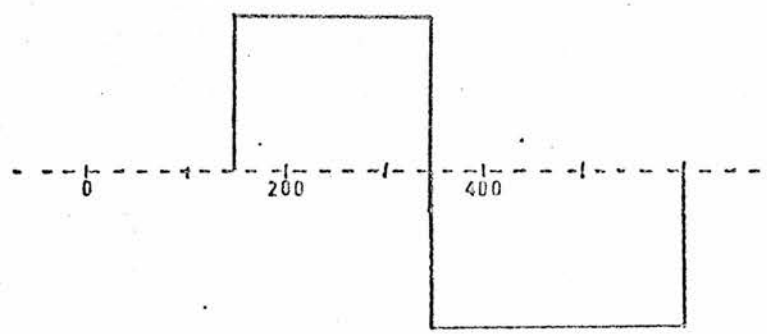

(d) Pulse profile delivered to cell.

Figure 17: Example of pulse generator output.

d) Galvanostat/Potentiostat.

The galvanostat/potentiostat used here was designed and constructed in the departmental electronic workshop and in the present context only the galvanostat operating facility will be described. Use was also made of the auxiliary inputs and a cell voltage offset facility. A circuit diagram of the device is shown in figure 18.

I Galvanostat Mode.

The reference potential circuit and LH00Z10K amplifier were used in a standard constant current generating configuration to supply currents as set by the current range selector. Currents applied to the cell in either the two or three electrode configuration were measured, either by the internal meter or by using the external current monitoring sockets shown on the amplifier at (B), figure 18.

II Auxiliary Input.

Auxiliary input from the pulse generator was applied to the summing point (A), of the LH00X10K amplifier. The standing current was set to zero and the current delivered to the cell was therefore controlled by the pulse generator or other external sources.

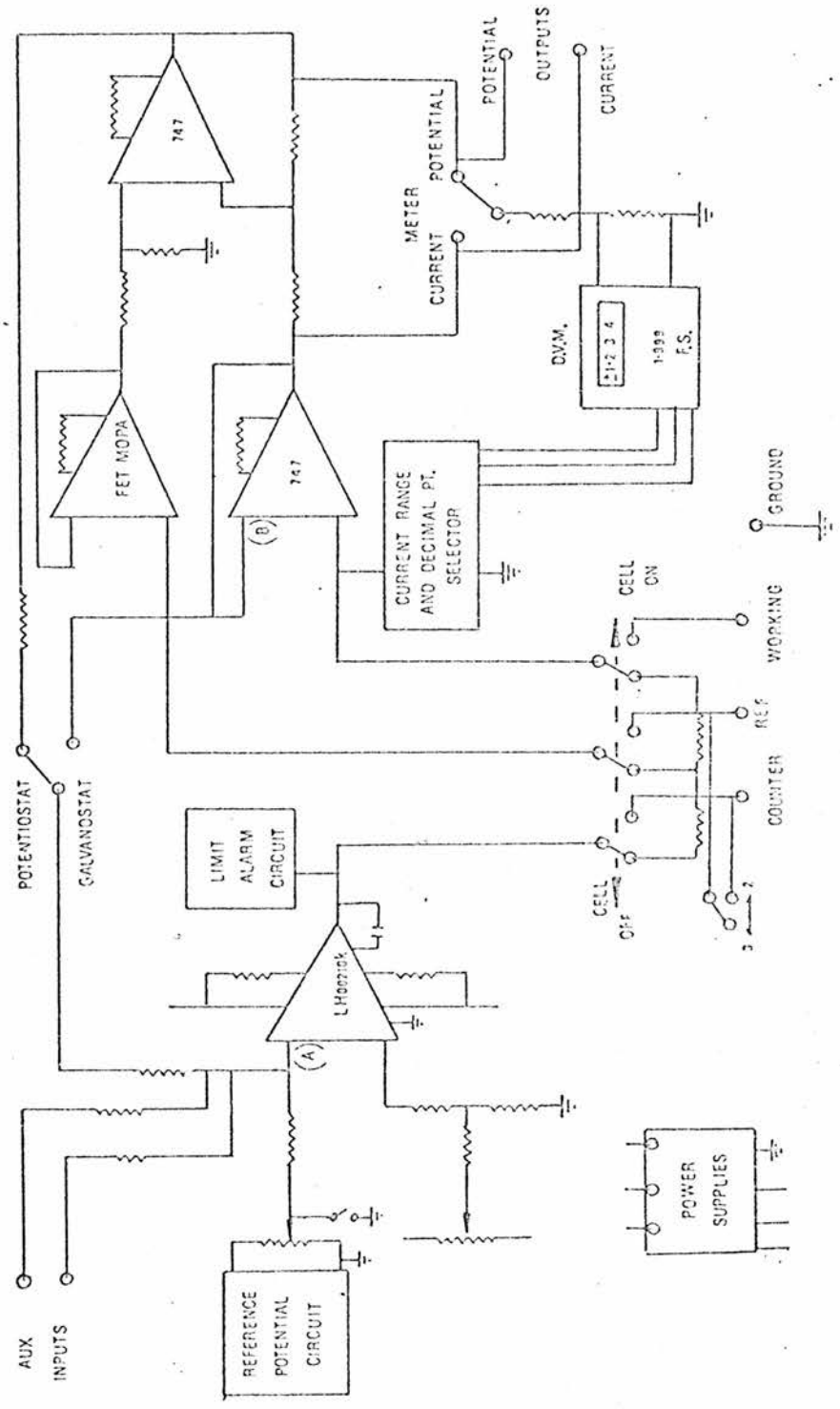

Figure 18:
Galvanostat circuit diagram.

III Cell Voltage Offset.

For applications in combination with the digital voltage recorder the cell voltage offset was used. This facility is not detailed on the circuit diagram. Its operation permitted the cell voltage to be offset with respect to the potential output to the voltage recorder, and consequently the most sensitive recording range of the voltage recorder could be used. The voltage range of the offset was $\pm$ 2.000 V using a ten turn precision potentiometer.

2.11.2 Experimental Procedure.

Prior to use several instrument checks had to be carried out on the apparatus. The zero standing current in the galvanostat was measured by attaching a dummy cell to the cell connection terminals, and monitoring current through the cell by means of a Solartron 7045 multimeter connected across the current measuring output on the rear panel of the galvanostat. This was brought close to zero by fine adjustment of the current setting potentiometer on the front panel. Further adjustments were carried out with a very sensitive current meter, (minimum measurable current 0.01 microampes), in series with the dummy cell, using the fine zero adjustment on the front panel.

The three electrode cell was then connected to the galvanostat and a DVM connected across the potential measuring output on the galvanostat rear panel. The cell was then switched on and the potential offset adjusted to produce an offset at the potential output corresponding to the cell voltage. The potential output of the galvanostat was then connected to the input of the Datarecorder or Solartron 7065, depending upon the pulse length being applied.

Cell temperature and initial cell voltage was measured using the electronic thermometer and Solartron 7045 respectively. The appropriate pulse generator was then set up and connected to the auxiliary input of the galvanostat and the cell switched on. The pulse was applied to the cell and the transient recorded by the appropriate voltage recorder. The cell was then immediately returned to open circuit.

When short pulse lengths were applied the pulse generator was set up to apply a deintercalating pulse immediately after the intercalating one (eg. figure 18), but for longer pulses (greater than 1 sec) then the polarity of the pulse generator had to be reversed in order to apply the deintercalating pulse. In both cases, the intercalation level of the cell was re-established at its original starting level.

The voltage recovery of the cell, to within a tenth of a millivolt of the original pre-pulse value was usually very rapid and once reached another repeat pulse could be applied if required.

Once the transient had been obtained it was transferred to the Tektronix 4052 microcomputer for signal averaging and transfer to the VAX/VMS mainframe, where further processing and storage could be carried out.

References.

[1] Bonino, F., Lazzari, M., McKechnie, J.S., Rivolta, B., Turner, L.D.S., Vincent, C.A., "Silver mono-, di-, and tetratungstates.", J. Inorg. Nucl. Chem., 1979, Vol. 41, p. 177.

[2] Takahashi, T., Ikeda, S., Yamamoto, O., "Solid-state ionics: A new high ionic conducting solid electrolyte $Ag_6I_4WO_4$ and use of this compound in a solid-electrolyte cell.", J. Electrochem. Soc., 1973, Vol. 120, No. 5, p. 647

[3] Chiodelli, G., Magistris, A., Schiraldi, A., "Some solid electrolyte cells.", Electrochemica Acta, 1974, Vol. 19, p. 655

[4] Smith, M.J., "Electrochemical Studies of Solid Solution Electrodes", Ph.D. Thesis, University of St.Andrews, 1982

[5] Henry, N.F.M., Lonsdale, K., "International Tables for X-Ray Crystallography", Kynoch Press, Manchester, 1969, Vol. 1, p. 304 & 266

[6] Jellinek, F., Brauer, G., Muller, H., "Molybdenum and Niobium Sulphides", Nature, No. 4710, 1960, p. 376.

[7] Henry, N.F.M., Lonsdale, K., "International Tables for X-Ray Crystallography", Kynoch Press, Manchester, 1969, Vol. 4, Table 2.2A, pages 75 & 82.

[8] Kadijk, F., Jellinek, F., "The system Niobium - Sulphur", Journal of the Less-Common Metals, 1969, Vol. 19, p. 421.

[9] Patriarca, M., Voso, M.A., Scrosati, B., Bonino, F., Lazzari, M., "Behaviour of transition metal disulphides as intercalation electrodes in solid state cells.", Solid State Ionics, 1982, Vol. 6, No. 1, p. 15.

3 A Computer Model for Mixed-Phase Electrodes.

3.1 Introduction

The interfaces where the electrolyte and electrode materials meet are a very important factor in the overall specific power of any cell, since it is at such interfaces that diffusion and charge transfer processes for the cell occur, (i.e. diffusion to and charge transfer at), as described in Chapter 1. The rates of these processes in turn determines the current density for the cell. Now, since the current density is normalised with respect to area, i.e. current density = i/nFA, (where i, total current drawn from the cell; A, total surface area at the electrode/electrolyte interface; F, Faraday's constant; n, number of electrons in the charge transfer reaction), it follows that if the contact area between the electrode and electrolyte, (i.e. A), could be increased then so also would the total current that could be drawn from the cell, since the current density for the various processes is fixed for a given contact area. In other words, the specific power of any cell can be increased by increasing the contact area at the electrode/electrolyte interface.

With conventional cells using liquid electrolytes, the problem of maximising the area in contact with the electrode is not so difficult as for cells with solid electrolytes, since in the former the electrodes can be immersed in the electrolyte and providing the

electrolyte does not have a prohibitively large surface tension, the area of contact will be equal to the actual area of the electrode surface. In many of these cases the contact area can be increased by using a porous or sintered electrode material. With solid electrolytes, however, great care must be taken to ensure that the contact between the two solids is more than simply point areas of contact as shown in figure 1.

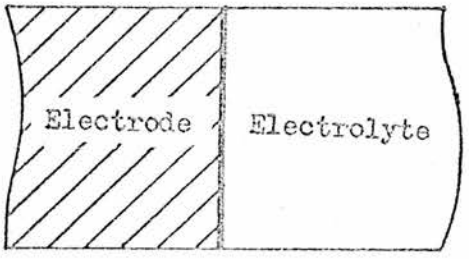

(a) Ideal Case

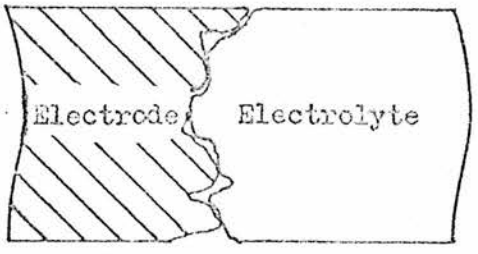

(b) Actual Case

Figure 1: Contact Area between solids

One way of ensuring a good contact area might be to polish the two surfaces to a very high standard before bringing them into contact(i.e. polish down to the atomic level if possible). This would be extremely difficult and time consuming and would result in an

area of contact limited to the geometric area of the electrode.

A different approach is to mix the electrode and electrolyte phase in a powdered form and then compress them together to form an electrode. Assuming an ideal arrangement which consists of identical particles packed together (i.e. the electrode and electrolyte materials comprise of particles of equal size and shape which can make contact with six neighbours) then a representation of this is shown in figure 2a), the particles are shown as spheres, but this need not be the case. The area of contact between any two particles will have some mean value, $\bar{a}$, dependant upon the nature of the components, and the manner in which pressure, heat, etc. have been applied during the formation of the electrode, figure 2b). As described in Chapter 1, the term 'composite' or 'mixed-phase' electrode will be used to describe an agglomeration of small grains of an electrode material bound together by another phase, usually but not necessarily a soft solid electrolyte[1,2] (figure 3).

In order to predict (and hence optimise) the effect of geometrical configurational changes on the contact area of a mixed-phase electrode, a simple computer model was developed and its application is described below.

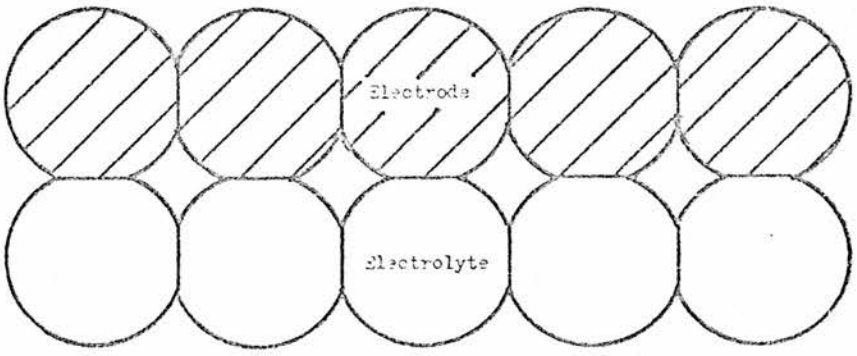

Figure 2 (a): Representation of contact area between electrolyte/electrode.

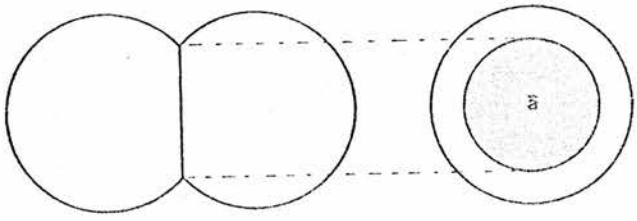

Figure 2 (b) : Mean Contact Area.

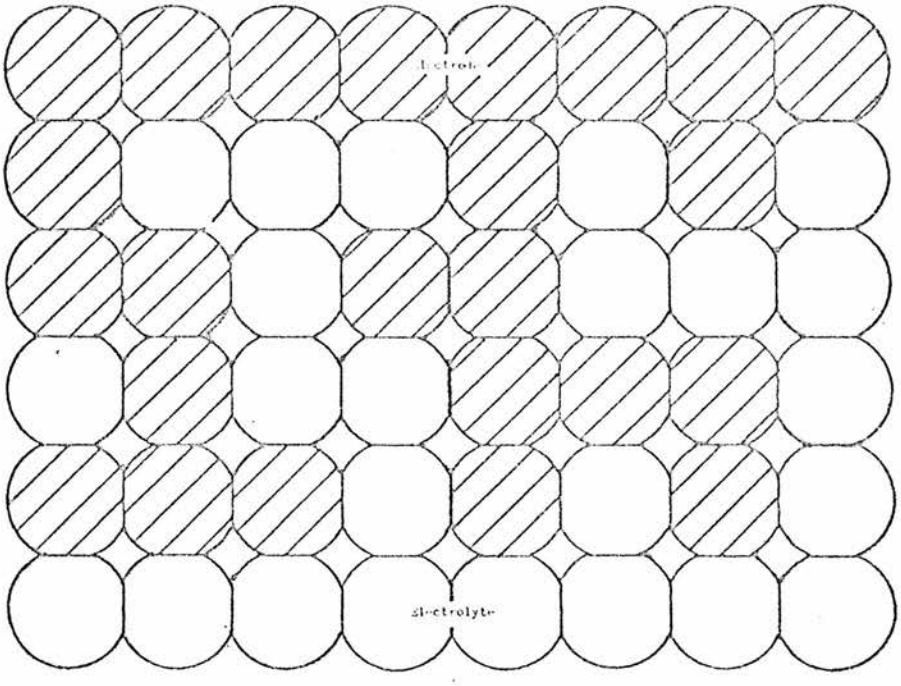

Figure 3: Representation of a Composite.

3.2 Computer Model.

As a starting point it was assumed that the composite electrode consisted of a close packed arrangement of equally sized particles, (i.e. a NaCl type of structure of two interleaved face centred cubic arrangements), and that these particles were identical in all aspects, as well as also being ideally mixed in the lattice. i.e. the positions of the particles on the lattice are totally random, and each particle has six nearest neighbours, figures 2 & 3.

Thus it was possible to model the above situation using an array (of dimensions i, j, k) whereby each position on the array corresponded to the centre of a particle. Each particle representing an electrode particle was labelled A and each electrolyte particle labelled B. An array randomly filled with A's and B's would therefore correspond to the situation of a composite region randomly filled with particles of electrolyte and electrode material. (N.B. the A's and B's represent particles of material and not atoms or molecules). Finally it was assumed that the upper layer and beyond consisted of pure electrode material (i.e. pure A) and the lower layer and beyond consisted of pure electrolyte material (i.e. pure B). This is illustrated by figure 4.

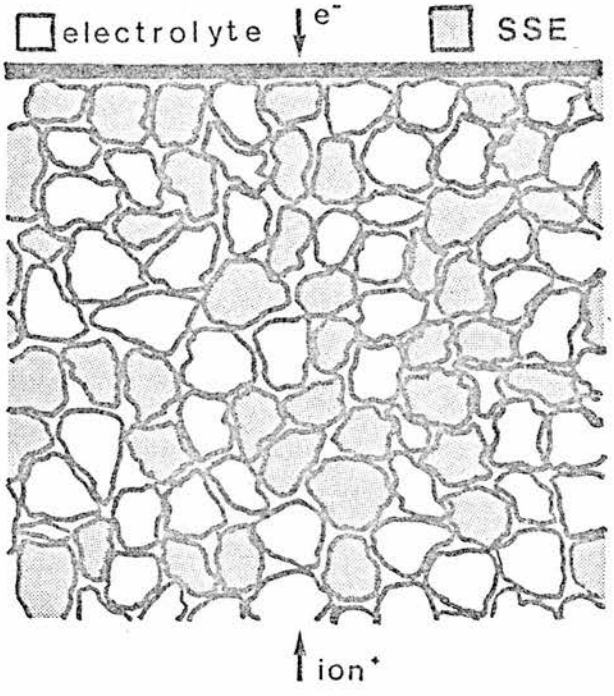

Figure 4 (a): Composite Electrode

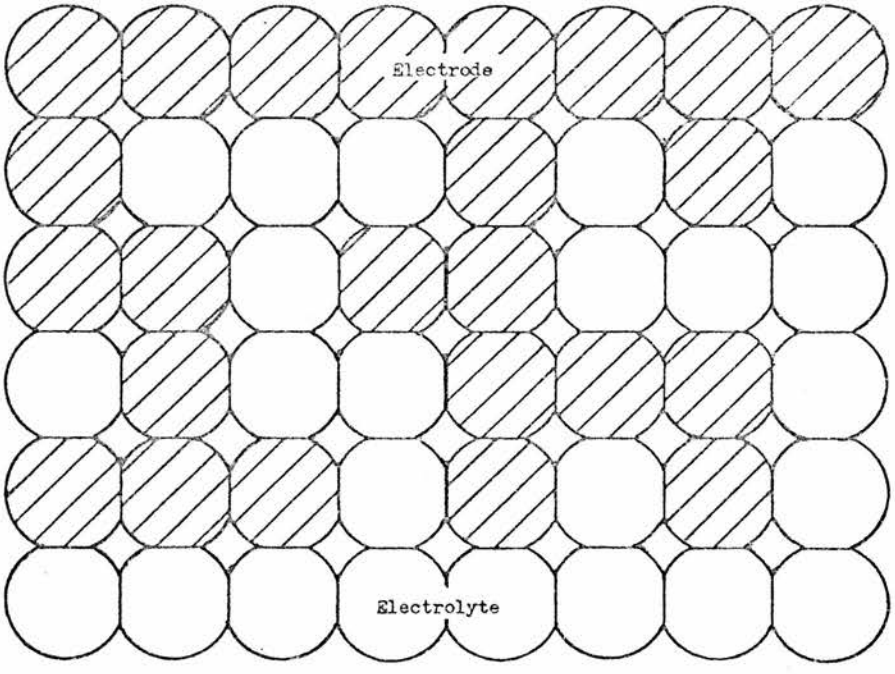

Figure 4 (b): Simulation Model of Composite Electrode

```
A A A A A A A A A A A A A A A A
A A B A B B A A A B B A A B A B
A B B A A B B B A A B A A B A A
A B B A B B A A B B B A B A B B
A A B B A B A A B A A A B B B A
B B B B B B B B B B B B B B B B
```

Figure 4 (c): Randomly distributed A and B particles.

```
A A A A A A A A A A A A A A A A
A A B A B B A A A B B A A   A
A B B A A B B B A A B A A   A A
A B B A B B     B B B A B   B B
A A B B   B     B A A A B B B
B B B B B B B B B B B B B B B B
```

Figure 4 (d): Non-isolated A's and B's

```
A A A A A A A A A A A A A A A A
    |   | |       | |
A A-B-A-B B-A A A-B B-A A   A
  |     |   | |   |
A-B B-A A-B B B-A A-B-A A   A A
        |       | |     |   | |
A-B B-A-B B     B B B-A-B   B B
  |   |           | |
A A-B B   B     B-A A A-B B B
| |               | | |
B B B B B B B B B B B B B B B B
```

Figure 4 (e): 'Links' between A's and B's.

Now in the situation described above, which is assumed to be the case of a completely non-blocking electrode, some of the particles of electrolyte will be totally surrounded by particles of electrode material (i.e. an A particle is surrounded by six B's). This means that there is no path joining this isolated particle to that of its pure bulk electrolyte; in other words, there is no path along which ionic species may travel to reach it and hence there is no possibility of substantial charge transfer reaction occurring at the interface of this particle with that of the electrode material. Therefore this particle does not contribute in any way to increasing the area of contact where charge transfer can occur, and so can effectively be ignored and simply considered as a region of empty space or void. The same argument holds true for particles of electrode type material which are completely surrounded by electrolyte, such electrode particles can also be considered as being isolated.

In this model only the A's which are directly joined through chains of A's back to the top layer of pure A need be considered and any other A's may be ignored. A similar situation applies to the B's which are not linked to the lowermost layer of pure B. This is illustrated by figure 4 d) in which all the isolated particles of A and B are ignored.

It is now possible to find a measure of the effective contact area simply by counting the number of times that a particle of A is adjacent to a particle of B, figure 4 e). The word 'link' will be used to indicate each A and B that are adjacent, and so the total number of links for a system will give an indication of the total effective contact area, via the product of the total number of links and $\bar{a}$, the mean contact area between two particles.

3.3 Two Dimensional Model

A computer program was written in Basic to investigate the above model on a two dimensional scale (i.e. each particle has only four neighbours) with equal numbers of A and B particles. Details of this program will not be given because of its limited application, but the more general program (for three dimensions) is described in appendix IV and could, if required, be modified to two dimensions. The former program was run on a Tektronix 4052 for various sizes and shapes of array, a typical array is shown in figure 5 a) and the processed array is shown in figure 5 b). The contact area between the A's and B's is given by the total number of links in the system, which in this case is 92. Any single particle can have a number of links ranging from zero to three.

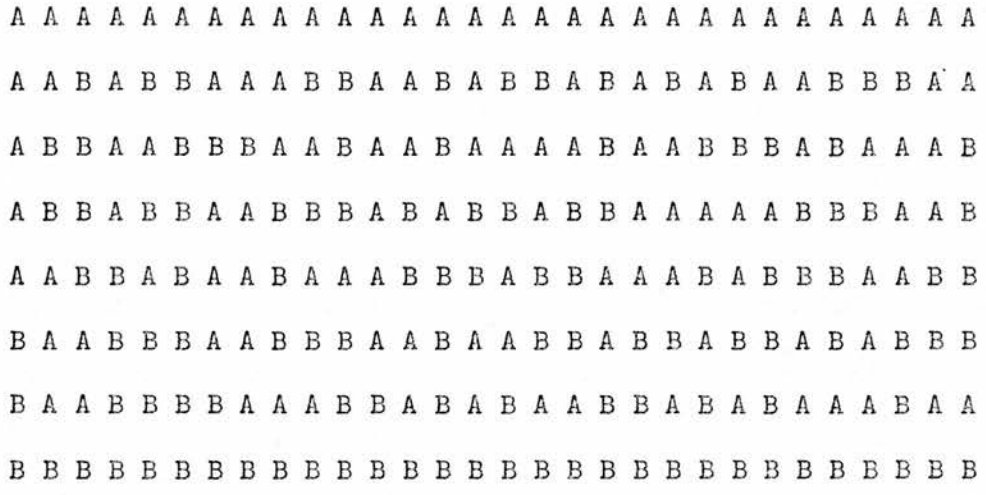

Figure 5 (a): Raw array

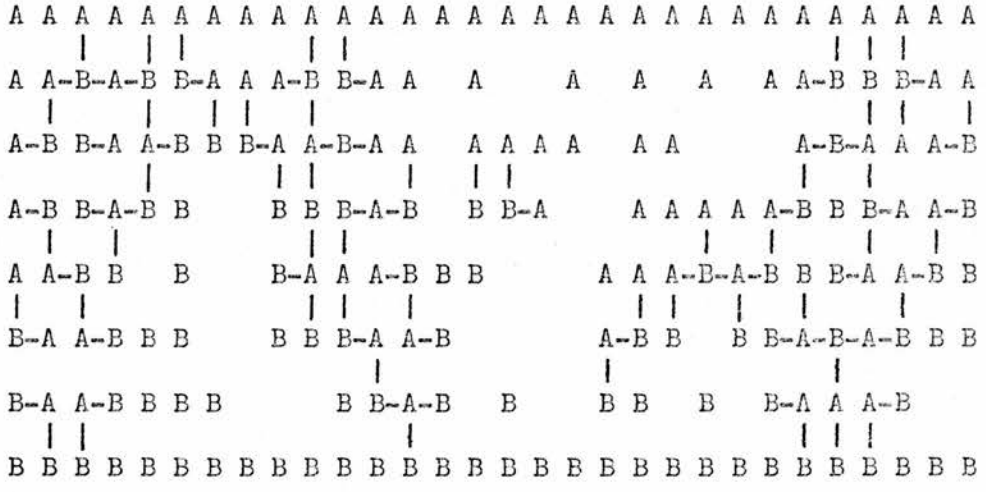

Figure 5 (b): Processed array (92 links)

A number of interesting points emerged from running this program. One which was immediately obvious was that there were indeed chains of each constituent protruding from the pure bulk. Another obvious point was that there was a very large amount of empty space in the array (i.e. areas where particles of A and B are not connected back to their pure form). These points can be seen in figure 5 b). It was found that the dimensions of the array had a very great effect on this phenomenon. For arrays which were thin the amount of empty space was minimal; for arrays which were thicker the amount of empty space was considerable; for arrays which were almost square the amount of empty space was so large that in many cases the particles of A and B were totally separated. This variation in the amount of empty space can be seen in figure 6.

Figure 6 (a): Rows = 6, Columns = 30, links = 70

Figure 6 (b): Rows = 8, Columns = 30, links = 36

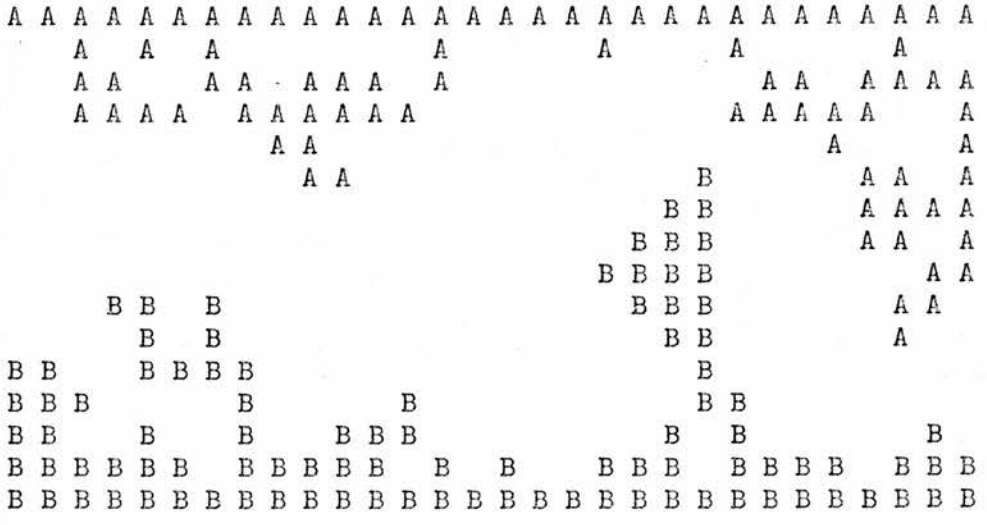

Figure 6 (c): Rows = 14, Columns = 30, links = 0

In the limiting case where there is no composite layer present, the contact area will equal the length of the rows. But as soon as a composite layer is introduced, it was anticipated that this area would increase. This was indeed found to be the case, but only for very thin arrays. As soon as the thickness of the array was increased to any great extent the area of contact fell and continued to fall to zero as the thickness increased. The total number of links is shown in figures 6 a) b) c) and it can be seen in figure 6 c) that the contact area is zero.

To summarise the two dimensional case, there are chains of material interwoven in the composite region which do increase the contact area between the two components as was described in the introduction. But the amount of isolated particles present is quite considerable, with the array dimensions playing a significant part in determining the grand total. The array dimensions also considerably influence the total number of links present.

3.4 Three Dimensional Model

The model described in the previous section was generalised to three dimensions with the same assumptions as before, i.e. identical particles with each particle having six neighbours and a totally random arrangement of particles within the composite region. The area

of contact between the two phases could be found by counting the number of links between the particles, but this time the number of links can range from 0 to 5, since each particle is surrounded by six others.

The programs to carry out the calculations were written in Salgol and run on a main-frame computer (VAX/VMS system), since the Tektronix 4052 was not capable of handling the complex computations required. A description of the relevant programs can be found in appendix IV. These programs can alter the dimensions of the array being studied as well as the relative ratio's and sizes of A and B.

3.5 Results from Three Dimensional Model

The data obtained from the computer model is stored on the accompanying magnetic tape, (tape A), and a directory and description of the files is given in appendix V.

3.5.1 Equal Ratios and Sizes of Particles.

The programs were run a large number of times with fixed dimensions for the array and a fixed number of A and B particles, but with different random distributions in the array to find how the values given for the contact area etc. deviated from each other. It

was found that the deviation from the mean was less than one percent. This implied that it was only necessary to run the program a few times for any single configuration in order to obtain reliable results.

All the configurations studied in the main investigation had square bases, i.e. the number of rows was equal to the number of columns (the rows being equivalent to the x-axis, the columns the y-axis and the layers the z-axis in cartesian coordinates), so that the arrays had a box shape with a square base and various thicknesses. To ensure that this symmetrical shape of the base was not distorting the results a number of runs were made on different shaped arrays (i.e. rectangular boxes of various dimensions). These runs confirmed that the shape of the base had no effect on the results.

To determine whether or not the overall size of the array would significantly affect the model, (i.e. whether edge effects were important), the program was run a number of times while keeping the ratio of A to B constant at one to one (i.e. 50 % of the total number of elements in the array were A's) and varying the dimensions of the base.

The area of the base was varied while the thickness of the array was kept constant. The plot of the number of links versus the number of elements in the array can be seen in figure 7 and as can be seen a straight line was obtained, implying that as the number of elements increases so does the contact area. The gradient indicates by how much each new element increases the contact area, and the intercept is

zero, as expected, since a base area of zero implies a contact area of zero.

The area of the base was next kept constant while the thickness of the array was varied. A plot of the number of links versus the number of layers in the array for various areas of base is show in figure 8.

As can be seen the plot is linear, implying that the area in contact increases uniformly as the thickness of the array increases. Thus even for extremely thick arrays the contact area increases, unlike the case of the two-dimensional model. The gradient of the line gives the number of links per layer (i.e. the number of links that each new layer contributes to the overall system). If the gradient is divided by the base area, then the resultant value will be the number of new links that each element in the new layer contributes to the total number of links and as can be seen this is approximately equal for the different sizes of base area and means that there are no edge effects influencing the results.

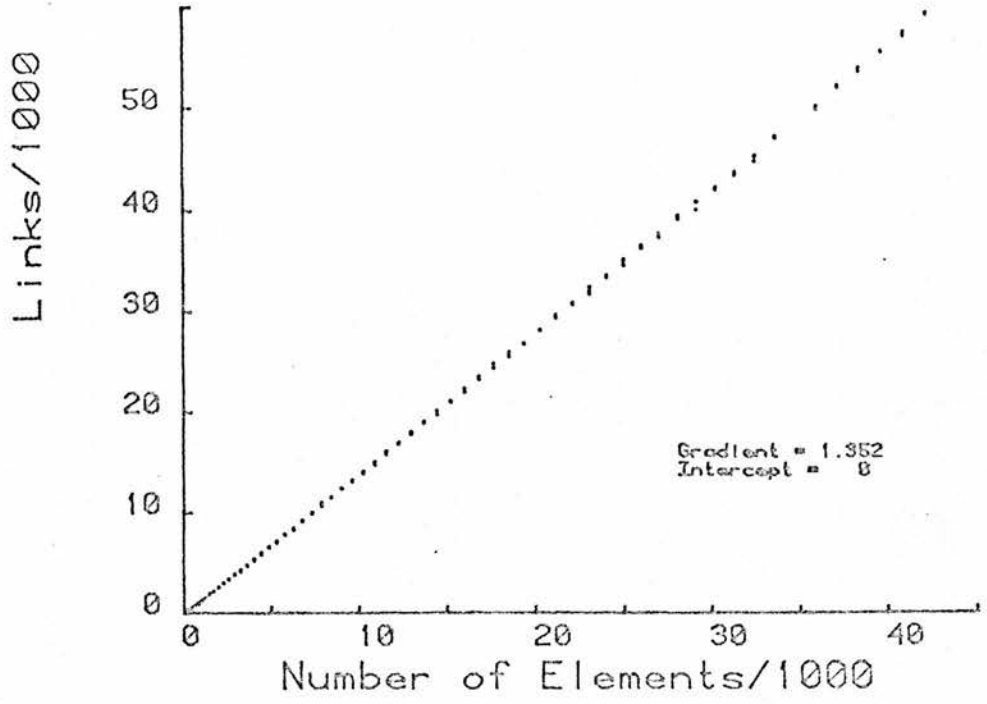

Figure 7: Number of 'links' as a function of array size. (No. layers = 10)

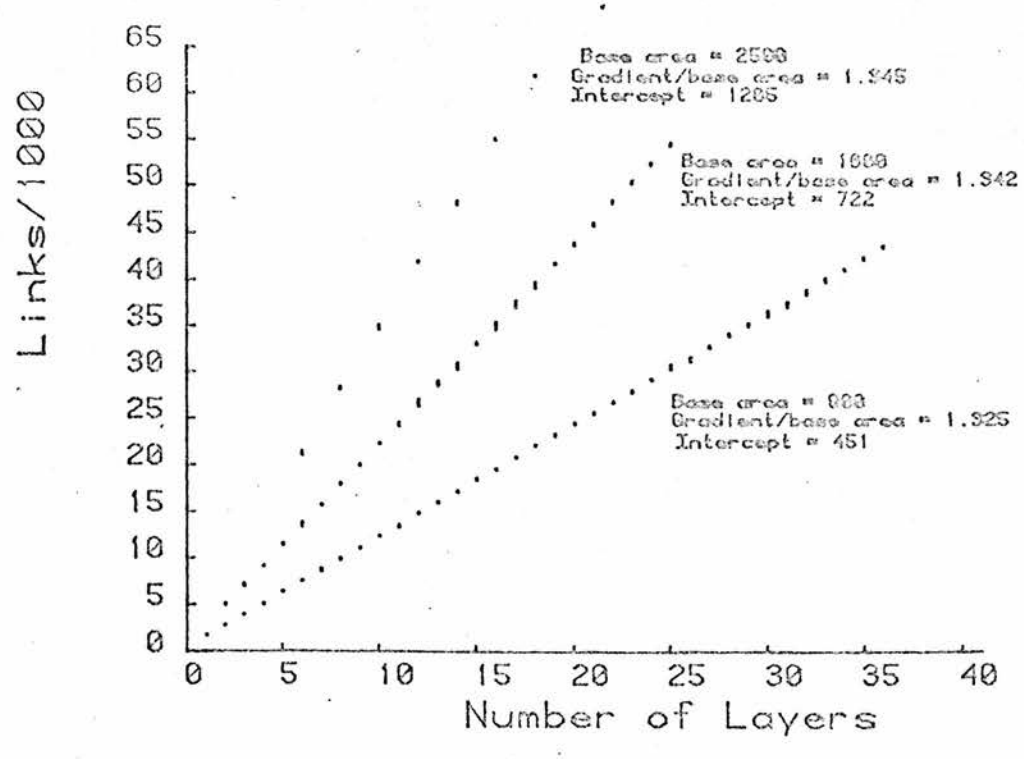

Figure 8: Number of 'links' as a function of the number of layers for various base areas.

The intercept of the plot gives the number of links that would be present if there were no layers present. Since if there were no composite region present, the contact area would equal the area of the base, it can be seen that the calculated intercept for the various arrays is low. This can be explained by the fact that for arrays of two layers or more there is a possibility of an A (or B) particle being completely surrounded by B (or A) particles, (or even by other A particles) this then means that some of the particles present are not contributing to the total number of links, and this total number therefore will be lowered. However in the case of zero or one layer there is no possibility of any A (or B) particles being completely surrounded, thus the total number of links will be higher than might be expected by extrapolating from data based on two or more layers.

The values from figures 7 and 8 were now normalised so that results obtained from different arrays could be compared. To do this the contact area due to the base was first subtracted from the total number of links in order to find the number of extra links produced by the composite layer. Then the resultant value was divided by the volume of the array (i.e. by the total number of elements present in the composite) to produce a normalised value. The 'normalised link number' for the various arrays (shown in figures 7 and 8) are plotted against the volume of the array in figure 9.

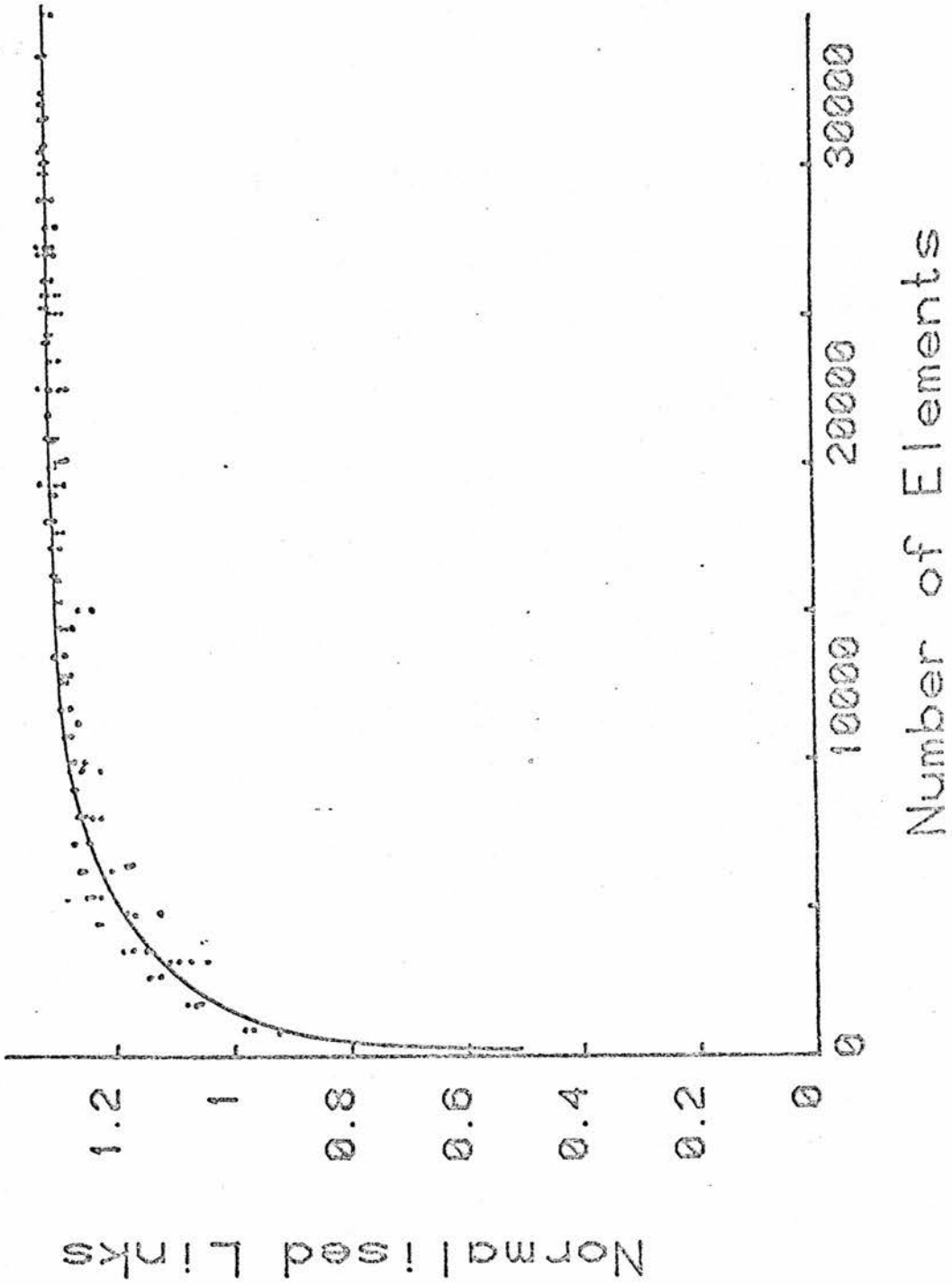

Figure 9: Normalised number of 'links' as a function of array size. Base areas 900-2500; equal numbers of particles of both components.

As can be seen the normalised link number for all the arrays tend towards a constant value of approximately 1.34. This proved that it was not necessary to use extremely large arrays to obtain consistent values for the contact area. Arrays of 10000 or more elements are seen to be adequate. The value of 1.34 obtained is the average number of links per element within the composite, for equal ratios of A and B. This is an increase over the number of links per element which occurs in the case of two pure forms in contact, (which can only have 1 link per element). Thus the efficiency of use of the particles has been increased by the use of the composite by 34% per element.

The levelling out of the graph implies that the total number of links within the array is directly proportional to the volume of that array, (after approximately 10000 elements), the constant of proportionality being 1.34. This means that the shape of the array does not affect the total contact area, (i.e. edge effects are negligible after 10000 elements), provided that the volumes of the arrays are the same. This of course does not take into account the contact area due to the base layer, if it did then the array with the larger base area would have the greater total contact area.

Without doubt the most important conclusion to be drawn from figure 9 is that there is no fall of in the effectiveness of particles, (i.e. in the normalised link number), as the thickness of the electrode region is increased and particles at the extremities become progressively separated from the base layer. This was not the

case in the two dimensional model where the number of links fell off rapidly with the thickness of the electrode region. It also means that the contact area for a composite region can be increased, without limit, simply by increasing the total amount of composite present.

Mention was made in the two dimensional model of how much 'empty space' was present in the array due to isolated particles. Figure 10 is a plot of the number of isolated particles, (expressed as a percentage of the total volume), plotted against the number of layers in the array.

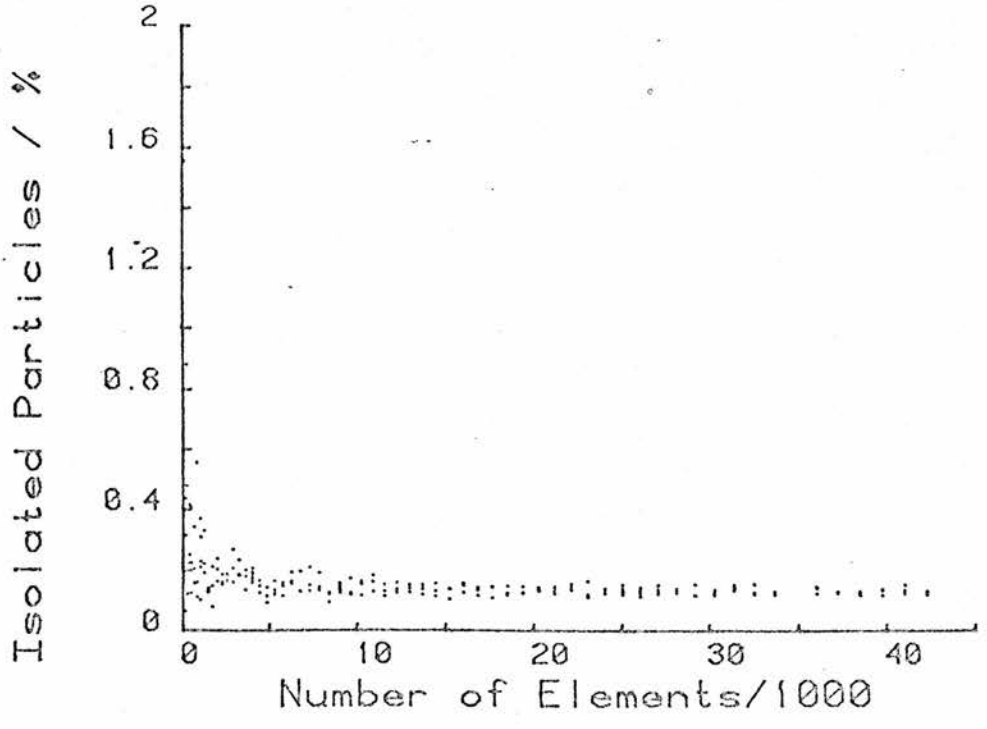

Figure 10: Percentage of isolated particles as a function of array size.

As can be seen the number of isolated elements is very low, and does not increase as the thickness of the array rises. Again this is quite different from the situation found in the two dimensional case. Since the amount of empty space is so low this must mean that the structure of the array is more like a sponge, with small pockets of isolated particles rather than the chain structure found in two dimensions, (this was borne out by inspection when some typical arrays were printed on acetate sheeting).

The reason that there is so many less isolated particles in three dimensions than in two is because in two dimensions four particles are required to completely surround another particle (i.e. there is only a 1 in 14 chance of the particles being completely surrounded) whereas in three dimensions six particles are required (i.e. a 1 in 42 chance of completely surrounding a particle). Thus there is far less likelihood of a particle being completely surrounded in three dimensions since it only requires one particle in six to connect back to the pure form for that particle not to be isolated.

3.5.2 Different Ratios.

All the results obtained in the previous sections were configurations with equal ratios of A to B. The following results refer to variable percentages of A, with respect to the total number of elements in the array. A plot of the normalised links versus percentage of A is shown in figure 11.

As can be seen the plot produces a symmetrical curve which has its maximum at 50% and minimum at 0% (and 100%). This means that the largest increase in contact area is obtained when a 1:1 ratio of A to B is used. The curve shows that the introduction of a composite region increases the contact area to a significant extent, and the effect extends over a wide range, say from approximately 38 % to 62 % Thus the particles contribute significantly to the establishment of links over nearly half the possible composition range of the mixed phase system.

The percentage of isolated A's (i.e. voids) is plotted in figure 12, as a function of composition and, as can be seen, is very low for much of the composition range. This means that there is very little wastage of particles and confirms that the efficiency of use of the constituents is very high for most of the composition range. An identical form of curve is obtained for the isolated B's, only the curve is the mirror image (around 50%) of the one shown in figure 12.

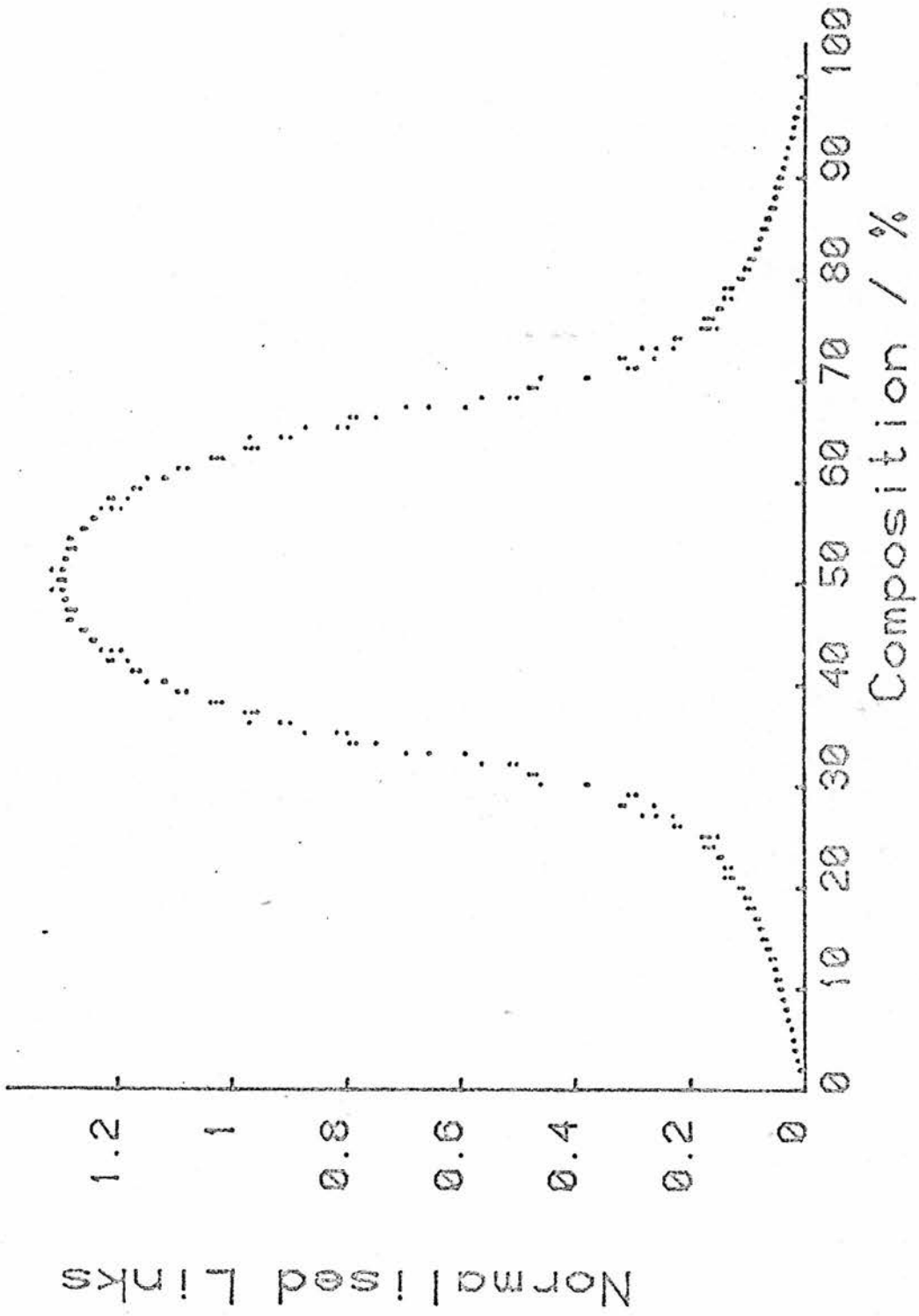

Figure 11: Normalised links as a function of composition.

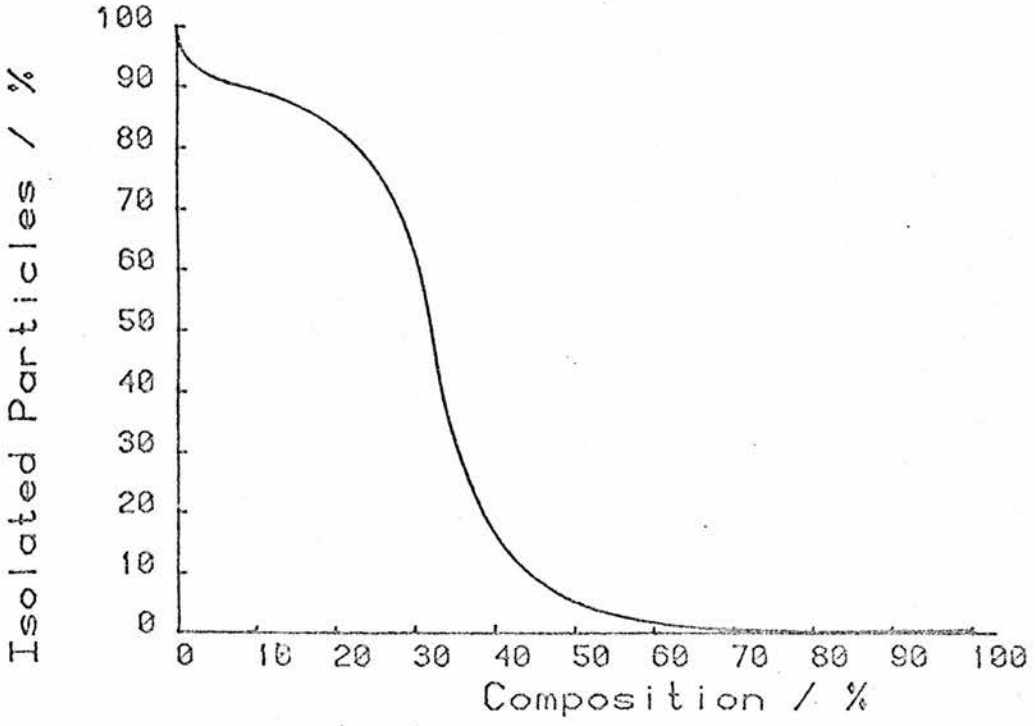

Figure 12: Percentage of isolated particles as a function of composition.

3.5.3 Different Sizes.

The effect of varying the relative sizes of the particles in the composite region was studied and the results are shown in figure 13. For each of the curves shown the size of particle A was increased twofold, while particle B was kept constant. As can be seen, as the size disparity increases, the normalised link number decreases implying that the effectiveness of the particles is decreasing. The curve also becomes skewed as the size disparity increases.

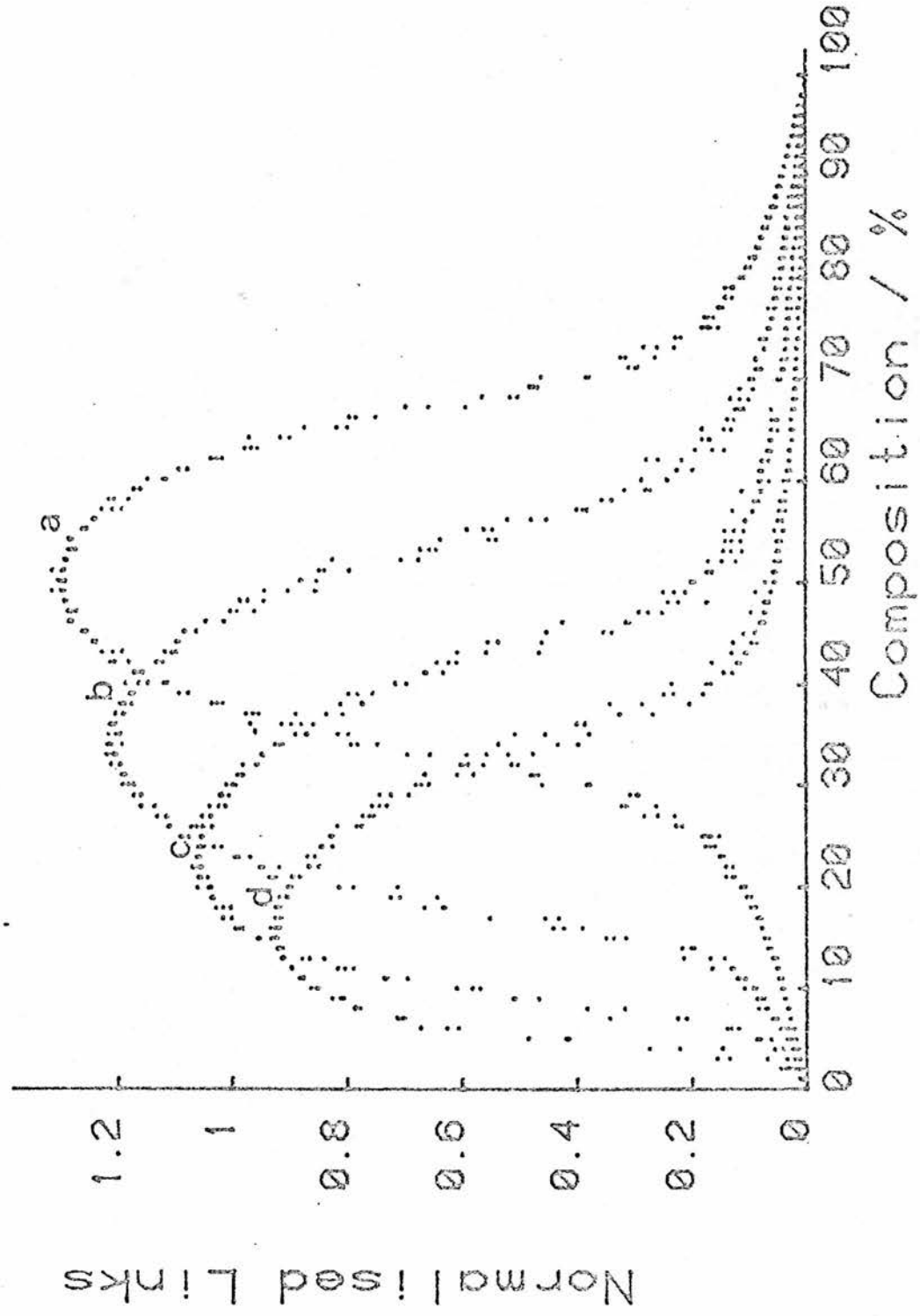

Figure 13: Effect of varying particle size ratio, (a) 1:1 (b) 1:2 (c) 1:4 (d) 1:8

3.5.4 Pseudo-Ionic Conductance.

In all the cases up to now both the particles have been considered 'ideal', i.e. they have only been allowed to conduct one type of charge species, e.g. the electrode material electrons, and the electrolyte ions. Now we consider an effect which we have called 'pseudo-ionic conductance' whereby one of the particles acts in such a way that it may be considered to conduct both types of charge.

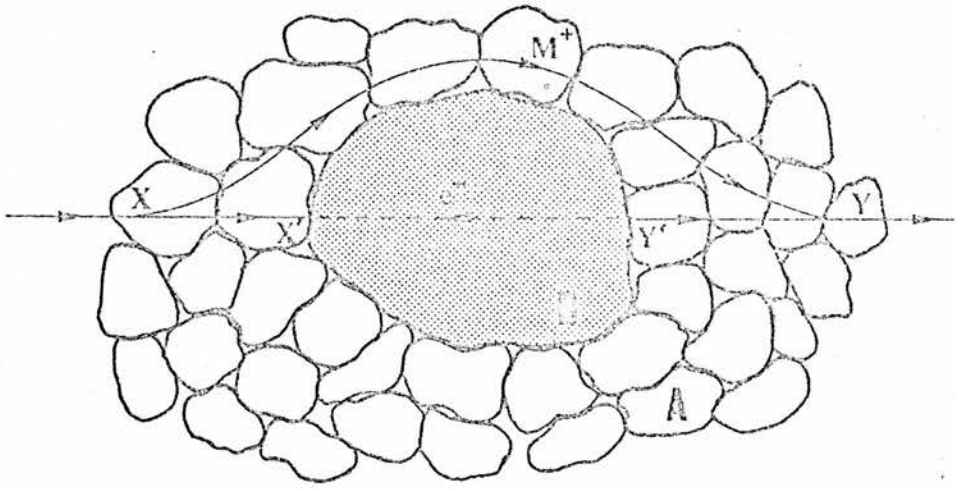

Figure 14: Mechanism for pseudo-ionic conductance where A is a silver electrolyte and B an isolated silver particle.

In figure 14, let B represent an isolated particle of electronic conductor (eg. silver), surrounded by a silver-conducting electrolyte, A, and let there be a flux of positive charge from left to right. From X, charge can be carried to Y by ionic transport around the silver particle. Alternatively, if the exchange current at the surface of the latter is high, the following sequence will also result in transport of an ion from X to Y :-

$$M^+(X) \xrightarrow[\text{transport}]{\text{ionic}} M^+(X')$$

$$M^+(X') + e \longrightarrow M(X')$$

$$e(Y') \xrightarrow[\text{transport}]{\text{electronic}} e(X')$$

$$M(Y') - e \longrightarrow M^+(Y')$$

$$M^+(Y') \xrightarrow[\text{transport}]{\text{ionic}} M^+(Y)$$

B could also be a solid state electrode phase containing the mobile component (figure 15) although it is now necessary to allow for the re-equilibration of the mobile species within the host lattice.

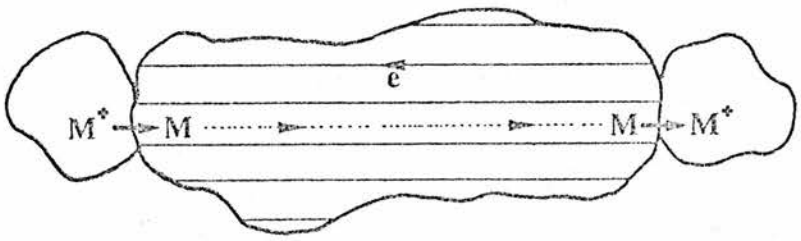

Figure 15: Mechanism for pseudo-ionic conductance for an isolated particle of an SSE phase.

If the model is modified to accommodate a mechanism of this sort then the result is shown in figure 16, and as can be seen the curve is no longer symmetrical, as was the case previously (figure 11) for the particles of equal size. The effectiveness of the particles has increased at high compositions of A, but is unaltered below 50%.

When the relative sizes of the particles are altered (still using the above mechanism) then figure 17 results, which is similar to that obtained previously (figure 13).

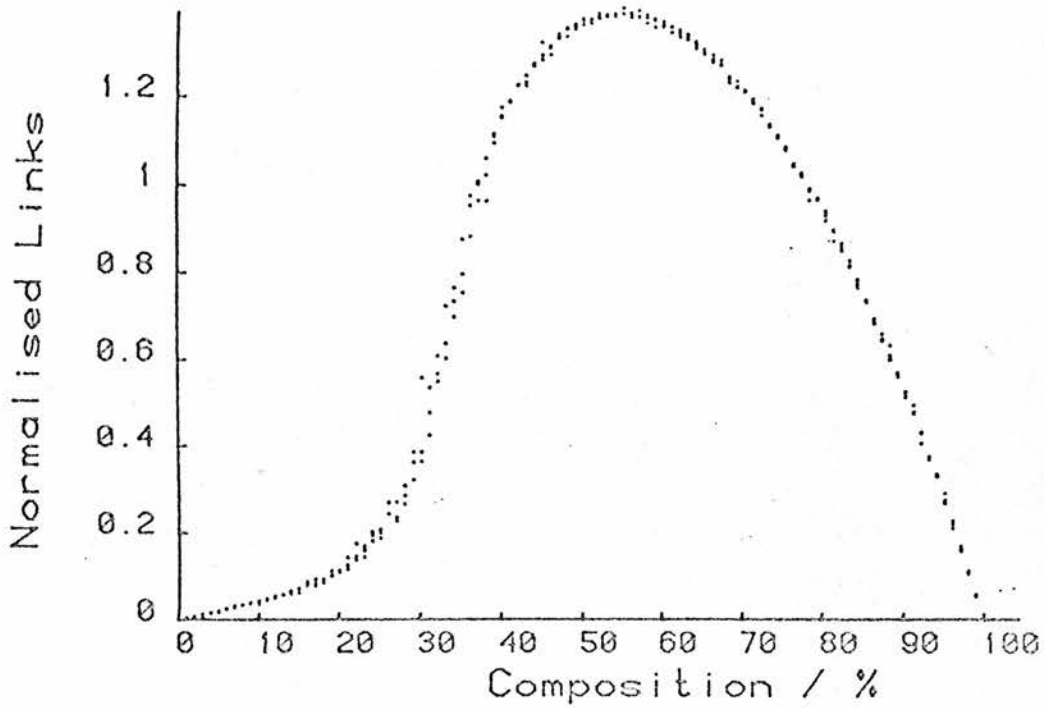

Figure 16: Normalised links as a function of composition where one component can participate in pseudo-ionic conductance.

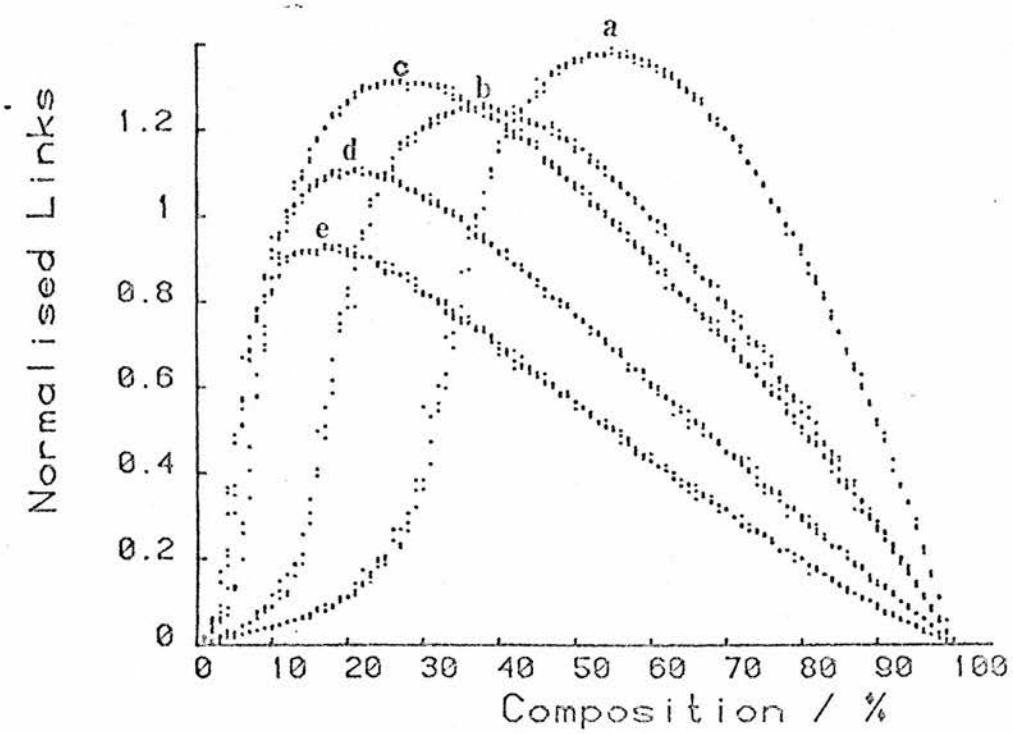

Figure 17: Normalised links as a function of composition for various particle size ratios where one component can participate in pseudo-ionic conductance. (a) 1:1 (b) 1:2 (c) 1:4 (d) 1:6 (e) 1:8.

3.6 Conclusions.

The conclusions to be drawn from this chapter are that the introduction of a composite layer does increase the contact area at the electrode/electrolyte interface to a considerable extent. For identical particles in equal ratios then the increase in the effectiveness of each particle, as far as contact area is concerned, is in the order of 34% per element, whereas for particles of different (relative) sizes, the increase in effectiveness is diminished slightly as the difference in sizes increases. This means that the contact area between the electrode and electrolyte phases can be significantly increased, without limit, by increasing the amount of composite present, i.e. by making the composite region thicker.

The optimum composition, as far as contact area is concerned, for a mixed-phase layer depends upon the relative sizes of the particles. The equal sized particles have a symmetrical curve and the optimum composition occurs at 50%. As the relative size disparity increases then the composition curve becomes skewed and the effectiveness of the particles is lowered slightly.

The numbers of isolated particles in the composite electrode is relatively small (less than 50%) for a large composition range (up to 65%) and the structure is rather like that of a sponge, where there are relatively few holes present.

For any chosen component and size ratio, then the total effective contact area can be increased without limit by expanding the thickness of the mixed-phase region. However the model does not take into account the impedance introduced by ionic (or electronic) motion within the phases, and so the thicker the layer, the greater the resistance due to the ionic motion within it. Thus in designing the best mixed-phase electrode it is therefore necessary to balance the need for a high contact area (in order to reduce the reaction impedance) with the conflicting requirement of minimum thickness and tortuosity (in order to reduce the electrolyte resistance). This balance depends on the nature of the particular materials used.

References.

[1] Oxely, J.E., Owens, B.B., "Solid state batteries.", Power Sources 3, (Proceedings of the 7' Internat. Symposium at Brighton), Editor Collins, Oriel Press, Newcastle, 1971, p. 535.

[2] Atlung, S., Zachau-Christiansen, B., West, K., Jacobsen, T., "The composite insertion electrode. Theoretical part. Equilibrium in the insertion compound and linear potential dependence.", to be submitted to J. Electrochem. Soc.

4 Electrochemical techniques for the study of rate processes in cells.

4.1 Introduction

When a galvanic cell undergoes charge or discharge, there are three general divisions that can be made to describe transmission of charge within it. These are

(a) electron flow in the electronic conductors,

(b) ion flow in the electrolyte, and

(c) charge transfer reactions at the electrode/electrolyte interfaces.

The rates at which each of these processes occurs determine the total current that the cell can deliver, and if any one of the rate processes is unable to maintain as high a rate as the others then it becomes the current limiting process. When any electrochemical cell is being charged or discharged (at a particular current) then a polarisation voltage or overpotential is observed, (i.e. the observed voltage is higher {or lower} than its equilibrium value), and has two main causes,

(I) Ohmic or 'iR drop' in the bulk of the electronic conductors and electrolyte phases, separators etc., due to the internal resistance of the bulk phases, and

(II) Electrode losses at the electronic/ionic phase boundaries which can involve many different phenomena, but can be divided into two general processes involving, charge transfer reactions, and mass transport of the electroactive species.

When an electrode process is charge transfer controlled (i.e. the current is determined by the rate of electron or ion transport at the electrode/electrolyte interface) then the rate of the process is determined directly by the potential difference across the double layer, and hence by the potential of the electrode. 'Charge transfer' is considered here to include the whole process of chemical bond formation and scission, solvation changes, etc. which must accompany the successful transfer of an electron or ion across an electrode/electrolyte interface.

In addition to the basic interfacial charge transfer reaction, many processes involve a further associated step in the vicinity of the phase boundary. For example a 'crystallisation' overvoltage can be distinguished which is caused by a hindrance in the inclusion or release of 'ad-atoms', into or from, respectively, the ordered lattice of a solid metal electrode. Another example is a 'reaction' overvoltage which is due to some slow chemical reaction, whose rate is independent of the electrode potential.

When the electrode process is mass transport controlled the current is restricted by the availability of the electroactive species at the electrode surfaces. Mass transport of the electroactive species may involve either diffusion in a concentration gradient or migration in an electric field. (In addition convection effects are important in cells with liquid phases.) If a high concentration of ions is present in the electrolyte which are not involved in the electrode process, (i.e. supporting or indifferent electrolyte) then the transport by electromigration is small. But if the electroactive species are responsible for carrying all the current in the electrolyte phase then it is not simple to distinguish mass transport polarisation and ohmic potential drop.

If mass transport is due to pure diffusion (i.e. motion of species in a concentration gradient only) then the concentration of the electroactive species can be found for simple systems by solving Fick's equations with appropriate boundary conditions and hence diffusion coefficients, etc., for various systems can be determined. Most of the work discussed in this thesis is concerned with cells which are limited by this type of transport control and so only the electrochemical measurement techniques that are available to study mass transport processes will be discussed here.

4.2 Electrochemical Measuring Techniques.

Electrochemical measuring techniques have the advantage of making thermodynamic and transport quantities available, by converting them into easily and precisely measurable electrical quantities. In other words it is possible to measure directly the absolute rate of the arrival/departure of the electroactive species at the electrode surface via the current passing through the cell, since the current is directly related to the rate of the charge transfer reaction through the condition of charge neutrality. Similarly it is possible to measure directly the exact activity of the electroactive species at the electrode surface by using the potential of the cell and applying the Nernst equation. For fast charge transfer reactions the assumption of pseudo-equilibrium of the electroactive species can be made, which means that the exact activity of the electroactive species at the electrode surface can be found. Another advantage of these techniques is that they form the basis of non-destructive methods of testing cells or electrode systems for practical applications.

A number of review articles discuss the various techniques available for studying solid state cells and the kinetic parameters that can be obtained using them.[1,2] Basically there are four methods available, viz.,

(a) Potential Step,

(b) Potential Sweep,

(c) A.c impedance, and

(d) Current Step.

A short explanation of each now follows, along with their advantages and disadvantages.

4.2.1 Potential Step.

In the potential step method it is assumed that an electrode initially has a uniform concentration of the mobile electroactive species M, of C_o, corresponding to an equilibrium voltage E_o with respect to a suitable reference electrode. At t = 0 a new activity (and therefore concentration) of M is imposed on the electrode surface by applying a voltage step between the sample and the reference electrode. The new concentration of M at the electrode/electrolyte interface (x = 0) is C_s. Chemical diffusion now occurs due to the concentration gradient imposed within the electrode. As a result, the electroactive species must be continuously supplied/removed by transport through the electrolyte phase in order to keep the surface concentration constant at the imposed value C_s, until the electrode reaches the composition C_s everywhere. The magnitude of this transient current provides a measure of the chemical diffusion flux as a function of time.

In the field of solid state cells this technique has been used in the study of oxides (e.g. wustite, urania, ceria, etc.) using zirconia electrolyte by Weppner et al[3,4] and Steele[5,6,7] and has been applied to powdered samples in liquid electrolytes by van Buren.[8]

An advantage of using the potential step method is that side reactions such as the nucleation of new phases can be avoided if the voltages are controlled within the stability range of the single phase. It also has the advantage that the rate of the charge transfer reaction is time-independent, since the potential across the double layer is constant. A disadvantage of the method is that an infinitely large current should pass through the cell initially in order to fulfil the imposed boundary conditions precisely, and means that the recording device may be overdriven, and some time may be required for the amplifier to recover, so that accurate readings can be displayed. Also, because the iR drop is time-dependent, it is very difficult to compensate for it. Another disadvantage is that there is typically a small initial current transient related to the accumulation of charge at the electrode/electrolyte interface which also cannot be readily allowed for.

4.2.2 Potential Sweep.

Linear potential sweep chronoamperametry is similar to the potential step method except that the potential applied to the galvanic cell is varied linearly with time, (i.e. the applied signal is a voltage ramp). This method is a popular technique for initial electrochemical studies of new systems and is very useful in obtaining information about fairly complicated electrode reactions, as well as obtaining various kinetic parameters. It has found its greatest application in the field of organic electrochemistry. The method is especially useful for studying multi-component systems.

It has the same advantage as the potential step method, in that the potential range that is swept can be controlled within the stability range of the SSE phase. But it also has the added advantage that,although there is an accumulation of charge associated with the double layer, (as in the potential step method), as long as the change in potential applied to the cell is known, then the change in current associated with the double layer can be compensated for, since the capacity of the double layer will be constant. The disadvantage for the potential sweep method is the same as that for the potential step method, namely that the iR drop is time-dependant and difficult to compensate for.

Armand et al[9] has used the method to determine the diffusion coefficient for lithium in RuO_2 using polymeric electrolytes, as well as determining the relationship between the particle dimensions and the sweep rate for the limiting cases of thin film diffusion and semi-infinite diffusion for a reversible process.

4.2.3 A.C. Impedance.

In a.c. impedance measurements the real (or Faradic) and complex (or capacitative) impedance of the system is measured as a function of frequency. The frequency range of the measurements can be very large, (from mHz to MHz), but for impedance measurements involving diffusion processes then the lower frequencies are of more interest, (i.e. less than 10 Hz).

From the complex plane plot of real against imaginary impedance it is possible to obtain, (via the Randles equivalent circuit and Warburg impedance), a quantity known as the diffusion impedance. At high frequencies the diffusion impedance is negligible, and the complex plane plot observed is one of an interactive RC circuit, giving rise to the familiar semi-circle. As the frequency decreases however, the diffusion impedance becomes significant and the complex plane plot becomes a straight line of slope 45^{o}.

The disadvantages of the a.c. method are that the theory derived to explain the diffusion process is very complicated, also reliable experimental results are difficult to obtain at the lower frequencies, where the measurements are carried out at. Another disadvantage is that by using a continuous a.c. waveform to perturb the system, there is no relaxation period between cycles in which to allow the mobile species to completely re-establish their pre-perturbation equilibrium. This will mean therefore that consistent results will not be obtained from the system, until a pseudo-steady state is reached by the mobile species. This means therefore that the exact initial and boundary conditions that apply to the system are complex.

Armstrong et al[10,11] have used this method to determine the diffusion coefficient for Cd in alkaline solution. Dawson and John[12] have extended the analysis theoretically to determine equations relating the diffusion factors for two separate electroactive species diffusing in one system, (the diffusion factor is a function of the diffusion coefficient and the thickness of the diffusion layer).

4.2.4 Current Step.

In the galvanostatic pulse technique a constant current is applied through a galvanic cell, between the working and counter electrodes. This causes the passage of a constant flux of electroactive species across the electrode/electrolyte interface. Chemical diffusion will then occur due to the time-independent concentration gradient imposed on the system, and this diffusion of electroactive species can be monitored by recording the potential difference between the working and reference electrodes during the current pulse.

This technique has the advantage that the iR drop of the cell is time-independent, (unlike the potential step model): it is merely added to the cell overpotential as a constant and does not affect the shape of the voltage transient. Also the instrumentation for galvanostatic experiments is simpler than the potentiostats required in the constant voltage experiments, and there is also no danger of the devices being overdriven with large currents at any point of the measurement, (unlike some of the potentiostatic methods). Another advantage of the galvanostatic pulse technique is that the total charge passed by the cell is easily determined, so that the change in concentration of the SSE material can be calculated precisely and, as in the present case, restored to its original value by passing an identical pulse of opposite polarity, (assuming the electrochemical reaction to be reversible). A disadvantage of the galvanostatic technique however is that there is no control over the intercalation

levels imposed on the SSE and close attention must be paid to ensure that the stability range of the SSE material is not exceeded, (e.g. phase changes could occur outwith certain intercalation levels). Another disadvantage is that the potential across the double layer is continuously changing and this means that the rate of the charge transfer reaction will not be time-independent, and hence will be difficult to correct for.

Another galvanostatic pulse techniques is known as the short pulse mode. In this method a short galvanostatic current pulse is applied to the cell, which alters the concentration of the mobile species in a narrow region at the electrode/electrolyte interface, and the time-dependent relaxation of the voltage is then observed. In order to meet the boundary conditions for this solution in the diffusion equation, the duration of the pulse must be short when compared to r^2/D, (where r is the physical dimension of the particles). This diffusion problem then is similar to that used in many radiotracer diffusion experiments and has the advantage that any external rate-limiting processes, (such as the transport of ions across high resistance electrolytes or the electrode/electrolyte interface), are eliminated. However one disadvantage with the technique is that large local surface concentrations may be applied and this may produce large variations in the diffusion coefficient.

A related galvanostatic technique is known as the Galvanostatic Intermittent Titration Technique (GITT) used by Weppner and Huggins and others[13-18] which combines transient and equilibrium measurements. With GITT, galvanostatic currents are applied to the

cell for a short time interval, in order to study the voltage transient as a function of time and determine the chemical diffusion coefficient (from the transient). This also produces a very small, but measurable, change in the stoichiometry of the SSE by coulometric titration. After each titrating pulse a new equilibrium cell voltage is established and the whole process can be repeated, thus enabling kinetic parameters such as the chemical diffusion coefficient to be studied as a function of stoichiometry.

Deroo et al[19] has used a galvanostatic cycling method, using a current square wave to study the coulombic efficiency and diffusion coefficient for the reversible intercalation of lithium in MoO_2 after several charge/discharge cycles. The technique is similar to the a.c. impedance method, in that the system is perturbated by a cyclic waveform, but unlike the a.c. technique, Deroo has allowed the system a rest period after each charge/discharge cycle. They have shown that the coulombic efficiency for the MoO_2 cell levels of very rapidly with increasing charge/discharge cycles, and after four cycles the efficiency is effectively constant. This indicates that a change in the electrode morphology and structure is taking place in the first few cycles, but rapidly stabilizes to form an electrode system which can sustain a large number of charge/discharge cycles.

References.

[1] Weppner, W., Huggins, R.A., "Electrochemical methods for determining kinetic properties of solids.", Annual Review of Materials Science, Vol. 8, 1978, p. 269.

[2] Steele, B.C.H., "Electrical conductivity in ionic solids", in 'MTP Internat. Review of Science, Inorganic Chemistry, Series One', Ed. L.E.J. Roberts, Vol. 10, 1972, Univ. Park Press, London, Butterworths, Baltimore, p. 117.

[3] Chu, W.F., Rickert, H., Weppner, W., "Electrochemical Investigations of chemical diffusion in wustite and silver-sulphide", in 'Fast Ion Transport in solids', Ed. W. van Gool, 1973, North-Holland Press, Amsterdam/London, p. 181.

[4] Rickert, H., Weppner, W., "Electrochemical investigation of chemical diffusion in wustite using a solid oxide electrolyte", Z. Naturforsch, Vol. 29, Part A, No. 12, 1974, p. 1849.

[5] Steele, B.C.H., Riccardi, C.C.,"Measurements of chemical diffusion coefficients in nonstoichiometric oxides using solid state electrochemical techniques", in 'Metallurgical Chemistry', Ed. O. Kubascheuski, 1972, Her Majesty's Stationary Office, London, p. 123

[6] Steele, B.C.H., "Measurements of chemical diffusion coefficients in nonstoichiometric oxides, using solid state electrochemical techniques", in 'Mass Transport Phenomena in Ceramics', Eds. Cooper, Heuer, Vol. 9, 1975, Plenum Press, New York/London, p. 269.

[7] Steele, B.C.H., "Measurements of chemical diffusion coefficients in nonstoichiometric oxides using solid state electrochemical techniques", Materials Science Res., Vol. 9, 1975, p. 269.

[8] van Buren, F.R., Broers, G.H.J., Boumen, A.J., Boesveld, C., "An electrochemical method for the determination of oxygen ion diffusion coefficients in lanthanum strontium cobaltate ($La_{1-x}Sr_xCoO_{3-y}$) compounds. Theoretical aspects", J. Electroanal. Chem. and Interfacial Electrochem., Vol. 87, No. 3, 1978, p. 389.

[9] Armand, M., Dalard, F., Deroo, D., Mouliom, C., "Modelling the voltametric study of intercalation in a host structure: application to lithium intercalation in RuO_2",

[10] Armstrong, R.D., Bell, M.F., Metcalfe, A.A., "The a.c. impedance of complex electrochemical reactions", in 'Electrochemistry -(Chemical Society. Specialist Periodic Reports)', Vol. 6, 1978, p. 98.

[11] Armstrong. R.D., Edmondson, K., "The impedance of cadmium in alkaline solution", Electroanal. Chem. and Interfacial Electrochem., Vol. 53, 1974, p. 371.

[12] Dawson, J.L., John, D.G., "Diffusion impedance - an extended general analysis", J. Electroanal. Chem., Vol. 110, 1980, p. 37.

[13] Weppner, W., Huggins, R.A., "Determination of the kinetic parameters of mixed-conducting electrodes and application to the system Li_3Sb.", J. Electrochem. Soc., Vol. 124, No. 10, 1977, p. 1569.

[14] Weppner, W., Huggins, R.A., "Electrochemical investigation of the chemical diffusion, partial ionic conductivities, and other kinetic parameters in Li_3Sb and Li_3Bi.", J. of Solid State Chem., Vol. 22, 1977, p. 297.

[15] Weppner, W., "Kinetic studies of mixed-conducting solids.", Solid State Ionics, Vol. 3/4, 1981, p. 1.

[16] Bottelberghs, P.S., Broers, G.H.J., "Diffusion and electromigration in solid Na_2WO_4.", Electrochemica Acta., Vol. 21, 1976, p. 719.

[17] Winn, D.A., Shemilt, J.H., Steele, B.C.H., "Titanium disulphide: A solid solution electrode for sodium and lithium.", Mat. Res. Bull., Vol. 11, 1976, p. 559.

[18] Scholtens, B.B., "Diffusion of silver in vanadium bronzes", Mat. Res. Bull., Vol. 11, 1976, p. 1553.
to be submitted to J. Electrochem. Soc.

[19] Dalard, F., Deroo, D., Mauger, R., "Electrochemical method for studying the reversibility of the lithium intercalation in secondary batteries", J. of Power Sources, Vol. 9, 1983, p. 321.

5 Response of Mixed-Phase Electrodes to Perturbation by Galvanostatic Pulses.

5.1 Introduction

The parameters which determine the discharge behaviour of a mixed phase electrode, under specified current load, can be related to the effective ionic and electronic conductivities of the two phases, the thickness of the electrode, the volume fraction of the components, the geometry and dimensions of the particles, the diffusion coefficient of the electroactive species, and the slope of the emf/composition curve for the insertion material. In principle if these parameters are known, then the discharge behaviour of the mixed phase region can be predicted. In general, the electrode behaviour can be classified in one of two limiting situations, (a) the discharge curve is dominated by diffusion of the electroactive species through the electrolyte within the mixed phase region, (e.g. when the thickness of the mixed phase region is relatively large or when the ionic conductivity of the electrolyte is poor), and (b) where the discharge curve is dominated by diffusion of the electroactive species in the SSE material, (e.g. when the electrolyte has a high ionic conductivity and the thickness of the mixed phase region is small). There is a third situation in which the discharge curve is characterised by both (a) and (b), but normally the electrode behaviour falls into one of the above two cases.

Atlung et al[1-3] have developed a simple theoretical model to derive equations which describe the distribution of potential and current within an ideal mixed phase electrode during discharge/charge operation by extending the theories applying to porous electrodes described by de Levie,[4] for both of the above limiting situations.

In the work described here the conductivity of the electrolyte was relatively high (0.09 S cm^{-1} at 50°C) and the thickness of the mixed-phase region has been kept low (less than 0.5 mm) so as to ensure that the response of the mixed phase region to a galvanostatic pulse would correspond to situation (b), i.e. the predominant influence on diffusion is due entirely to diffusion into the SSE particles.

When case (b) applies, the response of the mixed phase electrode to a galvanostatic pulse will follow either semi-infinite type of behaviour, (i.e. where the dimensions of the diffusion medium are assumed to be very much larger than the diffusion length) or bounded type of behaviour, depending upon the pulse length of the experiments.

When mass transport is due entirely to diffusion into the SSE particles then the principle factors that affect the response of the system are, D, the effective chemical diffusion coefficient for the electroactive species into the SSE material, and A, the real contact area at the electrode/electrolyte interface, i.e. Fick's first law,

$$F = - AD \frac{\partial C}{\partial x}$$

where F is the rate of transfer of the electroactive species, C the concentration of the species, and x the space coordinate.

For a particular level of intercalation of the electroactive species in the SSE material, then the value of D is constant, and so in order to increase the power available from a cell the real contact area, A, must be increased in comparison with a cell fabricated by placing pure electrode and electrolyte phases in contact,

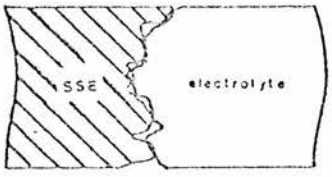

This can be achieved by introducing a mixed phase region, in which the electrode and electrolyte phases are mixed as powders and then treated with heat or pressure to produce an electrode. But as soon as a mixed phase region is introduced, the exact value for A is lost.

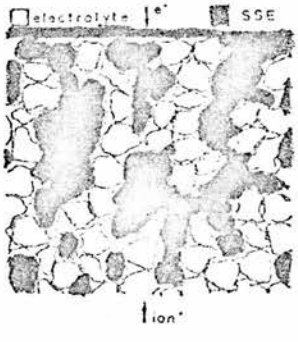

In all the measurement techniques described in chapter 4 and elsewhere, it is only possible to obtain values of D and A in combination with one another. It is noted here that in some bounded treatments it is possible to obtain values of D and r in combination, where r is the dimension of the particle involved. (e.g. if the particles were spheres then r would be their radius) But in each of these cases, r can be related back to A, and so the problem is again one involving A and D. In all the literature, where values of D have been quoted, an estimate of A has had to be made at some point in order to obtain D.

Although it is not possible to obtain absolute values for D and A, it is possible to obtain comparable values for one, by ensuring that the other value remains constant during the measurement. For example by fixing the intercalation level of the SSE material, the value of D will remain constant, and so comparative measurements of A are possible using cells containing similar samples of the SSE material and fabrication in an identical manner. On the other hand it is possible by using the same cell to study the effect of intercalation level on the value of D, since A remains constant.

When optimising the behaviour of an electrode system it is desirable to minimise the voltage polarisation of the electrode and this can be achieved by ensuring high values of A and D. A relatively large value for A can be achieved in a number of ways, for example by altering the system configuration, (e.g. introducing a mixed phase region), or its composition (i.e. the relative proportions of the

SSE/electrolyte in the region), or its method of formation (e.g. the pressure or temperature applied when producing the electrode), etc.

The work described in this chapter is involved in developing a reliable method of evaluating the merit of mixed phase electrode systems by measuring (and hence comparing) the relative contact area between different systems using the galvanostatic pulse technique. In the following chapter, this measurement method is applied to study some of the above mentioned ways of altering the contact area of a system.

5.2 Galvanostatic Pulse Measurements.

Three-electrode cells with (hexagonal) NbS_2 and silver ion conducting electrolyte as the mixed phase system in the working electrode, (in known ratios by weight) were prepared and intercalated to an appropriate level (e.g. $Ag_{0.05}NbS_2$) as described in Chapter 2.

The cells were loaded into cell holders which were mounted in a thermostated bath. A series of galvanostatic pulses of variable height and length were applied between the mixed phase working electrode acting as cathode and the silver counter electrode. The resultant electrochemical reaction at the cathode may be given as,

$$\delta\, Ag^{+} + \delta\, e^{-} + Ag_x NbS_2 \longrightarrow Ag_{x+\delta} NbS_2$$

The resulting voltage response between the mixed phase working electrode and the outer reference electrode were recorded as described in Chapter 2.

After each pulse the cell was brought back to its starting intercalation level using a reverse pulse and allowed to equilibrate until its potential was within 0.1 mV of its initial value. A schematic diagram of the galvanostatic pulse measurement is shown in figure 1.

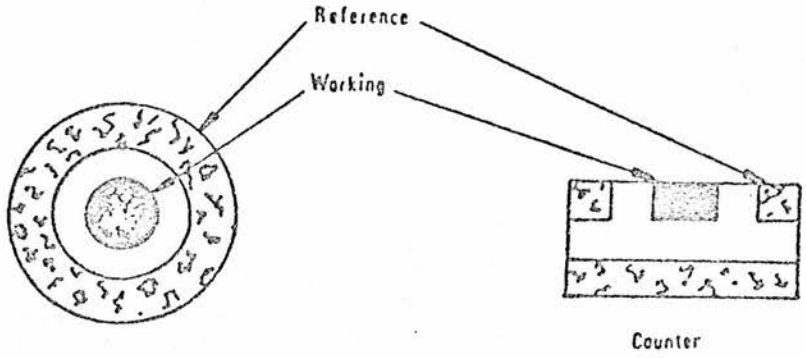

Figure 1 (a): Cell structure of 3 electrode cell

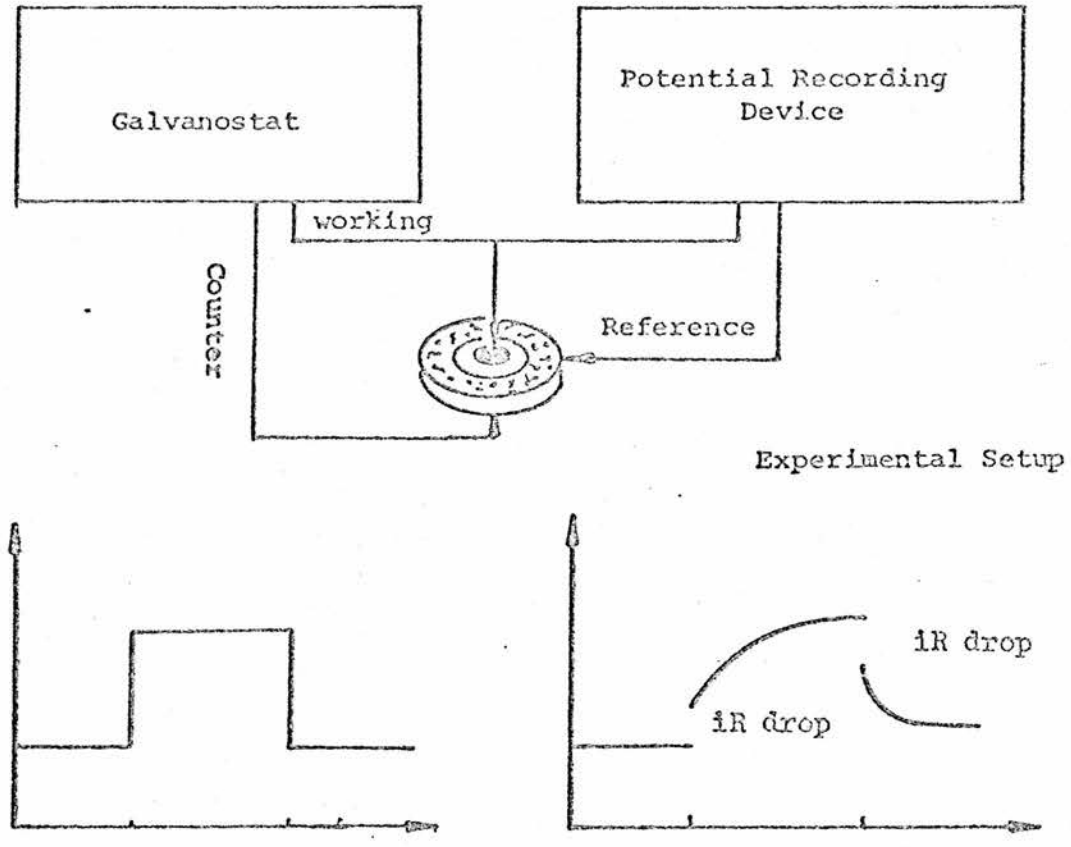

Figure 1 (b): Galvanostatic Pulse Technique

Currents from 1 microamp up to 5 milliamp and pulse lengths from 20 mS to 20000 secs were used. Larger currents and times were not applied for the following reasons,

a) the relationship relating overpotential to concentration of electroactive species at the electrode/electrolyte interface (derived later and in appendix I) only holds true for small perturbations of the cell from equilibrium,

b) larger currents and times could, if there were to be any charge transfer limitations on the electrode/electrolyte interface, take the electrode out of the linear Butler-Volmer region and any charge transfer resistance would then not be subsumed within the iR correction term,

c) to avoid any side reactions within the mixed phase region, such as nucleation of any new phases or dendrite formation.

Smaller times and currents gave voltage transients which could not reasonably be separated from random noise. Some typical transients are shown in figure 2. All the transients obtained during this investigation are stored on the accompanying magnetic tape, (tape A), and a directory and description of the tape is given in appendix V.

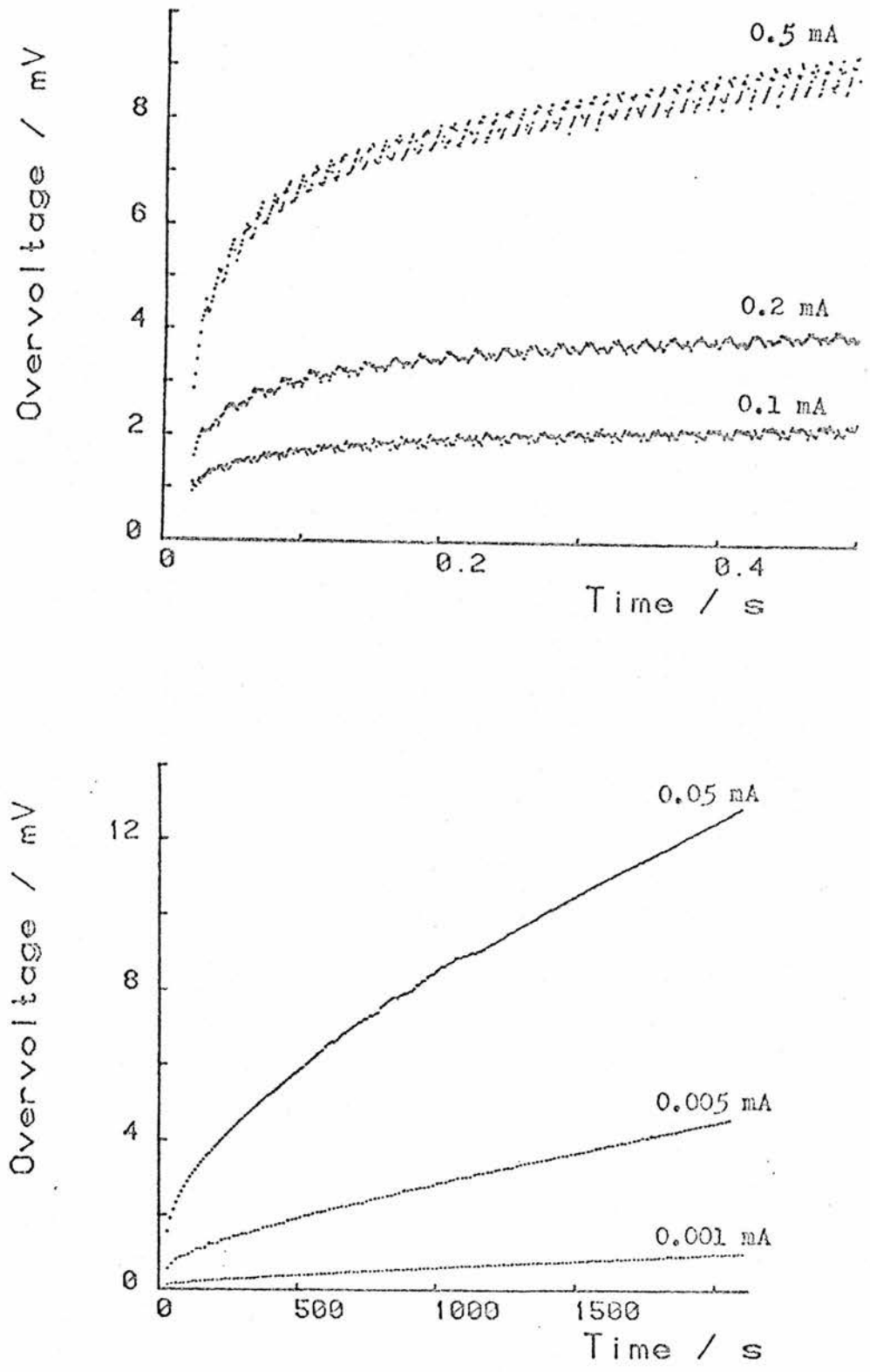

Figure 2: Some typical transients, pulsed with various currents.

5.3 Relating the Concentration of the Electroactive Species to the Cell Voltage.

In order to apply the equations detailed in the next section, which are derived in terms of concentrations of electroactive species at the surface of the SSE particle, C_o, and in the bulk, C, into an experimentally measurable quantity, (i.e. voltage between a reference electrode and the mass-transport limited SSE), the relationship between concentration of electroactive species (i.e. $C-C_0$) and cell overpotential must be found.

In a number of papers in the literature[5-9] the mass transport overpotential was directly related to concentration through the Nernst Equation,

$$\eta(t) = \frac{RT}{nF} \ln(C/C_0)$$

However careful thermodynamic studies of silver and lithium transition metal dichalcogenides[10-16] (figure 3) have shown that these electrode systems are far from ideal and that use of the Nernst Equation to relate concentration to overvoltage is completely inappropriate.

Armand[17] and other authors[1-3] have developed an equation of the form,

$$\eta = \frac{RT}{F} \{ \ln(\frac{1-X}{X}) - f(X - 0.5) \}$$

where $X = x/n$, the degree of intercalation and f is an 'interaction parameter'. The interaction parameter expresses approximately the effect of the electrostatic interactions associated with the insertion process and dominates the dependence of the potential on X. The typical range for this term is $10 < f > 20$, and the exact value depends upon the materials being studied.

This equation gives a very good approximation for the overpotential across a large range of x values. But for the situation studied in this work changes in the intercalation level are small and a simpler empirical relationship between concentration and overpotential has been used similar to that of Huggins and Weppner[10,11,13,18,19] and Worrell and coworkers.[14-16]

The concentration of electroactive species, C, can be related to the molar ratio, x, of electroactive species in the SSE material (i.e. Ag_xNbS_2) via the molar volume, V_m, of the SSE,

$$C = x/V_m$$

Assuming that the change in molar volume with composition is insignificant over the experimental conditions used, then the change in concentration and stoichiometry can be related by,

$$dC = \frac{d\delta}{V_m} \qquad [58]$$

where δ is the displacement of $A_{x+\delta}B$ from the initial composition A_xB. Expansion of this equation by dE leads to,

$$dE = \frac{dE}{d\delta} V_m dC$$

In other words, for small perturbations of the cell from equilibrium, we have,

$$\eta(t) = \frac{dE}{d\delta} V_m (C(t)-C_0) \qquad [59]$$

where $dE/d\delta$ is the gradient of the coulometric titration curve at a given value of x. Figure 3 shows the coulometric titration curve for the sample of NbS_2 used in this work, i.e. open circuit potential versus mole fraction of Ag in Ag_xNbS_2. Also included in figure 3 for comparison is the emf data obtained from reference 8. As can be seen from the graph there is a discontinuity in the curve around x = 0.15, indicating that a phase change in the SSE material is taking place. For x values up to x = 0.1 the curve is continuous, indicating that the NbS_2 is acting as a true SSE compound, (i.e. no phase changes are present). As a consequence all the measurements carried out in this work were done at an intercalation level of x = 0.05.

In order to find the gradient of the coulometric titration curve (i.e. $dE/d\delta$) a polynomial of large degree has been used to describe the curve. Exact details of how to obtain the gradient can be found in appendix I.

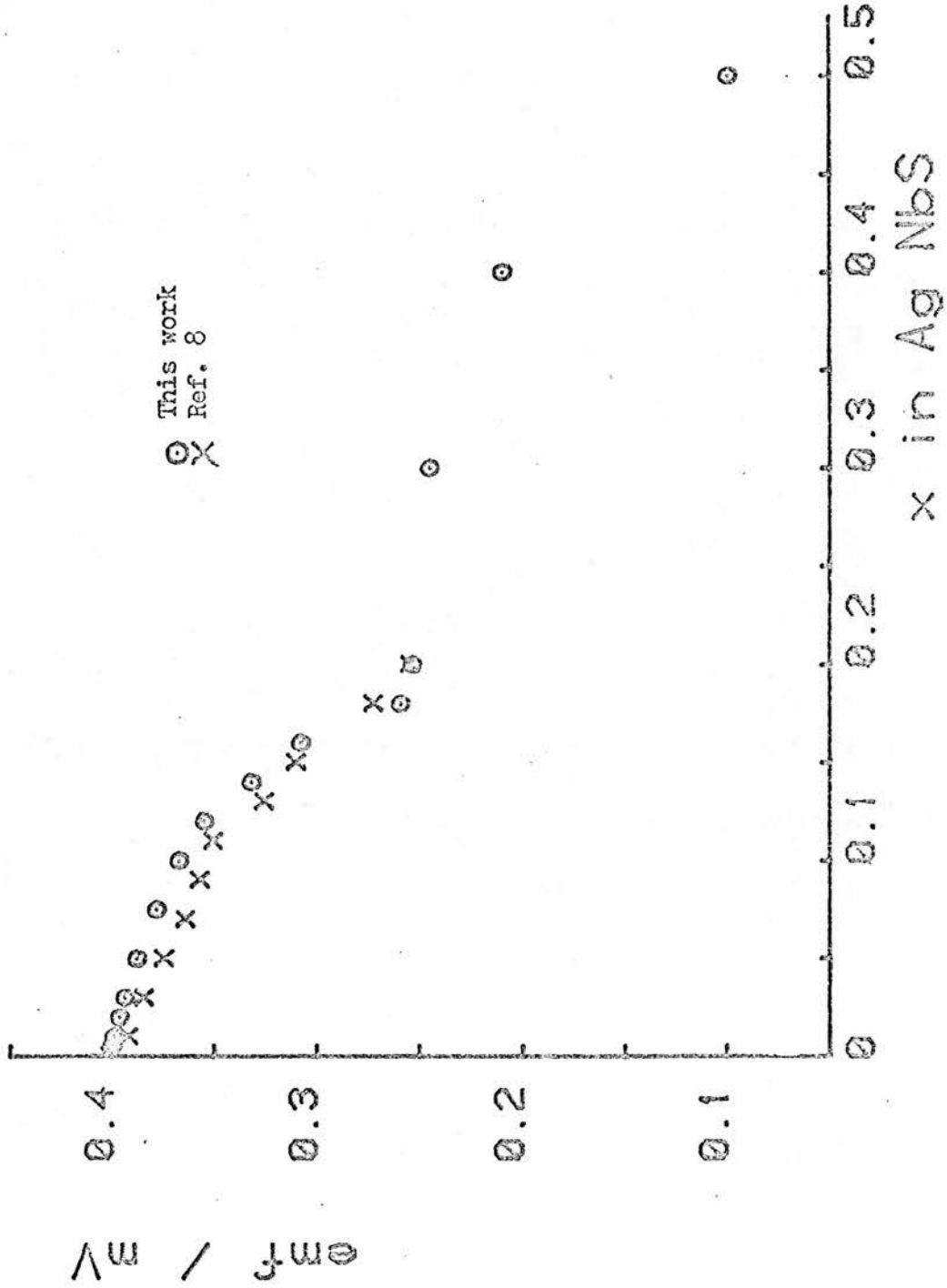

Figure 3: Equilibrium emf values for the intercalation of silver in NbS_2 as a function of x at 50°C.

5.4 Mathematical Models for Interpreting Diffusion in Mixed Phase Electrodes.

5.4.1 Simple Semi-Infinite Linear Diffusion.

One of the simplest models for analyzing a diffusion process in an electrode, uses 'semi-infinite' boundary conditions in which the dimensions of diffusion medium are assumed to be very much larger than the diffusion length. This model results in a very simple relationship between the concentration of the electroactive species at the electrode/electrolyte interface, which is related to the overpotential of the cell via the gradient of the coulometric titration curve as described above, and the length of time the galvanostatic pulse has been applied to the cell. It may be shown that the overpotential of the cell is directly proportional to the square root of the time. The full derivation of the equation is given in appendix I (equation [60] of appendix I) and yields,

$$\eta(t) = \frac{2(dE/d\delta)V_m i\, t^{1/2}}{nF\,\pi^{1/2}AD^{1/2}}$$

where $dE/d\delta$ is the gradient of the coulometric titration curve at a given value of δ, V_m is the molar volume of the solid state electrode (SSE) material, (for NbS_2 this is 33.97 cm^3 per mole)[20], i is the total current applied to the cell, n is the number of electrons

involved in the charge transfer reaction for silver, (i.e. 1), F is Faraday's constant, (96490 C equiv^{-1}), D is the chemical diffusion coefficient, and A is the real contact area at the electrode/electrolyte interface as described earlier.

The same relationship can be derived from using an approximation to the finite models described later, where the pulse length of the experiments are small (i.e. $t << r^2/D$, where r is the dimension of the diffusion medium).

If the conditions for semi infinite diffusion are correct then the equation can easily be fitted to a potential transient by plotting overpotential as a function of the square root of time and from the gradient of the line that results a value for $AD^{1/2}$ may be obtained. i.e.

$$AD^{1/2} = \frac{2(dE/d\delta)V_m i}{nF\pi^{1/2}\ \text{Gradient}}$$

Many authors, (eg. Huggins, Weppner, Wen, Atlung and co-workers[10-16], have used this 'root t' method to calculate values of $AD^{1/2}$, and hence D, (by assuming A to be the geometric area of the cell). In figure 4 an example of this type of treatment is shown for a $Li_{0.46}TiS_2/Li_3N$ mixed phase region[21] pulsed with 0.1 milliamp where the transient is plotted with respect to the square root of time. As can be seen a reasonable fit is obtained only for short times, thereafter the fit progressively deteriorates as the semi-infinite boundary condition breaks down.

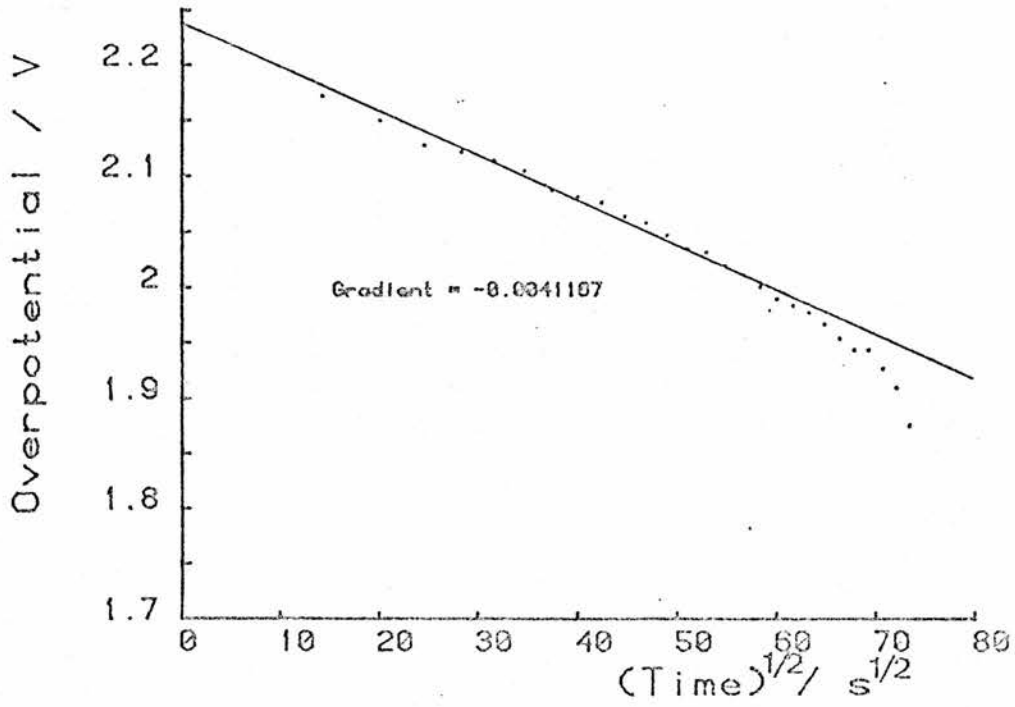

Figure 4: Example of square root time fit for $Li_{0.46}TiS_2/Li_3N$.

Two parameters are obtained from the above fit: a) $AD^{1/2}$ and b) iR drop. The Mean Square Residual (MSR) for the overall fit is also obtained. The smaller the MSR is for the transient then the better the model has described the transient. For the transient in figure 4, $AD^{1/2} = 2.21*10^{-4}$ $cm^3sec^{-1/2}$ and iR drop = 0.0296 V.

As a rough guide, a MSR less than 10^{-8} indicates that the fit is very good, whereas a MSR greater than 10^{-5} indicates a poor fit and the area between 10^{-8} and 10^{-5} indicates that the fit is reasonable.

All the transients obtained earlier were fitted by this semi-infinite model, and table 1 shows the data that was obtained.

As can be seen from table 1 there is a distinct trend in the parameters being measured, and the quality of the fit progressively deteriorates as the amount of charge applied to the cell is increased. For most of the transients the quality of the fit is very poor (i.e. greater than 10^{-6}). The values obtained for $AD^{1/2}$, which should be constant, are also increasing with the total charge passed, (by a factor of five).

This deterioration in the quality of the fit and in the failure of $AD^{1/2}$ to remain constant indicates therefore that the semi-infinite model cannot adequately describe the physical phenomenon that is taking place within the cell.

The principle assumption made in this model is that the diffusion of the electroactive species is semi-infinite, i.e. the solid state electrode material through which the species diffuse is infinitely large. Since, of course, the SSE particles are of finite size this assumption is likely to break down under the experimental conditions being studied.

Pulse Height (mA)	Pulse Length (secs)	$AD^{1/2}$ $*10^{-5}$	M.S.R. $*10^{-5}$	Pulse Height (mA)	Pulse Length (secs)	$AD^{1/2}$ $*10^{-5}$	M.S.R. $*10^{-5}$
5.000	300.00	4.156	6085.00	0.200	0.05	0.490	0.02
5.000	200.00	4.745	1074.70	0.200	0.02	0.470	0.01
5.000	100.00	4.979	169.32	0.100	300.00	1.521	21.86
5.000	50.00	4.785	86.91	0.100	200.00	1.735	12.41
5.000	10.00	5.938	5.56	0.100	100.00	2.116	1.34
5.000	0.50	3.945	159.57	0.100	50.00	2.454	0.12
5.000	0.20	2.191	85.12	0.100	10.00	3.172	0.02
5.000	0.10	1.528	81.31	0.100	0.50	0.994	0.21
5.000	0.05	0.956	81.62	0.100	0.20	0.705	0.04
5.000	0.02	0.550	50.53	0.100	0.10	0.549	0.02
2.000	300.00	3.726	4338.00	0.100	0.05	0.515	0.03
2.000	200.00	3.013	1292.40	0.100	0.02	0.536	0.01
2.000	100.00	2.925	258.41	0.050	2000.00	1.306	925.75
2.000	50.00	3.393	49.38	0.050	1500.00	1.377	242.46
2.000	10.00	5.011	0.73	0.050	1000.00	1.460	146.12
2.000	0.50	3.602	12.69	0.050	500.00	1.658	37.08
2.000	0.20	0.716	24.32	0.050	250.00	1.856	0.48
2.000	0.10	0.805	30.42	0.040	2000.00	1.166	946.99
2.000	0.05	1.641	2.34	0.040	1500.00	1.236	0.02
2.000	0.02	0.474	65.96	0.040	1000.00	1.328	98.32
1.000	300.00	2.293	438.75	0.040	500.00	1.459	14.28
1.000	200.00	2.513	135.97	0.040	250.00	1.522	0.60
1.000	100.00	2.690	59.76	0.030	2000.00	1.172	116.70
1.000	50.00	3.098	9.86	0.030	1500.00	1.166	107.80
1.000	10.00	3.636	0.01	0.030	1000.00	1.236	63.43
1.000	0.50	3.028	1.49	0.030	500.00	1.351	5.15
1.000	0.20	2.904	0.55	0.030	250.00	1.386	0.39
1.000	0.10	0.676	2.86	0.020	2000.00	1.044	249.90
1.000	0.05	0.544	0.75	0.020	1500.00	1.101	57.89
1.000	0.02	0.457	0.31	0.020	1000.00	1.142	59.59
0.500	300.00	2.406	17.47	0.020	500.00	1.312	10.25
0.500	200.00	2.393	32.12	0.020	250.00	1.430	0.19
0.500	100.00	2.515	17.46	0.010	2000.00	1.213	88.65
0.500	50.00	2.881	0.33	0.010	1500.00	1.313	0.01
0.500	10.00	3.139	0.01	0.010	1000.00	1.378	6.50
0.500	0.50	1.127	3.75	0.010	500.00	1.389	6.93
0.500	0.20	0.803	1.56	0.010	250.00	1.238	0.45
0.500	0.10	0.597	0.49	0.005	20000.00	0.389	197.01
0.500	0.05	0.501	0.17	0.005	15000.00	0.458	150.17
0.500	0.02	0.414	0.02	0.005	10000.00	0.455	172.64
0.200	300.00	3.102	4.55	0.005	5000.00	0.570	120.23
0.200	200.00	3.239	3.90	0.005	2000.00	0.677	112.58
0.200	100.00	3.568	0.15	0.005	1500.00	0.742	35.67
0.200	50.00	3.560	2.29	0.005	1000.00	0.841	15.58
0.200	50.00	3.326	0.04	0.005	500.00	1.025	4.54
0.200	20.00	3.055	1.81	0.005	250.00	1.171	0.71
0.200	10.00	3.246	0.01	0.001	2000.00	0.606	7.13
0.200	1.00	1.386	0.81	0.001	1500.00	0.663	2.60
0.200	0.50	1.040	0.79	0.001	1000.00	0.752	1.46
0.200	0.20	0.714	0.17	0.001	500.00	0.963	0.69
0.200	0.10	0.576	0.07	0.001	250.00	1.101	0.11

Table 1

5.4.2 Diffusion in Finite Particles.

Diffusion into a particle of finite size can occur in one of three distinct geometrical constraints corresponding to, a) one dimensional geometry, (eg. through a thin layer or film), b) two dimensional geometry, (eg. in a cylinder) and c) three dimensional geometry, (eg. in a sphere).

The derivations of the appropriate equations which relate the concentration of the electroactive species at the electrode/electrolyte interface to the duration of the pulse, and hence (via the gradient of the coulometric titration curve) to the overpotential of the cell for the above three geometries are given in appendix I where it is shown that the three distinct equations can all be expressed in one general form, containing constants which depend upon the geometry being considered, viz,

$$\eta(t) = \frac{Q_1(dE/d\delta)V_m i}{C_1 nFAr \ln(P)} \left\{ 1 - \frac{C_1}{Q_1} t \ln(P) - \sum_{j=1}^{\infty} \frac{C_2}{Q_j} P^{(Q_j t/Q_1)} \right\}$$

where $P = \exp(-Q_1 D/r^2)$, r is the dimension of the particle, and C_1, C_2 and Q_j are constants, the values of which are given in table 1 of appendix I. The other constants have been given earlier.

This above equation was fitted (as described in appendix III) to all the transients and table 2 shows the mean squared residuals of the fits for each of the different geometries. The 'square root time' fit is also given for comparison.

Pulse Height (mA)	Pulse Length (secs)	Mean Squared Residuals				
		Root t	Linear t	Cylinder	Thin Layer	Sphere
		*10-7	*10-7	*10-10	*10-10	*10-10
5.000	300.00	608500	412250	90756	104440	127790
5.000	100.00	16932	283230	103610	125570	163820
5.000	0.50	15957	26574	24650	25460	26697
5.000	0.05	8161	20280	2538.1	2740.7	2968.1
5.000	0.02	5052	15111	606.2	659.3	710.2
2.000	300.00	433800	1340400	867560	929220	1021200
2.000	100.00	25841	32449	1642.2	1191.5	724.7
2.000	0.50	1269	2662	1875.2	1967	2117.9
2.000	0.05	233	746	102.3	113	125.1
2.000	0.02	6595	8826	1681	1696.2	1710.8
1.000	300.00	43875	67511	3048.7	3910.1	5760.4
1.000	100.00	5976	12602	1632.9	1422	1758.1
1.000	0.50	149	494	305.9	329.7	369.1
1.000	0.05	74	297	247.9	274.8	305.6
1.000	0.02	30	45	112	114.7	117.4
0.500	300.00	1747	43569	6696.9	8842.4	12673
0.500	100.00	1746	3545	390.9	468.9	687.3
0.500	0.50	375	1089	857	911.1	998.1
0.500	0.05	17	60	51.4	56.1	61.6
0.500	0.02	2	5	8.8	9.1	9.5
0.050	2000.00	92580	277700	65	199	303
0.050	1000.00	14620	62990	71	90	207
0.040	2000.00	94690	207200	111	107	343
0.040	1000.00	9832	58760	156.4	30.4	366.7
0.030	2000.00	11670	290400	316.8	127.7	695.8
0.030	1000.00	6343	38000	126.4	19.8	278.1
0.020	2000.00	24990	82200	38.9	60.4	119
0.020	1000.00	5959	18640	28.9	28.2	64.5
0.010	2000.00	8865	11880	41.6	11.3	73.4
0.010	1000.00	649	7179	59.5	16.6	92.3
0.005	2000.00	11260	3808	3.6	9	2.9
0.005	1000.00	1558	1176	3.1	4.3	3.9
0.001	2000.00	712	303	0.8	1.1	0.7
0.001	1000.00	146	89	0.6	0.6	0.5

Table 2

Also listed in table 2 are the MSR's for a 'linear t' fit. This has been included because many authors (eg. Huggins, Weppner, Atlung, etc.[1-3,16-19]) have used a 'linear model' as an approximation to diffusion in a bounded region at long times. (i.e. when $t >> r^2/D$ then the sum of exponentials is insignificant). In other words the previous equation becomes,

$$\eta(t) = \frac{(-dE/d\delta)V_m i\, t}{nFAr} + \frac{(-dE/d\delta)V_m ir}{C_1 nFAD}$$

But as can be seen from table 2 the 'linear model' is much worse than any of the finite models and so the sum of exponentials under these conditions cannot be ignored. These authors have also used the 'square root t' fit (i.e. the equation for 'semi-infinite' diffusion) as an approximation to the previous equation at short times (i.e. $t << r^2/D$), but as can also be seen, this is an over-simplification for the values of D, r, t, etc. found in this system. Figure 5 shows a plot of the spherical model (using ten terms in the sum of exponentials) with appropriate values of D, i, etc. along with the straight line and root t approximations.

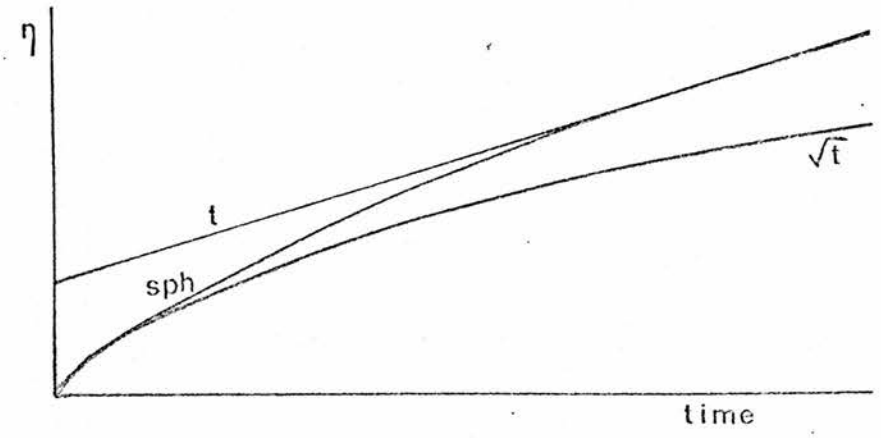

Figure 5: Plot of the spherical model along with the linear and root t approximations.

Figure 6 shows some of the MSR's plotted as a function of charge for different models. What can be seen immediately from this figure (and table 2) is that the three finite models have MSR's which are all approximately one thousand times smaller than those for the semi-infinite model indicating that any one of the finite models provides a better description of the diffusion process.

What can also be seen from table 2 is that the cylindrical model is slightly better at describing the transient than the thin layer model, which is in turn better than the spherical model. This is understandable since the SSE material (NbS_2) used has a layered type structure through which the electroactive species can diffuse,[22,23] as shown in plates 1 and 2 and figure 6. Diffusion normal to the layers does not occur to any great extent, so that the boundary condition for the process approximates to that of a cylinder.

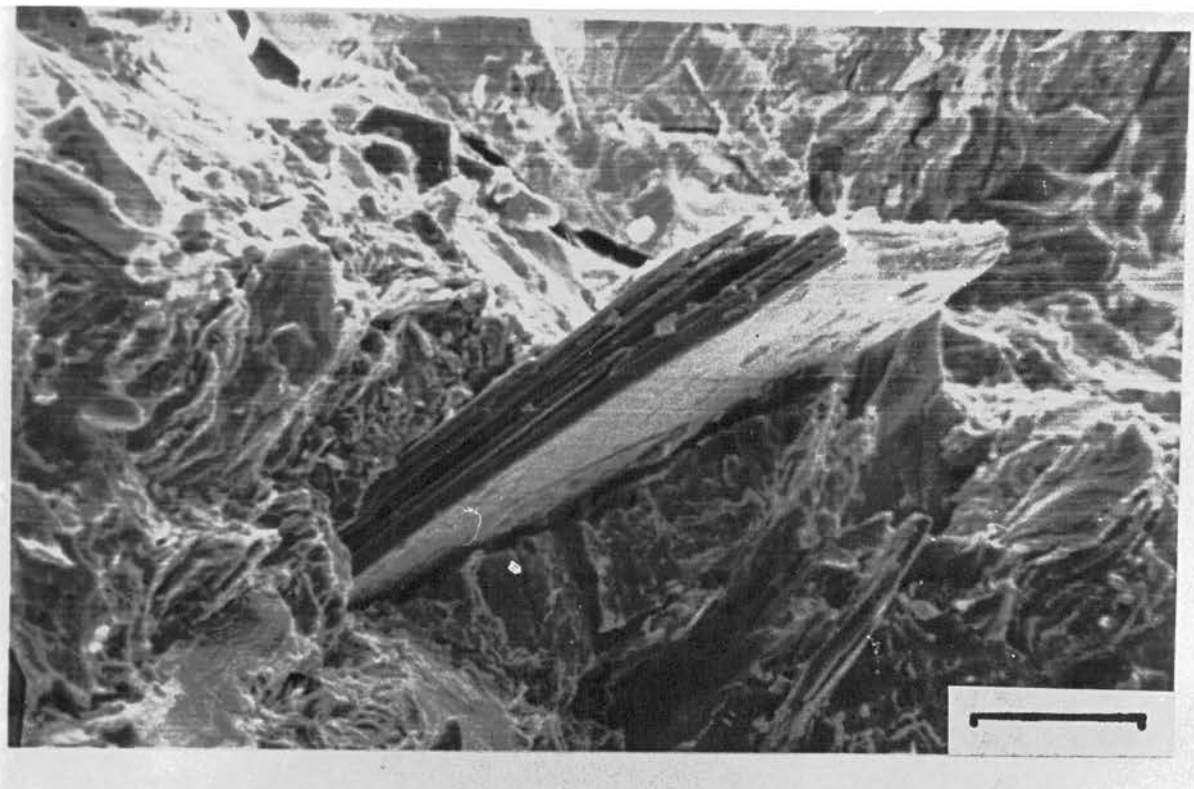

Plate 1: NbS_2 crystal. (20μ)

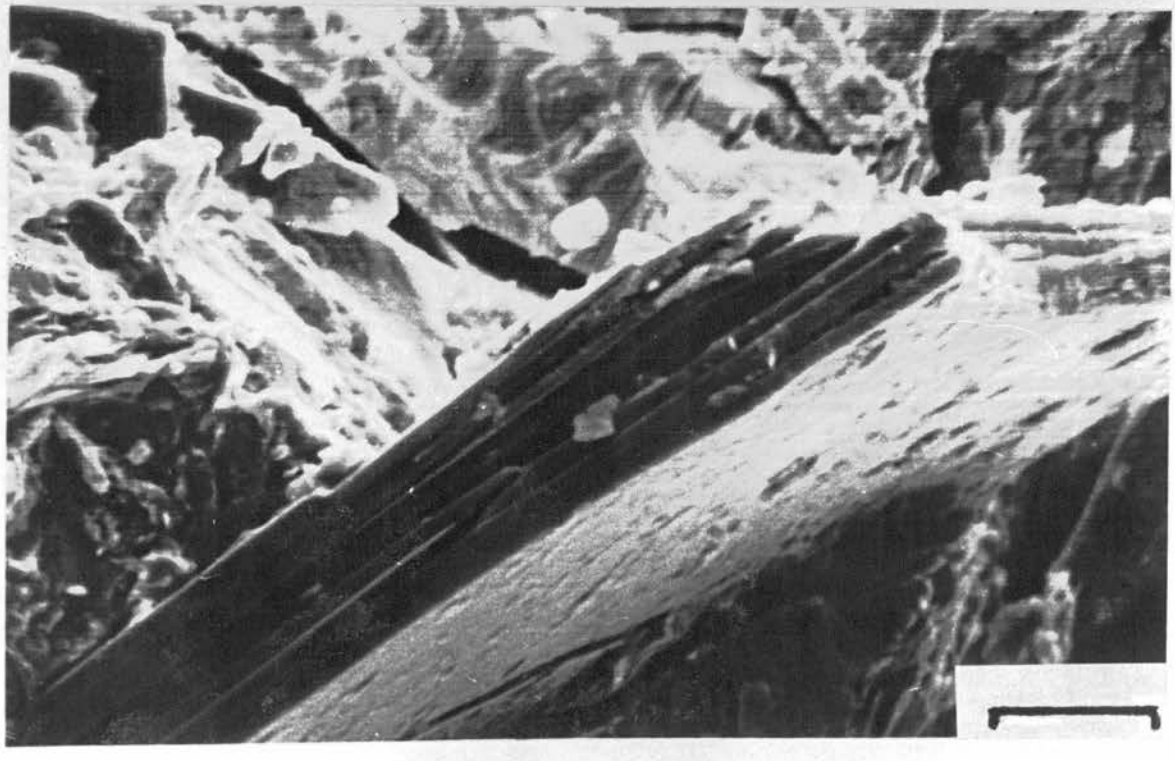

Plate 2: Enlargement of NbS_2 crystal. (10μ)

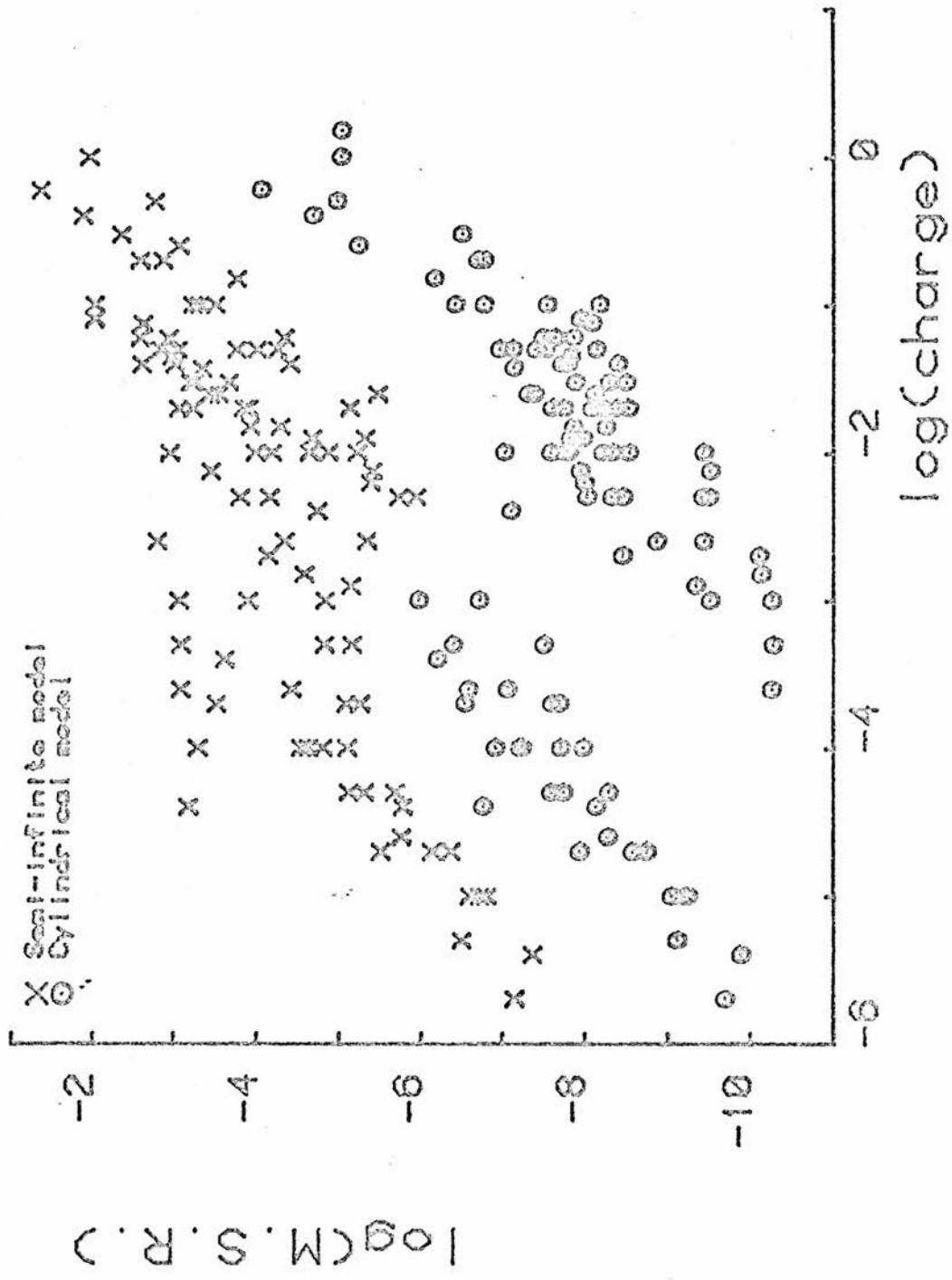

Figure 6: Mean Squared Residuals as a function of charge for various models.

When any one of the finite diffusion models are fitted to a transient then there are three parameters obtained, namely a) D/r^2, a measure of the effective chemical diffusion coefficient, b) $AD^{1/2}$, a measure of the total surface area between the electrode and electrolyte and c) the iR drop for the cell. The details of how these parameters are obtained is given in appendix III. Figure 7 shows an example of three transients which have been fitted by the cylindrical model, and the values for the parameters obtained are given in the adjacent table.

We shall concentrate on fitting and interpretation of data based on the cylindrical model since it gave the best fit for the SSE material used here, but the results and trends for the other two finite boundary models were found to be similar.

Table 3 shows a selection of the values for the parameters obtained by fitting the cylindrical model to the transients obtained previously. Figures 8 and 9 show plots of the two important parameters (D/r^2, $AD^{1/2}$) plotted as a function of pulse length for the various currents used.

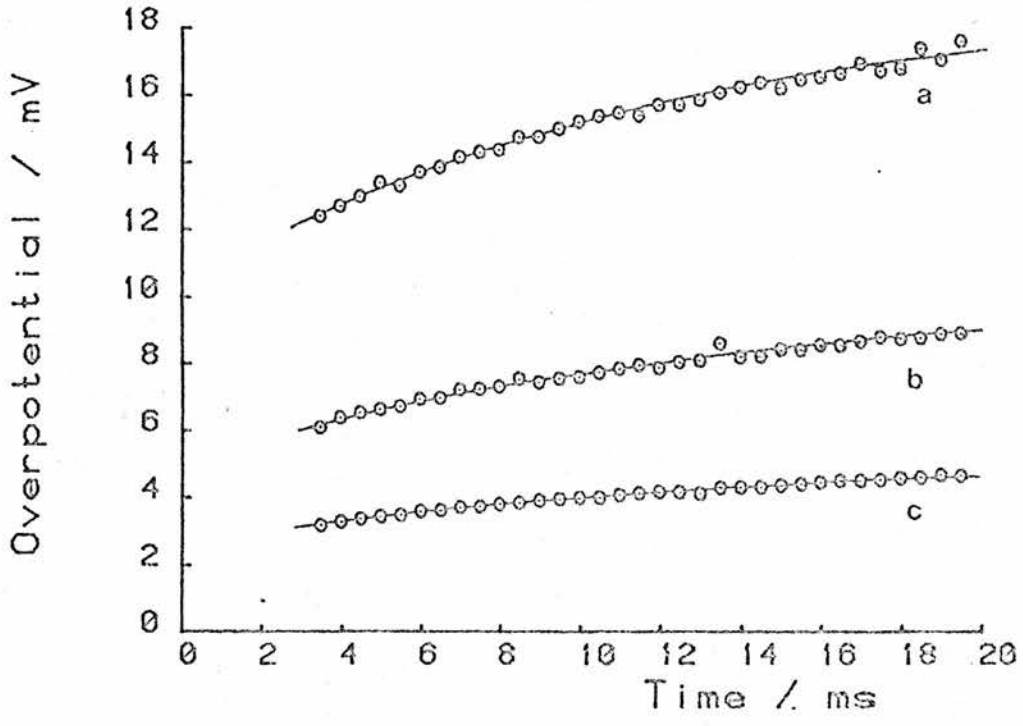

	a	b	c
Pulse Height/mA	2.0	1.0	0.5
IR drop/mV	10.1	4.84	2.43
$D^{1/2}r^{-1}$ /s$^{-1/2}$	1.41	1.48	1.51
$(AD^{1/2}$ /cm^{3}s$^{-1/2})$ x 10^6	4.63	4.86	3.71

Figure 7: Data points - responce of a mixed phase $Ag_{0.05}NbS_2$/ $Ag_6I_4WO_4$ electrode to (a) 2.0 mA (b) 1.0 mA and (c) 0.5 mA pulses at 50°C. Lines - curves fitted using the cylindrical diffusion model. Table shows the fitted parameters obtained from the model.

Pulse Height (mA)	Pulse Length (secs)	iR drop (mV)	D/r^2 ($secs^{-1}$) $*10^{-3}$	$AD^{1/2}$ ($cm^3 secs^{-0.5}$) $*10^{-4}$	M.S.R. $*10^{-10}$
5.00	300.00	0.083	1.589	0.682	90756
5.00	100.00	0.076	1.263	0.608	103610
5.00	0.50	0.039	235.400	0.522	24650
5.00	0.10	0.032	974.100	0.226	3919
5.00	0.05	0.030	1555.000	0.149	2538
5.00	0.02	0.027	2717.000	0.088	606
2.00	300.00	0.041	0.340	0.444	867560
2.00	100.00	0.015	0.398	0.300	1642
2.00	0.50	0.085	250.700	0.478	1875
2.00	0.10	0.013	920.400	0.111	2791
2.00	0.05	0.036	1487.000	0.228	102
2.00	0.02	0.098	2591.000	0.062	1681
1.00	300.00	0.014	1.008	0.329	3048
1.00	100.00	0.011	0.518	0.288	1632
1.00	0.50	0.028	247.000	0.387	305
1.00	0.10	0.061	883.700	0.082	1188
1.00	0.05	0.053	1476.000	0.065	247
1.00	0.02	0.047	2873.000	0.054	112
0.50	300.00	0.080	0.364	0.287	6696
0.50	100.00	0.093	2.774	0.354	390
0.50	0.50	0.046	250.500	0.144	857
0.50	0.10	0.030	877.000	0.071	177
0.50	0.05	0.026	1523.000	0.060	51
0.50	0.02	0.023	3106.000	0.049	8
0.20	300.00	3.880	0.579	0.397	225
0.20	100.00	4.190	1.321	0.439	243
0.20	0.50	1.790	236.000	0.132	189
0.20	0.10	1.120	873.900	0.069	26
0.20	0.05	1.010	1514.000	0.058	5
0.20	0.02	0.888	1142.000	0.050	1
0.10	300.00	1.570	2.008	0.271	31
0.10	100.00	0.879	0.398	0.217	45
0.10	0.50	0.871	232.800	0.125	50
0.10	0.10	0.533	861.400	0.065	6
0.10	0.05	0.486	1493.000	0.061	7

Table 3

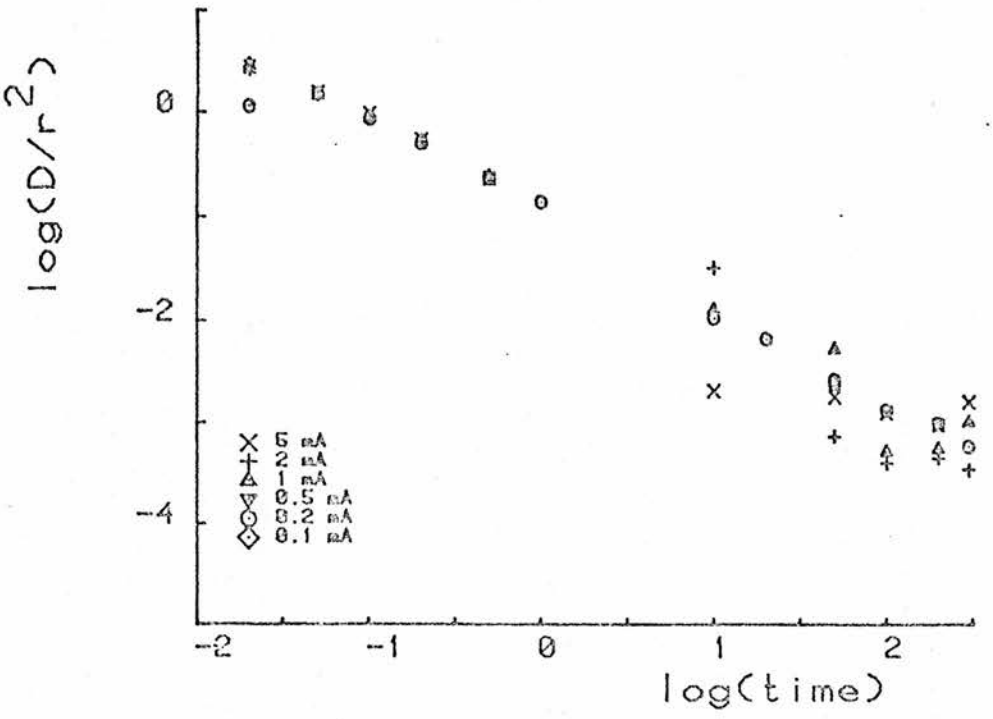

Figure 8: D/r^2 as a function of time for various pulse currents.

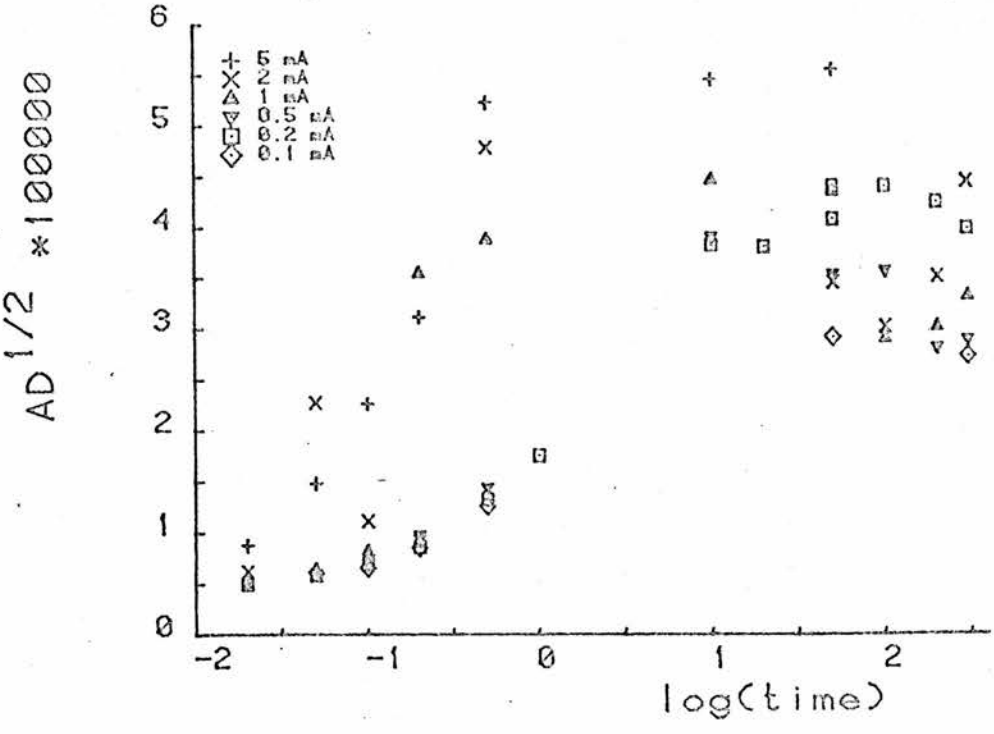

Figure 9: Effective contact area ($AD^{\frac{1}{2}}$) as a function of time for various pulse currents.

What is obvious from this data is that the parameters, which again should be constant, are still dependant on the pulse length. It would appear that as the pulse length increases, so D/r^2 decreases and $AD^{1/2}$ increases, although the latter levels out at pulse lengths greater than about 50 secs.

In order to investigate the time dependence further, transients with longer pulse lengths (up to 20000 secs) and smaller pulse heights were recorded. The currents applied had to be decreased to compensate for the increase in pulse length, so that the change in the overpotential of the cell would remain small and not invalidate the relationship between cell potential and concentration of electroactive species described in the derivation of the diffusion equations. (section 5.3)

The parameters obtained from these longer pulses are shown in table 4, and plots of D/r^2 and $AD^{1/2}$ versus pulse length are shown in figures 10 and 11.

Pulse Height (mA)	Pulse Length (secs)	iR drop (mV)	D/r^2 ($secs^{-1}$) $*10^{-3}$	$AD^{1/2}$ ($cm^3 secs^{-1/2}$) $*10^{-4}$	M.S.R. $*10^{-10}$
0.050	2000	1.985	0.095	0.180	65.00
0.050	1500	2.107	0.110	0.184	80.00
0.050	1000	2.416	0.180	0.197	71.00
0.050	500	2.728	0.368	0.218	75.10
0.050	250	2.793	0.703	0.231	103.70
0.040	2000	1.898	0.105	0.164	111.00
0.040	1500	2.015	0.123	0.169	134.00
0.040	1000	2.162	0.168	0.176	156.40
0.040	500	2.256	0.307	0.185	174.60
0.040	250	2.177	0.584	0.186	163.30
0.030	2000	1.343	0.063	0.147	316.80
0.030	1500	1.480	0.106	0.154	143.70
0.030	1000	1.646	0.167	0.163	126.40
0.030	500	1.689	0.305	0.170	135.80
0.030	250	1.607	0.624	0.170	111.10
0.020	2000	0.803	0.086	0.141	38.90
0.020	1500	0.829	0.092	0.142	50.60
0.020	1000	1.058	0.195	0.157	28.90
0.020	500	1.184	0.332	0.170	29.00
0.020	250	1.183	0.589	0.175	34.10
0.010	2000	0.770	0.102	0.168	41.60
0.010	1500	0.771	0.105	0.169	54.50
0.010	1000	0.758	0.144	0.170	59.50
0.010	500	0.673	0.259	0.164	46.42
0.010	250	0.568	0.573	0.153	13.30
0.005	20000	0.945	0.014	0.061	542.00
0.005	15000	0.985	0.028	0.072	39.34
0.005	10000	0.963	0.027	0.071	90.37
0.005	5000	0.041	0.076	0.089	35.81
0.005	2500	0.078	0.189	0.114	9.21
0.005	2000	0.043	0.237	0.121	3.62
0.005	1500	0.388	0.275	0.127	3.00
0.005	1000	0.419	0.337	0.134	3.13
0.005	500	0.449	0.457	0.143	3.65
0.005	250	0.463	0.805	0.152	4.51
0.001	2000	0.056	0.261	0.114	0.77
0.001	1500	0.065	0.317	0.121	0.73
0.001	1000	0.078	0.463	0.135	0.55
0.001	500	0.084	0.559	0.143	0.52
0.001	250	0.089	1.204	0.160	0.55

Table 4

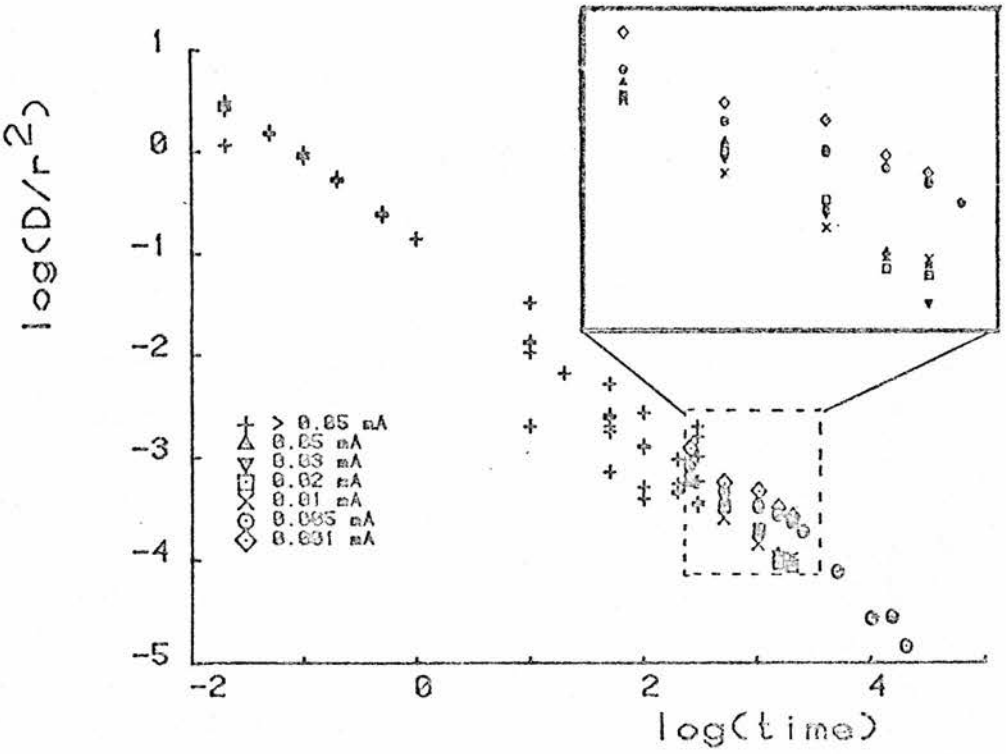

Figure 10: D/r^2 as a function of time for various pulse currents.

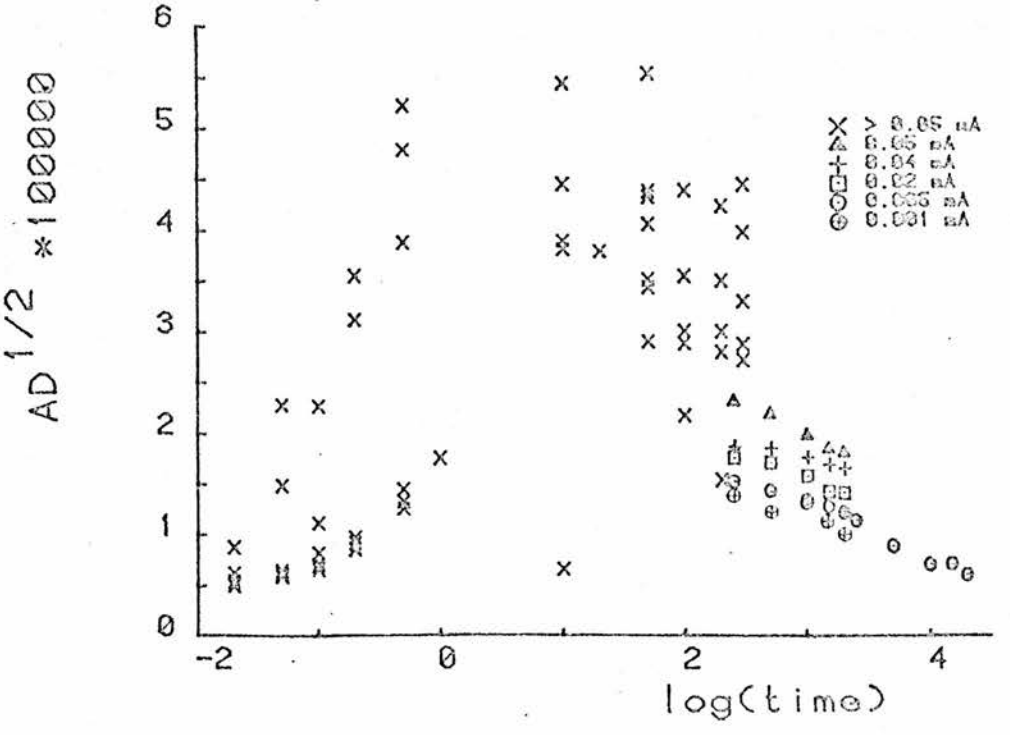

Figure 11: Effective contact area ($AD^{\frac{1}{2}}$) as a function of time for various pulse currents.

As can be seen from figures 10 and 11, the fitted parameters continue to change with the pulse length, although not to such a large extent as for the shorter pulse lengths, (table 3). D/r^2 continues to decrease as the pulse length increases; now $AD^{1/2}$ decreases slightly as the pulse length increases, but much less rapidly than the increase observed for short pulse lengths.

Another point which is obvious from figure 11, (also figure 9 to a lesser extent) is that the value of $AD^{1/2}$ increases as the current is increased, but that the value of D/r^2 is unaffected by the change in current.

This failure of the fitted parameters to remain constant as the applied pulse is altered suggests that there is some effect taking place in the cell which the above models have not taken into account. One assumption which must be made when deriving the finite models is that the size distribution of the SSE particles is uniform and that all the particles are of equal size and shape. This assumption must be made in order to solve exactly the partial differential equations associated with diffusion. Obviously though, the particle size of a SSE material are not in practice uniform and investigation of the effect of particle size on the voltage transient was now undertaken.

5.5 The Effect of Particle Distributions on Diffusion.

The simplest distribution to study (apart from a uniform one) is one in which there are only two different particle sizes present. For ease in visualising the situation a spherical model was used, but the arguments and results hold equally well for the cylindrical and thin layer models.

Thus we initially postulate a particle distribution consisting of a number of spheres of radius r_1 and r_2 (where $r_1 \neq r_2$). The numbers of each type of sphere can be varied and since the radius of the sphere has also been fixed, then the surface area of the spheres can be calculated, (viz. $A = N4\pi r^2$), or conversely if the radius and surface area of the spheres are known then the number of spheres (of that radius) can be found. In a similar manner, the volume of the spheres can be found given their number and radius, (viz $V = N4\pi r^3/3$): thus if any one of three quantities are known (i.e. N or A or V) then the other two may be calculated.

The equation governing diffusion in a sphere (equation [64], appendix I) is given below and as can be seen from this the overpotential at a fixed time (for any particular current, D, etc.) is dependent only upon the value of radius and area, all the other parameters having constant values.

$$\eta(t) = \frac{Q_1(dE/d\delta)V_m i}{C_1 nFAr \ln(P)} \left\{ 1 - \frac{C_1}{Q_1} t \ln(P) - \sum_{j=1}^{\infty} \frac{C_2}{Q_j} P^{(Q_j t/Q_1)} \right\}$$

where $P = \exp(-Q_1 D/r^2)$ and C_1, C_2 and Q_j are constants, the values of which are given in table 1 of appendix I.

Thus the overpotential at a given time can be generated for a uniform particle distribution given the radius and surface area of the particle and using the above equation, (where in practice the sum to infinity has been curtailed to three terms). In this manner a complete transient can be generated for a uniform particle distribution.

In a similar manner the voltage transient for a two sphere system may be found, since the overpotential at any given time for the sphere of radius r_1 (surface area A_1) is only dependent upon the proportion of current that these spheres receive. In other words, if V_1 and V_2 denotes the overpotentials, (at a given time), for the spheres of radius r_1 and r_2 respectively then,

$$V_1 = \frac{i_1}{A_1 r_1} f(r_1) \quad \text{and} \quad V_2 = \frac{i_2}{A_2 r_2} f(r_2)$$

$$\text{where} \quad f(r) = \frac{Q_1 (dE/d\delta)V_m}{C_1 nF \ln(P)} \left\{ 1 - \frac{C_1}{Q_1} t \ln(P) - \sum_{j=1}^{\infty} \frac{C_2}{Q_j} P^{(Q_j t/Q_1)} \right\}$$

i.e. a function which only depends upon r at any given time.

Thus by choosing the correct values for i_1 and i_2 it may be arranged for $V_1 = V_2$ since all the other quantities {A, r, f(r)} are fixed to their initial values (i.e. the value for V_1 may be increased simply by increasing i_1 and V_2 may be decreased by decreasing i_2). When $V_1 = V_2$ then this value will be the overpotential that results for a two sphere system and the value for i_1 and i_2 will correspond to the amount of current that each type of sphere receives.

In this manner a voltage transient for arrays of spheres of two sizes can be generated, (along with the proportion of current that each sphere receives), by progressively altering i_1 (and i_2) until the overpotentials match (i.e. $V_1 = V_2$). Figure 12 shows the voltage transient which results from a two particle distribution, where the surface area of the two sets of spheres has been set equal (at 0.3 cm^2) and the two sets of radii are 0.01 cm and 0.005 cm.

In figure 12, curve a) corresponds to the transient which would result for a uniform particle distribution of radius 0.005 cm, curve b) for radius 0.01 cm and curve c) the transient for the combination of the two spheres, where the surface area of each is equal, at 50% of a) {or b)}. As can be seen the resultant transient {c)} is always between the two extreme cases, but as the time of the pulse increases, so it tends towards the lower curve, i.e. towards the transient for the larger spheres {c)}. Figure 13 shows the current distribution which results from the two sphere system and it can be seen that the current distributes itself towards the larger spheres as the pulse progresses.

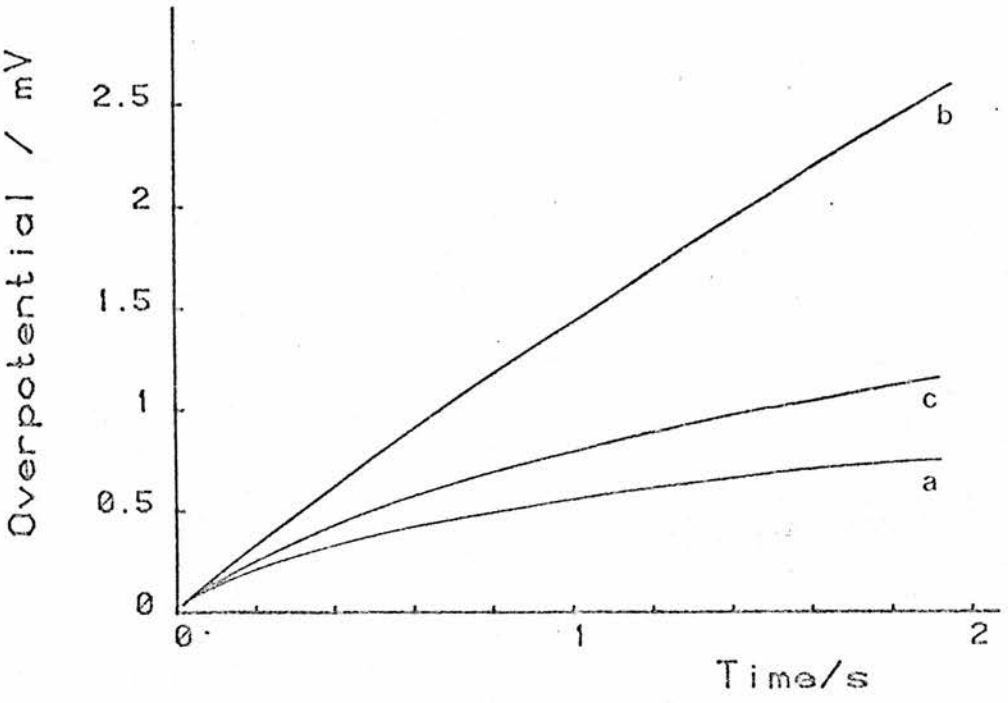

Figure 12: Voltage transient for electrodes consisting of two sets of spherical particles; each set has the same total area, but the radii of the spheres have a ratio of 1:10. (a) larger spheres, (b) smaller spheres and (c) mixture of the larger and small spheres, each having 50% of the total area in (a) or (b).

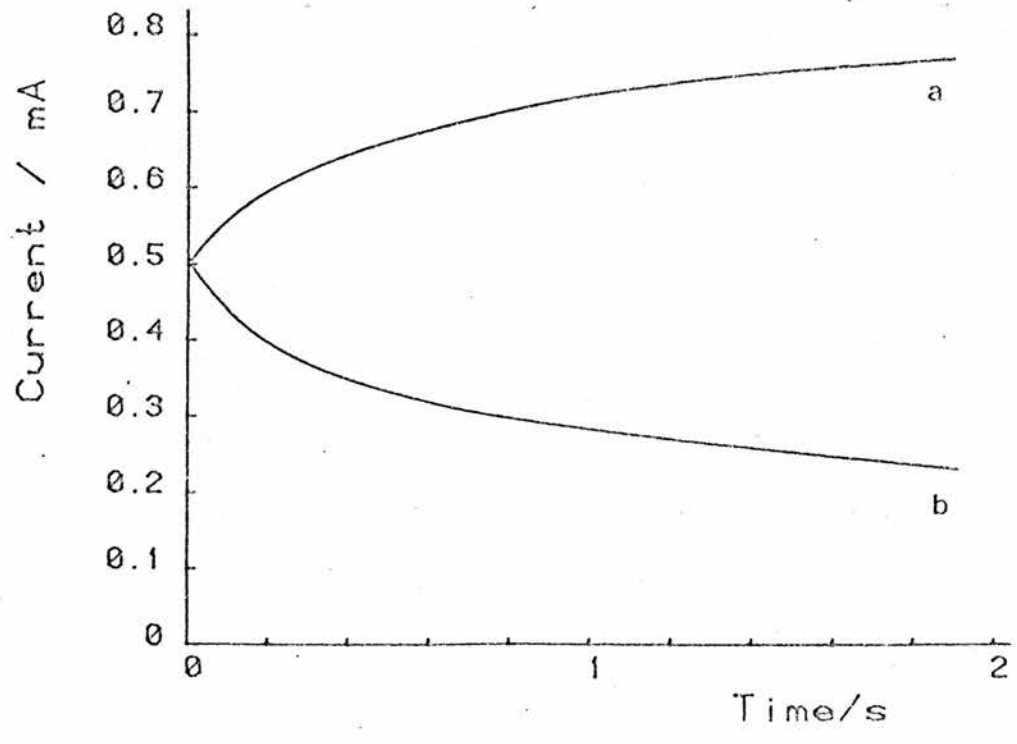

Figure 13: Distribution of 1 mA between two sets of spherical particles (as above). (a) larger spheres (b) smaller spheres.

This suggests that as the electrolysis time increases the larger spheres play a more predominant role in determining the shape of the voltage transient. In order to investigate this further, transients were generated for a two sphere distribution of various pulse lengths, and these were then fitted by the spherical model detailed in appendix III. The fitted parameters obtained are listed below in table 5.

Pulse Length (secs)	D/r^2 $(secs^{-1})*10^{-3}$	$AD^{1/2}$ $(cm^3 secs^{-1/2})*10^{-4}$
10	20.7	1.98
8	22.2	2.02
6	24.3	2.07
4	28.4	2.14
2	46.5	2.16

Table 5

As can be seen the fitted parameters are changing as the pulse length changes. As the pulse length increases then so D/r^2 and $AD^{1/2}$ decrease. This is the same trend as was seen in the experimental data for the longer pulse lengths.

If instead of a distribution of two spheres with equal area being used, one with equal volume or number of spheres is used then the same trend in the parameters is observed.

In a real SSE system the distribution of particles is likely to include more than just two particle sizes, and will probably be a distribution of sizes with more small particles being present than large ones. Such a situation of various particle sizes is simulated by taking the logarithm of the normal distribution with a standard deviation of 0.003, (figure 14), where the radii range from 0.001 cm up to 0.05 cm, with the distribution of particles being skewed towards the lower radius end. The mean radius of the curve is 0.01 cm, with the total weight being 4.6 mg (the surface area of each particle size can be found from the weight of material via its density and volume).

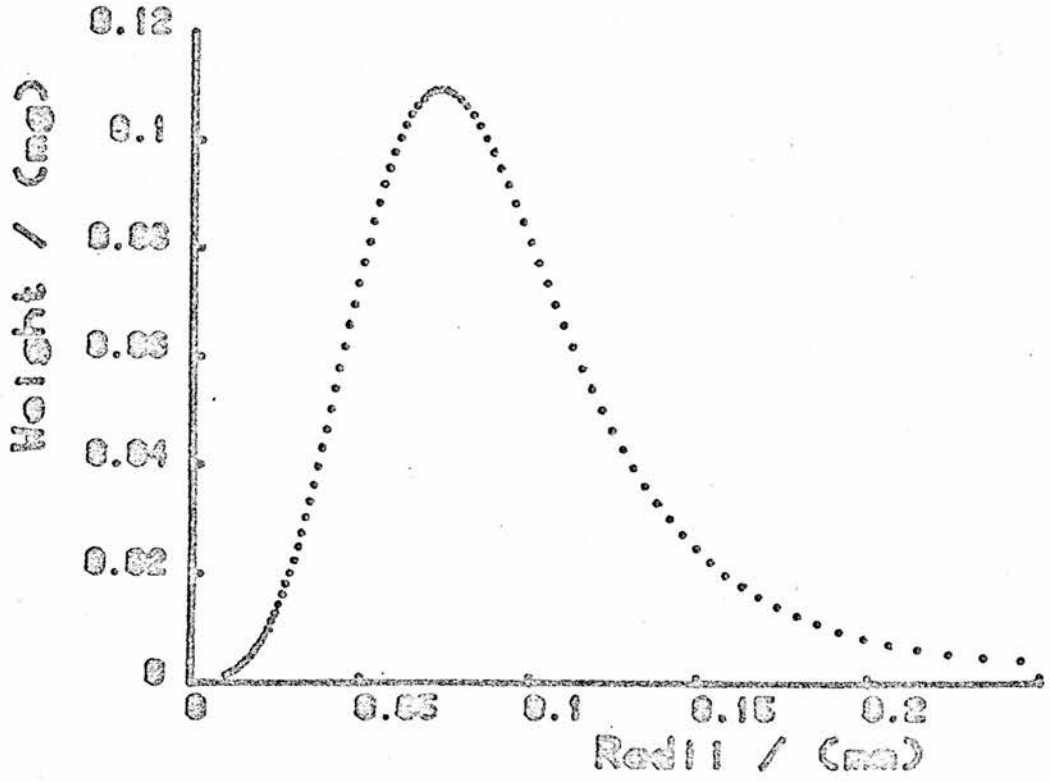

Figure 14: Log of the normal distribution

The voltage transient for the above distribution was obtained by using a similar iterative method to before. An initial value for the overpotential, V, (for a fixed time and total current) was selected, usually being a value calculated for an electrode of uniform particle distribution with radius and weight corresponding to the mean values for the skewed distribution. The current, i_j, associated with each particle of radius, r_j, and area, A_j, was then found, assuming V to be correct. The current distribution, i_j, for the range of radii was thus obtained. If the total current in this distribution (sum of i_j's) was greater (or less) than the total given current, i, then the voltage, V, was altered accordingly and the entire procedure repeated until the total current for the particle distribution was the same as the total current given. The value of V obtained in this manner corresponds to the voltage that would be obtained for the above distribution of particles at a given time.

The transient thus produced is shown in figure 15 and gave the current distribution shown in figure 16. The current has been normalised by dividing the current distribution at each time interval by the current distribution obtained at the smallest time interval, (i.e. 0.02 secs). The cross-over point on the graph occurs at the most probable radius for the skewed distribution.

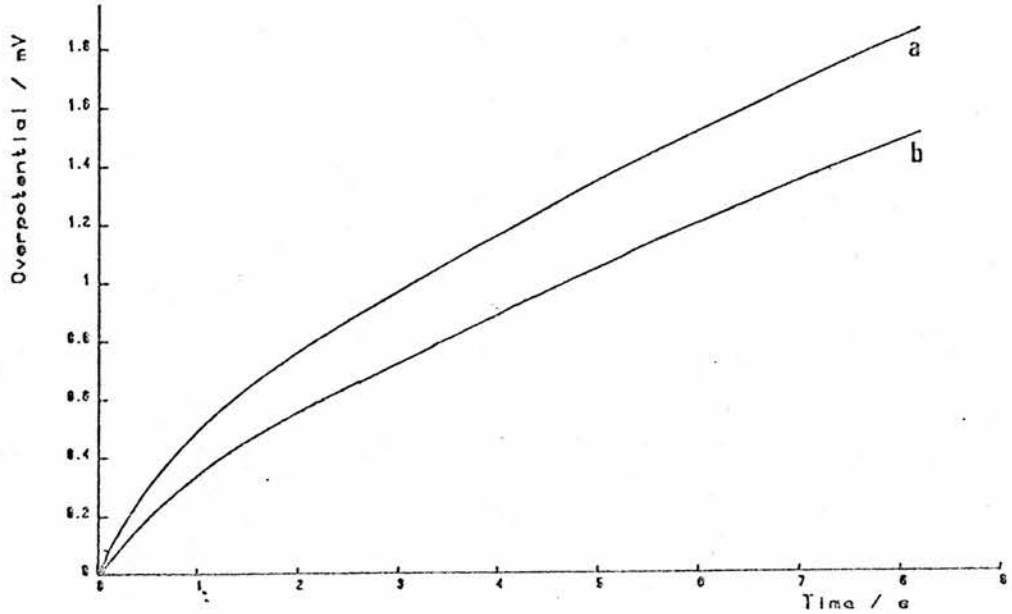

Figure 15: Voltage transient for electrodes consisting of spheres of various radii; (a) spheres of radius 0.01 cm and weight 4.6 mg and (b) spheres of various radii and weights, depicted in figure 14.

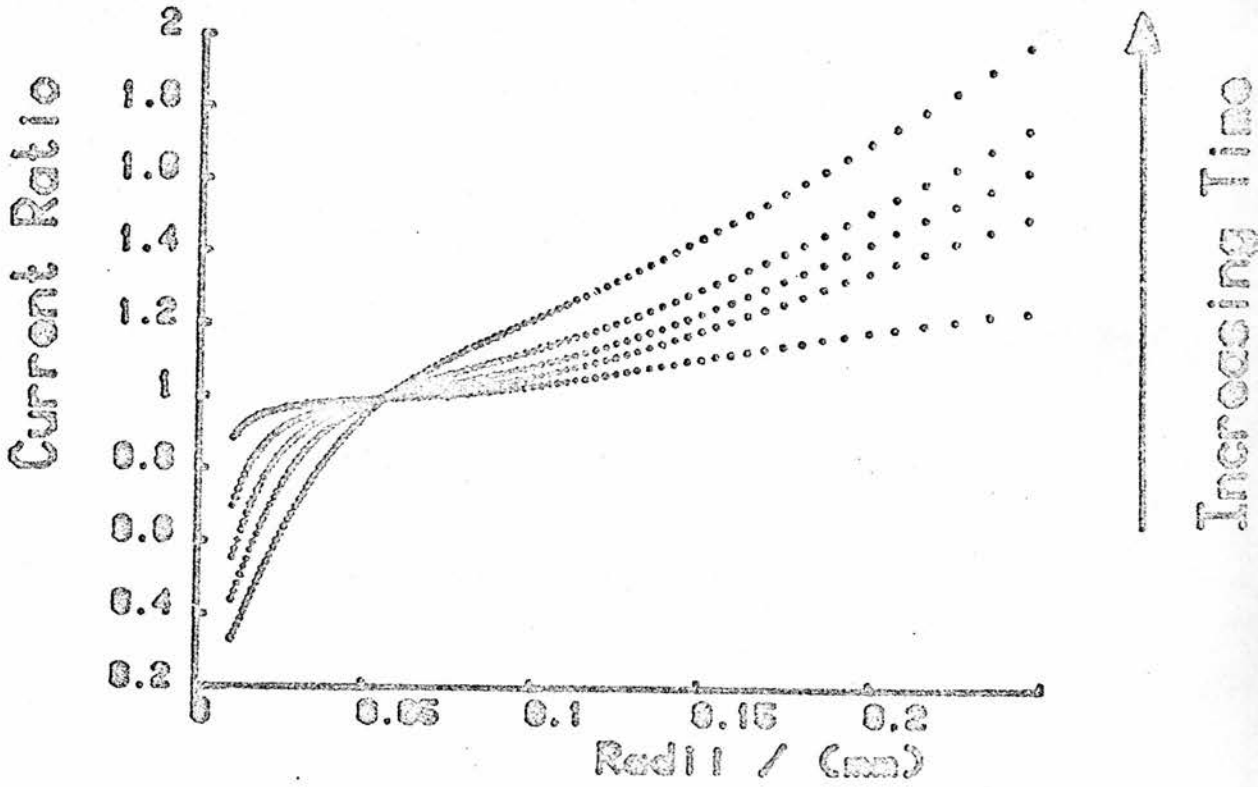

Figure 16: Normalised current for an electrode consisting of spheres of various radii as depicted in figure 14.

As can be seen from figure 16 the current is again distributing itself towards the larger spheres as the pulse progresses. This is the same trend as was observed for the two sphere model and again implies that the larger particles play a greater role in determining the shape of the transient at long times, whereas at short times it is the smaller particles which determine the shape. It can be considered that at the beginning of the pulse, all the particles play an equal role in determining the shape of the transient, but as the pulse progresses, so the smaller particles become "saturated" by the electroactive species and are in effect "switched-out" from playing a part in the shape of the transient, and as more and more of the smaller particles are "switched-out" so more larger particles govern the transient's shape, hence the trend for the measured value of r to increase with pulse length.

It is therefore concluded that particle size distributions form a reasonable basis for the decrease in the fitted value of D/r^2 with increasing pulse length. The value of $AD^{1/2}$ in the generated data decreases as the pulse length increases: this suggests that only the experimental data obtained for long pulse lengths (eg. above 100 secs) is valid as analysed by the finite diffusion models.

This influence of particle size also offers an explanation for the variation of $AD^{1/2}$ and D/r^2 with currents, since a larger current will "switch-out" the smaller particles more rapidly than the smaller currents, hence a decrease in D/r^2 and $AD^{1/2}$ for larger currents is to

be expected.

This trend has also been observed by Scholz et al[21] in their studies of silver diffusion in TaS_2 and TiS_2. They have shown, using optical methods, that the dimensions of the particles play a significant role in determining the rate at which the intercalation process occurs.

Thus to summarise, the trend observed in the fitted parameters is considered due to the distribution of particles sizes in the SSE material and the trend is for the apparent value of particle radius to increase as the pulse length (and height) increases.

5.6 Cell Comparisons.

From the last section it is obvious that it is not possible to obtain absolute values for the fitted parameters, D/r^2 and $AD^{1/2}$, since many factors influence them. However it is possible to make comparative measurements between cells if the pulse length and height used in the measurements are kept the same.

Measurements (using a constant pulse length and height) of the variation of these parameters with intercalation level, temperature, etc., permits the effect of the variables on cell response to be evaluated, provided that the same cell is used throughout a series of measurement. Similarly comparisons of the mixed phase electrodes

formed under different conditions (e.g. with different ratios of components) are possible provided that the same sample of SSE material is used. i.e. the particle distribution (of sizes and shapes) are very similar in each cell.

Comparative measurements of the chemical diffusion coefficient for different SSE materials is possible only if the SSE materials have very similar distributions of particle sizes and shapes, i.e. the SSE material must be of a similar nature and type and be prepared to as near an identical particle distribution as possible.

In order to confirm that consistent determinations of D/r^2 and $AD^{1/2}$ could be obtained a series of pulses were carried out on three different cells of identical construction using the same sample of NbS_2. A pulse length of 2000 secs and pulse height of 20 microampes was chosen for the measurements. The parameters obtained are listed in table 6 below. The three cells all had a $NbS_2/Ag_6I_4WO_4$ ratio of 1/2.

Cell	Weight of NBS_2 (mg)	D/r^2 ($secs^{-1}$) $*10^{-4}$	$AD^{1/2}$ ($cm^3 secs^{-1/2}$) $*10^{-4}$	Normalised $AD^{1/2}$ ($cm^3 secs^{-1/2} g^{-1}$) $*10^{-3}$
1	9.143	0.856	0.141	1.941
2	10.252	0.210	0.190	1.854
3	9.748	0.612	0.173	1.770

Table 6.

The values of $AD^{1/2}$ were normalised by dividing them by the weight of SSE material in each cell. As can be seen, the values for D/r^2 were within the range 0.56 ± 0.30 $s.^{-1}$ The values for $AD^{1/2}$ were within 4.6% of each other which is encouraging since the error introduced from weighing (in constructing the cells) could be as high as 4%.

These results indicated that valid comparisons between cells of $AD^{1/2}$ and D/r^2 using the finite diffusion model was possible providing that the particle distribution of the SSE material was the same, and that the pulse length and height were kept constant.

5.7 Conclusions and Further Work.

In conclusion then, of the four different models studied,

a) Semi-Infinite Diffusion.

b) Finite Linear Diffusion.

c) Spherical Diffusion.

d) Cylindrical Diffusion.

the semi-infinite case was found to be the least appropriate under the experimental conditions used, while the other three were found to be applicable. The crystal structure of the SSE material used in the working electrode is likely to determine which of these is the most suitable.

For the SSE material studied here, NbS_2 has a structure which allows diffusion in two-dimensions and so the cylindrical model is the most suitable for this application.

When a range of pulses were applied, the cylindrical model could not satisfactorily describe transients of different pulse lengths and heights. The model requires a uniform particle size and in the case of the SSE material used here, we conclude that the trend introduced by a distribution of particle sizes is for the effective radius, (as measured from the transient), to increase as the pulse length (or height) increases. For pulse lengths greater than 100 secs the trends in the fitted parameters can be understood and explained. For pulse

lengths less than 100 secs, bounded diffusion models are not satisfactory for the particle sizes involved in the present survey. More work requires to be done on the question of the influence of particle size on the form of the transient at short times.

On the assumption that D is constant for a particular SSE material at a fixed level of intercalation, then the variable which determines the response of a mixed phase electrode is the area of contact between the phases.

Other workers have also noted anomalous behaviour at short times.[24] It is possible that early in the pulse a small concentration of silver ad-atoms are formed, or that other surface processes distort the expected shape of the transient in this region.

If the duration and height of the pulse is kept constant and long pulse lengths are used then very good comparisons of the interfacial contact area can be made between different cells. This provides a technique by which different cell configurations can be studied accurately and comparisons made, as has been done in Chapter 6.

References.

[1] Atlung, S., Zachau-Christiansen, B., West, K., Jacobsen, T., "The composite insertion electrode. Theoretical part. Equilibrium in the insertion compound and linear potential dependence.", to be submitted to J. Electrochem. Soc.

[2] Atlung, S., B., West, K., Jacobsen, T., "Dynamic aspects of solid solution cathodes for electrochemical power sources.", J. Electrochem. Soc., Vol. 126, No. 8, 1979, p. 1311.

[3] Atlung, S., B., West, K., Jacobsen, T., "Dynamic considerations in the design of batteries with insertion cathodes.", 'Materials for advanced batteries', Editors Murphy, Broadhead and Steele, NATO Conference Series, 1980, Plenum Publishing Corp., New York, p. 275.

[4] de Levie, R., "Electrochemical response of porous and rough electrodes", in 'Advances in electrochem. and electrochem. engineering', Eds. P. Delahay, C.W. Tobias, Vol. 6, 1967, Pub. J. Wiley & Sons, New York, London, p. 329.

[5] Bonino, F., Lazzari, M., Vincent, C.A., Wandlass, A.R., "Electro-intercalation and diffusion of silver in tantalum disulphide.", Solid State Ionics, Vol. 1, 1980, p. 311

[6] Bottelberghs, P.S., Broers, G.H.J., "Diffusion and electro-migration in solid Na_2WO_4.", Electrochemica Acta., Vol. 21, 1976, p. 719.

[7] Winn, D.A., Shemilt, J.H., Steele, B.C.H., "Titanium disulphide: A solid solution electrode for sodium and lithium.", Mat. Res. Bull., Vol. 11, 1976, p. 559.

[8] Scholtens, B.B., "Diffusion of silver in vanadium bronzes", Mat. Res. Bull., Vol. 11, 1976, p. 1553.

[9] Bonino, F., Lazzari, M., Patriarca, M., Scrosati, B., Voso, M.A., "Behaviour of transition metal disulphides as intercalation electrodes in solid-state cells.", Solid State Ionics, Vol. 6, No. 1, 1982, p. 15.

[10] Wen, C.J., Boukamp, B.A.,Huggins, R.A.,Weppner, W., "Thermodynamic and mass transport properties of LiAl.", J. Electrochem. Soc., Vol. 126, No. 12, 1979, p. 2258.

[11] Weppner, W., Huggins, R.A., "Determination of the kinetic parameters of mixed-conducting electrodes and application to the system Li_3Sb.", J. Electrochem. Soc., Vol. 124, No. 10, 1977, p. 1569.

[12] Smith, M.J., "Electrochemical Studies of Solid Solution Electrodes.", Ph.D. Thesis, University of St.Andrews, 1982

[13] Weppner, W., Huggins, R.A., "Electrochemical investigation of the chemical diffusion, partial ionic conductivities, and other kinetic parameters in Li_3Sb and Li_3Bi.", J. of Solid State Chem., Vol. 22, 1977, p. 297.

[14] Nagelberg, A.S., Worrell, W.L., "Electrochemical determination of the chemical potential and diffusivity of sodium in Na_xTaS_2 at 300 K", in 'Proceedings of the Symposium on Electrode Materials and Processes for Energy Conversion and Storage', Eds. McIntyre, Srinivasen and Hill, Electrochem. Soc., Princeton, 1977, p. 847.

[15] Basu, S., Worrell, W.L., "Electrochemical determination of the chemical potential of lithium in Li_xTaS_2 at 300 K", in 'Proceedings of the Symposium on Electrode Materials and Processes for Energy Conversion and Storage', Eds. McIntyre, Srinivasen and Hill, Electrochem. Soc., Princeton, 1977, p. 861.

[16] Basu, S., Worrell, W.L., "Chemical diffusivity of lithium in Li_xTaS_2 and Li_xTiS_2 at 30°C", in 'Fast Ion Transport in Solids', Eds. Vashishta, Mundy, Shenoy, North-Holland Press Amsterdam, 1979, p. 149.

[17] Armand, M., "Materiaux d'Electrode a Couple Redox Interne.", Ph.D. Thesis, University Grenoble, 1978.

[18] Weppner, W., Huggins, R.A., "Electrochemical methods for determining kinetic properties of solids.", Annual Review of Materials Science, Vol. 8, 1978, p. 269.

[19] Weppner, W., "Kinetic studies of mixed-conducting solids.", Solid State Ionics, Vol. 3/4, 1981, p. 1.

[20] Patriarca, M., Voso, M.A., Scrosati, B., Bonino, F., Lazzari, M., "Behaviour of transition metal disulphides as intercalation electrodes in solid state cells.", Solid State Ionics, 1982, Vol. 6, No. 1, p. 15.

[21] Private communication from Atlung, S., November 1983.

[22] Scholz, G., Joensen, P., Reyes, J.M., Frindt, R.F., "Intercalation of Ag in TaS_2 and TiS_2", Physica, Vol. 105b, 1981, p.214

[23] Chianelli, R.R., Scanlon, J.C., Rao, B.M.L, "In situ studies of electrode reactions: the mechanism of lithium intercalation in TiS_2", J. of Solid State Chem., Vol. 29, 1979, p. 323

[24] Green, M., "Electrochromic display cells based on the tungsten bronzes", in 'Electrochromism and Electrochromic displays' Ed. B. Scrosati, 1982, p. 39.

6 Galvanostatic Pulse Measurements on cells.

6.1 Introduction

As described in Chapter 1, the properties of the mixed phase region are dependant upon many factors, e.g. depth, component ratio, relative sizes and conductances of the two phases, etc. In the first part of this chapter the effect of varying the component ratio has been studied, using the galvanostatic pulse technique developed in Chapter 5, to measure the effective contact area between the phases in various cells. This work ties up with the computer model of Chapter 3. In the second section of this chapter the effect on the contact area of heating the cell has been studied.

6.2 The Effect of Composition Ratio on the Effective Contact Area.

Various cells containing different $NbS_2/Ag_6I_4WO_4$ ratios in the working electrode were constructed and, after being intercalated to a fixed level (i.e. $Ag_{0.05}NbS_2$) and equilibrated, pulsed with 20 microamperes for 2000 secs. All the transients produced for this work are stored on an accompanying magnetic tape, (tape A), and appendix V gives a directory of the tape.

6.2.1 Results of Galvanostatic Measurements.

The transients obtained for each cell were fitted by the cylindrical diffusion model, (as described in appendix III and chapter 5), and table 1 shows the values obtained from this fit. The values of $AD^{1/2}$ have been normalised by dividing by the total weight of NbS_2 in the cell.

Cell	Ratio of NbS_2 to $Ag_6I_4WO_4$	D/r^2	$\frac{AD^{1/2}}{\text{Wt. of } NbS_2}$
		$secs^{-1}$ $*10^{-4}$	$cm^3 sec^{-1/2} g^{-1}$ $*10^{-3}$
1	2/1	0.696	0.563
2	2/1	0.620	0.409
3	2/1	0.610	0.543
4	1/1	0.708	1.170
5	1/1	0.644	1.263
6	1/2	0.856	1.939
7	1/2	0.210	1.854
8	1/2	0.612	1.772
9	1/3	0.465	1.922
10	1/3	0.356	1.941
11	1/10	2.325	0.798
12	1/10	0.524	1.042
13	1/18	0.649	0.619
14	1/18	1.094	0.718

Table 1

As can be seen from table 1, the values of D/r^2 are all approximately the same, whereas the values for $AD^{1/2}$ have a distinct trend. This can be seen more clearly in figure 1 and indicates that the optimum composition ratio for a mixed phase electrode of the components studied is in the region of 20-35% by weight of NbS_2.

This curve is of the same form as that obtained in Chapter 3 for a mixed phase region where the ratio of particle sizes was approximately 3:1 in terms of NbS_2 to $Ag_6I_4WO_4$ (i.e. figure 2). This suggests therefore that the maximum effective contact area between the $NbS_2/Ag_6I_4WO_4$ is obtained when the composition of the mixed phase region is approximately 25%. No direct comparison between the curves is possible however, because the model developed in chapter 3 is for isotropic particles, whereas the NbS_2 system being studied here is anisotropic. It was also not possible to determine the relative sizes of the NbS_2 and $Ag_6I_4WO_4$ particles from SEM photographs because of the large distribution of sizes involved.

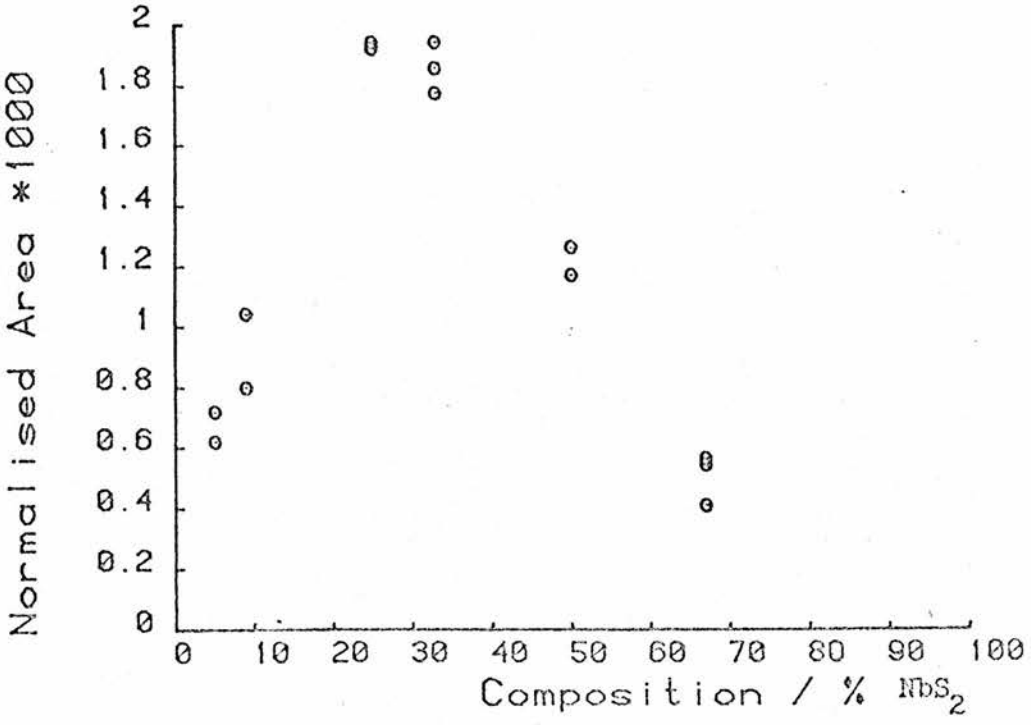

Figure 1: Effective Contact Area ($AD^{\frac{1}{2}}$) as a function of composition.

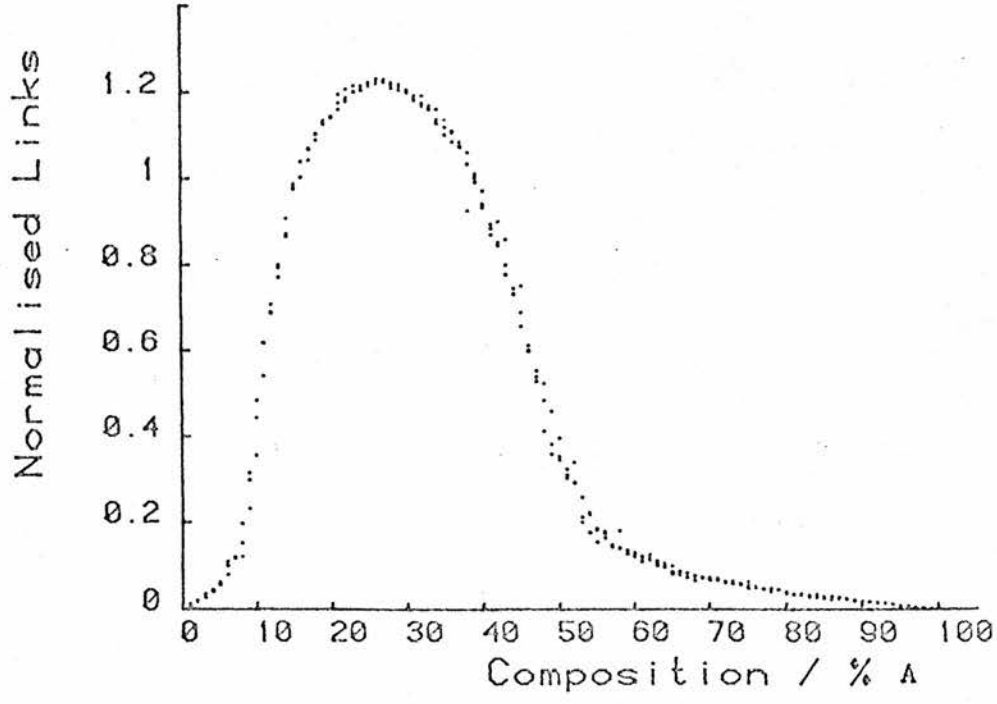

Figure 2: Normalised links as a function of composition for a particle size ratio of A:B = 3:1.

6.3 The Effect of Heating on the Effective Contact Area.

It was considered that the effective area of contact between the phases might be increased (and hence the electrode response improved) by annealing the mixed phase system at a temperature at which the vitreous electrolyte would flow and possibly wet the SSE particles. This procedure would also have the effect of raising the ionic conductivity by improving electrolyte-electrolyte grain contacts.

The melting point of the $Ag_6I_4WO_4$ electrolyte was found to be 293-295^{o}C and in order to determine the best temperature range for heating the cells, a number of scanning electron microscope (SEM) photographs of heated samples of pure electrolyte were taken. These are shown in plates 1 to 6.

Plates 1 and 2 show the unheated electrolyte: the particles have sharp pointed edges with very little coalescence between the individual particles. Plates 3 and 4 show the electrolyte after it has been heated at 300^{o}C (i.e. just above its melting point) for 30 mins, and as can be seen the particles have now very few sharp edges and have all melted into one large mass. An interesting phenomenon shown in these plates, are the large holes and craters that appear and are indicative of coalescence of voids, as the electrolyte melted. In plates 5 and 6 the electrolyte has been heated at 290^{o}C (i.e. just below its melting point) for 30 mins, and as can be seen the sample shows some characteristics of both previous cases, i.e. some sharp edged discrete particles and some coalescence of the material.

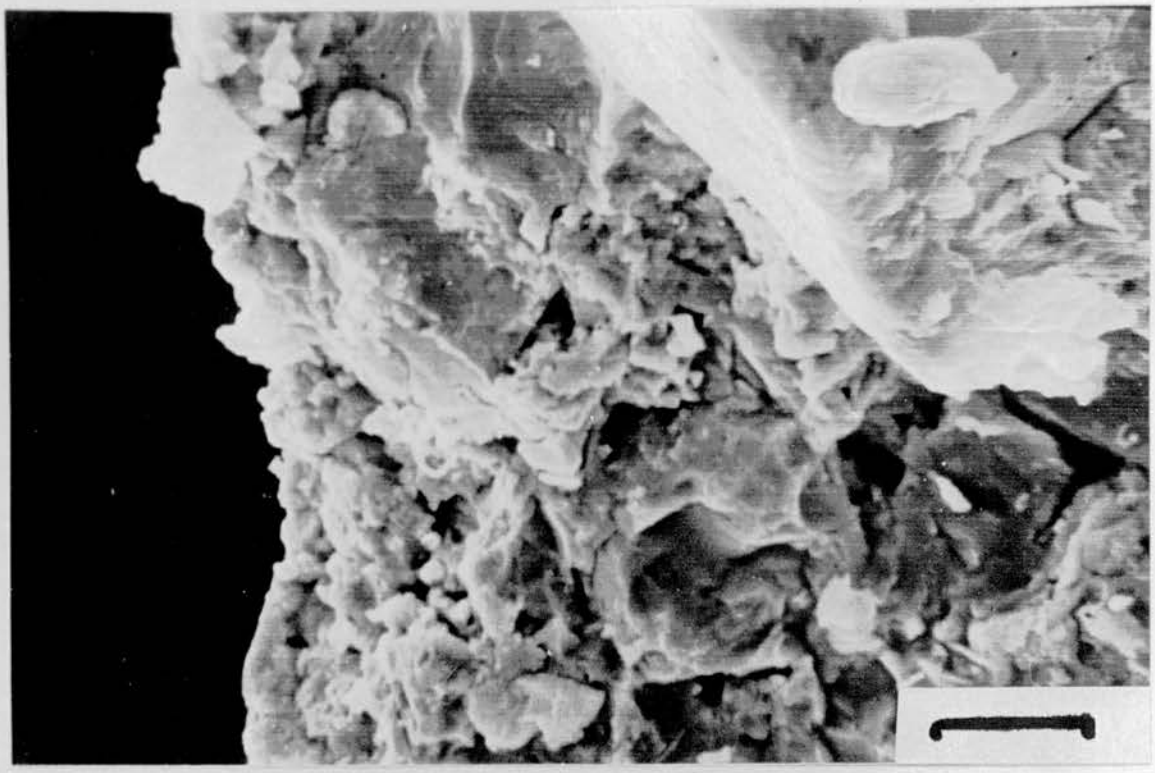

Plate 1: $Ag_6I_4WO_4$ electrolyte. No heat treatment. (10μ)

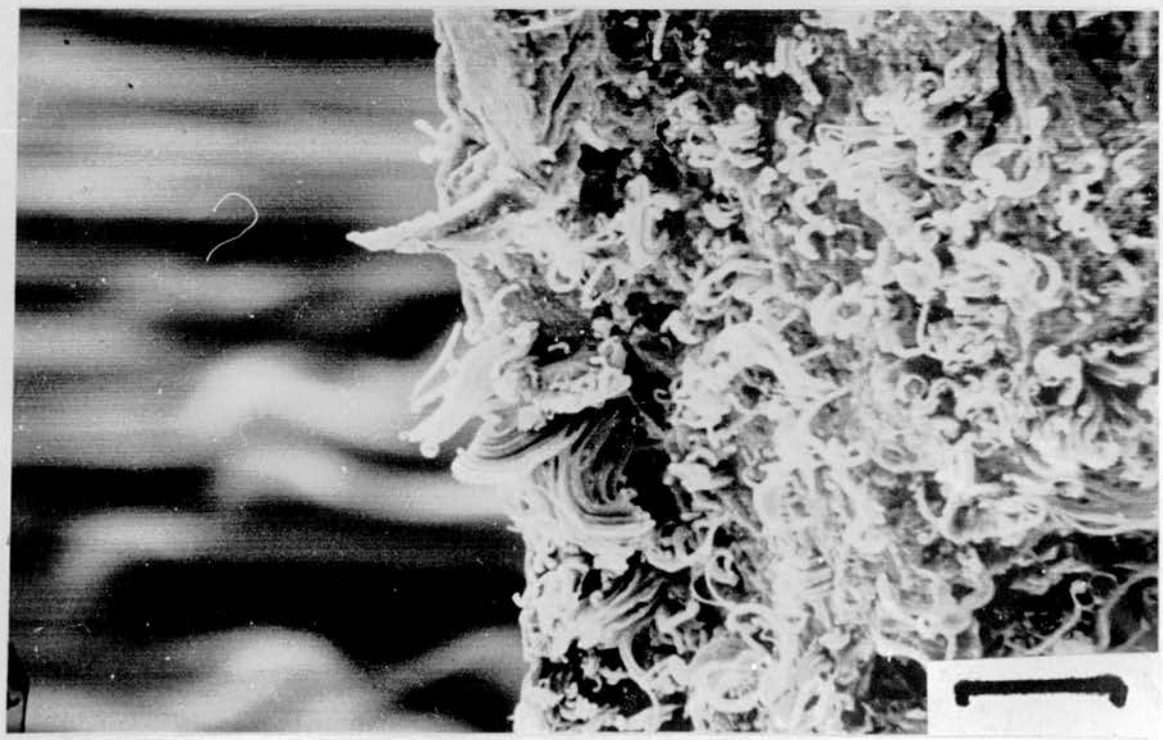

Plate 2: $Ag_6I_4WO_4$ electrolyte. No heat treatment. (20μ)

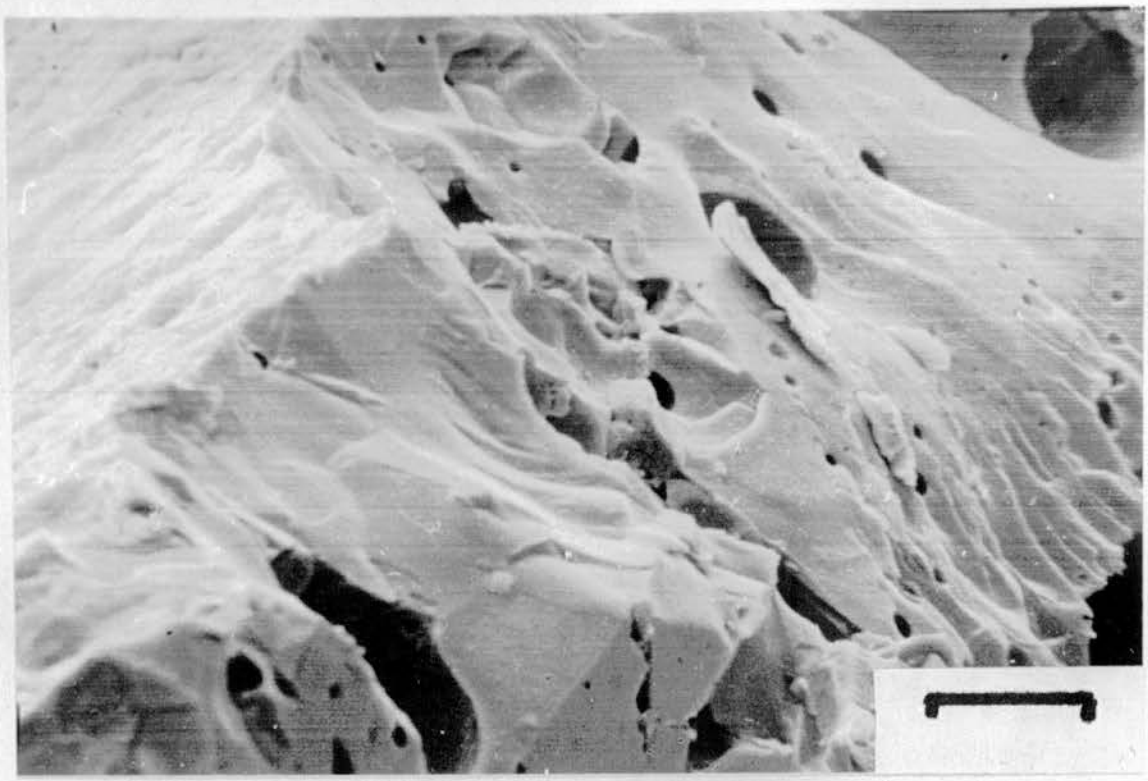

Plate 3: $Ag_6I_4WO_4$ electrolyte. 300°C
heat treated for 30 mins. (20μ)

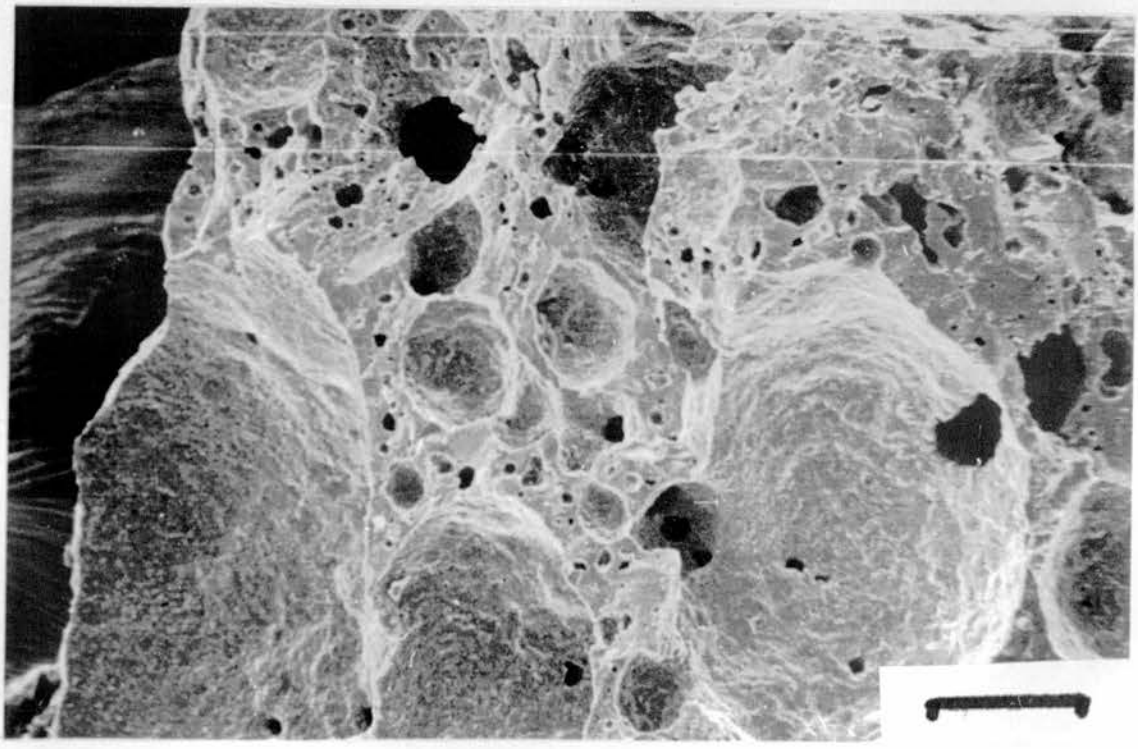

Plate 4: $Ag_6I_4WO_4$ electrolyte. 300°C
heat treated for 30 mins. (100μ)

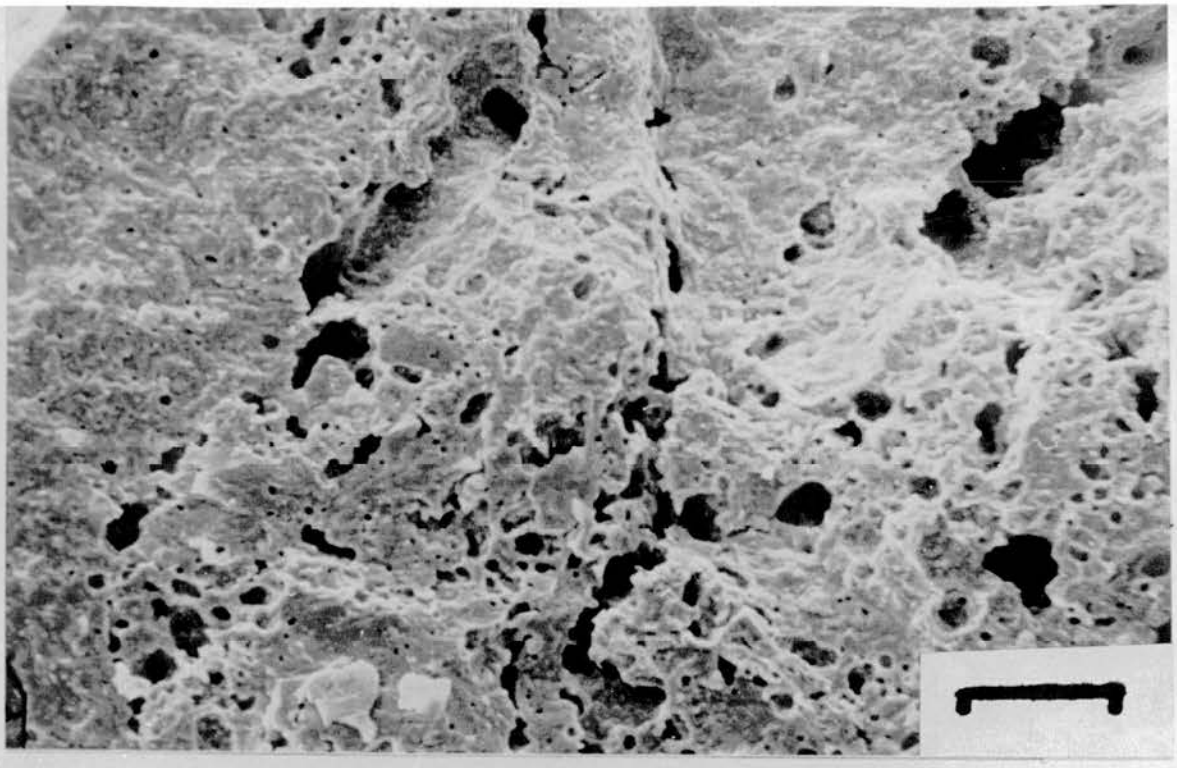

Plate 5: $Ag_6I_4WO_4$ electrolyte. 290°C
heat treated for 30 mins. (40μ)

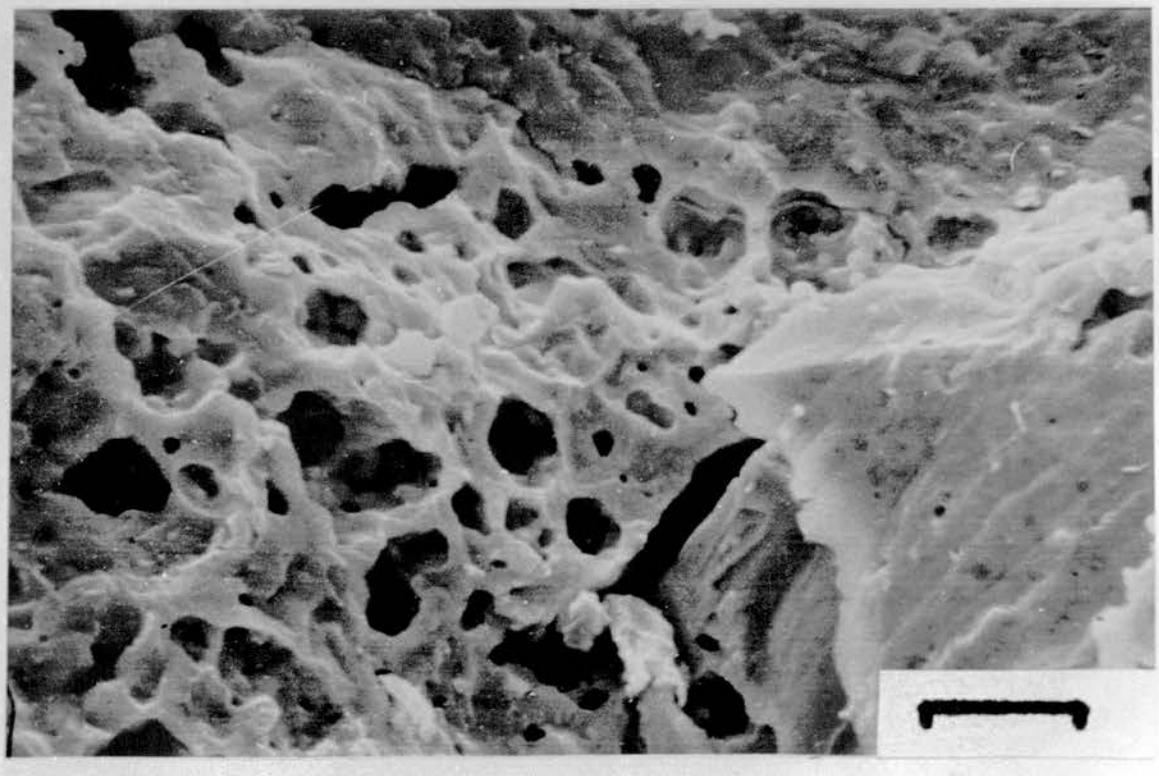

Plate 6: $Ag_6I_4WO_4$ electrolyte. 290°C
heat treated for 30 mins. (10μ)

In order to determine the 'wetting' effect of the electrolyte on the particles of NbS_2, a number of SEM photographs were taken of sections of a composite of $NbS_2/Ag_6I_4WO_4$ heated at 290°C and 300°C, plates 7 to 12.

Plates 7 and 8 show a unheated 'green' section and shows that the two phases have very little intimate contact. The electrolyte particles can be seen to have sharp edges characteristic of an unheated section. Plates 9 and 10 show the composite after it has been heated for 30 mins at 300°C, and as can be seen the electrolyte has melted, forming the characteristic craters and coalesced and flowed around the NbS_2 particles, apparently forming a much larger and more intimate area of contact. In plates 11 and 12 the composite has been heated to 290°C for 30 mins, and shows an intermediate type of structure with some electrolyte particles being discrete with sharp edges, but others have melted and coalesced around the NbS_2 forming a larger interfacial area.

In view of the above evidence it was decided to heat the cells at 290°C for 15 mins; if the cell was heated for longer or at a higher temperature then there was a possibility of the cell deforming and, in extreme cases short circuiting.

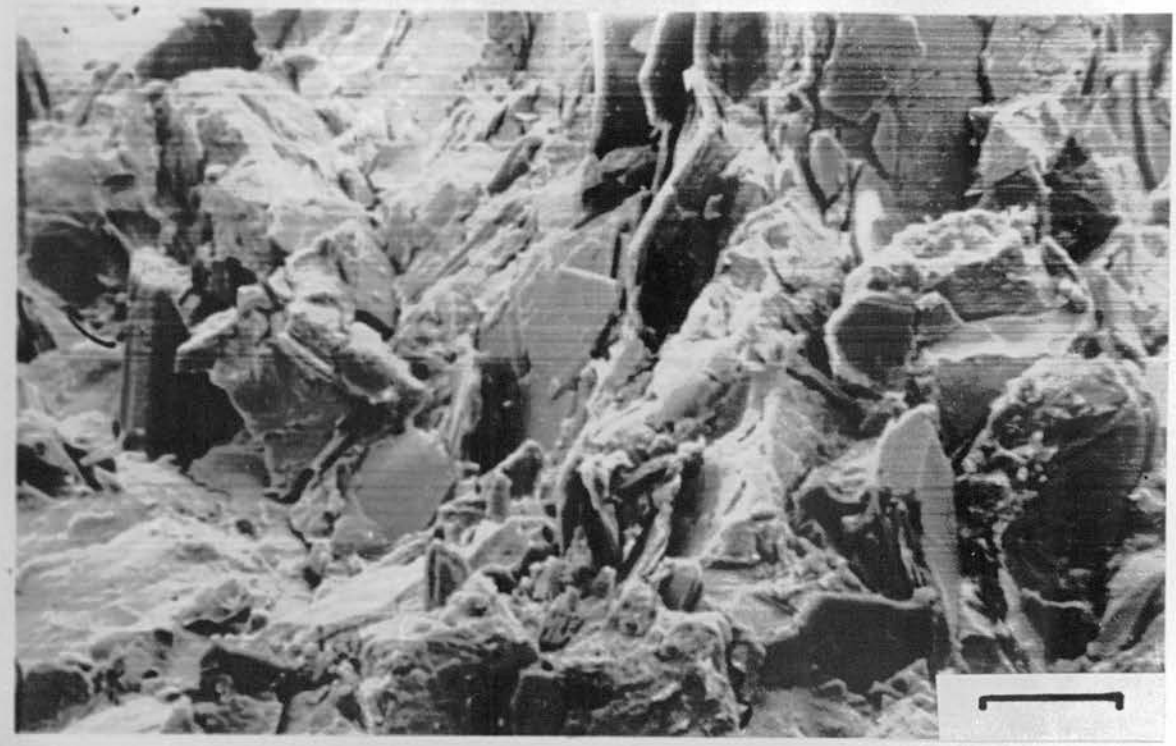

Plate 7: 'Green Pill', no heat treatment. (20μ)

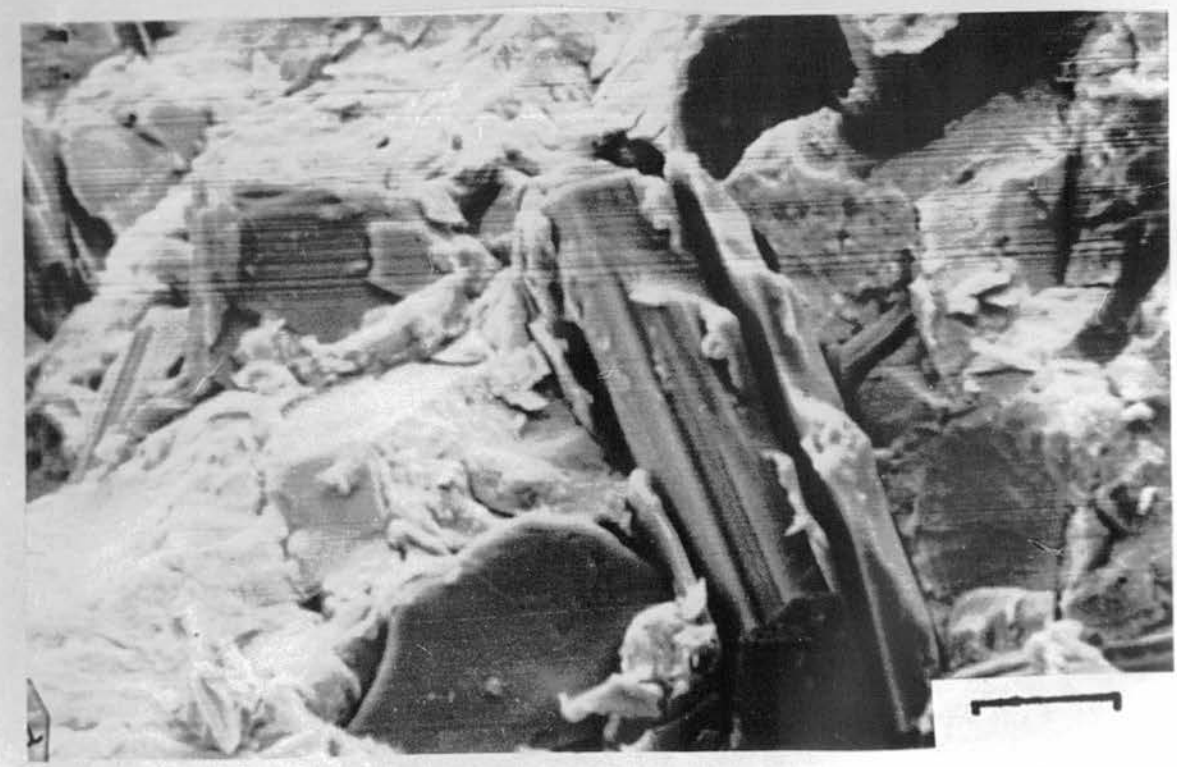

Plate 8: 'Green Pill', no heat treatment. (10μ

Plate 9: 300^{0}C heat treated for 30 mins. (20μ)

Plate 10: 300^{0}C heat treated for 30 mins. (20μ

Plate 11: 290^{0}C heat treated for 30 mins. (20μ)

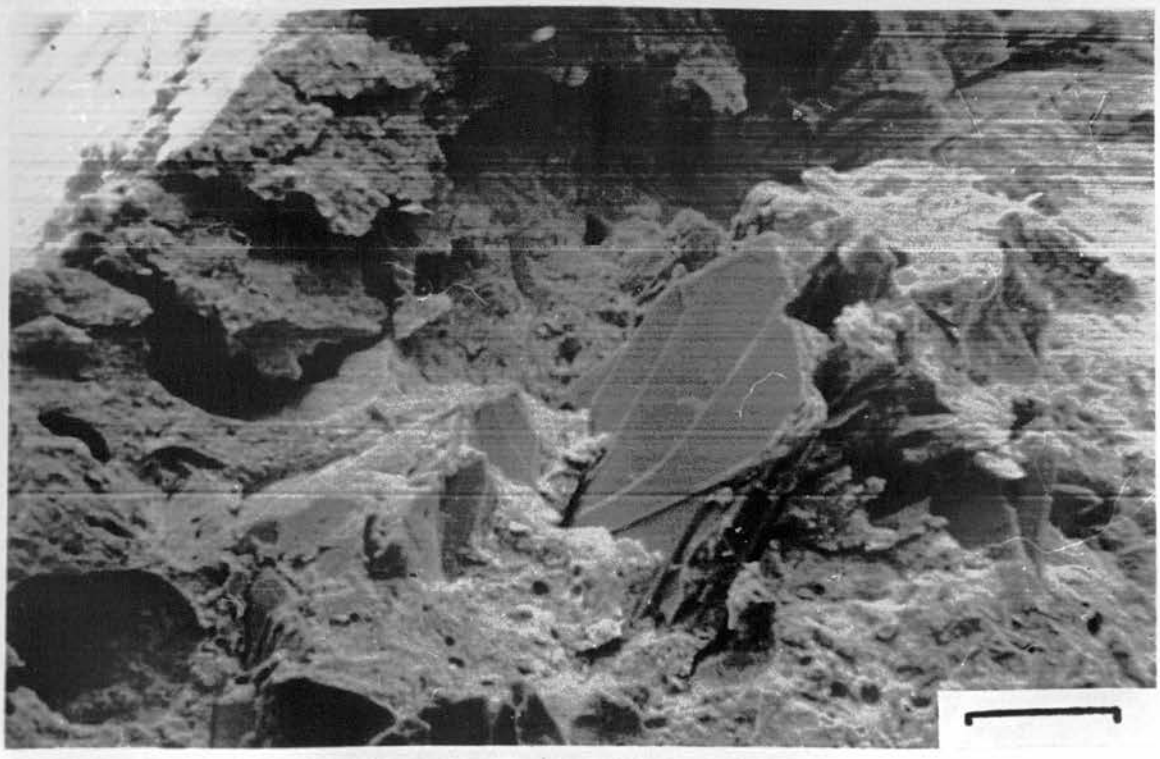

Plate 12: 290^{0}C heat treated for 30 mins. (20μ)

6.3.1 Results of Galvanostatic Measurements.

Three cells were constructed with a $NbS_2/Ag_6I_4WO_4$ ratio of 1/2 and intercalated to a fixed level, i.e. $Ag_{0.05}NbS_2$. The cells were then pulsed with 20 microamperes for 2000 secs and the transients thus obtained were stored on magnetic tape. Next, the cells were heated, in a nitrogen atmosphere, for 15 mins at 290°C, before again being pulsed with 20 microamperes for 2000 secs. It was necessary after heating, to re-intercalate the cells to a fixed level because it was found that the intercalation level of the cell had increased with the heat treatment. It is thought that this is due to some reaction occurring at the $NbS_2/Ag_6I_4WO_4$ interface which liberates a small amount of free silver.

It is noted here that, after heating, the cells were very much more brittle than before and had a tendency to crack or break when being handled, this effect was more pronounced at higher temperatures.

The transients obtained, are stored on the accompanying magnetic tape, (tape A), and a directory of the tape can be found in appendix V. The transients were fitted by the cylindrical diffusion model, described in appendix III, and the values obtained for the fitted parameters are shown in table 2.

Cell	Before heat treatment $\frac{AD^{1/2}}{\text{Wt. of } NbS_2}$ $cm^3 secs^{-1/2} g^{-1}$ $*10^{-3}$	After heat treatment $\frac{AD^{1/2}}{\text{Wt. of } NbS_2}$ $cm^3 secs^{-1/2} g^{-1}$ $*10^{-3}$	% increase in effective area
1	1.939	2.860	48
2	1.854	2.756	49
3	1.772	2.686	52

Table 2

As can be seen from the table the effective contact area between the unheated and heated cells has been increased significantly, with the average increase in the area being of the order of 50%.

6.4 Conclusions.

To conclude, it has been demonstrated that valid comparisons of the effective interfacial area between the electrode and electrolyte phases can be made between different cells using the galvanostatic pulse technique developed in Chapter 5.

It has also been demonstrated that the effective contact area can be maximised by using an optimum composition of constituents, (i.e. for the materials being used here, the maximum area is obtained when 25% (by weight) of the total composite electrode consists of NbS_2), and/or by tempering the cell for a period just below the melting point of the electrolyte. In the case demonstrated here the increase in area due to tempering is in the order of 50%.

Bonino et al[1] have shown that another factor influencing the interface morphology (and hence the effective contact area) is the pressure at which the working electrode was initially pressed. They have shown that the orientation of the layered SSE particles becomes less favourable (for diffusion) as the applied pressure is increased, and that for large pressures the SSE particles are orientated perpendicular to the direction of the applied pressure. Since diffusion occurs along the van der Waals gap between the SSE layers, this orientation will be disfavourable for diffusion if it occurs in the same direction as the pressure was applied, i.e. as is the case in most applications. Since, in all the cells studied in this work, the applied pressure was kept constant (and low), this factor will not influence the results obtained, but interesting results could be obtained by applying the galvanostatic pulse technique to cells constructed under various pressures.[2]

Thus for any cell comprising of particular materials, the maximum power that can be drawn from the cell can be increased by maximising the contact area by either of the methods described above.

References.

[1] Bonino, F., Lazzari, M., Mari, C.M., Vincent, C.A., "Interfacial properties in silver/silver glassy electrolyte/insertion electrode cells.", Solid State Ionics, Vol. 9&10, 1983, p. 677.

[2] Armstrong, R.D., Dickinson, T., Willis, P.M., "The impedance of the Pt/Ag_4RbI_5 and C/Ag_4RbI_5 interphases at anodic potentials", Electroanal. Chem. and Interfacial Electrochem., Vol. 48, 1973, p. 47.

Appendix I

Mathematics of Diffusion.

1 Introduction.

Mass transport in a chemical system may occur as a result of various perturbing forces. These can be classified under :-

a) Migration; as a result of an applied electric field.

b) Diffusion; as a result of a chemical potential gradient.

c) Convection; as a result of external mechanical forces being applied.

Experimental conditions are normally chosen so as to maximise the effect of the process under investigation and minimise the effect of the other two. In the present investigation transport due solely to the diffusion process is of interest.[1,2]

It is normally assumed that the driving force behind the diffusion process, the chemical potential gradient, can be approximated by the concentration gradient. In other words, the rate of transfer of diffusing substance through unit area of a section is proportional to the concentration gradient measured normal to the section. i.e.

$$F = - D \frac{\partial C}{\partial x} \qquad [1]$$

where F is the rate of transfer per unit area of section, C the concentration of diffusing substance, x the space coordinate measured normal to the section and D is called the diffusion coefficient. Equation [1] is known as Fick's first law of diffusion and for ideal systems D can be assumed to be constant.

If a disturbance is imposed upon the system which produces a concentration gradient somewhere in the system (which was previously at equilibrium) a diffusion process will occur which will eventually reach a new steady state condition. The fundamental differential equation which describes the above process is known as Fick's Second Law of Diffusion and will now be derived using equation [1] above.(1)

Consider an element of volume in the form of a rectangular parallelepiped whose sides are parallel to the axis of coordinates and are of lengths 2dx, 2dy, 2dz. Let the centre of the element be at P(x,y,z), where the concentration of diffusing substance is C. Let ABCD and A'B'C'D' be the faces perpendicular to the axis of x as in fig.1

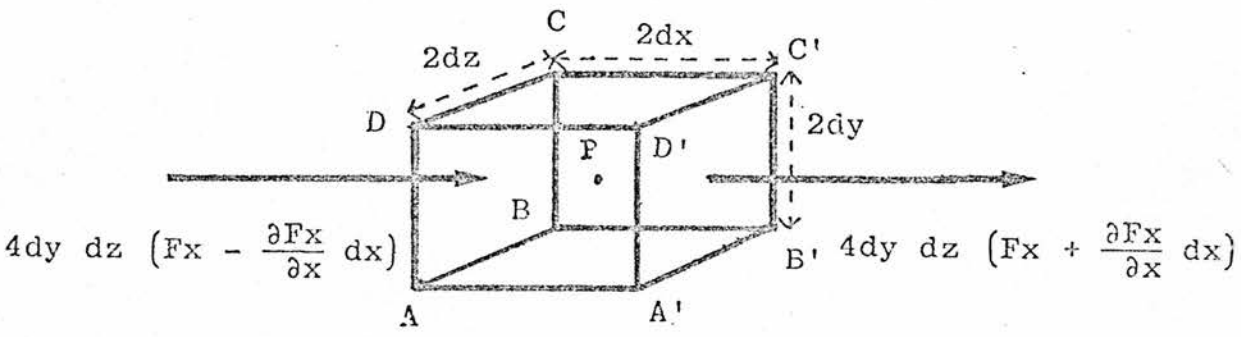

Figure 1

Then the rate at which diffusing substance enters the element through the face ABCD in the plane (x,dx) is given by,

$$4dydz(F_x - \frac{\partial F_x}{\partial x} dx)$$

where F_x is the rate of transfer through unit area of the corresponding plane through P. Similarly the rate of loss of diffusing substance through the face A'B'C'D' is given by,

$$4dydz(F_x + \frac{\partial F_x}{\partial x} dx)$$

The contribution to the rate of increase of diffusing substance in the element from these two faces is thus equal to,

$$-8dxdydz \frac{\partial F_x}{\partial x}$$

Similarly from the other faces we obtain,

$$-8dxdydz \frac{\partial F_y}{\partial y} \quad \text{and} \quad -8dxdydz \frac{\partial F_z}{\partial z}$$

But the rate at which the amount of diffusing substance in the element increases is also given by,

$$8dxdydz \frac{\partial C}{\partial t}$$

and hence we have,

$$-\frac{\partial C}{\partial t} + \frac{\partial F_x}{\partial x} + \frac{\partial F_y}{\partial y} + \frac{\partial F_z}{\partial z} = 0$$

if the diffusion coefficient is constant F_x, F_y and F_z are given by [1] and thus,

$$\frac{\partial C}{\partial t} = D\{ \frac{\partial^2 C}{\partial x^2} + \frac{\partial^2 C}{\partial y^2} + \frac{\partial^2 C}{\partial z^2} \} \qquad [2]$$

If diffusion is one-dimensional (i.e. if there is a gradient of concentration only along the x-axis) then [2] reduces to,

$$\frac{\partial C}{\partial t} = D \frac{\partial^2 C}{\partial x^2} \qquad [3]$$

which is known as Fick's Second Law of Diffusion.

Four separate diffusion models were considered, these were,

a) Semi-Infinite Linear Diffusion.

b) Finite Linear Diffusion.

c) Spherical Diffusion.

d) Cylindrical Diffusion.

The solutions to equation [2] for each of the four models will now be derived below when applied to the experimental conditions used here. The experimental conditions were that a short, cathodic, galvanostatic pulse was applied across the working counter electrodes of the cell. (fig 2.b)) As the current pulse was applied the voltage transient between the working and reference electrodes was recorded with respect to time. (fig 2.b)) After the cathodic, galvanostatic pulse was applied an identical anodic pulse was applied in order that the equilibrium concentration (C_0) of electroactive species not be changed by repeated measurements.

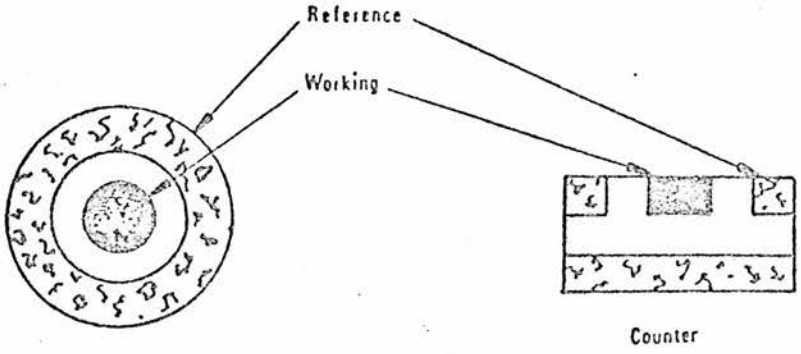

Figure 2 (a): Cell structure of 3 electrode cell

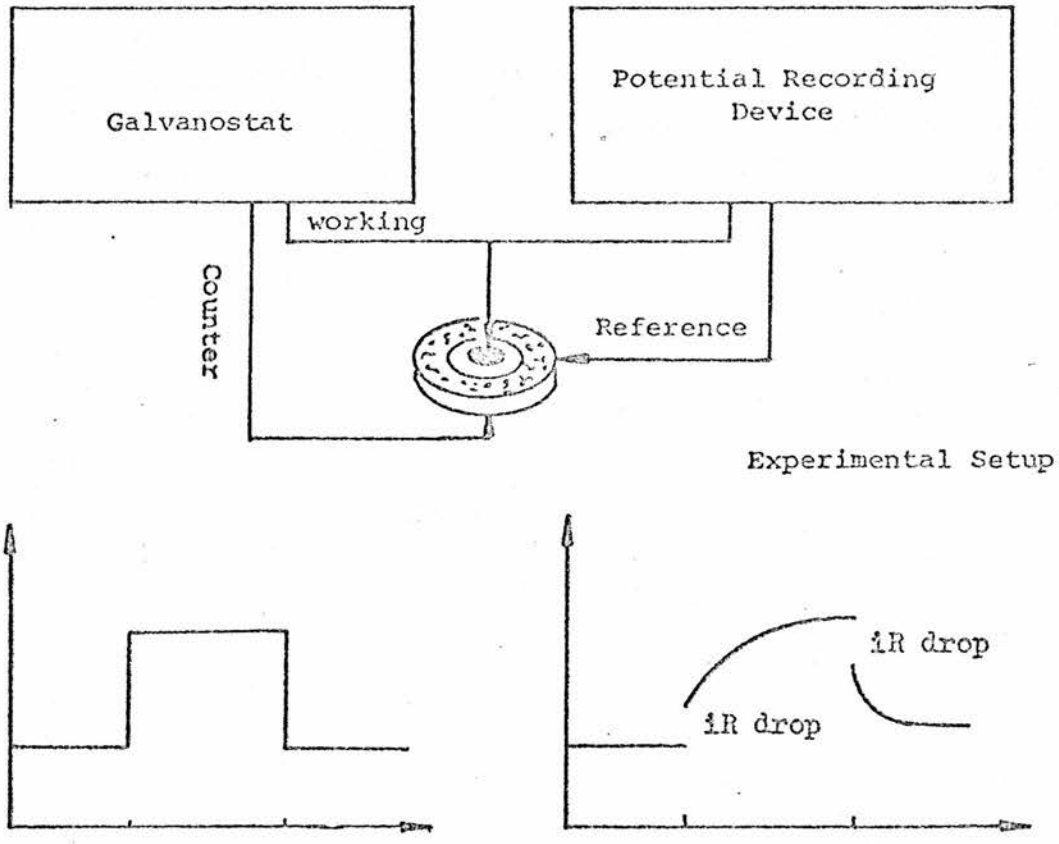

Figure 2 (b): Galvanostatic Pulse Technique

2 Solutions to Fick's Second Law of Diffusion.

2.1 a) Semi-Infinite Linear Diffusion.

For the case of semi-infinite diffusion in one-dimension[3,4] equation [2] simplifies to Fick's Second Law [3],

$$\frac{\partial C}{\partial t} = D \frac{\partial^2 C}{\partial x^2} \qquad [3]$$

with the initial condition that at t=0, $C=C_0$ throughout the system. i.e. the system is at a constant equilibrium concentration C_0. Also as x tends towards infinity, C must tend towards C_0. i.e. at very large distances from the electrode/electrolyte interface the concentration of diffusing species is invariant with time of the pulse. (the semi-infinite condition) There is also a second boundary condition that establishes the invariance of the flux of diffusing species at the electrode/electrolyte interface. i.e. from Fick's first law,

$$\left(\frac{\partial C}{\partial x}\right)_{x=0} = \frac{-F_0}{D}$$

where F_0 is the rate of transfer of diffusing species per unit surface area of the electrode/electrolyte interface. Since under the galvanostatic conditions imposed by the experiment, the current (i) is constant, the total rate of transfer of electroactive species across the electrode/electrolyte interface must therefore also be constant.

Thus Fick's second law [3] must be solved with the following initial and boundary conditions,

$$t = 0 \qquad x > 0 \qquad C = C_0 \qquad [4]$$

$$t > 0 \qquad x \to \infty \qquad C \to C_0 \qquad [5]$$

$$t > 0 \qquad x = 0 \qquad \left(\frac{\partial C}{\partial x}\right)_{x=0} = \frac{-F_0}{D} \qquad [6]$$

If the substitution, $C^* = C - C_0$ is now made, equations [3] to [6] become,

$$\frac{\partial C^*}{\partial t} = D \frac{\partial^2 C^*}{\partial x^2} \qquad [7]$$

for

$$t = 0 \qquad x > 0 \qquad C^* = 0 \qquad [8]$$

$$t > 0 \qquad x \to \infty \qquad C^* \to 0 \qquad [9]$$

$$t > 0 \qquad x = 0 \qquad \left(\frac{\partial C^*}{\partial x}\right)_{x=0} = \frac{-F_0}{D} \qquad [10]$$

Now taking the Laplace Transform of [7] leads to an ordinary differential equation,

$$p\bar{C}^* - C^*_{t=0} = D \frac{d^2\bar{C}^*}{dx^2}$$

and using [8],

$$D \frac{d^2\bar{C}^*}{dx^2} - p\bar{C}^* = 0 \qquad [\ 11\ ]$$

where p is the complex frequency variable, x the positional coordinate and $\bar{C}^*$ the Laplace Transform of C^*. Equations [9] and [10] become,

$$x \to \infty \quad \bar{C}^* \to 0 \qquad [\ 12\ ]$$

$$x = 0 \quad \frac{d\bar{C}^*}{dx}_{x=0} = \frac{-F_0}{D} \qquad [\ 13\ ]$$

The general solution of [11] is,

$$\bar{C}^{*} = A_1 \exp(-a_1 x) + A_2 \exp(a_1 x) \qquad [14]$$

where A_1 and A_2 are constants to be determined using equations [12] & [13] and $a_1 = (p/D)^{1/2}$.

From [12], in order that [14] tends towards zero as x tends towards infinity, A_2 must be equal to zero. Thus,

$$\bar{C}^{*} = A_1 \exp(-a_1 x) \qquad [15]$$

Now the differential of [15] with respect to x leads to,

$$\frac{d\bar{C}^{*}}{dx} = -A_1 a_1 \exp(-a_1 x)$$

for $x = 0$,

$$\left.\frac{d\bar{C}^{*}}{dx}\right|_{x=0} = -A_1 a_1$$

and using [13],

$$A_1 = \frac{F_0}{a_1 D}$$

Thus [15] becomes,

$$\bar{C}^* = \frac{F_0}{a_1 D} \exp(-a_1 x) \qquad [16]$$

Using tables to find the inverse Laplace Transformation of [16], and expressing the equation in terms of C and C_0 leads to,

$$C = C_0 + \frac{F_0}{D^{1/2}} \left\{ \frac{2t^{1/2}}{\pi^{1/2}} \exp(-x^2/\{4Dt\}) - \frac{x}{D^{1/2}} \operatorname{erfc}(x/\{2D^{1/2}t^{1/2}\}) \right\} \qquad [17]$$

where erfc(u) is the compliment of the error function, with the property that erfc(0) = 1.

Equation [17] is the required solution to Fick's second law for the initial and boundary conditions stated and gives the profile of concentration of the diffusing species as a function of time and distance from the reference plane. Since we are only interested in the concentration gradient at the electrode/electrolyte surface (i.e. x = 0), [17] simplifies to,

$$C = C_0 + \frac{2F_0 t^{1/2}}{\pi^{1/2} D^{1/2}}$$

Now F_0, the flux of diffusing species per unit area can be written as,

$$F_0 = \frac{i}{nFA}$$

where i is the total current applied to the cell, n the number of electrons involved in the charge transfer reaction, F Faraday's constant (96490 C equiv^{-1}) and A the total surface area for the electrode/electrolyte interface. Thus replacing F_0 we obtain,

$$C = C_0 + \frac{2it^{1/2}}{nFA\,\pi^{1/2} D^{1/2}} \qquad [\ 18\ ]$$

2.2 b) Finite Linear Diffusion.

For the case of linear diffusion[3,4,5] into a thin layer of material of thickness 2r (i.e. $-r < x > r$), equation [3] and the initial condition [4] and boundary condition [6] still hold. But the boundary condition [5] must be replaced by the condition that the flux of diffusing species cannot flow past x = 0 i.e.

$$\left(\frac{dC}{dx}\right)_{x=0} = 0$$

Thus we must now solve Fick's second law, [3] with the following conditions,

$$t = 0 \qquad x > 0 \qquad C = C_0 \qquad [19]$$

$$t > 0 \qquad x = 0 \qquad \left(\frac{dC}{dx}\right)_{x=0} = 0 \qquad [20]$$

$$t > 0 \qquad x = r \qquad \left(\frac{\partial C}{\partial x}\right)_{x=r} = \frac{-F_0}{D} \qquad [21]$$

As before the substitution $C^* = C - C_0$ can be made and the Laplace Transformation of the relevant equations can be taken leading to,

$$D\frac{d^2\bar{C}^*}{dx^2} - p\bar{C}^* = 0 \qquad [22]$$

with,

$$\left.\frac{d\bar{C}^*}{dx}\right|_{x=0} = 0 \qquad [23]$$

and

$$\left.\frac{d\bar{C}^*}{dx}\right|_{x=r} = \frac{-F_0}{D} \qquad [24]$$

Again the general solution to [22] is,

$$\bar{C}^* = A_1\exp(-a_1x) + A_2\exp(a_1x) \qquad [25]$$

where A_1, A_2 are constants and $a_1 = (p/D)^{1/2}$

Differentiating [25] with respect to x leads to,

$$\frac{d\bar{C}^*}{dx} = -a_1A_1\exp(-a_1x) + a_1A_2\exp(a_1x) \qquad [26]$$

Now, from [23], in order that [26] be zero at x = 0, $A_1 = A_2$. Thus,

$$\frac{d\bar{C}^*}{dx} = a_1 A_1 \exp(a_1 x) \{ 1 - \exp(-2a_1 x) \}$$

and from [24]

$$a_1 A_1 \exp(a_1 r) \{ 1 - \exp(-2a_1 r) \} = \frac{-F_0}{D}$$

so $$A_1 = \frac{-F_0 \exp(-a_1 r)}{Da_1\{1 - \exp(-2a_1 r)\}}$$

Thus equation [25] becomes,

$$\bar{C}^* = \frac{-F_0}{Da_1\{1 - \exp(-2a_1 r)\}} \{\exp(-a_1\{x+r\}) + \exp(a_1\{x-r\}) \} \qquad [27]$$

which on taking the inverse Laplace Transformation becomes,

$$C = C_0 - \frac{F_0 t^{1/2}}{D^{1/2}} \sum_{j=0}^{\infty} \{ \text{ierfc}(\frac{\{2j+1\}r - x}{2D^{1/2}t^{1/2}}) + \text{ierfc}(\frac{\{2j+1\}r + x}{2D^{1/2}t^{1/2}}) \}$$

where ierfc(u) is the first integral of the compliment to the error function and so the above equation can be rewritten as,

$$C = C_0 - \frac{F_0 r}{D}\left\{\frac{Dt}{r^2} + \frac{3x^2 - r^2}{6r^2} - \frac{2}{\pi^2}\sum_{j=1}^{\infty} Q_j\right\} \qquad [28]$$

$$\text{where } Q_j = \frac{(-1)^j}{j^2}\exp(-\pi^2 j^2 Dt/r^2)\cos(\pi jx/r)$$

Since, again, we are only interested in the concentration gradient at the electrode/electrolyte interface surface (x = r), equation [28] simplifies to,

$$C = C_0 - \frac{F_0 r}{D}\left\{\frac{Dt}{r^2} + \frac{1}{3} - \frac{2}{\pi^2}\sum_{j=1}^{\infty}\frac{1}{j^2}\exp(-\pi^2 j^2 Dt/r^2)\right\}$$

Let $P = \exp(-\pi^2 D/r^2)$, then

$$C = C_0 - \frac{F_0 r}{3D}\left\{1 + \frac{3Dt}{r^2} - \frac{6}{\pi^2}\sum_{j=1}^{\infty}\frac{1}{j^2}P^{j^2 t}\right\}$$

Substituting for D in terms of P, [i.e. $D = -(r^2/\pi^2)\ln(P)$] gives,

$$C = C_0 + \frac{F_0 \pi^2}{3r\ln(P)}\left\{1 - \frac{3t}{\pi^2}\ln(p) - \frac{6}{\pi^2}\sum_{j=1}^{\infty}\frac{1}{j^2}P^{j^2 t}\right\} \qquad [29]$$

As in the case for semi-infinite linear diffusion, F_0, the flux of diffusing species per unit area can be written as,

$$F_0 = \frac{i}{nFA}$$

where i, n, F & A are the same as before. (i.e. i is the total current applied to the cell, n is the number of electrons involved in the charge transfer reaction, F = 96490 C equiv^{-1} and A is the total surface area for the electrode/electrolyte interface) This changes [29] to,

$$C = C_0 + \frac{i\,\pi^2}{3nFV_m Ar\,\ln(P)}\left\{1 - \frac{3t}{\pi^2}\ln(P) - \frac{6}{\pi^2}\sum_{j=1}^{\infty}\frac{1}{j^2}P^{j^2 t}\right\} \quad [30]$$

where $P = \exp(-\pi^2 D/r^2)$.

2.3 c) Spherical Diffusion.

For the case of diffusion into a sphere[5] of radius r a change from cartesian coordinates to polar coordinates will be made to equation [2] to simplify matters. The relevant equations to alter the coordinates are,

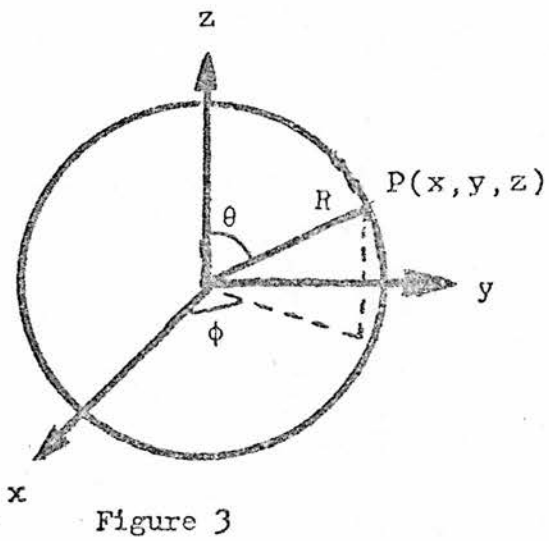

Figure 3
Spherical Coordinates

$$x = R\sin\theta\cos\phi$$

$$y = R\sin\theta\sin\phi$$

$$z = R\cos\theta$$

and after applying the above to equation [2] i.e.

$$\frac{\partial C}{\partial t} = D\left\{\frac{\partial^2 C}{\partial x^2} + \frac{\partial^2 C}{\partial y^2} + \frac{\partial^2 C}{\partial z^2}\right\} \qquad [2]$$

then the following is obtained,

$$\frac{\partial C}{\partial t} = \frac{1}{R^2}\left[\frac{\partial}{\partial R}\left(DR^2\,\frac{\partial C}{\partial R}\right) + \frac{1}{\sin\theta}\,\frac{\partial}{\partial \theta}\left(D\sin\theta\,\frac{\partial C}{\partial \theta}\right) + \frac{D}{\sin^2\theta}\,\frac{\partial^2 C}{\partial \phi^2}\right] \qquad [31]$$

and for the case where diffusion is purely radial (i.e. diffusion only occurs from the surface of the sphere into the centre) then,

$$\frac{\partial C}{\partial t} = \frac{1}{R^2}\left\{\frac{\partial}{\partial R}\left(DR^2\,\frac{\partial C}{\partial R}\right)\right\}$$

$$\frac{\partial C}{\partial t} = D\left\{\frac{\partial^2 C}{\partial R^2} + \frac{2}{R}\,\frac{\partial C}{\partial R}\right\} \qquad [32]$$

The initial and boundary conditions which apply to [32] are similar to those applying before, namely at $t = 0$, $C = C_0$ and that the flux of diffusing species at the electrode/electrolyte interface ($R = r$) is invariant with time. Thus equation [32] must be solved with equations [33] and [34] applying. A third condition which express's the symmetry of the situation will be introduced later, [38].

$$t = 0 \qquad R > 0 \qquad C = C_0 \qquad [33]$$

$$t > 0 \qquad R = r \qquad \left(\frac{\partial C}{\partial R}\right)_{R=r} = \frac{-F_0}{D} \qquad [34]$$

If the substitution $U = (C-C_0)R$ is made then we obtain,

$$\frac{\partial U}{\partial t} = D \frac{\partial^2 U}{\partial R^2} \qquad [35]$$

with the conditions,

$$t = 0 \qquad R > 0 \qquad U = 0 \qquad [36]$$

$$t > 0 \qquad R = r \qquad r \frac{\partial U}{\partial R} - U = \frac{-r^2 F_0}{D} \qquad [37]$$

In addition, since C is finite, and to describe the symmetry of the model,

$$t > 0 \qquad R = 0 \qquad U = 0 \qquad [38]$$

Equation [35] is in the form of Fick's second law, [3], and many problems involving radial flow in a sphere can be deduced immediately from those of the corresponding linear problem. But in this particular case condition [37] makes this impossible. If we now assume that the solution to equation [35] has separable variables then we can seek a solution of the form,

$$U = U_0(R,t) + P(R)T(t) \qquad [39]$$

where $U_0(R,t)$ is a function of R and t and satisfies [35], [37], [38] and P(R) & T(t) are functions of R and t respectively and satisfy [35], [38] and also [40],

$$rT\frac{dP}{dR} - TP = 0 \qquad \text{for } R=r \qquad [40]$$

and, as a whole, [39] satisfies [36].

i.e. the solution will be broken down into two parts, each part satisfying only certain of the conditions, but at the end of the derivation the sum of the two parts will satisfy all the initial and boundary conditions stated.

We will now derive the part containing the two separable functions, P(R) & T(t). Thus substituting the relevant part of [39] into equation [35] yields,

$$P\frac{dT}{dt} = DT\frac{d^2P}{dR^2}$$

i.e.
$$\frac{1}{T}\frac{dT}{dt} = \frac{D}{P}\frac{d^2P}{dR^2} \qquad [41]$$

Thus we have on the left-hand side of [41] an expression depending on t only, while on the right-hand side an expression depending only on R. Both sides must be equal to the same thing, namely a constant, which for convenience will be taken as $-a_1^2$. We have therefore two ordinary differential equations,

$$\frac{1}{T}\frac{dT}{dt} = -a_1^2$$

and

$$\frac{D}{R}\frac{d^2P}{dR^2} = -a_1^2$$

of which solutions are,

for a_1 non-zero

$$T = \exp(-a_1^2 t)$$

$$P = a_2 \sin(a_1 R/D^{1/2}) + a_3 \cos(a_1 R/D^{1/2})$$

and for $a_1 = 0$

$$T = \text{constant} = a_0$$

$$P = R$$

Thus [39] becomes,

$$U = U_0(R,t) + a_0 R + \exp(-a_1^2 t)\ \{a_2 \sin(a_1 R/D^{1/2}) + a_3 \cos(a_1 R/D^{1/2})\ \}$$

Now in order that [38] be true, $a_3 = 0$ and applying [41] gives,

$$ra_0 + r.\exp(-a_1^2 t).a_1/D^{1/2}.a_2.\cos(a_1 r/D^{1/2}) - ra_0 - \exp(-a_1^2 t).a_2.\sin(a_1 r/D^{1/2}) =$$

$$\frac{ra_1}{D^{1/2}} \cos(a_1 r/D^{1/2}) = \sin(a_1 r/D^{1/2})$$

$$\frac{ra_1}{D^{1/2}} \cot(ra_1/D^{1/2}) = 1$$

Let $b_j = a_1/D^{1/2}$, then rb_j must be the positive roots to the equation,

$$rb_j \cot(rb_j) = 1 \qquad [42]$$

in order that [41] be true. (see the end of this section for values of [42])

This reduces the solution to,

$$U = U_0(R,t) + a_0 R + \sum_{j=1}^{\infty} a_j \sin(b_j R) \exp(-b_j^2 Dt)$$

The sum of terms is introduced in order that all the solutions of [42] are taken into account, since they are all equally valid.

To find the part of the solution involving the function $U_0(R,t)$ we try the following,

$$U_0(R,t) = c_0 + c_1 t + c_2 t^2 + c_3 Rt + c_4 R^3$$

and apply the conditions stated previously. i.e. from [35],

$$\frac{\partial U_0(R,t)}{\partial t} = c_1 + 2c_2 + c_3 R$$

$$D \frac{\partial^2 U_0(R,t)}{\partial r^2} = 6c_4 DR$$

which implies that $c_2 = -c_1/2$ and $c_4 = c_3/(6D)$

Thus $$U_0(R,t) = c_0 + c_1 - c_1/2\ t^2 + c_3 Rt + c_3/(6D)\ R^3$$

and from [38]

$$U_0(0,t) = c_0 + c_1 - c_1/2\ t^2 = 0$$

which implies that $c_0 = c_1 = 0$

Therefore

$$U_0(R,t) = c_3 Rt + c_3/(6D)\ R^3$$

and finally from [37]

$$\left.\frac{\partial U_0(R,t)}{\partial R}\right|_{R=r} = c_3 t + c_3 r^2/(2D)$$

i.e.

$$rc_3 t + c_3 r^3/(2D) - rc_3 t - c_3 r^3/(6D) = \frac{-r^2 F_0}{D}$$

which implies that $c_3 = \frac{-3F_0}{r}$

This further reduces the solution to,

$$U = \frac{-3F_0}{Dr} \{ DRt + R^3/6 \} + a_0 R + \sum_{j=1}^{\infty} a_j \sin(b_j R) \exp(-b_j^2 Dt)$$

The only remaining condition is [36] which states that at $t = 0$, $U = 0$ therefore,

$$a_0 R + \sum_{j=1}^{\infty} a_j \sin(b_j R) = \frac{F_0 R^3}{2Dr}$$

The left-hand side of the above expression is in the form of a Fourier series and so the methods of Fourier analysis can be applied to find the coefficients a_0 and a_j. Thus to find a_0, multiply by R and integrate with respect to R over [0,r] i.e.

$$\int_0^r a_0 R^2 \, dR = \int_0^r \frac{F_0 R^4}{2Dr} \, dR$$

$$[a_0 R^3/3]_0^r = [F_0 R^5/(10Dr)]_0^r$$

$$a_0 r^3/3 = F_0 r^4/(10D)$$

$$a_0 = 3F_0 r/(10D)$$

and to find a_j, multiply by $\sin(b_j R)$ and integrate with respect to R over [0,r] i.e.

$$\int_0^r a_j \sin^2(b_j R)\, dR = \int_0^r \frac{F_0 R^3}{2Dr} \sin(b_j R)\, dR$$

$$a_j\left[\frac{R}{2} - \frac{\sin(b_j R)\cos(b_j R)}{2b_j}\right]_0^r = \frac{F_0}{2Dr}\left[\left(\frac{3R^2}{b_j^2} - \frac{6}{b_j^4}\right)\sin(b_j R) + \left(\frac{6R}{b_j^3} - \frac{R^3}{b_j}\right)\cos(b_j R)\right]_0^r$$

$$\frac{a_j}{2b_j}\{b_j r - \sin(b_j r)\cos(b_j r)\} = \frac{F_0}{2Dr}\left\{\left(\frac{3r^2}{b_j^2} - \frac{6}{b_j^4}\right)\sin(b_j r) + \left(\frac{6r}{b_j^3} - \frac{r^3}{b_j}\right)\cos(b_j r)\right\}$$

$$\frac{a_j}{2b_j}\tan(b_j r)\left\{\frac{b_j r}{\tan(b_j r)} - \cos^2(b_j r)\right\} =$$

$$\frac{F_0}{2Dr}\left\{\left(\frac{3r^2}{b_j^2} - \frac{6}{b_j^4}\right)\sin(b_j r) + \left(\frac{6r}{b_j^3} - \frac{r^3}{b_j}\right)\sin(b_j r)\cot(b_j r)\right\}$$

Now since, from [41], $\cot(b_j r) = 1/(b_j r)$ and $\tan(b_j r) = b_j r$ then,

$$\frac{a_j r}{2}\{1 - \cos^2(b_j r)\} = \frac{F_0 \sin(b_j r)}{2Dr}\left\{\frac{3r^2}{b_j^2} - \frac{6}{b_j^4} + \frac{6}{b_j^4} - \frac{r^2}{b_j^2}\right\}$$

$$\frac{a_j r}{2}\sin^2(b_j r) = \frac{F_0 r \sin(b_j r)}{Db_j^2}$$

$$a_j = \frac{2F_0}{Db_j^2 \sin(b_j r)}$$

Thus the end result is,

$$U = \frac{-3F_0}{Dr}\left\{ DRt + \frac{R^3}{6} - \frac{r^2R}{10} - \sum_{j=1}^{\infty} \frac{2r\sin(b_jR)\exp(-b_j^2Dt)}{3b_j^2\sin(b_jr)} \right\}$$

and returning to C gives,

$$C = C_0 - \frac{F_0r}{D}\left\{ \frac{3Dt}{r^2} + \frac{R^2}{2r^2} - \frac{3}{10} - \sum_{j=1}^{\infty} \frac{2\sin(b_jR)\exp(-b_j^2Dt)}{Rrb_j^2\sin(b_jr)} \right\}$$

Again we are only interested in the concentration gradient at the electrode/electrolyte interface (R = r) and so the above equation simplifies to,

$$C = C_0 - \frac{F_0r}{D}\left\{ \frac{3Dt}{r^2} + \frac{1}{5} - \sum_{j=1}^{\infty} \frac{2\exp(-b_j^2Dt)}{r^2b_j^2} \right\}$$

Let $P = \exp(-b_1^2D)$ then,

$$C = C_0 - \frac{F_0r}{5D}\left\{ 1 + \frac{15Dt}{r^2} - \frac{10}{r^2} \sum_{j=1}^{\infty} \frac{1}{b_j^2} P^{(b_j^2\, t/b_1^2)} \right\}$$

Substituting for D in terms of P, i.e. $D = -\ln(P)/b_1^2$ we get,

$$C = C_0 + \frac{F_0 b_1^2 r}{5\ln(P)} \left\{ 1 - \frac{15t}{r^2 b_1^2} \ln(P) - \frac{10}{r^2} \sum_{j=1}^{\infty} \frac{1}{b_j^2} P^{(b_j^2 \, t/b_1^2)} \right\} \qquad [43]$$

As in the case for semi-infinite and finite linear diffusion, F_0, the flux of diffusing species per unit area can be written as,

$$F_0 = \frac{i}{nFA}$$

where i, n, F & A are the same as before. (i.e. i is the total current applied to the cell, n is the number of electrons involved in the charge transfer reaction, F = 96490 C equiv^{-1} and A is the total surface area for the electrode/electrolyte interface) This changes [43] to,

$$C = C_0 + \frac{i b_1^2 r^2}{15nFV_m Ar \ln(P)} \left\{ 1 - \frac{15t}{r^2 b_1^2} \ln(P) - \frac{10}{r^2} \sum_{j=1}^{\infty} \frac{1}{b_j^2} P^{(b_j^2 \, t/b_1^2)} \right\} \qquad [44]$$

where $P = \exp(-b_1^2 D)$

and b_j are the positive roots to the equation

$rb_j \cot(rb_j) = 1$

2.3.1 Roots to the equation $X_i COT(X_i) = 1$

We wish to find the roots to the equation,

$$x_i \cot(x_i) = 1$$

i.e. $$x_i = \tan(x_i)$$

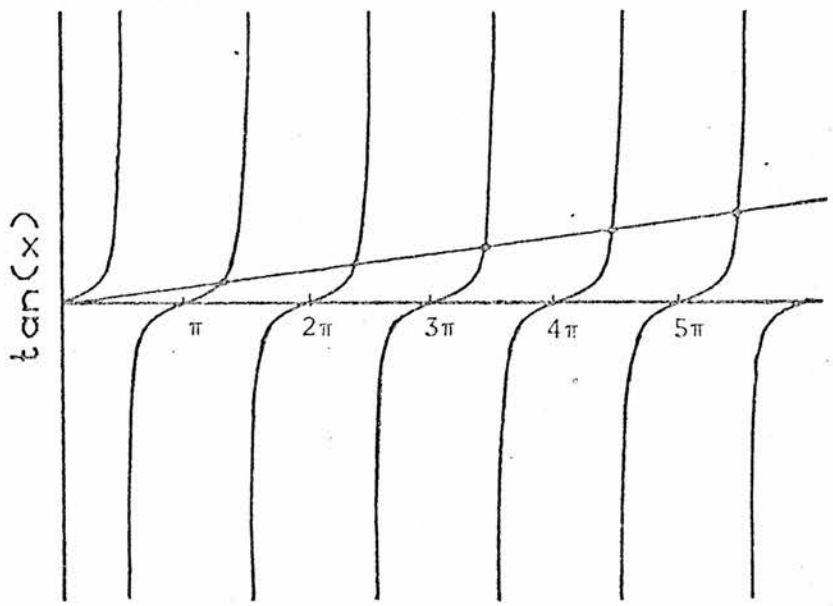

Figure 4.

Now from the graph of $\mathrm{Tan}(x_i)$, fig 4, it it obvious that as i tends towards infinity, x will tend to $(2i+1)^* \pi /2$. It is also obvious from the graph that all the roots to the equation must be of the form,

$$x_i = (2i+1)^* \pi /2 - e_i$$

where e_i is some small number corresponding to each root, which gets smaller as i gets larger.

Thus

$$\sin\{(2i+1)*\pi/2 - e_i\} = \sin\{(2i+1)*\pi/2\}\cos\{e_i\} - \cos\{(2i+1)*\pi/2\}\sin(e_i)$$
$$= (-1)^i\cos(e_i)$$

since $\sin\{(2i+1)*\pi/2\} = (-1)^i$ and $\cos((2i+1)*\pi/2) = 0$

$$\cos\{(2i+1)*\pi/2 - e_i\} = \cos\{(2i+1)*\pi/2\}\cos(e_i) + \sin\{(2i+1)*\pi/2\}\sin(e_i)$$
$$= (-1)^i\sin(e_i)$$

This leads to,

$$\tan\{(2i+1)*\pi/2 - e_i\} = \frac{1}{\tan(e_i)}$$

and since $\tan(x_i) = x_i$ we have therefore,

$$\tan(e_i) = \frac{1}{(2i+1)*\pi/2 - e_i}$$

i.e.

$$e_i = \tan^{-1}\{\frac{1}{(2i+1)*\pi/2 - e_i}\} \qquad [\ 45\ ]$$

Thus in order to find e_i (and hence x_i) all that is required is for a value of e_i to be guessed at and inserted into [45] and then refined by iteration to the desired accuracy.

The following short program illustrates this and calculates the value of x_1. Lines 110,120 fix the accuracy of comparison in line 170, in this case the first 15 digits must be equal for the IF statement to be true. Line 130 chooses which x_i is to be calculated and 140 chooses an arbitrary small value of e. The program then goes round in a loop using equation [45] until the desired accuracy of 15 digits is reached, at which point it prints the result and stops.

```
100 REM  Program to find the roots of X = TAN(X)
110 A = 15
120 FUZZ A,1.0E-64
130 I = 1
140 E = 0.5
150 T = E
160 E = ATN(1/(2*I+1)*PI/2 - E)     !ATN() is the INVERSE of TAN
170 IF E <> T THEN 150
180 PRINT E, (2*I+1)*PI/2 - E
190 END
```

This program produces the results,

$e_1 = 0.218979522476$ $x_1 = 4.49340945791$

$e_2 = 0.128729797037$ $x_2 = 7.72525183694$

$e_3 = 0.091452628135$ $x_3 = 10.9041216594$

$e_4 = 0.070973028323$ $x_4 = 14.0661939128$

$e_5 = 0.058004322813$ $x_5 = 17.2207552719$

and any others which are required.

2.4 d) Cylindrical Diffusion.

In order to solve Fick's 2nd law (equ [2]) for cylindrical diffusion a similar method to that used in the spherical case will be adopted. Firstly equation [2] will be rewritten in cylindrical coordinates. i.e.

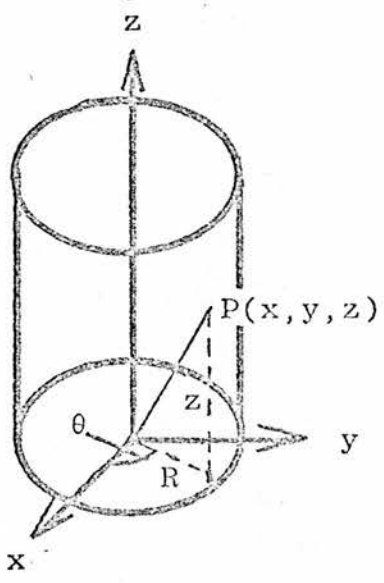

Figure 5
Cylindrical Coordinates

$$\begin{aligned} x &= R\cos\theta \\ y &= R\sin\theta \\ z &= z \end{aligned} \qquad [46]$$

and after applying these equations, [46], to equation [2] i.e.

$$\frac{\partial C}{\partial t} = D\left\{ \frac{\partial^2 C}{\partial x^2} + \frac{\partial^2 C}{\partial y^2} + \frac{\partial^2 C}{\partial z^2} \right\} \qquad [2]$$

we eventually obtain,

$$\frac{\partial C}{\partial t} = D\{ \frac{\partial^2 C}{\partial R^2} + \frac{1}{R} \frac{\partial C}{\partial R} \} \qquad [47]$$

The initial and boundary conditions which apply to [47] are the same as those which applied in the spherical case, namely

$$t = 0 \qquad R > 0 \qquad C = C_0 \qquad [48]$$

$$t > 0 \qquad R = r \qquad \frac{\partial C}{\partial R}_{R=r} = \frac{-F_0}{D} \qquad [49]$$

and if we again assume that the solution of [47] is separable then we can look for solutions of the form,

$$C = U_0(R,t) + P(R)T(t) \qquad [50]$$

where $U_0(R,t)$ is a function of R and t and satisfies [47] & [49] and P(R) & T(t) are functions of R and t respectively and satisfy [47] and

$$-D \frac{\partial (P(R)T(t))}{\partial R}_{R=r} = 0 \qquad [51]$$

But as a whole, [50] satisfies all the conditions [47], [48] and [49]. Concentrating on P(R) & T(t) first and applying these to [47] yields,

$$P \frac{dT}{dt} = DT \left\{ \frac{d^2P}{dR^2} + \frac{1}{R} \frac{dP}{dR} \right\}$$

i.e.
$$\frac{1}{T} \frac{dT}{dt} = \frac{D}{P} \left\{ \frac{d^2P}{dR^2} + \frac{1}{R} \frac{dP}{dR} \right\}$$

The left-hand side of this equation is the same as that obtained in the spherical case and so will have the same solution, namely

$$T(t) = \exp(-a_1^2 t)$$

Again applying the product T(t)P(R) to [47], but using the solution to T(t) just obtained this time gives,

$$-a_1^2 \exp(-a_1^2 t) P = \exp(-a_1^2 t) D \left\{ \frac{dP^2}{dR^2} + \frac{1}{R} \frac{dP}{dR} \right\}$$

i.e.
$$R^2 \frac{d^2P}{dR^2} + R \frac{dP}{dR} + \frac{R^2 a_1^2}{D} P = 0$$

Letting $V = Ra_1/D^{1/2}$ leads to

$$V^2 \frac{d^2P}{dV^2} + V \frac{dP}{dV} + V^2 P = 0$$

which is Bessel's equation of zero order and has the solution,

$$P(R) = A_j J_0(a_1 R/D^{1/2})$$

where A_j is some constant to be determined later. Thus,

$$P(R)T(t) = A_j \exp(-a_1^2 t) J_0(\frac{a_1 R}{D^{1/2}})$$

and applying this to condition [51] leads to,

$$\frac{-Da_1}{D^{1/2}} A_j \exp(-a_1^2 t) J_0'(\frac{a_1 r}{D^{1/2}}) = 0$$

In order for this to be true then,

$$\frac{dJ_0(\frac{a_1 r}{D^{1/2}})}{dR} = 0$$

Letting b_j be the zeros to this equation gives,

$$\frac{a_1 r}{D^{1/2}} = b_j$$

i.e. $$a_1 = \frac{b_j D^{1/2}}{r}$$

Thus the product of P & T becomes,

$$P(R)T(t) = \sum_{j=1}^{\infty} A_j \exp(-\frac{b_j^2 D}{r^2} t)\ J_0(\frac{b_j}{r} R)$$

where again the sum is introduced to ensure that all the solutions of [47] are considered.

Now that P(R)T(t) has been found we can set about finding $U_0(R,t)$. In a similar manner to the spherical case we first try the following function,

$$U_0(R,t) = c_1 + c_2 R^2 + c_3 t$$

which gives,

$$\frac{\partial U_0}{\partial t} = c_3 , \qquad \frac{\partial U_0}{\partial R} = 2c2R , \qquad \frac{\partial^2 U_0}{\partial R^2} = 2c_2$$

and applying these to [47] we find,

$$c_3 = D \{ 2c_2 + 2c_2 \}$$

$$c_3 = 4c_2D$$

That is $U_0(R,t) = c_1 + c_2R^2 + 4c_2Dt$

and applying [49] we get,

$$2c_2r = -F_0/D$$

$$c_2 = -F_0/(2rD)$$

i.e. $$U_0(R,t) = c_1 - \frac{F_0}{2rD} \{ R^2 + 4Dt \}$$

Thus putting this all together (i.e. into [50]) we get

$$C = c_1 - \frac{F_0}{2rD} \{R^2 + 4Dt\} + \sum_{j=1}^{\infty} A_j \exp(-\frac{b_j^2Dt}{r^2}) J_0(\frac{b_jR}{r})$$

Now the only remaining condition is [48]. (i.e. $C=C_0$ at $t=0$) For convenience let $c_1 = C_0 + A_0$, then at $t = 0$ we have,

$$0 = A_0 - \frac{F_0 R^2}{2rD} + \sum_{j=1}^{\infty} A_j J_0(b_j R/r)$$

i.e. $$A_0 + \sum_{j=1}^{\infty} A_j J_0(b_j R/r) = \frac{F_0 R^2}{2rD} \qquad [52]$$

As in the case for the sphere, the left-hand side of this expression is in the form of a Fourier Series and so the coefficients A_0 & A_j can be found by Fourier analysis.

In deriving A_0 & A_j certain useful results concerning the integrals of Bessel functions will be required, these have simply been stated below but derivations of them can be found on pages 196-199 of Carslaw and Jaeger[2].

$$\int_0^r R\, J_0^2(z_1 R/r)\, dR = \frac{r^2}{2} J_0^2(z_1) \qquad [53]$$

$$\int_0^r R\, J_0(z_1 R/r)\, J_0(z_2 R/r)\, dR = 0 \qquad [54]$$

$$\int_0^r R\, J_0(z_1 R/r)\, dR = 0 \qquad [55]$$

where z_1 & z_2 are different roots of $J_0^1(z_1) = 0$

[Note also that $J_0^1(z_1) = - J_1(z_1)$]

So to find A_0, multiply [52] by R and integrate with respect to R over [0, r].

$$\int_0^r \frac{F_0 R^3}{2rD}\,dR = \int_0^r A_0 R\,dR + \int_0^r A_j R\,J_0(b_j R/r)\,dR$$

$$[\,F_0 R^4/(8rD)\,]_0^r = [\,A_0 R^2/2\,]_0^r + 0 \quad \text{(from [55])}$$

$$F_0 r^3/8D = A_0 r^2/2$$

$$A_0 = F_0 r/(4D)$$

and to find A_j multiply by $RJ_0(b_j R/r)$ and integrate with respect to R over [0, r].

$$\int_0^r \frac{F_0 R^3}{2rD} J_0(b_j R/r)\,dR = \int_0^r \frac{F_0 r}{4D} R\,J_0(b_j R/r)\,dR + \int_0^r A_j R^2\,J_0^2(b_j R/r)\,dR$$

$$= 0 + A_j \frac{r^2}{2} J_0^2(b_j) \qquad \text{(from [55] \& [53])}$$

The left-hand integral must be evaluated by integration by parts and eventually leads to,

$$\frac{-F_0}{2rD}\frac{2r^4}{b_j^2} J_2(b_j) = A_j \frac{r^2}{2} J_0^2(b_j)$$

i.e. $$A_j = \frac{-2F_0 r\ J_2(b_j)}{Db_j^2\ J_0^2(b_j)}$$

Now from the recurrence formula for Bessel functions,

$$J_2(z) = \frac{2}{z} J_1(z) - J_0(z)$$

and since $J_1(z) = -J_0'(z)$, if z is the root to $J_0'(z) = 0$ then $J_2(z) = -J_0(z)$. Thus,

$$A_j = \frac{2F_0 r}{Db_j^2\ J_0(b_j)}$$

and therefore the end result is,

$$C = C_0 - \frac{F_0 r}{D} \left\{ \frac{R^2}{2r^2} + \frac{2Dt}{r^2} - \frac{1}{4} - 2 \sum_{j=1}^{\infty} \frac{\exp(-b_j^2 Dt/r^2)\ J_0(b_j R/r)}{b_j^2\ J_0(b_j)} \right\}$$

Once again we are only interested in the concentration gradient at the electrode/electrolyte interface (R=r) and so the above equation becomes,

$$C = C_0 - \frac{F_0 r}{4D} \left\{ 1 + \frac{8Dt}{r^2} - 8 \sum_{j=1}^{\infty} \frac{1}{b_j^2} \exp(-b_j^2 Dt/r^2) \right\}$$

Let $P = \exp(-b_1^2 D/r^2)$ then,

$$C = C_0 - \frac{F_0 r}{4D}\left\{ 1 + \frac{8Dt}{r^2} - 8\sum_{j=1}^{\infty} \frac{1}{b_j^2} P^{(b_j^2\, t/b_1^2)} \right\}$$

and substituting for D in terms of P {i.e. $D = -r^2 \ln(P)/b_1^2$ } we get,

$$C = C_0 + \frac{F_0 b_1^2}{4r\,\mathrm{Ln}(P)}\left\{ 1 - \frac{8t}{b_1^2}\ln(P) - 8\sum_{j=1}^{\infty} \frac{1}{b_1^2} P^{(b_j^2\, t/b_1^2)} \right\} \qquad [\ 56\ ]$$

Now as in all the previous cases, F_0, the flux of diffusing species per unit area can be written as,

$$F_0 = \frac{i}{nFA}$$

where i is the total current applied to the cell, n is the number of electrons involved in the charge transfer reaction, $F = 96490$ C equiv^{-1} and A is the total surface area for the electrode/electrolyte interface. This changes [56] to,

$$C = C_0 + \frac{i\, b_1^2}{4nFAr\ \mathrm{Ln}(P)}\left\{ 1 - \frac{8t}{b_1^2}\ln(P) - 8\sum_{j=1}^{\infty} \frac{1}{b_1^2} P^{(b_j^2\, t/b_1^2)} \right\} \qquad [\ 57\ ]$$

where $P = \exp(-b_1^2 D/r^2)$

and b_j are the positive roots of the

Bessel Function $J_1(b_j) = 0$.

2.5 Evaluation of Experimental Measurable Quantities.

In order to apply the above equations, [18], [30], [44] and [57], which are in terms of concentration into an experimentally measurable quantity (i.e. Voltage between a reference electrode and the mass-transport limited SSE) a relationship between concentration of electroactive species (i.e. $C-C_0$) and cell overpotential must be found.

As described in Chapter 5, the concentration of electroactive species, C, can be related to the molar ratio, x, of electroactive species in the SSE material (i.e. Ag_xNbS_2) via the molar volume, V_m, of the SSE,

$$C = x/V_m$$

and assuming that the change in molar volume with composition is insignificant over the experimental conditions used here, then the change in concentration and stoichiometry can be related by [58].

$$dC = \frac{d\delta}{V_m} \qquad [58]$$

where δ is the displacement of $A_{x+\delta}B$ from the initial composition A_xB and expansion of [58] by dE leads to,

$$dE = \frac{dE}{d\delta} V_m dC$$

In other words, for small perturbations of the cell from equilibrium, we have,

$$\eta(t) = \frac{dE}{d\delta} V_m (C(t)-C_0) \qquad [59]$$

where $dE/d\delta$ is the gradient of the coulometric titration curve at a given value of x. Fig. 6 shows a plot of open circuit potentials for NbS_2 versus mole fraction of Ag in Ag_xNbS_2.

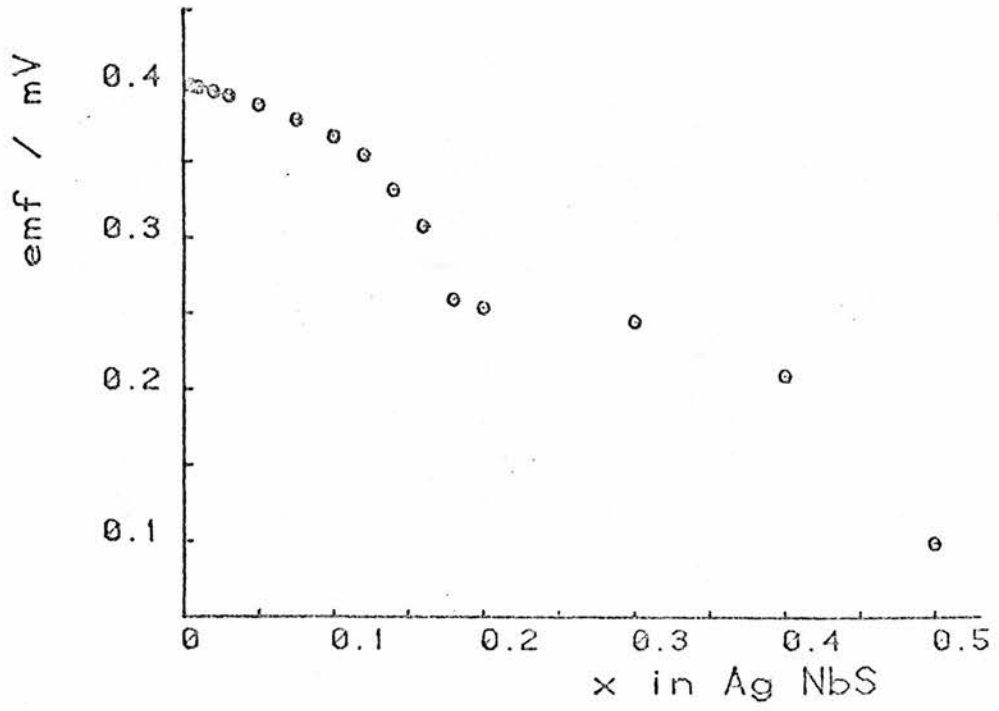

Figure 6.

Aside.

To obtain the gradient of the curve at any value of x (e.g. x_0), a polynomial of various powers of $(x - x_0)$ was fitted, i.e.

$$E(x-x_0) = \sum_{j=0}^{n} A_j(x-x_0)^j$$

where n is sufficiently large to ensure that the polynomial fits the curve reasonably well.

On differentiating the above with respect to x we obtain,

$$\frac{dE(x-x_0)}{dx} = \sum_{j=0}^{n} j\, A_j(x-x_0)^{j-1}$$

Thus $$\left.\frac{dE(x-x_0)}{dx}\right|_{x=x_0} = A_1$$

In other words the required gradient of the curve can be found from the coefficient of $(x - x_0)^1$ and all the other powers of $(x - x_0)$ in the polynomial are reduced to zero at $x = x_0$.

Thus on applying equation [59] to the four diffusion equations [18], [30], [44] and [57] we obtain,

a) Semi-infinite Linear Diffusion.

$$\eta(t) = \frac{2(de/d\delta)V_m it^{1/2}}{nFAD^{1/2}\pi^{1/2}} \qquad [60]$$

b) Finite Linear Diffusion.

$$\eta(t) = \frac{(dE/d\delta)V_m \pi^2 i}{3nFAr\ \ln(P)} \left\{ 1 - \frac{3t}{\pi^2}\ln(P) - \frac{6}{\pi^2}\sum_{j=1}^{\infty}\frac{1}{j^2}P^{j^2 t} \right\} \qquad [61]$$

where $P = \exp(-\pi^2 D/r^2)$

and $2r$ is the thickness of the thin layers.

c) Spherical Diffusion.

$$\eta(t) = \frac{(dE/d\delta)V_m r^2 b_1^2 i}{15nFAr\ \ln(P)} \left\{ 1 - \frac{15t}{r^2 b_1^2}\ln(P) - \frac{10}{r^2}\sum_{j=1}^{\infty}\frac{1}{b_j^2}P^{(b_j^2/b_1^2 t)} \right\} \qquad [62]$$

where $P = \exp(-b_1^2 D)$

and b_j are the positive roots to the equation

$rb_j \cot(rb_j) = 1$

d) Cylindrical Diffusion.

$$\eta(t) = \frac{(dE/d\delta)V_m b_1^2 i}{8nFAr\ \ln(P)} \left\{ 1 - \frac{8t}{b_1^2} \ln(P) - 8 \sum_{j=1}^{\infty} \frac{1}{b_j^2} P^{(b_j^2\, t/b_1^2)} \right\} \qquad [63]$$

where $P = \exp(-b_1^2 D/r^2)$

and b_j are the positive roots of

Bessel Function $J_1(b_j) = 0$.

The equations [61], [62] and [63] can all be written in a general form,

$$-\eta(t) = \frac{Q_1(dE/d\delta)V_m i}{C_1 nFAr\ \ln(P)} \left\{ 1 - \frac{C_1}{Q_1} t \ln(P) - \sum_{j=1}^{\infty} \frac{C_2}{Q_j} P^{(Q_j t/Q_1)} \right\} \qquad [64]$$

where $P = \exp(-Q_1 D/r^2)$ and C_1, C_2 and Q_j are constants, the values of which are given below in table 1 along with the generating function for the constant Q_j.

	Linear	Spherical	Cylindrical
C_1	3	15	8
C_2	6	10	8
Generating Function	$\sin(\pi j) = 0$	$rb_j \cot(rb_j) = 1$	$J_1(b_j) = 0$
Q_j	$\pi^2 j^2$	$(rb_j)^2$	b_j^2
Q_1	9.8696	20.1906	14.6819
Q_2	39.4784	59.6803	49.2186
Q_3	88.8264	118.8994	103.5001

Table 1.

References.

[1] Crank, J., "The Mathematics of Diffusion", Oxford Univ. Press, London, 2nd Edition, 1975

[2] Carslaw, H.S., Jaeger, J.C., "Conduction of Heat in Solids", Oxford Univ. Press, London, 2nd Edition, 1959

[3] Raistrick, I.D., Huggins, R.A., "The transient electrical response of electrochemical systems containing insertion reaction electrodes", Solid State Ionics, Vol. 7, No. 3, 1982, p. 213

[4] Wen, C.J., Boukamp, B.A., Huggins, R.A., "Thermodynamic and mass transport properties of 'LiAl'", J. Electrochem. Soc., Vol. 126, No. 12, 1977, p. 2258

[5] Atlung, S., West, K., Jacobsen, T., "Dynamic aspects of solid solution cathodes for electrochemical power sources", J. Electrochem. Soc., Vol. 126, No. 8, 1979, p. 1311

Appendix II

Data Smoothing Programs.

For all transients which have pulse lengths of less than one second there is a noise signal with constant period superimposed upon the basic transient, an example of which is shown in figure 1. This periodic noise is due to interference induced by the 50 Hz mains cycle (despite stringent precautions being taken to shield the apparatus) and the period of this waveform was found to be constant at one of the harmonics of the mains. (i.e. 25, 50, 100 Hz etc.) For transients of greater than one second duration the wavelength of this signal was too short to interfere with the measurement

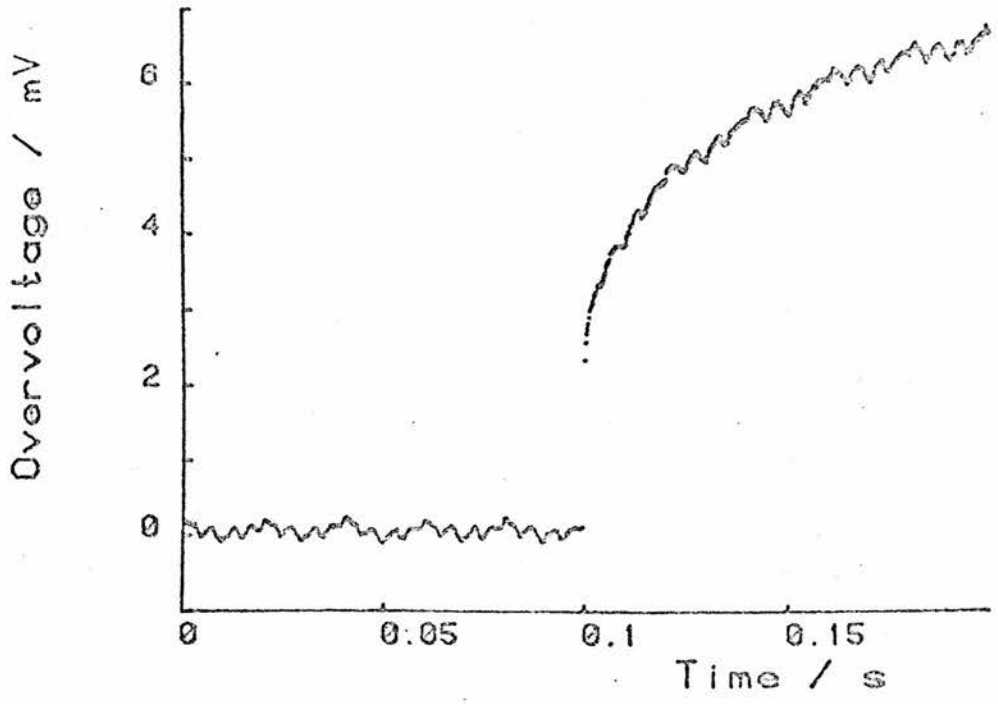

Figure 1: Raw transient

To eliminate this coherent interference a method was used which involved fitting a constant period waveform to the signal and then subtracting this fitted waveform to produce a smoothed transient. This is shown schematically in figure 2.

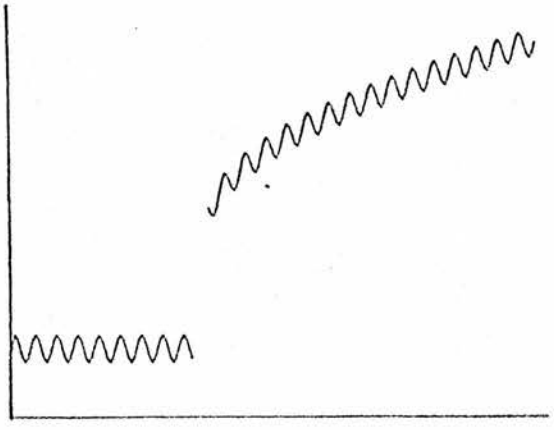

Figure 2 (a): Original noisy data.

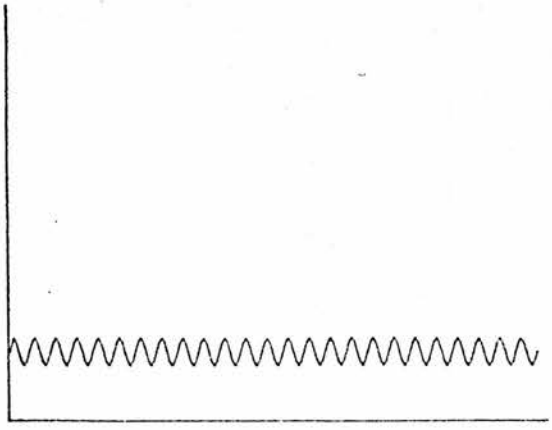

Figure 2 (b): Fitted noise wave of constant period, (derived from(a)).

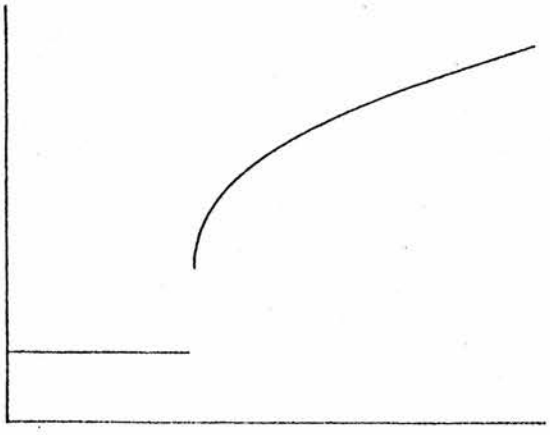

Figure 2 (c): Smoothed data (i.e. (a)-(b)).

The fundamental period of the noise wave can be calculated by dividing the period of the mains wave (i.e. 1/50 secs per wave) by the timescale of the transient. i.e. a transient which has a timescale of $5*10^{-4}$ points per second will have a noise wave of period, $0.02/5*10^{-4}$ = 40 points per wave.

In order to fit a noise waveform to an entire transient some mathematical function(s) must be found which adequately describes the basic transient upon which the noise is superimposed. In the case of the first half of the transient (i.e. the baseline) this is obviously a straight line. (i.e. $y = mx+c$) In the second half (i.e. the voltage response of the cell) this has been adequately described by a polynomial of large order. (i.e. $y = a + bx + cx^2 + dx^3 + ex^4 + fx^{0.5} + gx^{0.25} + hx^{0.125}$) It is to be emphasised that these functions (straight line & polynomial) are required only to enable the noise waveform to be fitted to the entire transient and that once the noise has been subtracted they play no further role in the fitting of the transient by a given model. Thus the original raw transient may be considered to be comprised of four parts; a) a noise wave of constant period, b) a straight line, c) a polynomial, d) data not described by a,b or c. When the transient is smoothed only part a), the fixed period noise waveform, is eliminated. This ensures that the transient is in no way distorted during the smoothing process.

A statistical package called GLIM (General LInear Model, developed by the working party on Statistical Computing of the Royal Statistical Society, London and implemented on the VAX/VMS mainframe computer at St.Andrews) was used to enable a fitting procedure as described above to be carried out.

For noise waveforms of periods less than or equal to 40 then GLIM can easily fit waveforms consisting of up to 40 entirely independently varying points and so ensuring that all the waveforms with periods less than 40 are also eliminated. Unfortunately for periods greater than 40 GLIM cannot cope with the large amount of computation required. However a method based on only fitting the first half of the transient (i.e. the baseline) with the most relevant coefficients present in the Fourier Transform of the waveform was found to be perfectly adequate in removing the noise from the entire transient, even though the fit only involved the first half of the signal.

Once the coherent noise waveform had been found and subtracted, the position (i.e. time) at which the current was first applied to the cell was found and the voltage data from this point onwards was stored on file ready for further processing and fitting by various models as described in appendix III. A schematic diagram of this smoothing process is shown in figure 3.

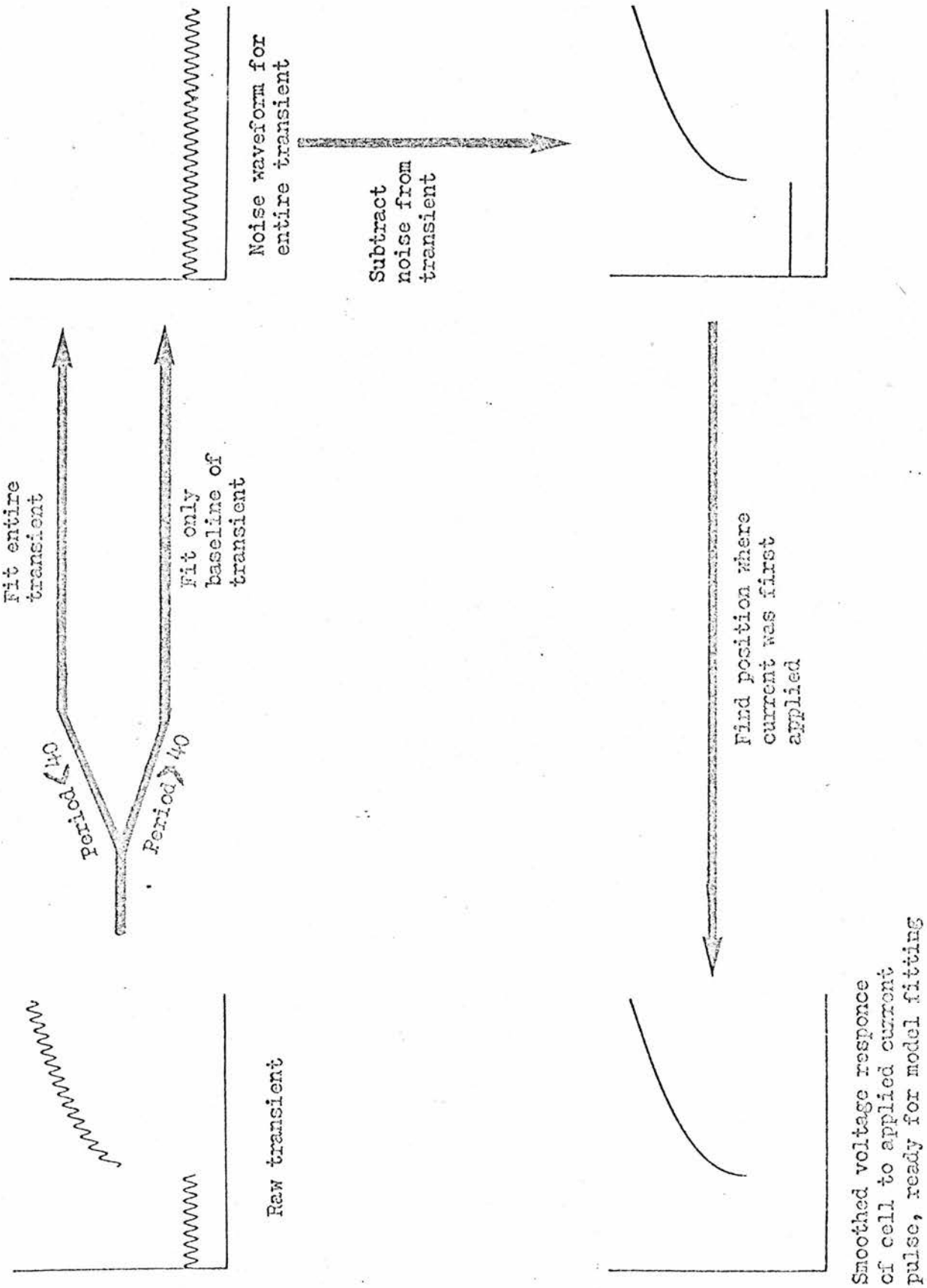

Figure 3: Schematic diagram of smoothing process.

This entire procedure of fitting a waveform and finding the start of the transient was done interactively at a terminal so that any spurious points or anomalies in the data could be removed or corrected at that stage of the process. The program which creates the necessary command file for GLIM is listed in program A2.1 and an example of a transient which has been smoothed by this method is shown in figure 4.

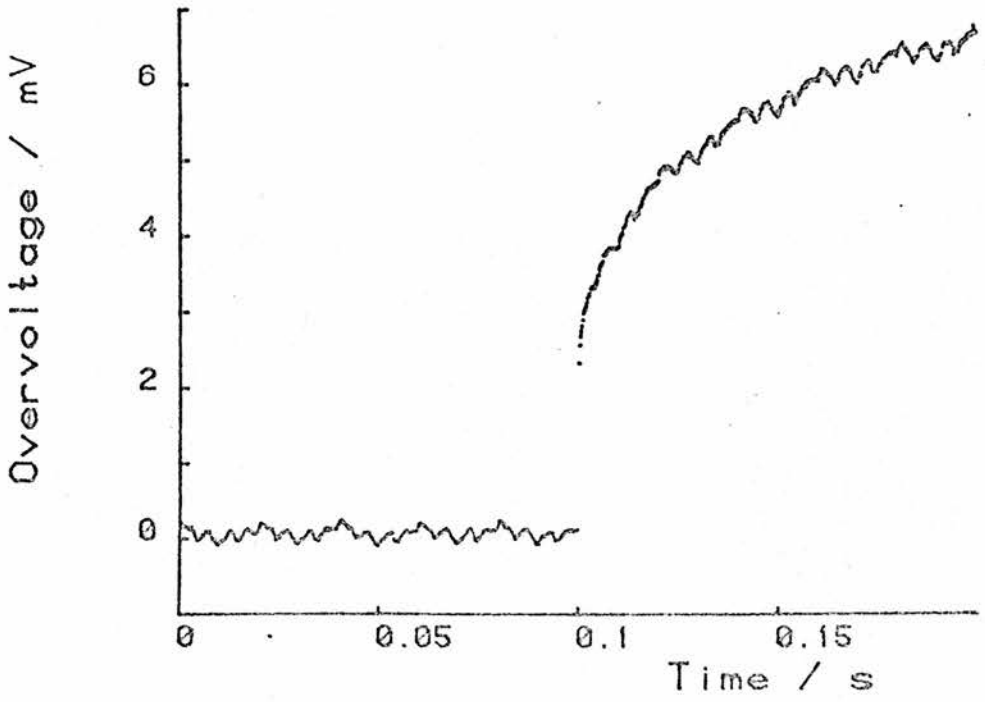

Figure 4 (a): Unsmoothed Voltage Transient.

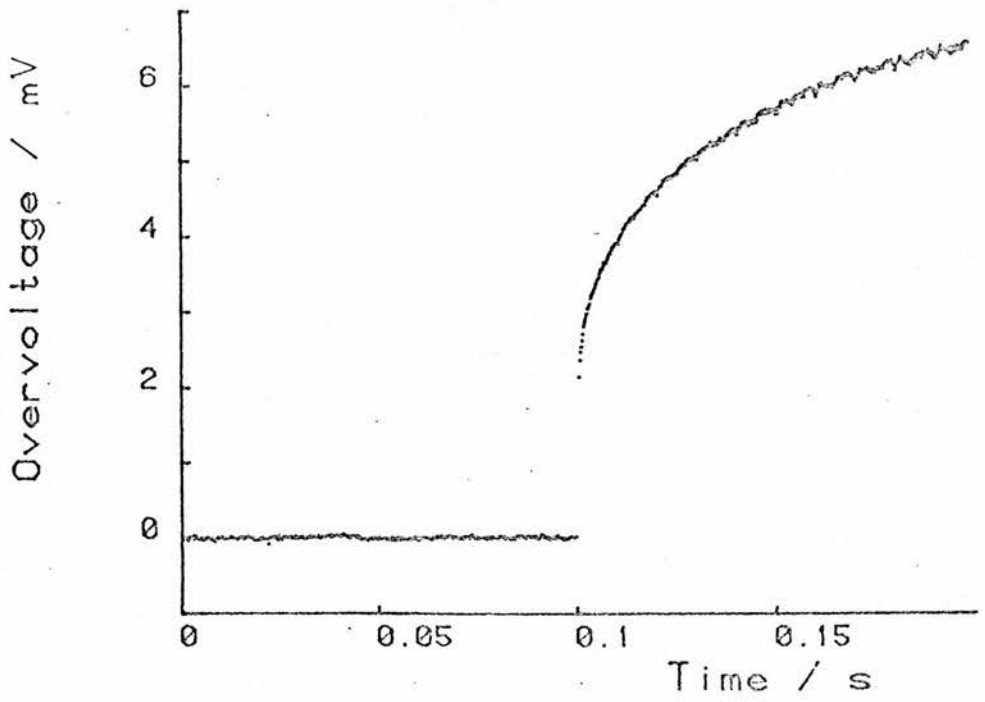

Figure 4 (b): Smoothed Voltage Transient.

Program A2.1

```
 1 -- !  Program to prepare a file (called <NAME>) to enable GLIM to
 2 -- !fit a waveform to data read from an input file (called <name>),
 3 -- !then output the smoothed data to a file for MLP to fit
 4 -- !a cylindrical model.
 5 --
 6 -- ! Set up constants for the particular solid state electrode
 7 -- !material being studied.  In this case NbS2
 8 --
 9 -- r.w := 8 ; i.w := 5 ; s.w := 1
10 -- let Mol.W = 157.034 ; let z = 1 ; let Molar.Vol = 33.9
11 -- let Grd = -0.37222 ; let Sample.Wt = 1
12 --
13 -- procedure elide (cfile in)
14 -- {     if in = s.i then {
15 --               while (peek(in)="'b" or peek(in)=" " or peek(in)="'t" or
16 --                        peek(in)="'p" )do{let skip.a.character=read(in)}
17 --               let skip.a.character = read(in)  }
18 --       else {  while ~eof(in) and (peek(in)=" " or peek(in)="'t" or
19 --               peek(in)="'p" or peek(in)="'n" or peek(in)="'o") do
20 --               { let skip.a.character = read (in) }   }  }
21 --
22 -- procedure read.number ( file F -> real )
23 -- {     let num := readr(F)
24 --       if peek(F) = "E" do { let d := read(F)
25 --               let p := readi(F) ; let PP := exp(p*ln(10))
26 --               num := num * PP  } ; elide(F) ; num  }
27 --
28 --
29 -- write"The period MUST = 0, 1, 2, 4, 10, 20, 40, 100, 200, 400,",
30 -- " points/wave'nand three questions will be asked.'n
31 -- 1. Enter data file to be smoothed 'n     (Default is SIGNAL.DAT )  :"
32 -- let name := read.a.line(s.i)
33 -- if name = "" do{ name := "SIGNAL.DAT" }
34 -- let Name := name(1|length(name)-4) ++ ".GLM"
35 -- write"'n2. Enter output file  (Default is ",Name," ) : "
36 -- Name := read.a.line(s.i)
37 -- if Name = "" do { Name := name(1|length(name)-4) ++ ".GLM" }
38 -- let time.ignore := 0.005
39 -- write "'n3. The first ",time.ignore:5," secs will be ignored."
40 --
41 -- let in = open(name,"a",0)
42 -- if in = nullfile do{write"'n",name," cannot be opened" ; abort }
43 --
44 -- ! Read constants and data from <name>
45 --
46 -- let title = read.a.line(in) ; let cell.no = read.a.line(in)
47 -- let time.scale = read.number(in) ; let temp = read.number(in)
48 -- let guest.conc = read.number(in) ; let current = read.number(in)
49 -- let duration = read.number(in) ; let starting.time = read.number(in)
50 -- let no.of.points = truncate(read.number(in))
51 -- let ignore = truncate(time.ignore/time.scale)
52 --
53 -- ! Calculate the period of the noise waveform
54 --
```

```
55 -- let period := truncate(0.1+1/(50*time.scale))
56 --
57 -- case period of
58 -- 0,1,2,4,10,20          : period := 40
59 -- 40 , 100 , 200 , 400   : {}
60 --       default :{write
61 --       The period must = 0, 1, 2, 5, 10, 20, 40, 100, 200 or 400"
62 --                 abort}
63 --
64 -- write"'n'nThe period of the noise wave is ",period," points.
65 --       and the first ",ignore," points will be ignored."
66 --
67 -- ! Find the approx. beginning  of the pulse.
68 --
69 -- let start = truncate(starting.time/time.scale)
70 -- if start+ignore > no.of.points do { write"
71 --                There is an error. The pulse does does not start
72 --                until after the ",no.of.points," point"  ; abort }
73 --
74 -- let end.of.pulse := truncate(duration/time.scale) + start - 5
75 -- if end.of.pulse>no.of.points do
76 --       {write"'nThe end of the pulse occurs at ",end.of.pulse,
77 --       "'nIt has therefore been set to ",no.of.points
78 --          end.of.pulse := no.of.points  }
79 --
80 -- ! Decide how much of the transient will be used in fitting
81 -- !the waveform    (i.e. All or only the BASELINE)
82 --
83 -- let finish := 0
84 -- case true of
85 --  period < 50          : finish := end.of.pulse
86 --  start<401            : finish := 400
87 --  default              : finish := start
88 --
89 -- !Read voltage data from <name>
90 --
91 -- let signal = vector 1::no.of.points of 0.0
92 -- for i=1 to no.of.points do{ signal(i):=read.number(in) }
93 -- close(in)
94 --
95 -- write"'n'nThe following data was taken from ",name
96 -- ,"'n'n",title,"'nThe pulse starts around address ",start
97 -- ,"'n'nThus will use  ",finish:4," points and try %K= ",start:4
98 --
99 -- ! Check that the arrays are small enough for MLP to handle.
100 -- !(if not curtail to 700 points)
101 --
102 -- let Step = ((end.of.pulse-start-ignore) div 701) + 1
103 -- write"'n'nMLP can only cope with 700 points. Therefore, since
104 -- there will be ",end.of.pulse-start-ignore," points, every ",Step
105 --  will be used.'n"
106 --
107 --
108 -- !Find the scaling factors required for MLP  (0.2<X>10 1<Y>100)
109 --
110 -- let max.x = (end.of.pulse-start)*time.scale
111 -- let min.x = (start+2)*time.scale
112 -- let scale.x := truncate(8/max.x*10000)/10000
```

```
113 -- if scale.x*min.x > 0.3 do
114 --       { scale.x := (truncate(10000/min.x)/10000+scale.x)/2}
115 --
116 -- let scale.y := 0
117 -- let mid.y = (signal(start+5)+signal(end.of.pulse-5))/2
118 -- case true of
119 --  mid.y > 1    : scale.y := 1
120 --  mid.y > 0.1  : scale.y := 10
121 --  mid.y > 0.01 : scale.y := 100
122 --  mid.y > 0.001        : scale.y := 1000
123 --  default      : scale.y := 10000
124 --
125 --
126 -- ! Output to GLIM the relevant data
127 --
128 -- let out := create(Name,"s","a","v",256)
129 -- if out = nullfile do {write"'n",Name," cannot be created" ; abort }
130 --
131 -- output out,"$ACC 9'n$UNI",finish," $DAT Y $READ 'n"
132 --
133 -- procedure list.number (int last )
134 -- { let col.count := 0
135 -- for i = 1 to last do
136 --       begin
137 --       if col.count = 6 do{ output out, "'n" ; col.count := 0 }
138 --       output out, fformat(signal(i),1,7)
139 --       col.count := col.count + 1
140 --       end
141 -- }
142 --
143 -- list.number(finish)
144 --
145 -- output out,"'n$CAL T=%GL(%NU,1)
146 -- $YVAR Y'n$CAL %N=%NU-6: %K=",start,": %L=",period,"'n"
147 --
148 -- if period < 50        then
149 --       begin      !Output commands to fit entire transient
150 --       output out,"$PRI 'The WHOLE data"
151 --       "set will be fitted and the pulse starts at (%K=)'%K$
152 --       $PRINT 'The period of the wave is (%L=) ' %L $
153 --       $PRINT 'Now use macro SMO1 to smooth the data' $
154 --       $PRINT 'Find %K first, then eliminate spurious points.' $
155 --       $CAL W=1   $WEI W'n$CAL S=%GL(%L,1)'n$FAC S %L'n$MACRO SMO1
156 --       $CAL U=%GE(T,%K):V2=(T-%K)*(T-%K):V=V2**0.5:
157 --       VQ=V**0.25:VE=V**0.125:EV=0.7**V
158 --       :RV=V**0.5:RV=RV*U:V=V*U:V2=V2*U:V3=V*V2:
159 --       V4=V2*V2:VQ=VQ*U:VE=VE*U:EV=EV*U
160 --       $FIT S+U+RV+VQ+VE+V+V2+V3+V4+T+EV -%GM'n$DEL V4 V3 VE VQ V2'n"
161 --       end
162 -- else
163 --       begin          !Output commands to fit only the baseline
164 --       output out,"$PRI 'Only the first ",finish
165 --       " points will be fitted and the period (%L=)'%L$
166 --       $PRINT 'Only eliminate spurious points. (Leave %K till later)' $
167 --       $PRINT 'Use macro SMO1 to initially smooth data' $
168 --       $CAL W=%LE(T,%K-5)   $WEI W
169 --       $CAL U=2*T*%PI/%L : %P=%PI/2
170 --       : S1=%SIN(1*U) : C1=%SIN(1*U+%P)
```

```
171 --        : S2=%SIN(2*U) : C2=%SIN(2*U+%P)
172 --        : S3=%SIN(3*U) : C3=%SIN(3*U+%P)
173 --        : S4=%SIN(4*U) : C4=%SIN(4*U+%P)
174 --        : S5=%SIN(5*U) : C5=%SIN(5*U+%P)
175 --        : S6=%SIN(6*U) : C6=%SIN(6*U+%P)
176 --        : S10=%SIN(10*U) : C10=%SIN(10*U+%P)
177 --        : S12=%SIN(12*U) : C12=%SIN(12*U+%P)
178 --        : S13=%SIN(13*U) : C13=%SIN(13*U+%P)
179 --        : S25=%SIN(25*U) : C25=%SIN(25*U+%P)
180 --        : S50=%SIN(50*U) : C50=%SIN(50*U+%P)
181 --        : S100=%SIN(100*U) : C100=%SIN(100*U+%P)
182 --        $MACRO SMO1'n$DEL R OR OT
183 --        $CAL S8=%SIN(8*U) : C8=%SIN(8*U+%P)'n"
184 --                case period of
185 --                100     :
186 --                    begin
187 --                    output out,": S9=%SIN(9*U) : C9=%SIN(9*U+%P)
188 --                    $FIT T+S1+S2+S3+S4+S5+S6+S8+S9+S10+S12+S13+S25+
189 --                    :+S50+S100+C1+C2+C3+C4+C5+C6+C8+C9+C10+C12
190 --                    :+C13+C25+C50+C100-%GM
191 --                    $DEL S8 C8 S9 C9'n"
192 --                    end
193 --                200     :
194 --                    begin
195 --                    output out,": S200=%SIN(200*U) : C200=%SIN(200*U+%P)
196 --                    $FIT T+S1+S2+S3+S4+S5+S6+S8+S10+S12+S13+S25+S50
197 --                    :+S100+S200+C1+C2+C3+C4+C5+C6+C8+C10+C12+
198 --                    :+C13+C25+C50+C100+C200-%GM
199 --                    $DEL S8 C8 S200 C200'n"
200 --                    end
201 --                400     :
202 --                    begin
203 --                    output out,": S200=%SIN(200*U)
204 --                    : C200=%SIN(200*U+%P)
205 --                    : S400=%SIN(400*U) : C400=%SIN(400*U+%P)
206 --                    $FIT T+S1+S2+S3+S4+S5+S6+S8+S10+S12+S13+S25
207 --                    :+S50+S100+S200+S400+C1+C2+C3+C4+C5+C6+C8
208 --                    :+C10+C12+C13+C25+C50+C200+C400-%GM
209 --                    $DEL S8 C8 S200 C200 S400 C400'n"
210 --                    end
211 --                default : {write"
212 --                An error has occurred in the CASE & period = "
213 --                period,"'n" }
214 --
215 --        output out,"$PRI '
216 --        Use the SECOND deviance & ignore the first ' $'n"
217 --        end
218 --
219 --
220 -- output out,"$CAL R=(%YV-%FV)*W*%SC**-0.5'n$SORT OR R : OT T R $
221 -- $PRI 'Use PLOT R T or CAL FY=%FV & PLOT FY T etc."
222 -- output out," to get plots of data' $
223 -- $LOOK 1 7 OT OR : %N %NU OT OR $
224 -- $PRI 'Use CAL W(i)=0 to obtain better fit' $
225 -- $PRI '%K = ' %K $
226 -- $PRI 'Use macro SMO2 to obtain the whole smoothed data' $
227 -- $ENDMAC'n$MACRO SMO2'n$OUT 10 $'n$DEL R OR OT'n"
228 --
```

```
229 -- !Output fitted noise waveform to file
230 --
231 -- if period > 50 then
232 --       { output out,"$CAL OR=%FV $VAR 400 R $CAL OR=OR*100000
233 --       $CAL OT=%LE(T,400) :R(OT*%CU(OT))=OR'n"
234 --       for i=1 to (end.of.pulse div 400 + 1) do
235 --       { output out,"$PRINT R$'n" }}
236 --   else
237 --       {  output out,"$EXTRA %PE'n$VAR %L R
238 --       $CAL %N=%PL+1 $VAR  %N OR OT$CAL OR=%PE :OT=%GL(%PL+1,1)
239 --       :OR=OR*100000 : OT=%LE(OT,%L+1) : OT(1)=0'n:R(OT*%CU(OT))=OR'n"
240 --       for i=1 to (end.of.pulse div period + 1) do
241 --       { output out,"$PRINT R$'n" }}
242 --
243 -- output out,"$OUT 6
244 -- PRI 'Use STOP & INP 9 to obtain the whole smoothed data set' $
245 -- $ENDMAC'n$RETURN'n"
246 --
247 -- close(out)
248 --
249 --
250 -- !Create file <NAME> containing the entire transient and commands to
251 -- !subtract the noise waveform and also find the beginning of the pulse
252 --
253 -- let NAME = name(1!length(name)-4) ++ ".ALL"
254 --
255 -- out := create(NAME,"s","a","v",256)
256 -- if out=nullfile do{write"'nCannot create ",NAME ; abort}
257 --
258 -- output out,"$ACC 9'n$UNI ",end.of.pulse," $DAT Y'n$READ'n"
259 --
260 -- list.number(end.of.pulse)
261 --
262 -- output out,"'n$CAL T=%GL(%NU,1)
263 -- $YVAR Y'n$CAL %N=%NU-6'n$DATA W'n$DINPUT 10
264 --
265 -- !Subtract the noise waveform
266 --
267 -- $CAL W=W/100000 :Y=Y-W : %K = ",start,"
268 -- $PRINT 'The data has been smoothed.' $
269 --
270 -- !Find the beginning of the pulse
271 --
272 -- $PRINT 'Now find %K and any outliers by using macro SM03' $
273 -- $CAL W=%GT(T,",start-10 :4,") $WEI W'n$MACRO SM03'n$DEL OT OR
274 -- $CAL U=%GE(T,%K):V2=(T-%K)*(T-%K):V=V2**0.5
275 -- :VQ=V**0.25:VE=V**0.125:EV=0.7**V
276 -- :RV=V**0.5:RV=RV*U:V=V*U:V2=V2*U:V3=V*V2
277 -- :V4=V2*V2:VQ=VQ*U:VE=VE*U:EV=EV*U
278 -- $PRI 'Use PLOT R T or  PLOT FY T etc. to get plots of data' $
279 -- $FIT U+RV+VQ+VE+V+V2+V3+V4+T+EV -%GM
280 -- $DEL V4 V3 VE VQ V2'n$CAL R=(%YV-%FV)*W*%SC**-0.5
281 -- $SORT OR R : OT T R $'n$LOOK 1 7 OT OR : %N %NU OT OR $
282 -- $PRINT 'Use CAL %K=? &  CAL Y(i)=%FV(i) to obtain better fit' $
283 -- $PRINT 'The START of the pulse (%K) = ' %K $
284 -- $PRINT 'Use macro OOT to prepare MLP FILE when data is smoothed' $
285 -- $ENDMAC
286 --
```

```
287 -- !Create file containing the smoothed transient to enable MLP
288 -- !to fit a cylindrical model.
289 --
290 -- $MACRO OOT'n$DEL W U OT OR RV V R EV
291 -- $CAL %K=%K+1+",iformat(ignore),"
292 -- : W=%GT(T,%K)*%GE(%TR(T/",Step,"),T/",Step,")
293 -- : %N=%CU(W) $VAR %N U V
294 -- $CAL U=%GL(%NU,1) + ",iformat(ignore)," :V(W*%CU(W))=Y
295 -- : U=U*",fformat(time.scale,1,7),"*",Step:3,"
296 -- $PRI 'Every ",Step," points will be used in MLP' $'n$OUT 8$
297 --
298 -- ! MLP commands to fit model
299 --
300 -- $PRINT 'CAPTION ",title(1|50),";' $
301 -- $PRINT 'CAPTION |",title(51|length(title)-50),";' $
302 -- $PRINT 'CAPTION ",time.scale,ignore,current,duration,
303 -- fformat(scale.x,4,2)," ",scale.y," ;' $
304 -- $PRINT 'CAPTION ",Sample.Wt,Molar.Vol,Mol.W,Grd," ;' $
305 --
306 -- !Output smoothed data
307 --
308 -- $PRINT 'DATA' $'n$PRI*6  U 'n$PRI*9 V $'n$PRI ';' $
309 --
310 -- !MLP fitting commands
311 --
312 -- $PRINT 'ECHO ;' $
313 -- $PRI 'CON 0.544885 0.1625405 3.352302 0.0772951 7.049413 ",
314 -- fformat(scale.x,4,2)," ",iformat(scale.y),";' $
315 -- $PRI 'NAMES C1=A,B,C,D,E,SX,SY V1=X,Y,Z P1=R ;' $
316 -- $PRI 'DER(2) X=X*SX Y=Y*SY ;' $
317 -- $PRI'MODEL(2) Z=(1-A*LOG(R)*X-A*R**X-B*R**(X*C)-D*R**(X*E))/LOG(R);'$
318 -- $PRI 'OPTION 1 2 2 2 0 0 3 1 4 ;' $
319 -- $PRI 'INITIAL 0.7 ;' $
320 -- $PRI 'FUN(2) C10=-SX*A/8*1000*LOG(P1) ' $'n"
321 -- let c = current*Grd*Mol.W/96490
322 -- output out,"$PRI 'C11=",fformat(c*10000,3,12),"/P2*SY/SX/A ' $
323 -- $PRI 'C12=P3/SY*100 ;' $
324 -- $PRI '10 11 12 ;' $'n$PRI 'FIT MODEL ;' $'n$PRI 'END ;' $'n$OUT 6 $
325 --
326 -- $PRI 'The file assigned to for008 is ready for use by MLP' $
327 -- $PRI 'Submit '" FIT ",name(1|length(name)-4),
328 -- " to system queue to fit data.' $
329 -- $ENDMAC'n$RETURN'n"
330 -- close(out)
331 --
332 -- write"'nThe file ",Name," is ready for use with GLIM.
333 --    Use   @SMOOTH   to initiate the smoothing." ?
```

The program listed (A2.1) produces two files: the first contains the necessary data for producing a fitted noise waveform and the other the data required to produce a smoothed transient ready for fitting by the MLP package (described in appendix III). The listings and a short description of each file will now be given.

Program A2.2, listed below, contains the data and GLIM commands for a transient with noise period less than 40, so that the entire transient will be fitted to find the noise waveform. The first two lines inform GLIM of the accuracy to which numbers must be read, (eg. to 9 places), of the number of points that will follow the READ statement and arrange to place this data into array Y. (There would then follow 695 voltage data points). The corresponding time data does not required to be entered, but is calculated within GLIM (line 9). The next 8 lines then set up constants and arrays (any letter preceded by a % is a constant, all other letters being arrays) as well as notifying which array contains the data to be fitted and what weights are to be associated with the fit. Lines 17 & 18 set up array S as the noise waveform with period %L (i.e. 40, as set in line 11). Line 19 notifies GLIM that a macro-loop called SM01 is beginning and this loop can be run once or repeatedly during the interactive section, by typing $USE SM01, until an adequate fit is obtained. Lines 20 to 22 then set up the arrays necessary in fitting a polynomial (with powers of 0, 0.125, 0.25, 0.5, 1, 2, 3 and 4) and line 23 commands GLIM to fit this polynomial to the second half of the transient (starting at %k [initially 500] upwards) along with a

straight line (from 1 to %k) and the noise waveform to the entire transient.

Lines 25 to 28 then calculate the residuals for the data and print the fourteen largest. Lines 32 & 33 tell GLIM that the macro-loop SM01 has finished and that a new loop SM02 is beginning. SM02 (lines 33 to 57) outputs the fitted noise waveform to the file assigned to channel 10, ready for further processing by the program listed in A2.4.

Program A2.2

```
 1 -- $ACC 9
 2 -- $UNI  695  $DAT Y $READ
 3 --  0.0052649 0.0052891 0.0052475 0.0052923 0.0052844 0.0052551
 4 --
 5 --    ( 695 voltage points )
 6 --
 7 --  0.0052711 0.0052794 0.0053147 0.0053271 0.0053408 0.0053507
 8 --  0.0053656 0.0053851 0.0053797 0.0053840 0.0053970
 9 -- $CAL T=%GL(%NU,1)
10 -- $YVAR Y
11 -- $CAL %N=%NU-6: %K=  500 : %L=   40
12 -- $PRI 'The WHOLE data set will be fitted. Pulse starts at (%K=)'%K$
13 -- $PRINT 'The period of the wave is (%L=) ' %L $
14 -- $PRINT 'Now use macro SM01 to smooth the data' $
15 -- $PRINT 'Find %K first, then eliminate spurious points.' $
16 -- $CAL W=1   $WEI W
17 -- $CAL S=%GL(%L,1)
18 -- $FAC S %L
19 -- $MACRO SM01
20 -- $CAL U=%GE(T,%K):V2=(T-%K)*(T-%K):V=V2**0.5:VQ=V**0.25
21 -- :VE=V**0.125:EV=0.7**V:RV=V**0.5:RV=RV*U:V=V*U:V2=V2*U
22 -- :V3=V*V2:V4=V2*V2:VQ=VQ*U:VE=VE*U:EV=EV*U
23 -- $FIT S+U+RV+VQ+VE+V+V2+V3+V4+T+EV -%GM
24 -- $DEL V4 V3 VE VQ V2
25 -- $CAL R=(%YV-%FV)*W*%SC**-0.5
26 -- $SORT OR R : OT T R $
27 -- $PRI 'Use PLOT R T or PLOT %FY T etc. to get plots of data' $
28 -- $LOOK 1 7 OT OR : %N %NU OT OR $
29 -- $PRI 'Use CAL W(i)=0 to obtain better fit' $
30 -- $PRI '%K = ' %K $
31 -- $PRI 'Use macro SM02 to obtain the whole smoothed data' $
32 -- $ENDMAC
33 -- $MACRO SM02
34 -- $OUT 10 $
35 -- $DEL R OR OT
36 -- $EXTRA %PE
37 -- $VAR %L R
38 -- $CAL %N=%PL+1 $VAR  %N OR OT$CAL OR=%PE :OT=%GL(%PL+1,1)
39 -- :OR=OR*100000 : OT=%LE(OT,%L+1) : OT(1)=0
40 -- :R(OT*%CU(OT))=OR
41 -- $PRINT R$
42 -- $PRINT R$
43 -- $PRINT R$
44 -- $PRINT R$
45 -- $PRINT R$
46 -- $PRINT R$
47 -- $PRINT R$
48 -- $PRINT R$
49 -- $PRINT R$
50 -- $PRINT R$
51 -- $PRINT R$
52 -- $PRINT R$
53 -- $PRINT R$
54 -- $PRINT R$
55 -- $OUT 6
56 -- $PRI 'Use STOP & INP 9 to obtain the whole smoothed data set' $
57 -- $ENDMAC
58 -- $RETURN
```

If the period of the noise waveform is greater than 40, then only the baseline of the transient is fitted by the most relevant coefficients of its Fourier Transform, and the commands to do so are listed in A2.3 below.

The first fifteen lines are the same as those in A2.2. Lines 16 to 32 then set up the arrays necessary to fit the 28 most relevant Fourier coefficients, while lines 33 & 34 contain the commands to fit these arrays to the baseline data contained in array Y. Lines 35 to 56 are the same as in A2.2. i.e. lines 37 to 40 calculate and print the 14 largest residuals, while lines 45 to 55 contain a macro-loop (SM02) which outputs the fitted waveform to the file assigned to channel 10, ready for use by program A2.4.

Program A2.3

```
 1 -- $ACC 9
 2 -- $UNI  500  $DAT Y $READ
 3 --  0.0000174 0.0000094 0.0000268 0.0000158 0.0000130 0.0000242
 4 --
 5 --    ( 500 voltage points )
 6 --
 7 --  0.0000297 0.0000024 0.0000361 0.0000056 0.0000064 0.0000038
 8 --  0.0011877 0.0014045
 9 -- $CAL T=%GL(%NU,1)
10 -- $YVAR Y
11 -- $CAL %N=%NU-6: %K=  500 : %L=  100
12 -- $PRI 'Only the first 500 points will be fitted. Period (%L=)'%L$
13 -- $PRINT 'Only eliminate spurious points. (Leave %K till later)' $
14 -- $PRINT 'Use macro SMO1 to initially smooth data' $
15 -- $CAL W=%LE(T,%K-5)   $WEI W
16 -- $CAL U=2*T*%PI/%L : %P=%PI/2
17 -- : S1=%SIN(1*U) : C1=%SIN(1*U+%P)
18 -- : S2=%SIN(2*U) : C2=%SIN(2*U+%P)
19 -- : S3=%SIN(3*U) : C3=%SIN(3*U+%P)
20 -- : S4=%SIN(4*U) : C4=%SIN(4*U+%P)
21 -- : S5=%SIN(5*U) : C5=%SIN(5*U+%P)
22 -- : S6=%SIN(6*U) : C6=%SIN(6*U+%P)
23 -- : S10=%SIN(10*U) : C10=%SIN(10*U+%P)
24 -- : S12=%SIN(12*U) : C12=%SIN(12*U+%P)
25 -- : S13=%SIN(13*U) : C13=%SIN(13*U+%P)
26 -- : S25=%SIN(25*U) : C25=%SIN(25*U+%P)
27 -- : S50=%SIN(50*U) : C50=%SIN(50*U+%P)
28 -- : S100=%SIN(100*U) : C100=%SIN(100*U+%P)
29 -- $MACRO SMO1
30 -- $DEL R OR OT
31 -- $CAL S8=%SIN(8*U) : C8=%SIN(8*U+%P)
32 -- : S9=%SIN(9*U) : C9=%SIN(9*U+%P)
33 -- $FIT T+S1+S2+S3+S4+S5+S6+S8+S9+S10+S12+S13+S25+S50+S100
34 -- :+C1+C2+C3+C4+C5+C6+C8+C9+C10+C12+C13+C25+C50+C100-%GM
35 -- $DEL S8 C8 S9 C9
36 -- $PRI 'Use the SECOND deviance & ignore the first as irrelevant' $
37 -- $CAL R=(%YV-%FV)*W*%SC**-0.5
38 -- $SORT OR R : OT T R $
39 -- $PRI 'Use PLOT R T or PLOT %FY T etc. to get plots of data' $
40 -- $LOOK 1 7 OT OR : %N %NU OT OR $
41 -- $PRI 'Use CAL W(i)=0 to obtain better fit' $
42 -- $PRI '%K = ' %K $
43 -- $PRI 'Use macro SMO2 to obtain the whole smoothed data' $
44 -- $ENDMAC
45 -- $MACRO SMO2
46 -- $OUT 10 $
47 -- $DEL R OR OT
48 -- $CAL OR=%FV $VAR 400 R $CAL OR=OR*100000
49 -- $CAL OT=%LE(T,400) :R(OT*%CU(OT))=OR
50 -- $PRINT R$
51 -- $PRINT R$
52 -- $PRINT R$
53 -- $OUT 6
54 -- $PRI 'Use STOP & INP 9 to obtain the whole smoothed data set' $
55 -- $ENDMAC
56 -- $RETURN
```

Once the noise waveform has been calculated and output to file (assigned to channel 10) the GLIM package is exited at the interactive stage (by typing $STOP) and re-entered so that all the arrays and variables are completely cleared and initialised ready for the next stage in the smoothing. The next stage is initiated by the commands listed in program A2.4.

The first nine lines are again the same as those for A2.2. (i.e. read in the raw data into array Y). Lines 10 & 11 then reads the noise waveform (assigned to channel 10) into array W and line 12 subtracts this noise from the raw data contained in array Y. Line 15 sets up the weights required for fitting a polynomial to Y in order to find where the current was first applied to the cell. Lines 16 to 30 then set up a macro-loop (called SM03) which fits a polynomial to the transient (from the %K th point upwards) to find the beginning of the pulse and outputs the largest residuals. This loop (SM03) enables not only the beginning of the pulse to be found, but also any spurious points present to be removed. These spurious points can be removed by typing $CAL Y(i) = %FV(i) at the interactive stage to set the i th data point to its fitted value. Once an adequate set of data has been obtained it is output to file (assigned to channel 8) by the macro-loop OOT, this loop also outputs the commands required by the MLP statistical package as described in appendix III. (lines 38 to 42 and 44 to 54).

Program A2.4

```
 1 -- $ACC 9     $UNI 994  $DAT Y
 2 -- $READ
 3 --  0.0064723 0.0064464 0.0064223 0.0064172 0.0064361 0.0064314
 4 --    ( 994 voltage points )
 5 --  0.0064711 0.0064868 0.0065443 0.0065419 0.0065482 0.0065803
 6 --  0.0065508 0.0065777 0.0065723 0.0066062
 7 -- $CAL T=%GL(%NU,1)
 8 -- $YVAR Y
 9 -- $CAL %N=%NU-6
10 -- $DATA W
11 -- $DINPUT 10
12 -- $CAL W=W/100000 :Y=Y-W : %K =   500
13 -- $PRINT 'The data has been smoothed.' $
14 -- $PRINT 'Now find %K and any outliers by using macro SM03' $
15 -- $CAL W=%GT(T, 490 ) $WEI W
16 -- $MACRO SM03
17 -- $DEL OT OR
18 -- $CAL U=%GE(T,%K):V2=(T-%K)*(T-%K):V=V2**0.5:VQ=V**0.25
19 -- :VE=V**0.125:EV=0.7**V:RV=V**0.5:RV=RV*U:V=V*U:V2=V2*U:V3=V*V2
20 -- :V4=V2*V2:VQ=VQ*U:VE=VE*U:EV=EV*U
21 -- $PRI 'Use PLOT R T or PLOT %FY T etc. to get plots of data' $
22 -- $FIT U+RV+VQ+VE+V+V2+V3+V4+T+EV -%GM
23 -- $DEL V4 V3 VE VQ V2
24 -- $CAL R=(%YV-%FV)*W*%SC**-0.5
25 -- $SORT OR R : OT T R $
26 -- $LOOK 1 7 OT OR : %N %NU OT OR $
27 -- $PRINT 'Use CAL %K=? &  CAL Y(i)=%FV(i) to obtain better fit' $
28 -- $PRINT 'The START of the pulse (%K) = ' %K $
29 -- $PRINT 'Use macro OOT to prepare MLP FILE when data is smoothed' $
30 -- $ENDMAC
31 -- $MACRO OOT
32 -- $DEL W U OT OR RV V R EV
33 -- $CAL %K=%K+1+25 : W=%GT(T,%K)*%GE(%TR(T/    1 ),T/    1 )
34 -- : %N=%CU(W) $VAR %N U V
35 -- $CAL U=%GL(%NU,1) + 25 :V(W*%CU(W))=Y : U=U* 0.0002000*  1
36 -- $PRI 'Every     1  points will be used in MLP' $
37 -- $OUT 8$
38 -- $PRINT 'CAPTION Smoothed data for cell pulsed with 0.5 mA for 1;'$
39 -- $PRINT 'CAPTION |00 mS (3 runs) 1/7/82;' $
40 -- $PRINT 'CAPTION   2.e-04    25   5.e-04      0.1    45.47  1000  ;'$
41 -- $PRINT 'CAPTION     1     33.9   157.034 -0.37222  ;' $
42 -- $PRINT 'DATA' $
43 -- $PRI*6  U       $PRI*9 V $        $PRI ';' $
44 -- $PRINT 'ECHO ;' $
45 -- $PRI 'CON 0.544885 0.1625405 3.352302 0.0772951 7.049413 45.47 1000;'$
46 -- $PRI 'NAMES C1=A,B,C,D,E,SX,SY V1=X,Y,Z P1=R ;' $
47 -- $PRI 'DER(2) X=X*SX Y=Y*SY ;' $
48 -- $PRI 'MODEL(2) Z=(1-A*LOG(R)*X-A*R**X-B*R**(X*C)-D*R**(X*E))/LOG(R);'$
49 -- $PRI 'OPTION 1 2 2 2 0 0 3 1 4 ;' $
50 -- $PRI 'INITIAL 0.7 ;' $
51 -- $PRI 'FUN(2) C10=-SX*A/8*1000*LOG(P1) ' $
52 -- $PRI 'C11=  -0.003028873224/P2*SY/SX/A ' $
53 -- $PRI 'C12=P3/SY*100 ;'          $PRI '10 11 12 ;' $
54 -- $PRI 'FIT MODEL ;'      $PRI 'END ;'      $OUT 6 $
55 -- $PRI 'The file assigned to for008 is ready for use by MLP' $
56 -- $PRI 'Submit " FIT A35M41M1 "  to system queue to fit data.' $
57 -- $ENDMAC  $RETURN
```

Appendix III

Fitting Program

In order to fit equation [64] from appendix I, a number of alterations must first be made. Obviously the sum to infinity cannot be applied, therefore as an approximation only the first three terms are used. It was found that the exponential terms in the sum had a significant effect only at the very beginning of the pulse (i.e. for approximately the first 10% of the pulse length) and corresponded to the rapidly changing shape of the transient in this region. Thus when interpreting the results of the fit it must be remembered that the first part of the transient will not be fitted well because only three exponential terms have been used, but that the rest of the transient will be adequately fitted by the curtailed series. Thus equation [64] can be written as,

$$\eta(t) = iR + \frac{Q_1(dE/d\delta)V_m i}{C_1 nFAr \ln(P)} \{1 - \frac{C_1}{Q_1} t\ln(P) - \frac{C_2}{Q_1} P^{t} - \frac{C_2}{Q_2} P^{(Q_2 t/Q_1)} - \frac{C_2}{Q_3} P^{(Q_3 t/Q_1)} \} \qquad [65]$$

where $P = \exp(-Q_1 D/r^2)$ and C_1, C_2, Q_1, Q_2 & Q_3 are constants, the values of which are given in table 1 of appendix I.

The statistical package which was used to fit this equation is called MLP (Maximum Likelihood Program, available from the Lawes Agricultural Trust, Rothamsted Experimental Station, 1980) and is particularly suited to fitting exponentials of the type in [65]. Unfortunately, the data to be fitted must first be scaled in order for MLP to work properly. The X data (i.e. time data) must be in the range 0 to 10 and the Y data (i.e. overpotential data) in the range 0 to 100. Thus if X is used to indicate the scaled time and Y the scaled overpotential and S_x & S_y the scale factors involved, we then have that $\eta = Y/S_y$ and $t = X/S_x$, leading to,

$$Y = S_y iR + \frac{S_y(dE/d\delta)V_m i}{C_1 nFAr \ln(P)} \{1 - \frac{C_1 t}{Q_1 S_x}\ln(P) - \frac{C_2}{Q_1}P^{(X/S_x)} - \frac{C_2}{Q_2}P^{(Q_2X/Q_1S_x)} - \frac{C_2}{Q_3}P^{(Q_3X/Q_1S_x)}\}$$

Letting $R = P^{(1/S_x)} = \exp(-Q_1 D/r^2 S_x)$ gives,

$$Y = S_y iR + \frac{S_y(dE/d\delta)V_m i}{S_x C_1 nFAr \ln(R)} \{1 - \frac{C_1}{Q_1}X\ln(R) - \frac{C_2}{Q_1}R^{X} - \frac{C_2}{Q_2}R^{(Q_2X/Q_1)} - \frac{C_2}{Q_3}R^{(Q_3X/Q_1)}\} \quad [66]$$

If we now let,

$$I = S_y iR$$

$$K = \frac{S_y(dE/d\delta)V_m i}{S_x C_1 nFAr}$$

and A, B, C, D, E, F be constants as denoted in table 1 below, then equation [66] becomes,

$$Y = I + \frac{K}{\ln(R)}\{ 1 - AX\ln(R) - BR^X - CR^{DX} - ER^{FX} \} \qquad [67]$$

Constant	Value	Cylindrical	Spherical	Thin Layer
A	C_1/Q_1	0.5449	0.7429	0.3040
B	C_2/Q_1	0.5449	0.4953	0.6079
C	C_2/Q_2	0.1625	0.1676	0.1520
D	Q_2/Q_1	3.3523	2.9559	4
E	C_2/Q_3	0.0773	0.0841	0.0676
F	Q_3/Q_1	7.0495	5.8889	9

Table 1

Equation [67] is thus the equation which is ultimately fitted by the MLP package. Three separate parameters are obtained (I, K and R) from the fit and these in turn lead to the values of the iR drop, D/r^2 and Ar via,

$$\text{iR drop} = I/S_y$$

$$D/r^2 = \frac{S_x}{Q_1} \ln(R)$$

$$Ar = \frac{S_y (dE/d\delta) V_m i}{S_x C_1 nF K}$$

In order to obtain comparable values to those obtained for the semi-infinite linear model the values of Ar and D/r^2 are combined to give rise to a value of $AD^{1/2}$. Thus three values will be quoted for each fit: these are a) the iR drop of the cell, b) D/r^2 (a measure of the effective diffusion coefficient), and c) $AD^{1/2}$ (a measure of the total surface area between the electrode and electrolyte).

The command file necessary to enable MLP to fit equation [67] is listed in A3.1 below. The first two lines indicate a title. (MLP has a maximum line length of 60 characters, therefore a title longer than 60 must be split into two). Lines 3 & 4 give constant values required in the evaluation of D/r^2 and Ar. (eg. V_m, $dE/d\delta$, i etc.) There then follows the data values to be fitted. Unlike the GLIM package which calculates the time data within the program, MLP requires it to

be specified. The semi-colon in line 20 indicates that all the data has been read and lines 22 & 23 declare values for A, B, C, D, E and the scale factors for X and Y. Line 24 scales the data by the values given in SX & SY. (i.e. 0.004 and 1000 respectively) Lines 25 to 27 sets the model up as well as indicating a rough initial value for R to begin the fit with. Lines 28 to 31 evaluate the values for D/r^2, Ar and the iR drop. (i.e. C10 = D/r^2, C11 = Ar & C12 = iR drop) Finally line 32 commands MLP to fit the model described in line 25.

Program A3.1

```
 1 -- CAPTION Raw data, 1 run, 0.01 mA, 2076 secs, (290 C, 15 mi;
 2 -- CAPTION |ns) on 28/4/84;
 3 -- CAPTION       3.     0   1.e-05    2076.  0.00400  1000  ;
 4 -- CAPTION     1    33.97   157.034 -0.37222  ;
 5 -- DATA
 6 --        1.       4.       7.      10.      13.
 7 --       16.      19.      22.      25.      28.
 8 --
 9 --       (1975 time data points)
10 --
11 --     1951.    1954.    1957.    1960.    1963.
12 --     1966.    1969.    1972.    1975.
13 --  0.000716375  0.000907375  0.001033375  0.001141375  0.001201375
14 --  0.001341375  0.001427375  0.001478375  0.001592375  0.001548375
15 --
16 --       (1975 voltage data points)
17 --
18 --  0.007852375  0.007827375  0.007857375  0.007842375  0.007856375
19 --  0.007876375  0.007847375  0.007887375  0.007859375
20 -- ;
21 -- ECHO ;
22 -- CON  0.5448848 0.1625405 3.3523020 0.0772951 7.0494130 0.004 1000;
23 -- NAMES C1=A,B,C,D,E,SX,SY V1=X,Y,Z P1=R ;
24 -- DER(2) X=X*SX Y=Y*SY ;
25 -- MODEL(2) Z=(1-A*LOG(R)*X-A*R**X-B*R**(X*C)-D*R**(X*E))/LOG(R);
26 -- OPTION 1 2 2 2 0 0 3 1 4 ;
27 -- INITIAL 0.7 ;
28 -- FUN(2) C10=-SX*A/8*1000*LOG(P1)
29 -- C11=  -0.000060577464/P2*SY/SX/A
30 -- C12=P3/SY*100 ;
31 -- 10 11 12 ;
32 -- FIT MODEL ;
33 -- END ;
```

To fit the required model the above command file must be assigned to the input channel of MLP before the package can be run. When this has been done then the fitting of the model can proceed by running the MLP package. The relevant data (i.e. fitted parameters, residuals, fitted values etc.) is automatically output to file where it can be plotted. An example of the plots and parameters obtained is shown in figure 1.

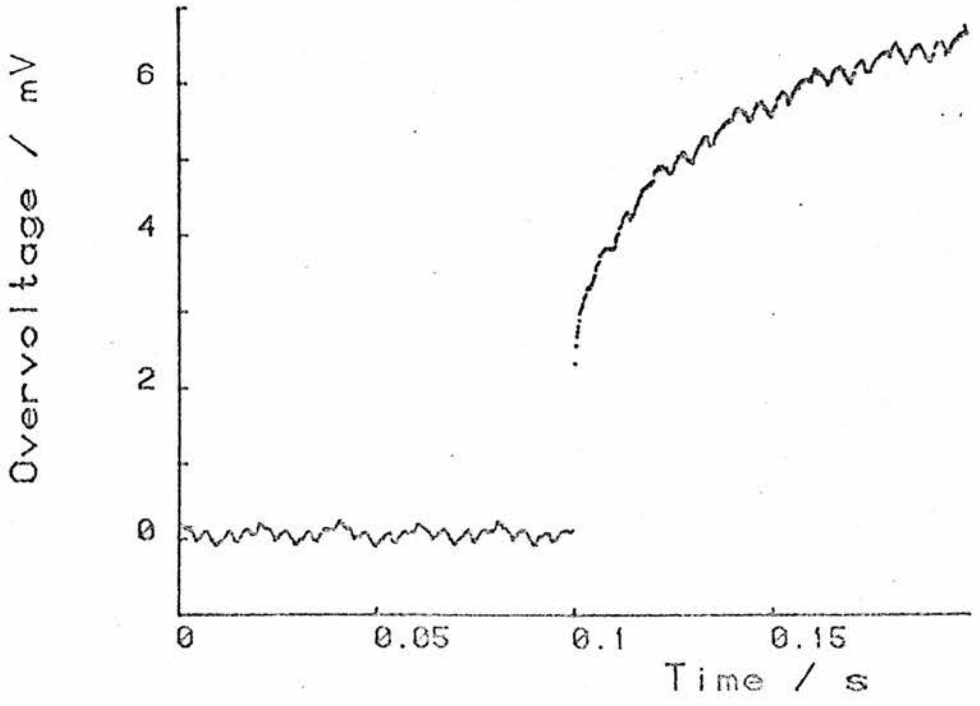

Figure 1 (a): Original Voltage Transient.

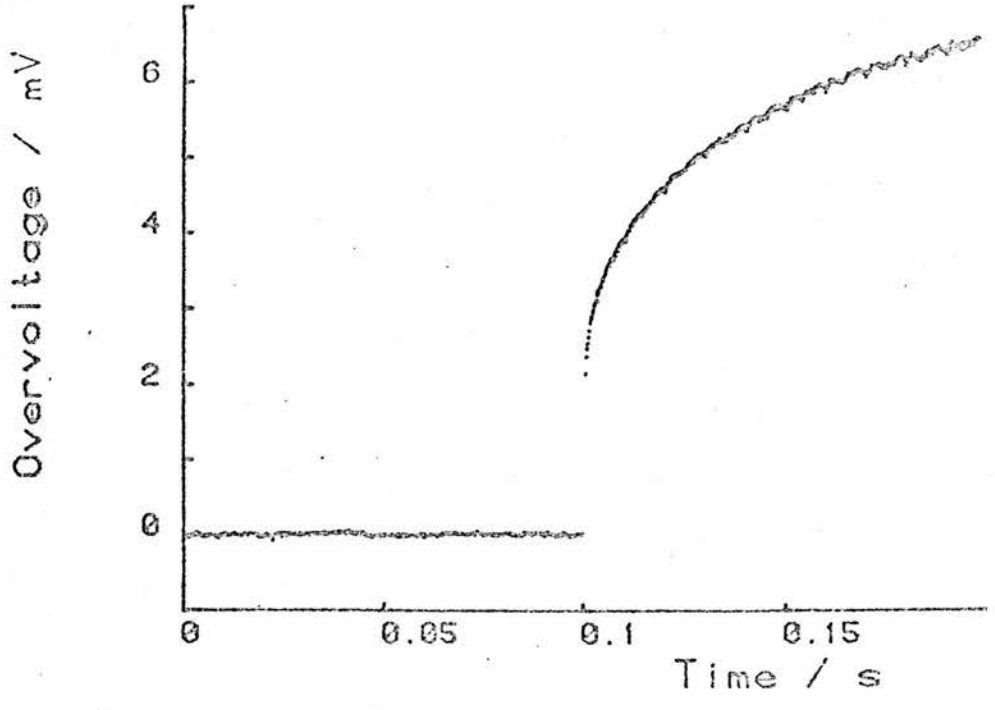

Figure 1 (b): Smoothed Voltage Transient.

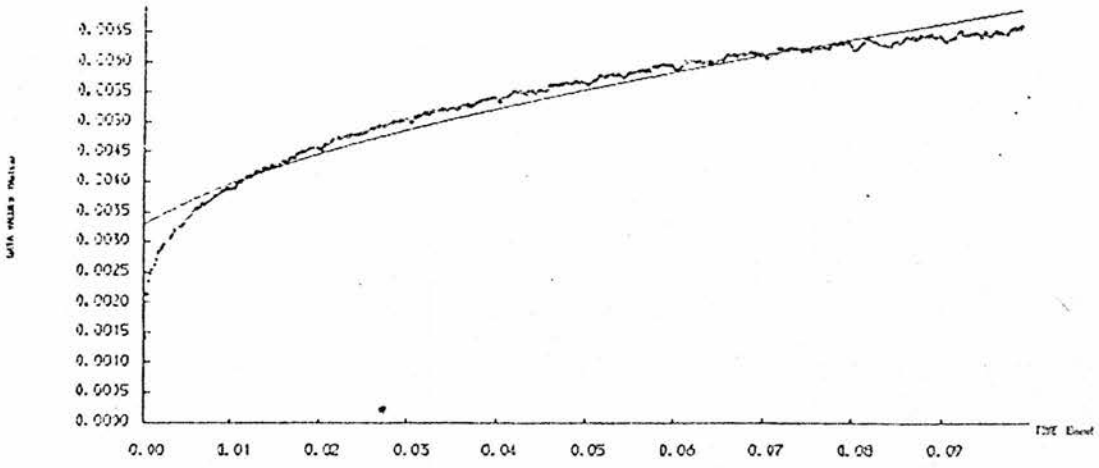

Figure 1 (c): Smoothed data and fitted curve for the cylindrical model.

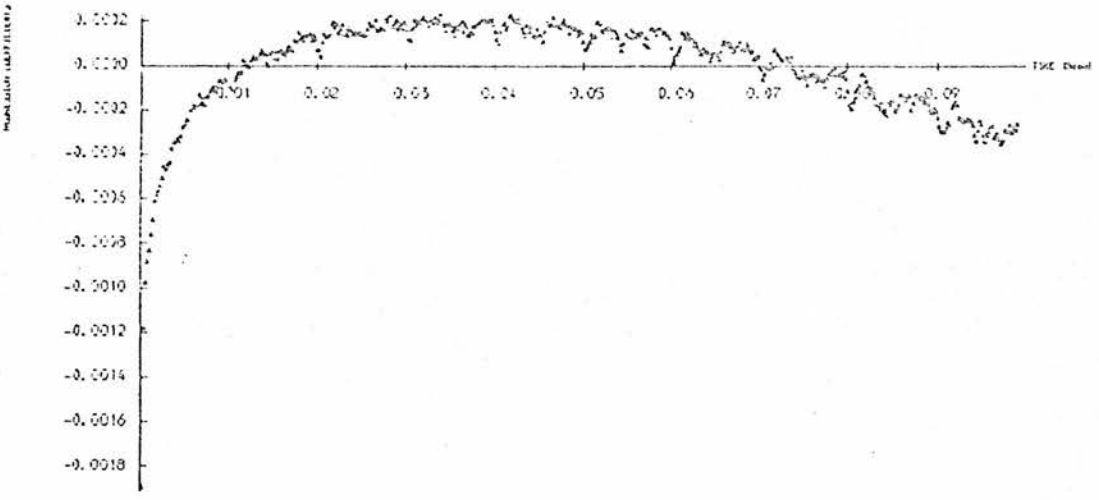

Figure 1 (d): Standardised Residuals for the cylindrical model.

Fitted parameters obtained from the above transient,

Pulse current	= 0.5 mA
D/r^2	= 1.305 $secs^{-1}$
$AD^{\frac{1}{2}}$	= 6.964 10^{-6} $cm^3 secs^{-\frac{1}{2}}$
iR drop	= 2.850 mV
R.M.S.	= 4.757 10^{-8}

Appendix IV

Mixed Phase Electrode Model Programs.

Four programs were required to carry out the calculations involved in the mixed phase electrode model described in Chapter 3. These are,

(a) ARRAY.COM, command file to carry out repeated runs.

(b) RAND.GLM, command file for GLIM to generate random numbers.

(c) SETSEED.S Salgol program to generate seeds required by (b).

(d) SORTARRAY.S Salgol program to generate and process a lattice.

Each of these programs is listed (with short descriptions) at the end of this appendix.

The functions these programs perform can be separated into three processes which are run repeatedly. First, programs (b) and (c) set up the necessary parameters which are required by the statistical package GLIM to produce a file containing randomly distributed 1's and 0's in a preselected ratio. Program (d) then creates a three dimensional array and, using the previously created file, fills it with 0's and 1's according to the particular random scheme generated. A point on the array with value 0 corresponds to an ionic conducting or "A" particle on the real lattice; a point with value 1 corresponds to an electronic conducting or "B" particle. The array is then processed so that all the A's and B's which are not linked to their

pure form are deleted. Finally the number of "links" (see Chapter 3) between the A's and B's are calculated, together with the number of A's and B's which have 0, 1, 2, 3, 4 or 5 links, and this information is sent to file for storage.

Program (a) is the command file which controls the above three processes. It can perform several runs in sequence and permits various parameters to be altered, eg. the number of layers, percentage composition, etc. This program keeps track of the central processing unit (CPU) time that has been used and, if it is approaching one hour (the maximum CPU time allowed for any one session), then it aborts and resubmits itself to continue running at a new session where it has left off.

The reason for using the GLIM statistical package to create the random array (instead of using a simple random number generator available through the normal high level language compiler) is to avoid any 'structure' occurring in the randomness of the array. With a single random number generator there is the possibility of certain random numbers occurring more frequently than they should. By using GLIM it was possible to use three separate random number generators to produce a single set of random numbers with no structure. This was done by generating three separate sets of random 0's and 1's, and then using the first set to decide which of the other two sets were to be chosen, as shown in figure 1.

Set 1	Set 2	Set 3	Resultant Random Number
0	1	0	1
0	0	1	0
1	1	0	0
1	1	1	1
0	1	0	1
1	0	0	0
0	1	1	1

Figure 1

i.e. a zero in set 1 means, 'use the random number found in set 2' and a one in set 1 means, 'use the random number found in set 3'.

It is at this stage that the relative proportion of A to B (i.e. 0's to 1's) is decided; for example a composition comprising of 50% A corresponds to an equal number of 0's and 1's being output, whereas 25% A corresponds to three times the number of 1's to 0's and so on.

After the random number file has been generated, the main program, SORTARRAY.S, is run. This program first creates an array (of the required dimensions) and fills it with 1's and 2's: a zero in the random number file produces a 1 in the array; a one in the file produces a 2 in the array.

A 1 is defined to correspond to an A which has not yet been examined to find out if it eventually connect back to the bulk constituent. When this has been checked, and if it is indeed so

connected, the description parameter is set to 3, if not it is set to 0, indicating an isolated particle. Likewise a 2 corresponds to an unchecked B and a 4 to a B which is connected back to its respective bulk layer. Also, by definition, the first (top) layer is considered to be pure A and so is set to 3, while the last (bottom) layer is pure B and set to 4.

The program therefore examines all the 1's in the array, starting at the second layer and working down. If one of the six neighbours to a 1 is a 3, (i.e. a particle of A connected to its bulk layer), then the 1 is set to 3. If the 1 is surrounded by 0's, 2's or 4's, then this indicates that the element is isolated from the bulk layer and so it is set to 0. If, on the other hand, the 1 is connected to another 1, then this second 1 must be examined to see if it connects back to its bulk constituent, before a decision on the first element can be made. In this situation it may be necessary to follow a long chain of 1's (wherever they lead) before a decision can be made on the first 1 encountered.

Once the program has worked down through the whole array examining all the 1's, (resetting them to 0 or 3), it then repeats the process for the 2's, setting any 2 connected to a 4, (i.e. a particle of B connected to its bulk), to a 4 and any isolated 2's to a 0. This time the program starts at the bottom of the array and works upwards.

After the array has been processed in this manner it will only contain 3's and 4's corresponding to A's and B's that are connected to their respective bulk layers, and 0's which correspond to isolated A's and B's. In the final stage of the program the number of 'links' existing between the 3's and 4's is determined. This is done by examining all the 3's in the array, (i.e. A's which are connected to their bulk layer), starting at the top and working down. The six neighbours of each 3 is examined and if a 4 is encountered, then the total number of links is incremented by one. This not only generates the total number of links (between the 3's and 4's), but also the number of 3's (and 4's) that have 0, 1, 2, 3, 4, 5 links with a 4.

Once the array has been processed the relevant data (i.e. total number of links, number of 3's with 0, 1, 2, 3, 4, 5 links, number of isolated 3's, etc.) is output to file for storage.

The four programs (with short descriptions) are listed below.

(a) ARRAY.COM

This program is the main command program which controls the running of the other three programs. It can increment the parameters the model examines (e.g. change the thickness or composition ratio of the region); it also measures the total CPU time used and estimates whether enough time remains to complete another run, or whether the program must be resubmitted to the queue. The command file is run as

a batch file from a queue called SLOW$BATCH which allows the program one hour of CPU time, and also allows it to 'chain' itself repeatedly (i.e. resubmit the file to the queue for another run).

Program A4.1

```
 1 -- $ set default [chrin.array]
 2 -- $ on error then goto abort
 3 -- $start:
 4 -- $ delete randomary.dat;*
 5 -- $! Time is in 1/100 th's of a second.
 6 -- $ tstart = 'f$getjpi("","CPUTIM")'
 7 -- $ tlimit = 'f$getjpi("","CPULIM")'
 8 -- $ P2 = 'P2'
 9 -- $ P1 = 'P1' + 1
10 -- $ if P1.GE.3 then goto change
11 -- $cont:
12 -- $ if P2.GT.100 then goto leave
13 -- $ row = 50
14 -- $ col = 50
15 -- $ lay = 10
16 -- $ perc = 'P2'
17 -- $! Calculate the number of seeds GLIM requires.
18 -- $ n = row * col * lay/2000
19 -- $! Write n and perc to file perc.dat
20 -- $ open/write out perc.dat
21 -- $ write out perc
22 -- $ write out n
23 -- $ close out
24 -- $ sr setseed
25 -- $ delete perc.dat;*
26 -- $ ASSIGN RAND.GLM FOR005
27 -- $ ASSIGN SEED.GLM FOR011
28 -- $ ASSIGN RANDOMARY.DAT FOR008
29 -- $ run sys$user:glim3a
30 -- $ delete seed.glm;*
31 -- $! Write the dimensions of the array to file, dim.dat
32 -- $ open/write outfile dim.dat
33 -- $ write outfile row
34 -- $ write outfile col
35 -- $ write outfile lay
36 -- $ write outfile perc
37 -- $ close outfile
38 -- $ run sortarray.exe
39 -- $ append tempdata.dat datachain.dat
40 -- $ delete tempdata.dat;*
41 -- $ purge dim.dat
42 -- $! Time in 1/100 secs
43 -- $ trun = 'f$getjpi("","CPUTIM")' - 'tstart'
44 -- $ if(f$getjpi("","CPUTIM")+trun).LT.(tlimit-500) then goto start
45 -- $subslow:
46 -- $ purge array.log
```

```
47 -- $ submit/queue=slow$batch/log_file=[chrin.array] -
48 --         /priority=1/cputime=01:00:00 -
49 --       array.com   -
50 --         /parameters=('P1','P2')
51 -- $ exit
52 -- $change:
53 -- $ P2 = P2 + 1
54 -- $ P1 = 0
55 -- $ goto cont
56 -- $abort:
57 -- $ P1 = P1 - 1
58 -- $ n = P1 +1
59 -- $ t = f$getjpi("","CPUTIM")/100
60 -- $ if(f$getjpi("","CPUTIM")).GE.(tlimit-100) then goto subslow
61 -- $ open/write out mail.dat
62 -- $ write out "An error has occurred in VAXB:[CHRIN.ARRAY]ARRAY.COM"
63 -- $ write out "and the values of P1 = ''n' & P2 = ''P2'"
64 -- $ write out "with cputime = ''t' secs."
65 -- $ close out
66 -- $ send chrin =[chrin.array]mail.dat
67 -- $ delete [chrin.array]mail.dat;*
68 -- $ goto subslow
69 -- $ exit
70 -- $leave:
71 -- $ send me end
72 -- The array.com has run 3 times with values :-.
73 --                Rows    =   50
74 --                Columns =   50
75 --                Layers  =   10
76 --
77 --       and approx.  0-100 % of 1's to total no. of elements.
78 --       where the 1's are 5 times the size of the 2's.
79 -- $stop
```

Line 1 is the default directory to which all the files are written or from which they are read. Line 2 directs execution to the label "ABORT" (line 56) if an error occurs during any stage of the program. If the error is due to the CPU time limit being exceeded then the job (command file) is resubmitted from where it left off before the error; otherwise the user is notified of the error and the job is resubmitted, (lines 56 to 69).

Line 4 clears space on the disc in readiness for a new run, while line 6 and 7 record the time the program was started and the time limit for the job, (i.e. 1 hour). In this example the composition of the array is incremented by one from 0% to 100% and P2 is the variable containing the current value of composition, line 8. The program is run three times at each value of composition, and the counter for the number of runs is P1, which is incremented by one each time the program is run, line 9. In line 10, if P1 is greater than 3 then execution is sent to line 52, where P2 is incremented by one and P1 is reset to 0 before execution is continued, (i.e. sent to line 11). In line 12 if the value of composition has reached 100% then execution is terminated, (line 70). Lines 13 to 16 set up constants which the main program SORTARRAY requires, (i.e. the composition and dimensions of the array). Line 17 to 25 then set up and run the program SETSEED, which creates seeds for the random number generators used by GLIM and outputs the seeds to file (SEED.GLM). Lines 26 to 30 assign the necessary files to GLIM, which is then run creating a file (RANDOMARY.DAT) of random 0's and 1's with the required ratio.

Lines 31 to 37 create a file (DIM.DAT) containing the data required by the SORTARRAY program and line 38 sets the program running. SORTARRAY then runs indicating, as it progresses, what stage it has reached, (see listing for SORTARRAY). When the program has been successfully completed, then execution can continue from line 39, which appends the file TEMPDATA.DAT (the data from a single run of SORTARRAY) to a file, DATACHAIN.DAT, containing data from all the

previous runs.

Lines 42 to 51 then decide whether or not there is enough CPU time remaining for another run of the programs. If there is, the execution is sent back to the start, line 3, but if not, execution is terminated and a new job is submitted which carries on from where this job left off.

(b) RAND.GLM

This program contains the commands which GLIM requires to generate a set of unstructured random 0's and 1's. It requires a file (assigned to channel 11) containing the relative proportions of 0's to 1's that is required, as well as a set of seeds for the random number generator. This file (at channel 11) is created by the SETSEED program which is described in part (c). The set of random 0's and 1's are output to the file assigned to channel 8, RANDOMARY.DAT.

Program A4.2

```
 1 -- $C THIS GLIM PROGRAM OUTPUTS RANDOM NUMBERS
 2 -- $C WITHOUT ANY STRUCTURE.
 3 -- $UNIT 2000
 4 -- $C UNI <INTEGER> IS THE NUMBER OF RANDOM NUMBERS CALCULATED
 5 -- $C WITHIN THE LOOP EACH TIME IT IS PERFORMED. %L IS THE
 6 -- $C NUMBER OF TIMES THAT THE LOOP IS PERFORMED.
 7 -- $C %L & %P ARE READ IN, %P IS THE PERCENTAGE OF 0'S TO 1'S.
 8 -- $C SEEDS MUST BE RANDOM INTEGERS BETWEEN 1 AND 4095,4095,2047
 9 -- $C %P AND SEEDS TAKEN FROM A FILE IN CHANNEL 11
10 -- $C X TAKES THE VALUE 1 WHEN SR IS GREATER THAN OR EQUAL TO %P
11 -- $INPUT 11
12 -- $MAC LOOP
13 -- $INPUT 11
14 -- $CAL A=%GE(%SR(0),%P)
15 -- $INPUT 11
16 -- $CAL B=%GE(%SR(0),%P)
17 -- $INPUT 11
18 -- $CAL C=%GE(%SR(0),0.5)
19 -- $CAL X=%EQ(C,1)*A+%EQ(C,0)*B
20 -- $OUT 8
21 -- $PRINT *1 X $
22 -- $CAL %K=%K+1 : %E=%LT(%K,%L)
23 -- $ENDMAC
24 -- $CAL %K=1 : %E =1 $WHILE %E LOOP $
25 -- $STOP
```

Line 3 sets up the number of elements each array can hold. The maximum number of elements GLIM can hold in a single array is 2000: thus in order to create more than 2000 random numbers the whole procedure must be repeated by a loop. The entire program is set up as a macro loop (called LOOP, lines 12 to 23) which is run and controlled by the WHILE statement in line 24. Line 11 reads in from the file assigned to channel 11 (SEED.DAT) the total number of times LOOP is to be run and the ratio of 0's to 1's required, (e.g. the line at channel 11 could read, $CAL %L=5 : %P=0.5 meaning 10000 random numbers are required with a ratio of 1:1). %K is the loop counter which is initially set to one (line 24) and incremented (line 22) after each set of 2000 random numbers have been output. The WHILE statement (line 24) to control LOOP is itself controlled by a logical variable, %E, which is true when %K < %L but false when %K > %L (line 22).

Lines 12 to 23 contain the macro loop (LOOP) which generates three separate sets of random numbers, (contained in arrays A, B, C) and from these, selects one set of random numbers with no structure (contained in array X). Lines 13 to 18 stimulate the random number generator to fill A, B, C using the seeds found at channel 11 (e.g. the line at channel 11 might read, $SSEED 211 3978 1977 $RETURN). The random number generator {$SR(0)} generates real numbers between 0 and 1, which are then compared to the value of %P, (the required ratio of 0's to 1's), if $SR(0) => %P then the result is 1, if $SR(0) < %P then the result is 0. In this way a set of random 0's and 1's (of the desired ratio) are created from a set of random real numbers. In line

19 the three sets of random numbers are combined, as described earlier, to create an unstructured set which is then output to the file assigned to channel 8 (RANDOMARY.DAT) by lines 20 and 21.

(c) SETSEED.S

This program generates a file containing data required by RAND.GLM, the random number generator described above. The first line of the file contains information telling RAND.GLM how many times its internal loop must be run and what ratio of 0's to 1's is required. The rest of the file contains sets of three seeds that are used by RAND.GLM. The information concerning the above (i.e. ratio of 1's to 0's and total number of times to run the loop) is read from a file called PERC.DAT created initially by ARRAY.COM.

Program A4.3

```
! Program to generate seeds for the GLIM random number generator.
!     (i.e. GLIM requires 3 seeds per run)
!     This program is set up for the ARRAY.COM program.
! Output seeds to file SEED.GLM
let name = "SEED.GLM"
let out = create(name,"s","a","v",256)
if out=nullfile do { write "'n Cannot create ",name ; abort }
!Procedure to create a random number.
procedure b.not(int x -> int)
        if x=maxint then -maxint-1 else -(x+1)
procedure b.xor (int x,y -> int)
        b.and(b.or(x,y),b.not(b.and(x,y)))
procedure randint (int i -> int)
{       i := b.xor(shift.r(i,13),i)
        i := b.xor(shift.l(i,18),i)
        b.and(i,maxint) }
procedure plant.seed (-> int)
{       let seed.str = date(length(date)-1|2)
        let seed := decode (seed.str(1|1)) - 48
        seed := 10 * seed + (decode ( seed.str(2|1)) - 48)
        seed*seed       }
procedure random ( int seed -> real)
{       seed := randint(seed)
        seed*1/maxint   }
let s0 = "$CAL %L="
let s1 = " : %P="
let s2 = " $SSE "
let s3 = " $RETURN"
i.w := 4
s.w := 0
! Read the percentage of 1's to total from file, perc.dat.
let In = open("PERC.DAT","a",0)
if In=nullfile do {write"'n Cannot open PERC.DAT'n" ; abort }
let perc = readi(In)/100
let n = readi(In) + 1
close (In)
write "'n The % of 1's to total = ",perc*100
write"'n& the number r of seeds required by GLIM = ",n
output out, s0,n,s1,fformat(perc,2,6),s3,"'n"
s.w := 1
let seed := plant.seed
for i=1 to 3 * (n+1) do
        begin
        let r = vector 1::20 of 0.0
        for j=1 to 20 do
              { r(j) := random(see(d)
                seed := truncate(r(j)*maxint)   }
        let seed1 = truncate(r(3) * 4095)
        let seed2 = truncate(r(11) * 4095)
        let seed3 = truncate(r(17) * 2047)
        output out, s2,seed1,seed2,seed3,s3,"'n"
        for j=1 to 33 do {let dummy = random(seed)
                  seed := truncate(dummy*maxint)}
        end
close(out)
?
```

Lines 5 to 7 create an output file (SEED.GLM) which will eventually contain all the required seeds. The seeds generated for RAND.GLM are themselves produced by a random number generator, but as Salgol does not have a built-in generator, lines 8 to 24 contain procedures {called RANDOM(seed)} which generate a random number between 0 and 1.

Lines 25 to 30 set up variables required later, while lines 32 to 36 read the relevant information from the input file, PERC.DAT. Line 39 outputs the required first line in SEED.GLM, e.g. $CAL %L = 5 : %P = 0.4 $RETURN. The FOR loop (lines 42 to 54) create the total number of seeds which RAND.GLM will require. The vector r, (line 44), contains twenty random numbers, (generated by lines 45 to 47), of which only three are chosen as seeds, lines 48 to 50. This 'excess' of random numbers are generated to ensure a 'true' random seed being output. Line 51 then outputs the seeds in the required format (i.e. $SSE 4011 2765 576 $RETURN). Lines 52 to 53 then ensure that the random number generator will be re-entered in a random manner and lines 55 to 56 terminate the program.

(d) SORTARRAY.S

This is the main program of the four and generates the randomly filled lattice, determines whether or not particles are connected to their respective bases, discards any isolated particles, and calculates the number of links which exist between the two types of particle. The progress of the program is output periodically along with the time taken for the section to be completed. At the end of the program the relevant data is output to TEMPDATA.DAT. This file contains the array dimensions, total number of 1's and 2's, total number of links and the number of 3's and 4's with 0, 1, 2, 3, 4, 5 links.

Program A4.4

```
 1 -- !   PROGRAM TO CALCULATE THE NUMBER OF LINKS
 2 -- ! BETWEEN TWO EQUAL PARTICLES RANDOMLY DISTRIBUTED
 3 -- ! ON A 3-DIMENSIONAL ARRAY, WHICH IS READ FROM
 4 -- ! A DISC FILE CALLED, RANDOMARY.DAT
 5 --
 6 -- procedure cputime(-> real )
 7 -- !   Returns the number of minutes the program has been running for.
 8 -- !  (remember that this time is the total amount of cputime used.
 9 -- !    i.e. for the whole section on the computer.)
10 -- {        let time.str := time
11 --          let min.str := time.str(4|2)
12 --          let sec.str := time.str(7|2)
13 --          let temp := decode(min.str(1|1)) - 48
14 --          let mins := 10*temp + decode(min.str(2|1)) - 48
15 --          temp := decode(sec.str(1|1)) - 48
16 --          let secs := 10*temp + decode(sec.str(2|1)) - 48
17 --          mins*1.0 + secs/60
18 -- }
19 --
```

```
20 -- let CHAIN.LEN := 0
21 -- let CHAIN.AVERAGE := 0.0
22 -- let CHAIN.CALL := 0
23 -- let first.time = cputime
24 --
25 --
26 -- s.w := 1
27 -- i.w:=  5
28 -- r.w := 5
29 --
30 -- ! Read the array dimensions of file, dim.dat
31 --
32 -- let Name="dim.dat"
33 -- let Inp= open(Name,"a",0)
34 -- if Inp = nullfile do{ write"'n",Name," cannot be opened."; abort }
35 --
36 -- let R = readi(Inp) + 2
37 -- write "'n The number of rows =",R-2
38 -- let C = readi(Inp) + 2
39 -- write "'n The number of columns =",C-2
40 -- let L = readi(Inp) + 2
41 -- write "'n The number of layers =",L-2
42 -- let perc = readi(Inp)
43 -- write"'n The % of 1's to total =",perc
44 -- close(Inp)
45 --
46 --
47 -- ! Read array from file randomary.dat.
48 -- ! There must be at least (R-2)*(C-2)*(L-2)
49 -- ! random 1's & 2's in randomary.dat
50 --
51 -- let name = "randomary.dat"
52 -- let inp = open(name,"a",0)
53 -- if inp = nullfile do{ write"The opening of",
54 --                       name," was unsuccessful.";abort}
55 --
56 -- let count.1 := 0
57 -- let count.2 := 0
58 --
59 -- let M.lat = vector 1::R,1::C,1::L of 0
60 --
61 -- for iL = 2 to L-1 do
62 --     begin
63 --     for iR = 2 to R-1 do
64 --         begin
65 --         for iC = 2 to C-1 do
66 --             begin
67 --             let numb = readr(inp)
68 --             case numb of
69 --              0.0 : count.1 := count.1 + 1
70 --              1.0 : count.2 := count.2 + 1
71 --             default : { write"'nOne of the data points in ",
72 --                                 name," = ",numb,"'n" ; abort }
73 --             M.lat(iR,iC,iL) := truncate( numb + 1 )
74 --             end
75 --         end
76 --     end
77 -- close(inp)
78 --
79 -- write"'n The array has been read from file in ",
80 --          cputime-first.time," mins."
81 --
82 -- ! Set top layer to 3 and bottom layer to 4.
83 -- for iR = 2 to R-1 do
```

```
84 --     { for iC = 2 to C-1 do
85 --                              { M.lat(iR,iC,1) := 3
86 --                                M.lat(iR,iC,L) := 4 }  }
87 -- write"'n",count.1+count.2,"points have been read in to the M.lat."
88 -- write"'n and it took ",cputime-first.time," mins."
89 --
90 -- procedure find.options(int r.ch,c.ch,l.ch,tar;string opt -> string)
91 --     {
92 --     if tar =1 then
93 --         begin      ! Tendency to go UP to top.
94 --         if ((l.ch - 1) >= 1 and M.lat(r.ch,c.ch,(l.ch-1)) = 1 )
95 --             do opt := "U"
96 --         if ((c.ch + 1) <= C and M.lat(r.ch,(c.ch+1),l.ch) = 1 )
97 --             do opt := opt ++ "R"
98 --         if ((r.ch + 1) <= R and M.lat((r.ch+1),c.ch,l.ch) = 1 )
99 --             do opt := opt ++ "F"
100 --         if ((c.ch - 1) >= 1 and M.lat(r.ch,(c.ch-1),l.ch) = 1 )
101 --             do opt := opt ++ "L"
102 --         if ((r.ch - 1) >= 1 and M.lat((r.ch-1),c.ch,l.ch) = 1 )
103 --             do opt := opt ++ "B"
104 --         if ((l.ch + 1) <= L and M.lat(r.ch,c.ch,(l.ch+1)) = 1 )
105 --             do opt := opt ++ "D"
106 --         end
107 --
108 --               else
109 --
110 --         begin   ! Tendency to go DOWN to bottom.
111 --         if ((l.ch + 1) <= L and M.lat(r.ch,c.ch,(l.ch+1)) = 2 )
112 --             do opt := "D"
113 --         if ((c.ch + 1) <= C and M.lat(r.ch,(c.ch+1),l.ch) = 2 )
114 --             do opt := opt ++ "R"
115 --         if ((r.ch + 1) <= R and M.lat((r.ch+1),c.ch,l.ch) = 2 )
116 --             do opt := opt ++ "F"
117 --         if ((c.ch - 1) >= 1 and M.lat(r.ch,(c.ch-1),l.ch) = 2 )
118 --             do opt := opt ++ "L"
119 --         if ((r.ch - 1) >= 1 and M.lat((r.ch-1),c.ch,l.ch) = 2 )
120 --             do opt := opt ++ "B"
121 --         if ((l.ch - 1) >= 1 and M.lat(r.ch,c.ch,(l.ch-1)) = 2 )
122 --             do opt := opt ++ "U"
123 --         end
124 --
125 --         opt ++ "N"
126 --
127 --     }
128 --
129 --
130 --
131 --
132 -- procedure follow.chain (int r.chain,c.chain,l.chain,target )
133 --     begin
134 --     if ( M.lat((r.chain + 1),c.chain,l.chain) ~= target and
135 --          M.lat((r.chain - 1),c.chain,l.chain) ~= target and
136 --          M.lat(r.chain,(c.chain + 1),l.chain) ~= target and
137 --          M.lat(r.chain,(c.chain - 1),l.chain) ~= target and
138 --          M.lat(r.chain,c.chain,(l.chain + 1)) ~= target and
139 --          M.lat(r.chain,c.chain,(l.chain - 1)) ~= target  )
140 --     then M.lat(r.chain, c.chain, l.chain) := 0
141 --     else
142 --         begin
143 --
144 --         CHAIN.CALL := CHAIN.CALL + 1
145 --         let set := 5
146 --         let chain.pos = vector 1::(R*L),1::3 of 0
147 --         let chain.opt = vector 1::(R*L) of " "
148 --         let chain.len := 1
```

```
149 --          let branch := 0
150 --          let test := false
151 --          let options := ""
152 --          options:=find.options(r.chain,c.chain,l.chain,target,options)
153 --          !   Store M.lat element temporarily in chain.pos.
154 --          chain.pos(1,1) := r.chain
155 --          chain.pos(1,2) := c.chain
156 --          chain.pos(1,3) := l.chain
157 --          chain.opt(1) := options
158 --          M.lat(r.chain,c.chain,l.chain) := 5
159 --
160 --
161 --          while ( ~test and (options ~="N" or branch ~= 0 )  )
162 --          do
163 --              begin
164 --              let move := options(1|1)
165 --              if options~= "N"do options:=options(2|(length(options)-1))
166 --              if branch ~= 0 then { chain.opt(branch) := options
167 --                                    branch := 0  }
168 --                                else chain.opt(chain.len) := options
169 --              case  move  of
170 --                  "U" : l.chain := l.chain - 1
171 --                  "D" : l.chain := l.chain + 1
172 --                  "L" : c.chain := c.chain - 1
173 --                  "R" : c.chain := c.chain + 1
174 --                  "B" : r.chain := r.chain - 1
175 --                  "F" : r.chain := r.chain + 1
176 --                  "N" :  {}
177 --              default : write"'nOne of the points has NO options."
178 --
179 --
180 --              options := ""
181 --              options:=find.options(r.chain,c.chain,l.chain,target,options
182 --
183 --              if  M.lat(r.chain,c.chain,l.chain) =  target do
184 --                 begin
185 --                 chain.len := chain.len + 1  !i.e. have a new point
186 --                 if chain.len > CHAIN.LEN do CHAIN.LEN := chain.len
187 --                 CHAIN.AVERAGE := CHAIN.AVERAGE+chain.len
188 --                 M.lat(r.chain,c.chain,l.chain) := 5
189 --                 chain.pos(chain.len,1) := r.chain
190 --                 chain.pos(chain.len,2) := c.chain
191 --                 chain.pos(chain.len,3) := l.chain
192 --                 chain.opt(chain.len) := options
193 --                 end
194 --
195 --              ! Test M.lat element to see if it is connected to Home.
196 --              if ( M.lat((r.chain - 1),c.chain,l.chain) = target + 2 or
197 --                   M.lat((r.chain + 1),c.chain,l.chain) = target + 2 or
198 --                   M.lat(r.chain,(c.chain - 1),l.chain) = target + 2 or
199 --                   M.lat(r.chain,(c.chain + 1),l.chain) = target + 2 or
200 --                   M.lat(r.chain,c.chain,(l.chain - 1)) = target + 2 or
201 --                   M.lat(r.chain,c.chain,(l.chain + 1)) = target + 2  )
202 --              do test := true
203 --
204 --              if test then set := target + 2
205 --                 else
206 --                 begin
207 --                 if options = "N" do
208 --                    begin     ! Look for branching in the chain
209 --                    branch := 1
210 --                    while chain.opt(branch) = "N" do branch := branch +1
211 --                    if branch <= chain.len
212 --                    then
213 --                    { r.chain := chain.pos(branch,1)
```

```
214 --                      c.chain := chain.pos(branch,2)
215 --                      l.chain := chain.pos(branch,3)
216 --                      options := ""
217 --              options:=find.options(r.chain,c.chain,l.chain,target,options
218 --                      chain.opt(branch) := options   }
219 --                  else { set := 0
220 --                         branch := 0
221 --                         options := "N"  }
222 --                  end
223 --              end
224 --          end
225 --
226 --          ! Set all points in chain to set
227 --          for i. = 1 to chain.len do
228 --           {M.lat(chain.pos(i.,1),chain.pos(i.,2),chain.pos(i.,3)):=set}
229 --          end
230 --
231 --
232 --      end
233 --
234 --
235 --
236 --
237 -- !                MAIN PROGRAM
238 -- !        Look for elements connected to Home.
239 --
240 -- let FOLLOW.CHAIN := 0
241 --
242 -- !   Proceed through the array from TOP to BOTTOM.
243 -- for iL = 2 to ( L - 1 )  do
244 --      begin
245 --      for iR = 2 to ( R - 1 )  do
246 --          begin
247 --          for iC = 2 to ( C - 1 ) do
248 --              begin
249 --              if M.lat(iR,iC,iL) = 1 do
250 --                begin
251 --                if (M.lat(iR,iC,(iL-1)) = 3 or M.lat(iR,iC,(iL+1)) = 3 or
252 --                    M.lat((iR-1),iC,iL) = 3 or M.lat((iR+1),iC,iL) = 3 or
253 --                    M.lat(iR,(iC-1),iL) = 3 or M.lat(iR,(iC+1),iL) = 3 )
254 --                then M.lat(iR,iC,iL) := 3
255 --                else { follow.chain(iR,iC,iL,1)
256 --                       FOLLOW.CHAIN := FOLLOW.CHAIN + 1 }
257 --                end
258 --              end
259 --          end
260 --      write"'n The",iL,"layer has been processed."
261 --      write"'n in ",cputime-first.time," mins"
262 --      end
263 --
264 -- write"'n All the 1's have been processed to 0's or 3's."
265 -- write"'n and it took ",cputime-first.time," mins"
266 --
267 -- !    Proceed through array from BOTTOM to TOP.
268 -- for iL = (L-1) to 2 by -1 do
269 --      begin
270 --      for iR = 2 to (R - 1) do
271 --          begin
272 --          for iC = 2 to (C-1) do
273 --              begin
274 --              if M.lat(iR,iC,iL) = 2 do
275 --                begin
276 --                if (M.lat(iR,iC,(iL-1)) = 4 or M.lat(iR,iC,(iL+1)) = 4 or
277 --                    M.lat((iR-1),iC,iL) = 4 or M.lat((iR+1),iC,iL) = 4 or
278 --                    M.lat(iR,(iC-1),iL) = 4 or M.lat(iR,(iC+1),iL) = 4 )
```

```
279 --                then M.lat(iR,iC,iL) := 4
280 --                else { follow.chain(iR,iC,iL,2)
281 --                       FOLLOW.CHAIN := FOLLOW.CHAIN + 1 }
282 --                end
283 --              end
284 --          end
285 --      write"'n The",iL," layer has been processed."
286 --      write"'n in ",cputime-first.time," mins"
287 --      end
288 --
289 -- write"'n All the 2's have been processed to 0's or 4's."
290 -- write"'n and it took ",cputime-first.time," mins"
291 --
292 --
293 -- ! This part calculates the number of relevant 3's and 4's and also
294 -- !    the number of links between them.
295 --
296 -- let link.3.to.0 := 0
297 -- let link.3.to.1 := 0
298 -- let link.3.to.2 := 0
299 -- let link.3.to.3 := 0
300 -- let link.3.to.4 := 0
301 -- let link.3.to.5 := 0
302 --
303 -- let link.4.to.0 := 0
304 -- let link.4.to.1 := 0
305 -- let link.4.to.2 := 0
306 -- let link.4.to.3 := 0
307 -- let link.4.to.4 := 0
308 -- let link.4.to.5 := 0
309 --
310 -- let cont.from.3 := 0
311 -- let cont.from.4 := 0
312 --
313 -- let no.of.links := 0
314 --
315 -- let flag := 0
316 --
317 -- for iL= 2 to (L-1) do
318 --     begin
319 --     for iR= 2 to (R-1) do
320 --         begin
321 --         for iC= 2 to (C-1) do
322 --             begin
323 --             case M.lat(iR,iC,iL)  of
324 --               0 : {}
325 --               3 : begin
326 --                   cont.from.3 := cont.from.3 + 1
327 --                   flag := 0
328 --                   if M.lat(iR-1,iC,iL) = 4 do { flag := flag + 1
329 --                                   no.of.links := no.of.links + 1 }
330 --                   if M.lat(iR+1,iC,iL) = 4 do { flag := flag + 1
331 --                                   no.of.links := no.of.links + 1 }
332 --                   if M.lat(iR,iC-1,iL) = 4 do { flag := flag + 1
333 --                                   no.of.links := no.of.links + 1 }
334 --                   if M.lat(iR,iC+1,iL) = 4 do { flag := flag + 1
335 --                                   no.of.links := no.of.links + 1 }
336 --                   if M.lat(iR,iC,iL-1) = 4 do { flag := flag + 1
337 --                                   no.of.links := no.of.links + 1 }
338 --                   if M.lat(iR,iC,iL+1) = 4 do { flag := flag + 1
339 --                                   no.of.links := no.of.links + 1 }
340 --                   case flag of
341 --                   0 : link.3.to.0 := link.3.to.0 + 1
342 --                   1 : link.3.to.1 := link.3.to.1 + 1
343 --                   2 : link.3.to.2 := link.3.to.2 + 1
```

```
344 --                      3 : link.3.to.3 := link.3.to.3 + 1
345 --                      4 : link.3.to.4 := link.3.to.4 + 1
346 --                      5 : link.3.to.5 := link.3.to.5 + 1
347 --                default : write"An element (3) has more than 5 links."
348 --
349 --                      end
350 --
351 --                  4 : begin
352 --                      cont.from.4 := cont.from.4 + 1
353 --                      flag := 0
354 --                      if M.lat(iR-1,iC,iL) = 3 do flag := flag + 1
355 --                      if M.lat(iR+1,iC,iL) = 3 do flag := flag + 1
356 --                      if M.lat(iR,iC-1,iL) = 3 do flag := flag + 1
357 --                      if M.lat(iR,iC+1,iL) = 3 do flag := flag + 1
358 --                      if M.lat(iR,iC,iL-1) = 3 do flag := flag + 1
359 --                      if M.lat(iR,iC,iL+1) = 3 do flag := flag + 1
360 --
361 --                      case flag of
362 --                      0 : link.4.to.0 := link.4.to.0 + 1
363 --                      1 : link.4.to.1 := link.4.to.1 + 1
364 --                      2 : link.4.to.2 := link.4.to.2 + 1
365 --                      3 : link.4.to.3 := link.4.to.3 + 1
366 --                      4 : link.4.to.4 := link.4.to.4 + 1
367 --                      5 : link.4.to.5 := link.4.to.5 + 1
368 --                default : write"An element (4) has more than 5 links"
369 --
370 --                      end
371 --           default : write"'n An element is not 0,3 or 4."
372 --              end
373 --          end
374 --      end
375 --
376 -- ! Add the number of links which the Home elements contribute.
377 -- for iR = 2 to (R-1) do{
378 --       for iC = 2 to (C-1) do { if M.lat(iR,iC,2) = 4 do
379 --                                          no.of.links :=no.of.links+1 }
380 --                           }
381 --
382 -- write"'n The array has been processed"
383 -- write"'n and it took ",cputime-first.time," mins"
384 --
385 -- if CHAIN.CALL ~= 0 do { CHAIN.AVERAGE := CHAIN.AVERAGE/CHAIN.CALL }
386 --
387 -- ! Store the above information on tempdata.dat.
388 -- i.w := 7  ! sets integer field width.
389 -- s.w := 1  ! trailing spaces
390 -- let file.name = "tempdata.dat"
391 -- let out = create(file.name,"s","a","v",256 )
392 -- output out,"'"Rows='"",R-2,"'"Cols='"",C-2,
393 -- "'"Lay ='"",L-2,"'"& %='"",perc,"'n"
394 -- output out, count.1, count.2, no.of.links, cont.from.3,cont.from.4,"'n"
395 -- output out, link.3.to.0,link.3.to.1,link.3.to.2,
396 -- link.3.to.3,link.3.to.4,link.3.to.5,"'n"
397 -- output out, link.4.to.0,link.4.to.1,link.4.to.2,
398 -- link.4.to.3,link.4.to.4,link.4.to.5,"'n"
399 -- output out, FOLLOW.CHAIN, CHAIN.CALL, CHAIN.AVERAGE, CHAIN.LEN
400 -- close(out)
401 -- ?
```

Lines 6 to 18 contain a procedure which gives the total CPU time used by the process and is called throughout the program to report on its progress. Lines 20 to 28 initialise constants, while lines 32 to 44 read the dimensions of the array and composition from the file, DIM.DAT. Lines 47 to 77 read the random 0's and 1's from RANDOMARY.DAT and fill a vector called M.lat, (short for Main Lattice, with dimensions R rows, C columns, L layers), with random 1's and 2's. Lines 82 to 86 then set the top layer to pure 3 and the bottom layer to pure 4.

Lines 90 to 127 contain a procedure called FIND.OPTIONS which examines an element in the array (either a 1 or 2) and decides which direction the chain of elements being followed can take, i.e. this procedure is used when a chain of 1's (or 2's) is being followed to see if it eventually connects back to its pure constituent. The procedure has a built in tendency to follow the chain upwards or downwards depending on whether the chain being followed consists of 1's or 2's. The abbreviations used stand for, Up or Down, (i.e. $\pm$ one layer), Left or Right, (i.e. $\pm$ one row), and Back or Forward, (i.e. $\pm$ one column).

Lines 132 to 232 contain the procedure called FOLLOW.CHAIN which will follow a chain of 1's (or 2's) wherever it goes until it either becomes isolated, (in which case all the elements in the chain are set to 0), or connect back to 3 (or 4), in which case all the elements are set to a 3 (or 4). This procedure uses FIND.OPTIONS and is called

from the main program when a 1 (or 2) is encountered which does not have a nearest neighbour that is a 3 (or 4).

The main program is situated from lines 237 onwards and lines 242 to 262 proceed through the array, from the top layer down, examining all the elements that are 1's and deciding whether or not they are isolated from their bulk. If they are, they are set to 0, if not, they are set to 3. Lines 267 to 287 then proceed through the array from the bottom to top examining all the 2's and deciding whether they are isolated (set to 0) or not (set to 4). When line 291 is encountered then the array has been fully processed and only 0's, 3's or 4's remain in the array.

Lines 293 to 380 calculate the number of links which exist between the 3's and 4's. It is at this stage that the number of 3's (and 4's) with 0, 1, 2, 3, 4, 5 links is also found. Finally lines 285 to 401 output the above data to file (TEMPDATA.DAT) for storage.

Appendix V

Directory of Magnetic Tape A.

The experimental data obtained from the experiments described in chapters 3, 5 and 6 are stored on the accompanying magnetic tape, A, (which is stored in the Computing Laboratory, under the label ECH344). A directory and explanation of the files on the tape is given below.

The following data concerns chapter 3,

File name	Array Dimensions Columns	Rows	Layers	Ratio of Particle sizes	Composition (% volume)
1105050XX.DAT	50	50	1->15	1:1	10
1205050XX.DAT	50	50	1->15	1:1	20
120XXXX15.DAT	1->50	1->50	15	1:1	20
1305050XX.DAT	50	50	1->15	1:1	30
1404040XX.DAT	40	40	1->25	1:1	40
1405050XX.DAT	50	50	1->15	1:1	40
1503030XX.DAT	30	30	1->35	1:1	50
1504040XX.DAT	40	40	1->25	1:1	50
150505010.DAT	50	50	10	1:1	50
15050505.DAT	50	50	5	1:1	50
1505050XX.DAT	50	50	1-15	1:1	50
150606010.DAT	60	60	10	1:1	50
150755010.DAT	75	50	10	1:1	50
150XXXX10.DAT	1->65	1->65	10	1:1	50
1505959XX.DAT	59	59	1->10	1:1	50
1XX404010.DAT	40	40	10	1:1	0->100
1XX404015.DAT	40	40	15	1:1	0->100
1XX505010.DAT	50	50	10	1:1	0->100
1XX606010.DAT	60	60	10	1:1	0->100
2XX505010.DAT	50	50	10	2:1	0->100
4105050XX.DAT	50	50	1->15	4:1	10
8105050XX.DAT	50	50	1->15	8:1	10
8156060XX.DAT	60	60	1->10	8:1	15
815XXXX10.DAT	1->65	1->65	10	8:1	15
8205050XX.DAT	50	50	1->15	8:1	20
820XXXX15.DAT	1->50	1->50	15	8:1	20
8305050XX.DAT	50	50	1->15	8:1	30
8405050XX.DAT	50	50	1->15	8:1	40
8505050XX.DAT	50	50	1->15	8:1	50
850606010.DAT	60	60	10	8:1	50
8506060XX.DAT	60	60	1->10	8:1	50

File name	Array Dimensions Columns	Rows	Layers	Ratio of Particle sizes	Composition (% volume)
850XXXX10.DAT	1->65	1->65	10	8:1	50
8605050XX.DAT	50	50	1->15	8:1	60
8805050XX.DAT	50	50	1->15	8:1	80
8XX505015.DAT	50	50	15	8:1	0->100
3XX505010.DAT	50	50	10	3:1	0->100
4205050XX.DAT	50	50	1->15	4:1	20
420XXXX15.DAT	1->50	1->50	15	4:1	20
4305050XX.DAT	50	50	1->15	4:1	30
4405050XX.DAT	50	50	1->15	4:1	40
4505050XX.DAT	50	50	1->15	4:1	50
450XXXX15.DAT	1->50	1->50	15	4:1	50
4605050XX.DAT	50	50	1->15	4:1	60
4805050XX.DAT	50	50	1->15	4:1	80
4XX505010.DAT	50	50	10	4:1	0->100
4XX505015.DAT	50	50	15	4:1	0->100
4XX606010.DAT	60	60	10	4:1	0->100
4XX606015.DAT	60	60	15	4:1	0->100
5XX505010.DAT	50	50	10	5:1	0->100
6XX505010.DAT	50	50	10	6:1	0->100
7XX505010.DAT	50	50	10	7:1	0->100
8XX606010.DAT	60	60	10	8:1	0->100
8XX606015.DAT	60	60	15	8:1	0->100
8XX707015.DAT	70	70	15	4:1	0->100
	The following data was obtained using the pseudo-ionic conductance model.				
1105050XX.ION	50	50	1->15	1:1	10
1205050XX.ION	50	50	1->15	1:1	20
120XXXX10.ION	1->65	1->65	10	1:1	20
1305050XX.ION	50	50	1->15	1:1	30
1405050XX.ION	50	50	1->15	1:1	40
1505050XX.ION	50	50	1->15	1:1	50
150XXXX10.ION	1->65	1->65	10	1:1	50
1605050XX.ION	50	50	1->15	1:1	60
1805050XX.ION	50	50	1->15	1:1	80
1XX505010.ION	50	50	10	1:1	0->100
1XX505015.ION	50	50	15	1:1	0->100
1XX606010.ION	60	60	10	1:1	0->100
1XX606015.ION	60	60	15	1:1	0->100
2XX505010.ION	50	50	10	2:1	0->100
3XX505010.ION	50	50	10	3:1	0->100
4XX505010.ION	50	50	10	4:1	0->100
5XX505010.ION	50	50	10	5:1	0->100
6XX505010.ION	50	50	10	6:1	0->100
7XX505010.ION	50	50	10	7:1	0->100
8XX505010.ION	50	50	10	8:1	0->100

The following data concerns chapter 5,

File name	Ratio of NbS_2 to $Ag_6I_4WO_4$	Weight of NbS_2 (mg)	Pulse Height (mA)	Pulse Length (secs)	Total No. of runs
A11M33P2.DAT	1/2	9.925	1.0	300	1
A11M43P2.DAT	1/2	9.925	0.1	300	1
A12M33P2.DAT	1/2	9.925	2.0	300	1
A12M43P2.DAT	1/2	9.925	0.2	300	1
A15M31M1.DAT	1/2	9.925	5.0	0.1	1
A15M32M1.DAT	1/2	9.925	5.0	0.2	1
A15M33P2.DAT	1/2	9.925	5.0	300	1
A15M35M1.DAT	1/2	9.925	5.0	0.5	1
A15M35M2.DAT	1/2	9.925	5.0	0.05	1
A15M43P2.DAT	1/2	9.925	0.5	300	1
A22M31M1.DAT	1/2	9.925	2.0	0.1	2
A22M32M1.DAT	1/2	9.925	2.0	0.2	2
A22M35M1.DAT	1/2	9.925	2.0	0.5	2
A22M41P0.DAT	1/2	9.925	0.2	1.0	2
A22M42P1.DAT	1/2	9.925	0.2	20	2
A22M45P1.DAT	1/2	9.925	0.2	50	2
A25M32M2.DAT	1/2	9.925	5.0	0.02	2
A25M42M1.DAT	1/2	9.925	0.5	0.2	2
A25M45M1.DAT	1/2	9.925	0.5	0.5	2
A31M31M1.DAT	1/2	9.925	1.0	0.1	3
A31M32M1.DAT	1/2	9.925	1.0	0.2	3
A31M32M2.DAT	1/2	9.925	1.0	0.02	3
A31M35M1.DAT	1/2	9.925	1.0	0.5	3
A31M35M2.DAT	1/2	9.925	1.0	0.05	3
A32M35M2.DAT	1/2	9.925	2.0	0.05	3
A35M41M1.DAT	1/2	9.925	0.5	0.1	3
A35M42M2.DAT	1/2	9.925	0.5	0.02	3
A35M45M2.DAT	1/2	9.925	0.5	0.05	3
A42M41M1.DAT	1/2	9.925	0.2	0.1	4
A42M45M2.DAT	1/2	9.925	0.2	0.05	4
A51M42M1.DAT	1/2	9.925	0.1	0.2	5
A51M45M1.DAT	1/2	9.925	0.1	0.5	5
A52M45M1.DAT	1/2	9.925	0.2	0.5	5
A61M41M1.DAT	1/2	9.925	0.1	0.1	6
A72M42M1.DAT	1/2	9.925	0.2	0.2	7
A81M42M2.DAT	1/2	9.925	0.1	0.02	8
A91M45M2.DAT	1/2	9.925	0.1	0.05	9
A92M42M2.DAT	1/2	9.925	0.2	0.02	9
LU121M5.DAT	1/2	9.143	0.01	2000	1
LU125M5.DAT	1/2	9.143	0.05	2000	1
LU125M6.DAT	1/2	9.143	0.005	2000	1
LU1225M6.DAT	1/2	9.143	0.0025	2000	1
LU121M6.DAT	1/2	9.143	0.001	2000	1
LU122M5.DAT	1/2	9.143	0.02	2000	1
LU123M5.DAT	1/2	9.143	0.03	2000	1
LU124M5.DAT	1/2	9.143	0.04	2000	1
VU125M610.DAT	1/2	9.143	0.005	10000	1
VU125M62.DAT	1/2	9.143	0.005	2000	1
VU125M620.DAT	1/2	9.143	0.005	20000	1

The following data concerns chapter 6 and the effect of composition on the contact area.

File name	Ratio of NbS_2 to $Ag_6I_4WO_4$	Weight of NbS_2 (mg)	Pulse Height (mA)	Pulse Length (secs)	Total No. of runs
LU121M5.DAT	1/2	9.143	0.01	2000	1
LU125M5.DAT	1/2	9.143	0.05	2000	1
LV121M5.DAT	1/2	10.353	0.01	2000	1
LV122M5.DAT	1/2	10.353	0.02	2000	1
LV123M5.DAT	1/2	10.353	0.03	2000	1
LD115M6.DAT	1/1	13.383	0.005	2000	1
LD113M5.DAT	1/1	13.383	0.03	2000	1
LD111M5.DAT	1/1	13.383	0.01	2000	1
LD112M5.DAT	1/1	13.383	0.02	2000	1
LE212M5.DAT	2/1	19.253	0.02	2000	1
LE213M5.DAT	2/1	19.253	0.03	2000	1
LE211M5.DAT	2/1	19.253	0.01	2000	1
LE215M6.DAT	2/1	19.253	0.005	2000	1
LI111M5.DAT	1/1	12.985	0.01	2000	1
LI112M5.DAT	1/1	12.985	0.02	2000	1
LJ131M5.DAT	1/3	7.606	0.01	2000	1
LJ132M5.DAT	1/3	7.606	0.02	2000	1
LS1101M5.DAT	1/10	2.340	0.01	2000	1
LS1102M5.DAT	1/10	2.340	0.02	2000	1
LN131M5.DAT	1/3	2.453	0.01	2000	1
LN132M5.DAT	1/3	2.453	0.02	2000	1
LF211M5.DAT	2/1	18.653	0.01	2000	1
LF212M5.DAT	2/1	18.653	0.02	2000	1
LK211M5.DAT	2/1	17.587	0.01	2000	1
LK212M5.DAT	2/1	17.587	0.02	2000	1
LQ1181M5.DAT	1/18	1.564	0.01	2000	1
LQ1182M5.DAT	1/18	1.564	0.02	2000	1
LT1101M5.DAT	1/10	2.323	0.01	2000	1
LT1102M5.DAT	1/10	2.323	0.02	2000	1
LW121M5.DAT	1/2	10.252	0.01	2000	1
LW122M5.DAT	1/2	10.252	0.02	2000	1
LX121M5.DAT	1/2	9.748	0.01	2000	1
LX122M5.DAT	1/2	9.748	0.02	2000	1
LR1181M5.DAT	1/18	1.461	0.01	2000	1
LR1185M6.DAT	1/18	1.461	0.005	2000	1
LR1183M6.DAT	1/18	1.461	0.003	2000	1

The following data concerns chapter 6 and the heat treatment of cells.

File name	Ratio of NbS_2 to $Ag_6I_4WO_4$	Weight of NbS_2 (mg)	Pulse Height (mA)	Pulse Length (secs)	Total No. of runs
	The following data sets refer to measurements carried out on the cells <u>before</u> they have been heat treated.				
LU121M5.DAT	1/2	9.143	0.01	2000	1
LU122M5.DAT	1/2	9.143	0.02	2000	1
LV121M5.DAT	1/2	10.353	0.01	2000	1
LV122M5.DAT	1/2	10.353	0.02	2000	1
LW121M5.DAT	1/2	10.252	0.01	2000	1
LW122M5.DAT	1/2	10.252	0.02	2000	1
LX121M5.DAT	1/2	9.748	0.01	2000	1
LX122M5.DAT	1/2	9.748	0.02	2000	1
	The following data sets refer to measurements carried out on the cells <u>after</u> they have been heat treated. (i.e. 15 mins at 290°C)				
TU121M5.DAT	1/2	9.143	0.01	2000	1
TU122M5.DAT	1/2	9.143	0.02	2000	1
TV121M5.DAT	1/2	10.353	0.01	2000	1
TV122M5.DAT	1/2	10.353	0.02	2000	1
TW121M5.DAT	1/2	10.252	0.01	2000	1
TW122M5.DAT	1/2	10.252	0.02	2000	1
TX121M5.DAT	1/2	9.748	0.01	2000	1
TX122M5.DAT	1/2	9.748	0.02	2000	1